Characterisation of Polyvinyl Alcohol Hydrogels modified with Chitosan for Cardiovascular Applications

by

David T. Mathews (*B.Eng.*)

Thesis presented to Dublin City University in fulfilment of the requirements for the degree of Doctor of Philosophy

Supervisors: **Dr. Garrett B. McGuinness**
Prof. Paul Cahill
Prof. M.S.J. Hashmi

School of Mechanical and Manufacturing Engineering,
Dublin City University,
Ireland

2006

Declaration

I hereby certify that this material, which I now submit for assessment on the programme of study leading to the award of Doctor of Philosophy, is entirely my own work and has not been taken from the work of others save and to the extent that such work has been cited and acknowledged within the text of my work.

Signed: David Mathews I.D No.: 97626619

David Mathews

Date: 21/7/06

Acknowledgements

There are many people who have contributed in numerous ways to this work. Firstly I would like to express my gratitude to my supervisor, Dr. Garrett McGuiness, to whom I am indebted for his help, guidance, support and patience throughout this project.

I am also very grateful to the staff (especially Prof. Saleem Hashmi) of the Mechanical and Manufacturing Engineering Department, Dublin City University for their support and help over the last few years. I am also appreciative to Dr. Triona Lally for her help and advice. Thanks also to Liam Dominican and his technical team for the advice and manufacture of many quality pieces. Special thanks to fellow members of the Bioengineering branch especially, Graham Gavin, John Hingston and Declan Noone.

Sincere thanks to Prof. Paul Cahill and all my former colleagues in the Vascular Health Research Centre where I have spent much of my time working and gained valuable biological experience. I particularly wish to thank Dr. Yvonne Birney and Dr. Catherine Sweeney for their continuous encouragement, support and especially their friendship over the past few years. Thanks to everyone in the Vascular Health Research Centre for "adopting the engineer" and always including me in all extracurricular activities!!

I would like to thank the Trinity Centre For Bioengineering, Trinity College Dublin for the use of their uniaxial tension tester during my hour of need!

I wish to thank Dublin City University and the Mechanical and Manufacturing Engineering Department who generously subsidised my travel to a number of conferences during my completion of this work.

Sincere thanks to my parents, Thomas and Margaret, and also my sisters, Caroline and Maura for their advice and unwavering support all my life! Thanks also to my friends for listening to me, especially during the tough times!!

Publications & Presentations

Mathews, D.T, Birney, Y.A., McGuinness, G.B., Cahill, P.A. Vascular cell viability on polyvinyl alcohol hydrogel modified with water-soluble and -insoluble chitosan. Journal of Biomaterials Research, Part B . *(Submitted)*

Mathews, D.T, McGuinness, G.B., Birney, Y.A., Cahill, P.A. Mechanical and biological evaluation of poly (vinyl alcohol) hydrogel modified with chitosan. Proceedings of Bioengineering in Ireland, 2006.

Mathews, D.T, McGuinness, G.B., Birney, Y.A., Cahill, P.A. Evaluation of poly (vinyl alcohol) hydrogels modified with chitosan as potential bioartificial materials. Proceedings of Bioengineering Materials, Poland, 2005.

Mathews, D.T, McGuinness, G.B., Birney, Y.A., Cahill, P.A. Attachment and growth of cultured endothelial and smooth muscle cells on PVA / chitosan combined hydrogels, Proceedings of Bioengineering in Ireland, 2005.

Mathews, D.T, McGuinness, G.B., Birney, Y.A., Cahill, P.A. Vascular cell growth on poly (vinyl alcohol) hydrogel membranes containing chitosan. Proceeding of Northern Ireland Biomedical Engineering Society, 2005.

Mathews, D.T, McNamara, B.P., McGuinness, G.B. Residual Strain effects on the stress/strain fields of an artery during physiological and non-physiological loading conditions. Proceedings of European Society of Biomechanics, Netherlands, 2004.

Mathews, D.T, McNamara, B.P., McGuinness, G.B. The Effect of Opening Angle Variations on the Strain Fields of an artery For Various Loaded States, Proceedings of Bioengineering in Ireland, 2004.

Awards

Finalist for the Institute of Engineers of Ireland Annual Biomedical Engineering Research Medal 2006. Paper and Presentation Title:

Mathews, D.T, Birney, Y.A., McGuinness, G.B., Cahill, P.A. Effect of water-soluble chitosan on the mechanical and biological properties of polyvinyl alcohol hydrogels. Institute of Engineers of Ireland Conference 2006.

Table of Contents

List of Figures

List of Tables

Abbreviations

BAEC	Bovine aortic endothelial cells
BASMC	Bovine aortic smooth muscle cells
BSA	Bovine serum albumin
DAPI	4'-6-Diamidino-2-phenylindole
DMSO	Dimethlysulphoxide
DNA	Deoxyribonucleic acid
EC	Endothelial cells
EDTA	Trypsin-Ethlyenediamine Tetracetic Acid
FACS	Fluorescent activated cell sorter
FBS	Foetal bovine serum
F-actin	Filamentous actin
HBSS	Hanks balanced salt solution
hr	Hour
IS	Water-insoluble
KOH	Potassium Hydroxide
min	Minutes
PBS	Phosphate buffered saline
PEG	Polyethylene gylcol
PI	Propidium iodide
P/S	Penecillin-streptomycin
PVA	Polyvinyl alcohol
RGD	Arginine-glycine-aspartic acid
RGDS	Arginine-glycine-aspartic acid-serine
RGES	Arginine-glycine-glutamic acid-serine
rpm	Rotations per minute
SEM	Scanning electron microscope
SMC	Smooth muscle cells
UV	Ultraviolet
WS	Water-soluble

Nomenclature

C_{ij}	Components of the right Cauchy-Green deformation tensor
E_{ij}	Components of Green-Lagrangian strain tensor
I_1, I_2, I_3	Stretch invariants
J	Jacobian determinant
R_i	Internal radius
R_o	External radius
S_{ij}	Components of the second Piola-Kirchoff stress tensor
W	Strain energy density
$\lambda_1, \lambda_2, \lambda_3$	Principal stretches
α	Opening angle
Θ_0	Polar angle
μ_k, α_k	Material constants for the Ogden model
a	Radius of rotation
p	Density
n	Viscosity
f	Frequency
g	Gram
µl	Microlitre
M	Molar
cm	Centimetre
cm^2	Centimetre squared
°C	Degrees celsius
kg	Kilogram
kD	Kilodaltons
σ_E	Engineering stress
ε_E	Engineering strain
σ_T	True stress
ε_T	True strain

Abstract

Title: Characterisation of Polyvinyl Alcohol Hydrogels Modified with Chitosan for Cardiovascular Applications

David T. Mathews (B.Eng.)

The use of Polyvinyl Alcohol (PVA) hydrogels combined with chitosan as a vascular tissue substitute for *in vitro* vascular cell culture studies was investigated. Hydrogels possess many characteristics that can be controlled and adjusted during the fabrication processes, such as tissue-like elasticity, mechanical strength and permeability. In order to develop a material with appropriate inherent material properties that may be used to fabricate a bioartificial vessel with appropriate structural properties, arterial wall mechanics were investigated. A three layer finite element model, incorporating the effects of circumferential and longitudinal residual stresses, was developed to identify the effect of vessel geometry, constitutive properties and residual stresses on the structural response of an arterial segment.

Chitosan was blended to the hydrogel to enhance cell adhesion and growth. The effect of fabrication parameters on the mechanical and morphological characterisation of the PVA-chitosan blended hydrogels was determined using uniaxial extension tests, bi-axial inflation tests, opening angle observations and scanning electron microscopy. PVA-chitosan hydrogel vessels were constructed, and the compliance was measured and compared with numerical predictions.

In vitro experiments have been conducted to investigate vascular endothelial and smooth muscle cell adhesion and growth to PVA-chitosan hydrogel surfaces. The structure and composition of the cultured cells on the PVA-chitosan hydrogel surfaces was studied using immunocytochemistry techniques. Cellular proliferation and viability under static and shear culture conditions have been explored using fluorescent activated cell sorter analysis.

The finite element analysis results showed that the constitutive properties had a significant affect on the overall structural response of the artery wall. The mechanical and morphological studies established that the PVA-chitosan blended hydrogel membranes could be fabricated with similar properties to porcine aortic tissue. The findings of the biological experiments demonstrated that vascular cells adhered to the PVA-chitosan membranes and exhibited comparable proliferation and apoptosis characteristics to control samples. The results described increase understanding of PVA-chitosan blended hydrogel membranes specifically with regard to the development of bioartificial vessels for use in *in vitro* vascular bioreactors.

Chapter 1

Introduction

Cardiovascular diseases remain among the most prominent health challenges despite many breakthroughs in cardiovascular medicine over recent years. Cardiovascular diseases are the leading cause of death in the western world, accounting for 37.3 % of all deaths in the United States [1]. An estimated 17 million people die globally due to cardiovascular disease per annum, which translates into one death every 30 seconds [2]. The incidence of cardiovascular disease in Ireland is above the European Union (EU) average, with 62 deaths per 100,000 population in 2004 compared to the EU average of 56 [3]. In addition, it is estimated that one quarter of people in the western world live with cardiovascular disease, resulting in a significant economic impact, both in terms of health care expenditures and lost productivity [1]. An increased understanding of the mechanisms underlying the pathology of cardiovascular diseases is imperative both in the prevention and management of this condition.

While the number of deaths related to cardiovascular diseases has increased over the past numbers of years, this increase would be significantly higher but for development of improved diagnostic equipment that can enable early diagnosis and more successful interventional procedures. It is generally accepted that the progression of atherosclerosis (narrowing or blocking of the artery due to the presence of plaque), in an arterial vessel is related to the mechanical forces experienced by the arterial wall [4], cigarette smoke, high blood pressure and high cholesterol. In order to prevent cardiovascular diseases, as well as treat them, and

reduce the number of deaths, the effect of specific mechanical stimuli on the arterial wall and on vascular cells needs to be understood.

There is a need for experimental systems which can apply physiological mechanical stimuli to endothelial (EC) and smooth muscle cells (SMC), in order to properly understand the effect on their behaviour. Specifically, there is a need for a bioartificial vessel which can support EC and SMC growth and form the basis for experiments involving physiological flow conditions and interventional procedures. The bioartificial vessel must be constructed from a biomaterial which will interact with fluid flow, pressure and mechanical procedures in a manner similar to vascular tissue.

Ultimately, such bioartificial vessels would prove to be invaluable biomedical research tools to examine the impact of various pharmacological and mechanical interventions and thereby avoid *in vivo* studies. Moreover, *in vitro* studies would contribute to the development of commercial bioartificial small diameter grafts for vascular reconstruction in patients where autologous blood vessels are not available.

1.1 Biomaterial Development

In order to develop a biomaterial for *in vivo* or *in vitro* applications there are a number of issues that need to be addressed including (i) appropriate cellular activity on the biomaterial and (ii) appropriate mechanical properties throughout the physiological stress range. The most important factor is the selection of a suitable biomaterial. Many synthetic biomaterials with the appropriate range of mechanical properties have been identified [5]. The next step is to determine which material can be processed and prepared to address the aforementioned issues. There are a number of biomaterial characteristics, processing parameters and preparation techniques that influence biomaterial effectiveness including:

1. **Biomechanical properties (elasticity)**
   There is a need to replicate both the elastic properties of arterial tissue and the structural properties of blood vessels. Control of mechanical properties would be advantageous. Therefore, the selection of appropriate

fabrication techniques is important as the mechanical properties may be influenced by the processing parameters.

2. **Porosity of the biomaterial**.

   This affects cellular and molecular adhesion and diffusion of nutrients [6]. Porosity can be induced in virtually any biomaterial, and is highly influential in controlling cell activity on the biomaterial.

3. **Surface coating and texture.**

   The biomaterial must support growth of EC and SMC in order to be suitable for *in vivo* or *in vitro* applications. The surface coatings (peptides and protein) promote cell adhesion [7-9] while the surface texture may affect cellular adhesion.

To fabricate a biomaterial that replicates the *in vivo* environmental conditions, a biomaterial with mechanical and biological properties representative of arterial tissue is required. Bioartifical arterial tubular vessels could then be manufactured with similar geometric and stress-strain characteristics of arterial tissue. Mechanical signals alter almost all aspects of cell function. Therefore, a bioartifical arterial tubular vessel with representative mechanical and geometric properties seeded with vascular cells *in vitro* will affect the biochemical signals produced by the cells. The mechanical properties of many biomaterials can be varied through different processing techniques, though the coupled effect on cellular activity may vary from one biomaterial to another. Validation of the biomaterial suitability is another important aspect in the development process. *In vitro* mechanical and biological experiments that reproduce one or more *in vivo* parameters are required to evaluate the biomaterials.

1.2 Research Objectives and Methodology

The objective of this research is to assess the use of polyvinyl alcohol (PVA) hydrogel combined with chitosan as a potential scaffold for use in *in vitro* vascular cell culture studies. In order to validate or refute continued development of the biomaterial as a potential vascular substrate, three research areas were investigated:

1. **Finite element analysis of vascular wall mechanics.**
   Finite element analysis was used to investigate the structural response of arterial walls under physiological conditions. This allowed an investigation of the importance of factors such as vessel geometry, constitutive properties and residual stresses (circumferential and axial) to the overall vessel behaviour.

2. **Mechanical characterisation of the PVA-chitosan blended hydrogels.**
   PVA hydrogels can be considered non-linear, elastic, isotropic, incompressible materials [10]. Uniaxial extension tests, bi-axial inflation tests and tubular inflation tests were used to characterise the mechanical properties of the PVA-chitosan blended hydrogels. In order to investigate the polymer network, the porosity characteristics of these PVA-chitosan blended hydrogels was analysed using scanning electron microscopy (SEM).

3. **Vascular cell adhesion to PVA-chitosan blended hydrogels.**
   Cell culture techniques were conducted to determine if adhesion and proliferation of vascular cells can be achieved on PVA-chitosan blended hydrogels. Cell morphologies were studied using immunocytochemistry staining to determine whether the membranes affected the structure and composition of the cells. Fluorescent activated cell sorter (FACS) analysis was used to establish proliferation and cell viability. Preliminary flow experiments were also performed to verify if the anchorage of cellular focal adhesion sites is sufficient to withstand shear stress.

If the PVA-chitosan blended hydrogels can be fabricated with appropriate mechanical properties and support vascular cell adhesion and proliferation then the biomaterial may be considered suitable for further investigation in vascular bioreactors. This would then be suitable for investigating vascular EC and SMC fate decisions, as well as other investigations relating to the use of medical devices such as balloon angioplasty and stent implantation.

Chapter 2

Literature Review

In order to develop a biomaterial that mimics arterial mechanical properties and may be used as a substrate for vascular cell culture experiments, it is important to understand the functions of the different layers of the arterial wall. The composition and biomechanical properties of arterial tissue are therefore reviewed in this chapter. Published information on the mechanical environment experienced by arterial tissue is reviewed, to provide an insight into how the substrate should be mechanically characterised. Commercial and non-commercial vascular cell culture systems are described and the biological responses of vascular cells to mechanical stimuli are also discussed. The chapter concludes with a review of selected natural and synthetic biomaterials that may be potentially used to fabricate a biomaterial for cardiovascular applications.

2.1 Vascular Structure and Function

2.1.1 Arterial Wall Classification

The arterial wall has multiple physiological functions and a complex structure (Figure 2.1). Arteries can be classified into two categories; elastic arteries and muscular arteries. Elastic arteries, which include the aorta, carotid and the iliac arteries, tend to be larger diameter vessels and are located close to the heart. However, muscular arteries, which include the coronaries, femorals and tibials, are smaller vessels located closer to the arterioles. Most arteries, however, display some of the characteristics of both types of artery. The human arterial wall comprises of

three concentric layers; the tunica intima, the tunica media and the tunica adventitia (Figure 2.2). The intima is the inner layer, the media is the middle layer and the adventitia is the outermost layer. Each arterial layer presents specific material properties to assume a particular role in the vascular wall.

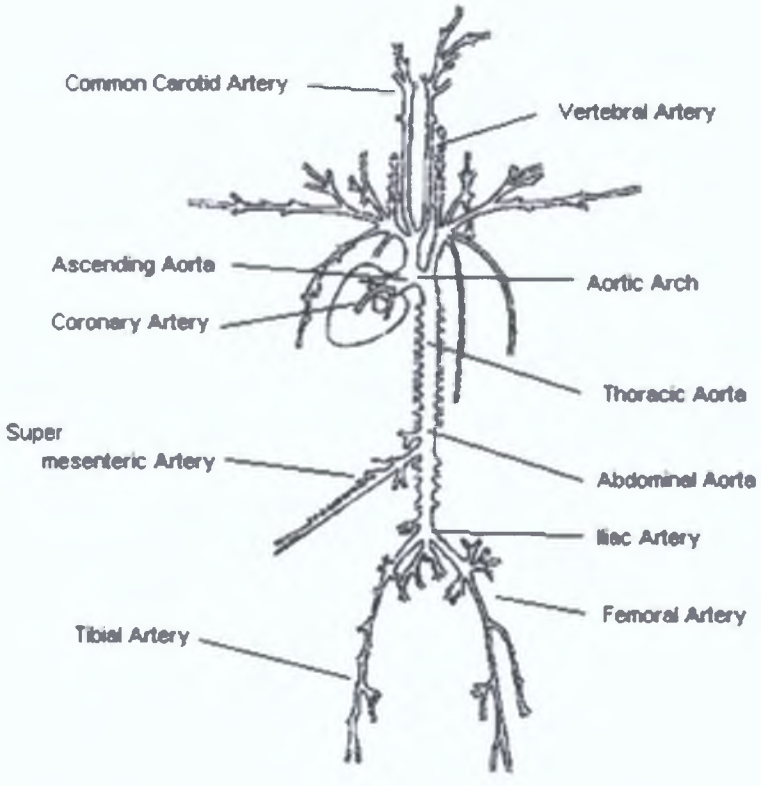

Figure 2.1 **Systemic arterial tree.** (based on diagram from [11], originally modified from McDonald [12])

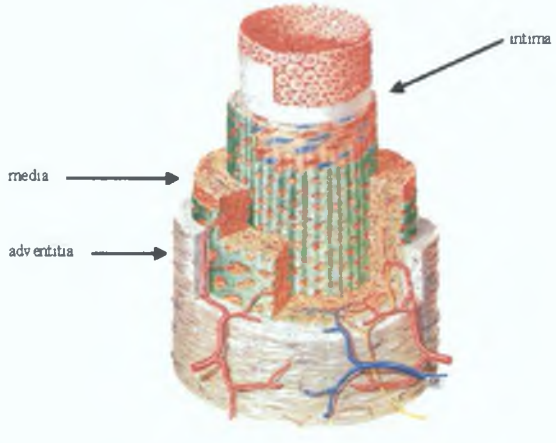

Figure 2.2 **Schematic of a human muscular artery: tunica intima, tunica media and tunica adventitia (Citied from [13]).**

2.1.2 The Intimal Layer

The intima is composed of a monolayer of endothelial cells (EC) lying on a thin basal membrane (the internal elastic lamina). The endothelium constitutes a selective barrier between the blood and tissues [14-16] and prevents bacteria in the blood entering the wall, as well as preventing thrombosis. The EC align with the direction of the blood flow. The internal elastic lamina is a flexible membrane that allows bending and changes in diameter associated with changes in blood pressure. The intima in young healthy individuals has little or no effect on the overall mechanical compliance of the vascular wall. However, the intima thickens with age and disease, which can have a significant effect on its mechanical properties [17].

2.1.3 The Medial Layer

The media consists of smooth muscle cells (SMC) in an extracellular network of elastin fibres and collagen fibrils [18]. The collagen fibres are interconnected between concentric layers of SMC and elastic fibres [14]. There are two sublayers between the intima and media, and the media and adventitia, known as the internal and external elastic lamina respectively. These laminae are much more pronounced in muscular arteries than in elastic arteries. The media has high strength, resilience and the ability to resist loads in both the longitudinal and circumferential directions. In a healthy artery the media is the most significant layer from a mechanical compliance standpoint [15].

2.1.4 Adventitial Layer

The adventitia is the outermost layer of the artery. It consists primarily (70 % to 80 %) of thick bundles of collagen fibrils together with fibroblasts, fibrocytes, nerves and vasa vasorum that form a "leathery" tissue [19]. The thickness of the adventitia can be between 10 % to 50 % of the total arterial thickness, depending on whether it is an elastic or muscular artery and on its location in the arterial tree (Figure 2.1). The compliance of the artery varies with the amount of collagen and elastin in the wall [14], with the collagen fibrils reinforcing the wall, offering stability and strength through its structure [15]. The adventitia also carries micro-

vessels that supply nutrients and oxygenated blood to the SMC [20].

The contribution to mechanical significance of each of the layers changes as the arteries age. In a young healthy individual the intima offers little mechanical resistance but this may become more significant for aged diseased arteries, as the intima becomes thicker and stiffer. The media and adventitia provide the arterial wall with strength and are essentially the load bearing layers of the artery. At physiological pressures, the arterial wall is subjected to low stress and the media is the load-bearing layer [21,22]. The adventitia is not as stiff as the media at low pressures. However, at high pressures the stiffness significantly increases as the collagen fibrils straighten. This increase in rigidity prevents overstretch and rupture of the artery [15].

Arteries exhibit both active and passive mechanical behaviour. The degree of contraction of SMC within the arterial wall determines the active mechanical behaviour of arterial tissue [15]. Passive mechanical properties of elastic or muscular arteries are dependent on the composition of the artery, specifically the amount of elastin and collagen present in the vessel wall.

2.2 Vascular Biomechanics

A number of assumptions or simplifications are often used to develop a biomechanical model for vascular tissue.

2.2.1 Heterogeneity

From histological studies, an arterial segment may be considered to have a uniform structure in the longitudinal and circumferential directions, but not in the radial direction [23]. The artery consists of a complex arrangement of many individual components (cells, muscle, fibres etc.). Each component has different physical and mechanical properties whose contents vary according to tissue type and location [24]. Therefore, the distinction between the layers and the constitutive homogeneity within each layer indicates that it may be realistic to assume that the properties of the artery vary by layer and not continuously with radius (ie: that each

layer of the artery may be considered homogeneous). However, it should also be noted, that the media of the vessel bears most of the load at physiological pressure since the media typically represents between 50 % to 90 % of the thickness of the vessel wall [18]. The assumption of homogeneity does not make any distinction between the specific contributions made by different constituents of the wall such as elastin and collagen. However, it is the overall mechanical behaviour of the arterial tissue and the contributions of all the constituents of the vessel, which is of interest.

2.2.2 Incompressibility

Arterial tissue in a similar fashion to other rubber-like materials which are capable of undergoing large elastic deformations, show a very low degree of compressibility [25,26]. The resistance of arterial tissue to volume changes is orders of magnitude greater than its resistance to shape changes [26]. The arterial wall, like most biological soft tissues, contains more than 70 % water, therefore the volume changes only slightly under loading [24]. Carew *et al* [25] and Dobrin and Rovick [27] considered the issue of incompressibility in the context of arterial tissue and reported that under physiologic conditions the assumption of incompressibility can be safely made.

2.2.3 Anisotropy

The arterial wall is anisotropic. This means that it has different stiffness characteristic in different directions [28-30]. Patel and Fry [28] excised segments of aorta, cannulated the segments at both ends, suspended them vertically from a ring stand and pressurised them at various axial loads. The rotation of the lower end of the aortic vessels was measured with respect to the fixed upper end as a function of pressurisation. Strain values were calculated from measurements of overall segment length, midwall radii and rotations. Patel and Fry [28] reported that under physiologic loading the shearing strain ($\varepsilon_{z\theta}$ and $\varepsilon_{z\theta}$) values for all segments of blood vessel tested were always small compared to the corresponding circumferential and axial strains ($\varepsilon_{\theta\theta}$ and ε_{zz}). In this study, it was concluded that the vessel may be treated as a cylindrically orthotropic tube. This implies that the elastic properties of

the vessel are almost symmetrical about the planes in the radial, circumferential and axial directions to the principal stresses under physiological loading.

2.2.4 Nonlinearity

Biological soft tissues under physiological loading exhibit material and geometric non-linearities. The artery behaves in a non-linear viscoelastic manner [31,32]. This behaviour is dependent on the location along the vascular tree. Each of the main structural components (collagen and elastin fibres) of the artery provides certain mechanical characteristics, and the degree of nonlinearity is determined by the ratios of these components.

Figure 2.3 shows the stress versus strain curve of the adventitia layer from non-diseased tissue of a diseased external iliac artery [33]. A non-linear stress versus strain relationship is evident. In the initial stages of extension (A) only the elastin resists extension (bears a load). In this region of the graph the curve rises almost linearly with a low slope. Further extension of a specimen (B) recruits the least taut collagen fibres first, and then gradually collagen fibres of different tortuosity are recruited. The stress versus strain curve rises gradually until all the collagen fibres are recruited and the tissue tears. Hence the nonlinear effect is due to the transfer of load from the elastin to collagen fibres as the strain increases.

The stress strain response of arterial tissue has generally been obtained by several researchers from uniaxial tensile tests. A number of studies have been conducted which have measured the non-linear stress versus strain relationship in uniaxial tension of different arterial tissue from different species as well as from different areas of the arterial tree [33-37]. In uniaxial tensile testing, dogbone-shaped longitudinal and circumferential specimens are clamped at each end and undergo cyclic uniaxial extension while continuously recording the force-elongation (width and gauge) relationship. Generally researchers have quantified the overall uniaxial stress versus strain response of arterial tissue (ie: 3 layers of the arterial wall). However, Holzapfel *et al* [33] separated the three layers of a human external iliac artery and performed uniaxial extension tests to obtain the stress strain relationship for each layer.

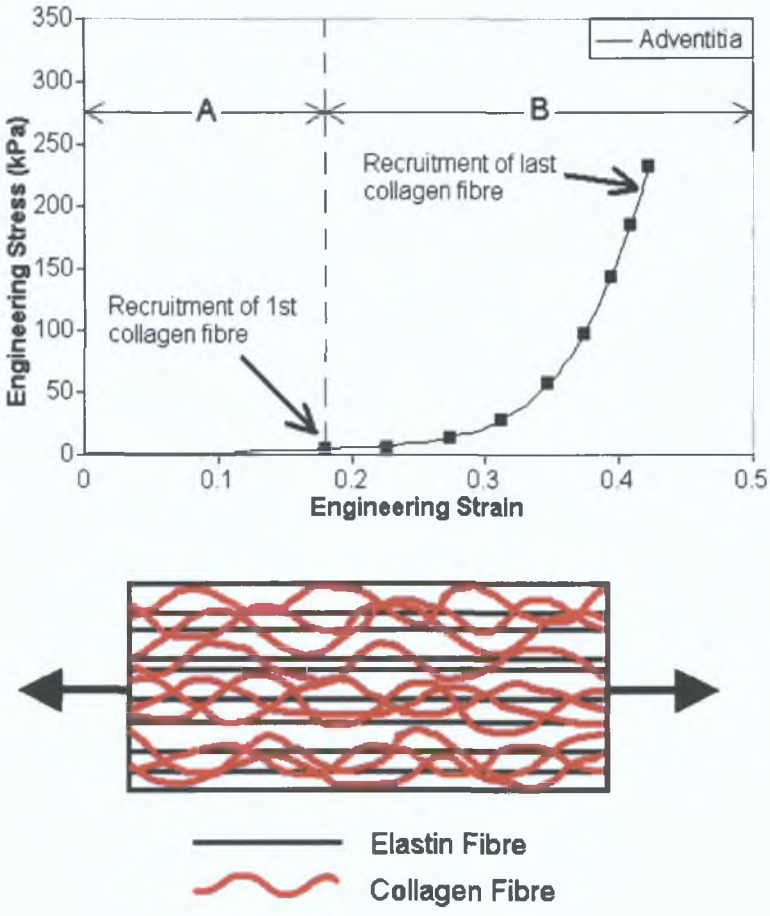

Figure 2.3 **Non linear behaviour of the adventita layer from a human specimen.** (Note: Stress versus Strain data obtained from Holzapfel *et al* [33].

The deformation response of arteries is strongly coupled in the principal directions (radial, longitudinal and circumferential directions) due to the complex organisation of the constituents of arterial tissue, namely the collagen and elastin content. Multiple uniaxial tests are insufficient to characterise arterial tissue due to nonlinear interactions (eg: an applied axial strain in arteries alters the circumferential stress versus strain curve [18]). Therefore in order to simultaneously determine the response of arterial tissue in the principal directions, biaxial testing is necessary.

If arterial tissue is considered incompressible, three-dimensional mechanical properties can be inferred from a two-dimensional test. This has led to a number of studies to estimate the biaxial response of arterial segments [38-41]. To perform biaxial testing, two boundary conditions must be controlled. The edges of a biaxially loaded sample must be free to expand since the sample is loaded in two principal orientations [42]. Therefore the use of solid clamping grips is excluded. The use of

numerous grips to grasp the sample to allow lateral extension necessitates the use of non-contact strain measurement in the central region of the test specimen at a distance from the sample edges to avoid the localised affect of the grips. An alternative method is to use a bubble inflation method, where a circular specimen is clamped down, sealed and inflated [40]. This technique assumes that the deformed specimen is spherical and only allows for equibiaxial testing.

Inflation and extension of excised intact arterial tissue specimens is another method used to gain a better understanding of the nonlinear and anisotropic arterial wall behaviour [39,43-45]. During inflation tests on arterial tissue, a longitudinal force and an internal pressure are applied to a cylindrical vessel. This method avoids traumatic excision of the arterial tissue and the mechanical environment is closer to physiological loading conditions. A pressure versus diameter relationship is used to describe the behaviour of the arterial segments.

Arteries show hysteresis under cyclic loading, stress relaxation under constant extensions and creep under constant loads [46]. It has also been noted that during the first few cycles of loading the stress mitigates (softens) (Figure 2.4). Preconditioning, the repeated loading and unloading of arterial tissue four or fives times before the actual test (loading to failure), has been deemed necessary to stabilise the tissue and reproduce the state of the tissue in the physiologic environment [37,47].

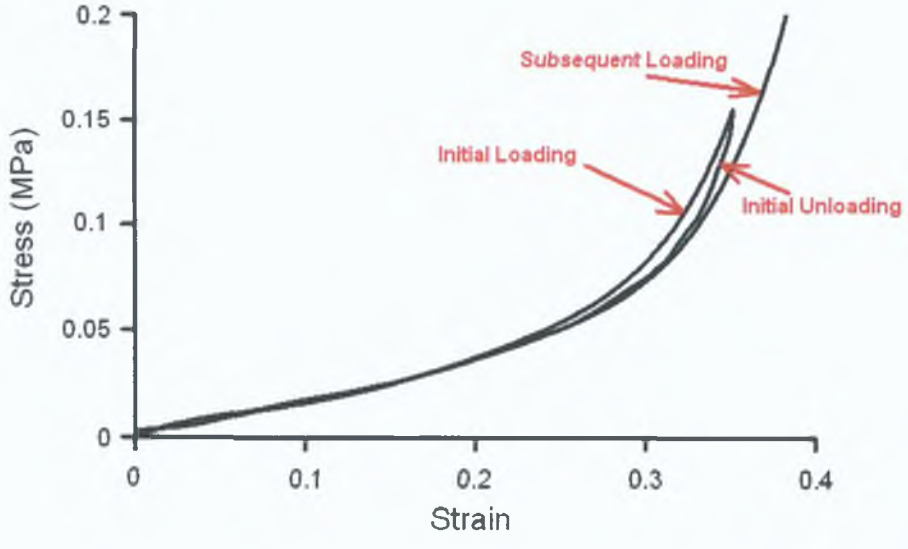

Figure 2.4 **A typical preconditioning curve showing the response become more extensible with one preconditioning cycle [48].**

2.2.5 Residual Stress

Residual stress is a tension or compression, which exists in the arterial wall without application of an external load [49]. The existence of arterial residual stresses was first reported by D.H. Bergel in 1960 [50]. He noted that a longitudinal cut in an arterial section resulted in the "unrolling" of the artery. Residual stresses have a strong influence on the stress and strain distributions across the arterial wall under physiological loading [15,51]. In order to accurately model the relationship between stress and strain, it is essential to identify the appropriate stress free reference configuration.

A radial cut of an unloaded intact arterial ring opens up because there is a reduction in the strain energy stored. This angle is known as the opening angle (Figure 2.5). Chuong and Fung [51] suggested that the radial cut leads to a zero stress state, in the arterial ring as it reduces the residual stresses.

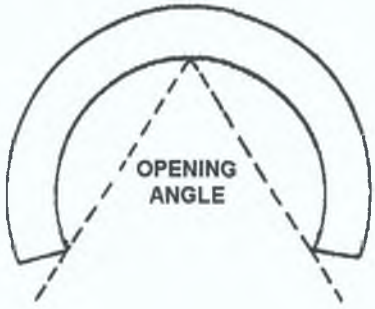

Figure 2.5 Schematic cross section of a cut vessel at zero stress, defining the opening angle.

Residual stresses have been examined from a variety of different viewpoints and there have been some conflicting findings. It has been reported that single radial cuts in the arterial rings capture most of the residual strain effect and that the location of the cut has very little effect on the value of the opening angle [52,53]. However it has also been suggested that the one radial cut is not sufficient to relieve all the residual stress in the artery [54]. Vossoughi *et al* [55], established that if the arterial ring is separated into inner and outer rings and then cut in the radial direction, different opening angles result for each ring. Greenwald *et al* [54] concluded the true stress free configuration can only be achieved by partial destruction of the vessel wall. In addition, this group also suggested that the different layers of the arterial

wall might each have different opening angles.

In order to assess the residual stresses in arterial segments, the length of the arterial segment is noted prior to harvesting and the opening angles of arterial rings are measured. It has been suggested that the elastin content is responsible for the residual stress in the arterial wall [56,57]. Fung and Liu [52] have shown that the opening angle of the artery varies with the location along the vascular tree (Figure 2.6) and is also affected by physical, chemical or biological stimuli, for example hypertension or diabetes [58]. According to experimental studies by Schulze-Bauer *et al* [59] the intima, media and adventitia of non-diseased, aged human external iliac arteries, when separated, spring open to form sectors which show different opening angles. Positive opening angles were reported for the intact wall sectors (ranging from 56° to 163°), as well as the separated media and adventitia. Conversely negative opening angles were evident in the intima layer. Schulze-Bauer *et al* [59] recognised that further data and improved knowledge are required to affirm these observations for the intimas.

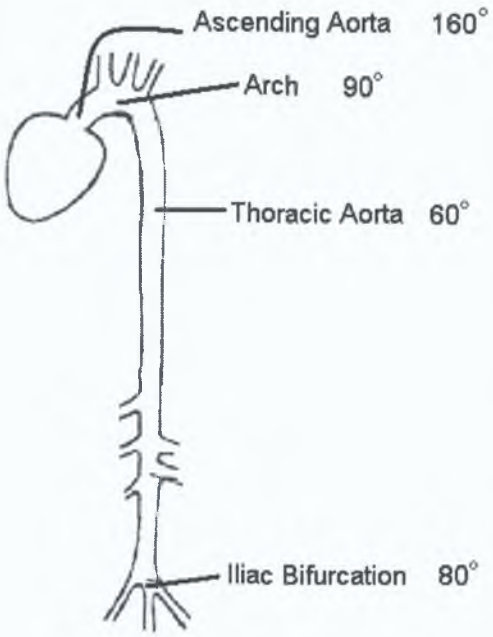

Figure 2.6 Variations in the opening angles along different sections of a rat aorta (Adapted from [60]).

2.3 Vascular Cell Mechanotransduction

Mechanotransduction is the process by which cells convert mechanical stimuli into biochemical signals. Mechanical stresses regulate a many physiological functions including the detection of fluid shear stress imparted by blood flow across vascular cells. Mechanical signals transform almost all aspects of cell function (growth, differentiation, migration, gene expression, protein synthesis, and apoptosis) while mechanical forces directly affect the form and function of tissues.

2.3.1 Mechanical Forces and Vascular Tissue

All tissues in the body are subjected to physical forces, which can originate either from environmental factors, or from tension created by the cells themselves [61-63]. Almost all vessels carrying fluids within the body are distensible, and interactions between internal blood flow and vessel wall deformation contribute both to a vessels biological function and dysfunction. The vascular wall is an integrated functional component of the circulatory system that is constantly exposed to mechanical forces of haemodynamic origin. *In vivo*, the artery experiences shear stress and tensile strain as a result of the pulsatile nature of the blood flow [64,65].

Pulse pressure, which is defined as the difference between peak systolic and diastolic blood pressure, acts as a compressive force perpendicular to the endothelial lining. The adventitia is normally at near atmospheric pressure. Arteries experience circumferential wall tension and stretch as a result of blood pressure. Humans experience a mean pulsatile pressure of approximately 100 mmHg and a pulse pressure variation of ~20 mmHg [38].

Shear stresses are small frictional forces acting in the full thickness of the artery wall that cause modest deformations. Under normal physiological conditions, EC are primarily subjected to this haemodynamic shear stress. However, under conditions of endothelial dysfunction or denudation, shear stress can also exert its effect on the underlying SMC. In arterial circulation, based on altering vessel wall diameters, the mean wall shear stress is 1.5-1.8 Pascals [66]. Changes in shear stress can be associated with changes in pulse pressure. EC, which contain shear stress

response elements, respond to physiological or pathological alterations in shear stress by releasing vasoactive agents and pro- or anti-atherogenic substances [61,64].

Another well characterised haemodynamic effect associated with the vasculature is cyclic circumferential strain. Cyclic strain in arterial vessels is due to the repetitive pulsatile force on the vessel wall due to arterial blood pressure. Cyclic strain can be multi-dimensional as the pulsatile force acts perpendicular to the blood vessel, resulting in "stretching" of the vascular cells in multiple planes. All cells of the vessel wall experience cyclic strain under normal physiological conditions. SMC, which constitute the major component of the vessel wall, together with elastin and collagenous components, experience most of the pressure-induced cyclic strain. Normal blood pressure is considered to be 120/80 mmHg, whereas blood pressures of above 140/90 mmHg and below 90/60 mmHg are considered high and low respectively [67]. Factors ranging from physical exertion to psychological stress can result in a transient rise in blood pressure, and a consequent transient increase in cyclic stress. Cyclic strain in arteries varies between 5 % to 10 % during the normal cardiac cycle but can exceed 20 % with physiological changes in arterial pressure [68].

2.3.2 Endothelial Cells (EC)

A single cell layer thick membrane of EC lines the entire circulatory system. This plays an important role in physiological haemodynamics and permeability of the blood vessels [64,69]. The endothelium is, in essence, a multifunctional organ. A healthy endothelial lining is fundamental to normal vascular function. Malfunctions in the function and structure of the EC can be critical factors in the pathogenesis of arterial diseases, namely thrombosis and arteriosclerosis [70]. The EC are extremely sensitive and act as signal transducers of shear stress to adapt smooth muscle cell regulation of vasomotor tone in the arterial wall. The vasculature responses to altered blood flow are arbitrated by the endothelium.

2.3.3 Smooth Muscle Cells (SMC)

SMC are generally situated in the medial layer of the artery. Several studies

have demonstrated a marked heterogeneity of SMC phenotypes (genetic makeup) in the vessel wall of both human and animal models [71,72]. These phenotypes are classified as synthetic and contractile. Whilst both the intimal and medial layers contain a mixture of both phenotypes, the synthetic phenotype is most commonly associated with the intimal layer. The contractile SMC, on the other hand, are most commonly associated with the tunica media, and express differentiated cell markers associated with contractile function, and are involved in the synthesis and maintenance of extracellular components of the vessel wall. SMC are considered the most important cell type involved in the pathogenesis of lesions in atherosclerosis [73].

2.3.4 *In Vitro* Cell Culture – Bioreactor Systems

In order to investigate the effect of the mechanical environment on cell response numerous *in vitro* systems (bioreactors) have been developed. Barron *et al* [74] defined a bioreactor as a system that simulates physiological environments for the creation, physical conditioning, and testing of cells, tissues, precursors, support structures and organs *in vitro*. There are numerous commercial systems and experimental apparatus' developed by research groups that attempt to mimic shear stress or/and cyclic strain conditions that are experienced by vascular cells *in vivo*. In an ideal bioreactor, biomechanical and biochemical controls are fundamental in the creation of a simulated physiological environment for cell growth [74].

Physiological Flow Bioreactors

Moore *et al,* [75] developed an experimental apparatus to expose EC to shear stress and circumferential cyclic strain. The apparatus consists of four cylindrical elastic tubes (Figure 2.7). Cells are cultured to the inner walls of the compliant tubes then a pulsatile pressure gradient controlled by a pump drive imposes a pulsatile shear stress and a cyclic expansion to the tubes. The following conditions may be investigated; (a) Static conditions – no shear or stretch, (b) shear stress only, (c) hoop stretch only and (d) shear and hoop stretch. For the tubes where no hoop stretch is desired, a rigid plastic casting is mounted around the elastic tubes to prevent expansion in the radial direction. A variety of physiological pressure, flow, stretch and temperature parameters may be produced using this system.

The CELLMAX Artificial Capillary System™ [76] is a commercially available apparatus that is used for the perfused transcapillary *in vitro* co-culture of vascular EC and SMC. This system simulates the highly efficient, three-dimensional function of the human capillary system and permits long term culture at precisely controlled flow rates. It is used to measure the effect on vascular cells of haemodynamic shear stress.

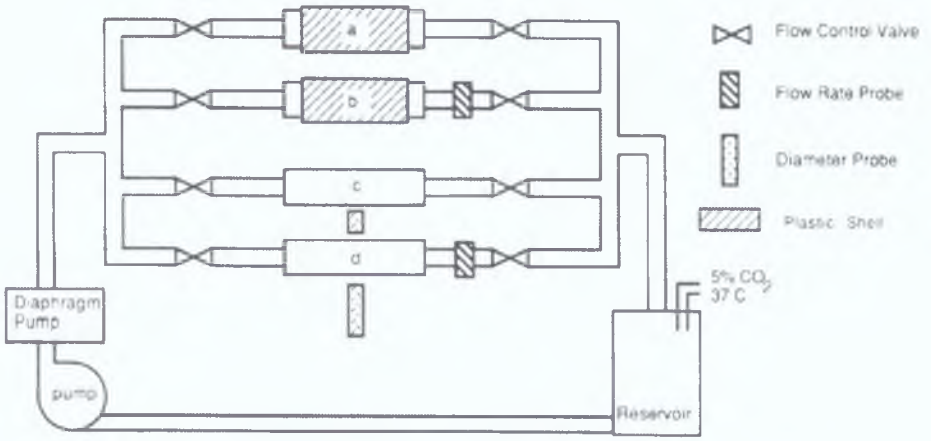

Figure 2.7 Schematic of the flow system used to subject EC to shear stress and hoop stretch [75].

The system (Figure 2.8) consists of a capillary bundle that contains 50 rigid semi-permeable capillaries and a positive-pressure displacement pump that circulates media at a chosen flow rate from a reservoir bottle through silicone rubber tubing. The media flows through an oxygen carbon dioxide exchange unit. Media enters the capillary bundle at the inlet endport and flows through the lumen of each individual capillary in the bundle before exiting at the outlet endport. The media is pumped back into the reservoir.

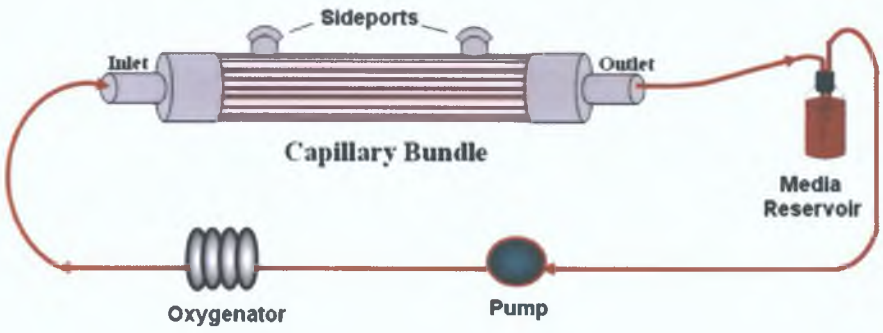

Figure 2.8 Schematic of perfused co-culture system representing the normal path flow of the perfused media [76].

SMC are seeded onto the extracapillary space (ECS) of the capillary bundle using the sideports and allowed to adhere and grow (Figure 2.9). EC are then seeded into the luminal space via the inlet ports. By regulating the fluid velocity the shear stress to which the EC are exposed can be altered. The two cultures, smooth muscle and EC do not make direct cell-to-cell contact but are exposed to the same culture medium. This allows diffusion of nutrients or secreted products released in both directions through the pores in the capillary wall (Figure 2.9).

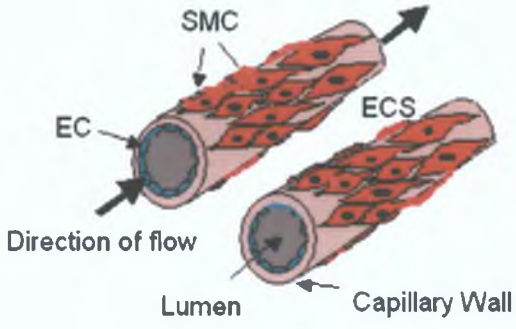

Figure 2.9 Schematic illustration of co-cultured SMC and EC on rigid semi-permeable capillaries [76].

Shear Stimulus Bioreactors

The dynamic flow system (Figure 2.10) developed by Blackman and co-workers is a cone and plate device that consists of culture well environment and a driver unit [77]. The complete system, which includes a transparent cone and the plate surface, is mounted onto a microscope stage and allows direct visualisation of the cells, adhered to the plate surface. The cells are examined using phase contrast microscopy under dynamic flow conditions. A timing belt connected to a programmable stepper motor controls the rotation of the cone. The system can replicate various waveforms ranging from simple laminar flows to more complex arterial waveforms through precise control of the motor. Constant exchange of fresh media is permitted through two circulation ports on the plate. The dynamic flow system is used to measure the response of EC to pulsatile shear stress waveforms encountered by the endothelium in the arterial circulation.

The parallel plate system is used to quantity the effects of fluid shear stress on cells (Figure 2.11). It consists of a polycarbonate chamber with entrance and exit flow slots, a vacuum port, a silicone membrane gasket and a glass slide [78]. The silicone gasket creates a rectangular flow channel and also prevents leeks. A vacuum

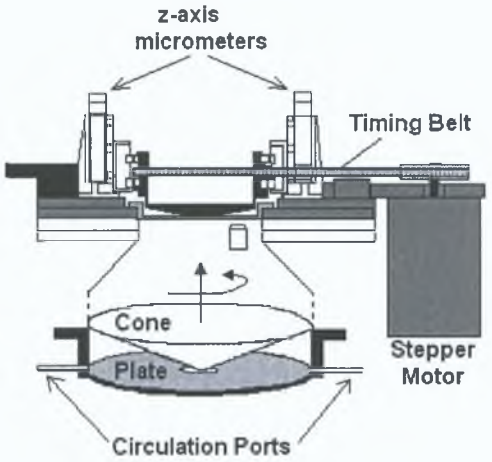

Figure 2.10 Dynamic flow system [77].

pump is attached to ensure a tight seal between the flow deck and the bottom of the culture dish. The flow deck may be adapted with a variety of inlet and outlet designs and silicon rubber gaskets with different sizes. This system is used to quantity the effects of fluid shear stress on cells.

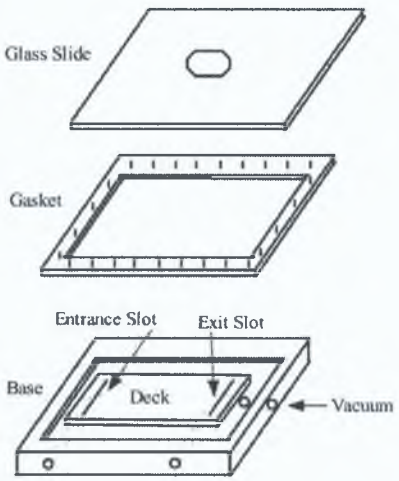

Figure 2.11 Schematic of parallel plate flow chamber configuration [79].

Strain Stimulus Bioreactors

The Flexercell® strain unit (North Carolina, US) is a commercially available system that provides regulated strain to cells in culture (Figure 2.12) [80]. It consists of a flexible bottom tissue culture plate with mesh like anchors at the culture well periphery for cell and matrix attachment. A control module regulates the pressure and rate of evacuation of the rubber bottom culture plates to control the mechanical load to the cells *in vitro*. Positive or negative pressures may be simulated. The positive pressure mode stretches the well bottom upwards producing a relatively

uniform, biaxial strain over the entire well surface. The well bottom stretches downward with a gradient in the negative pressure mode creating maximum strain at the well periphery and minimum at the well centre. The pressure and the rate of evacuation regulate a single deformation event of the rubber bottom plate. The deformations can be repeated at controlled frequencies. This system can apply reproducible cyclic or static tensile or compressive strains to cells cultured *in vitro*. Specified frequency, amplitude and duration of strain can be reproduced *in vitro* by regulating the degree and timing of the pressure applied to the flexible bottomed plates.

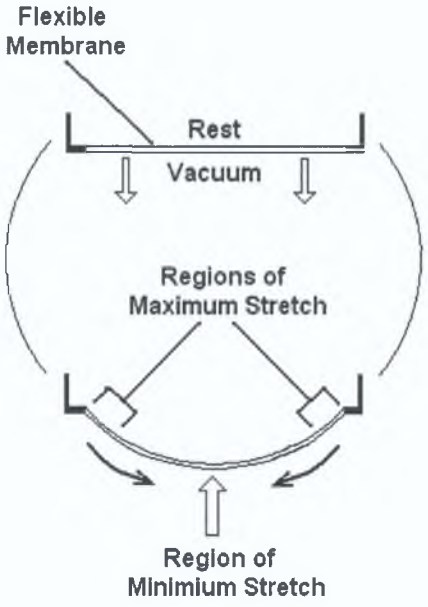

Figure 2.12 The Flexercell® plate base has a flat culture substrate at rest [80].

2.3.5 Response of Vascular Cells to Mechanical Stimuli

The primary function of EC is to act as a selectively permeable barrier regulating the exchange of substances between blood and tissue. Therefore EC have the ability to communicate (secrete substances) in two directions, outward to platelets and leukocytes and inward to SMC [81]. Being in direct contact with blood flow, the endothelium is exposed to a variety of biomechanical stimuli, namely mechanical forces generated by the pulsatile nature of blood flow (Figure 2.13). These include flow-induced shear forces, radial forces as a result of blood pressure, circumferential and axial forces due to cell-to cell contact and distension due to pressure. Some of these forces act directly upon the EC and induce changes, while

others are transduced across the endothelial layer to other components of the vessel wall including SMC [81]. Depending on the magnitude and direction of the blood flow induced forces, the EC express genes, which in turn produce different molecules (adhesion molecules, vascoactive molecules, cytokines, growth factors and prostanoids) as shown in Figure 2.13 [82]. Alterations to the blood flow and therefore the forces experienced by the endothelium may be affected by lifestyle, diseases such as atherosclerosis and aneurysms as well as the implantation of medical devices.

The shape and orientation of EC are determined primarily by blood flow [83]. The nuclei of EC are ellipsoid in shape and their major axis is aligned in the direction of the blood flow [84]. Shear stress also affects the function of the EC. These functions include cell proliferation [85], expression of adhesion molecules [81], growth factors [86] and modulators of thrombogenity [67]. The multitude of responses indicates that shear activates numerous signal transduction pathways. For example, the vasomotor agents released by the endothelial under shear stress initiate signalling between the endothelium and medial SMC [87].

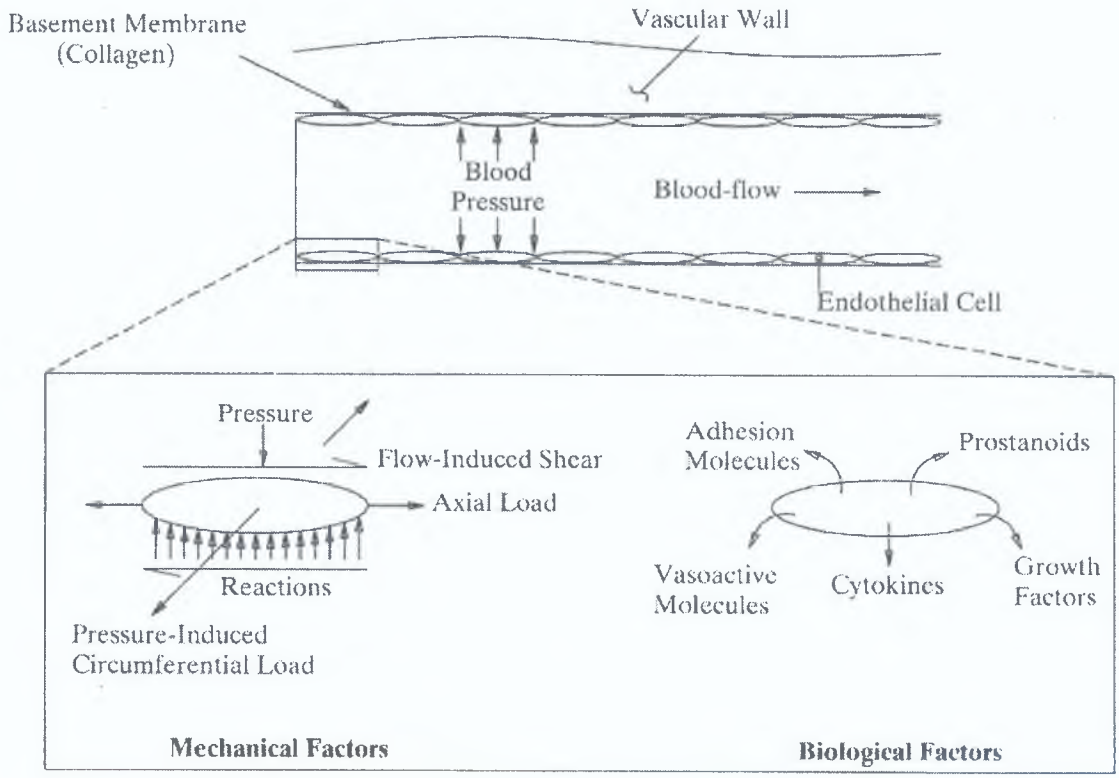

Figure 2.13 Schematic showing various mechanical loads acting on a single cell [82].

Shear stress also affects the repair process of EC [68]. Repair of a circumferential wound on an artery occurs more rapidly than in a longitudinal wound. This is because in a longitudinal wound the cells have to realign perpendicular to flow. A reduction in the shear stress slows repair due to the fact that the contact between neighbouring cells weakens. Without cell-to-cell adhesion, important signals concerning the direction of repair are no longer received [68].

Interactions between EC and SMC cells are essential for a number of physiological processes and are important for the maintenance of normal tissue physiology. In the arterial environment there are structural and metabolic interactions between EC and SMC. Communication between cells may involve humoral mechanisms (cell secretions) or direct cell-to-cell contact [16]. Humoral communication between EC and SMC includes the regulation of smooth muscle proliferation and vasoactivity (constriction and dilation of artery). Endothelial derived growth factors and growth inhibitors control smooth muscle proliferation whereas smooth muscle vasoactivity is regulated by endothelial-derived relaxing factors [16]. Cell-to-cell contact is based on the presence of myoendothelial junctions (areas where EC and SMC are in contact) in arteries. These junctions allow communication between the EC and SMC [88].

There are numerous factors, mechanical forces, vasoactive substances and interactions between cells that can affect vascular cells. Vascular cell fate defines the change in a cell in response to various stimuli. Cell fate is divided into four main categories; proliferation, differentiation, migration and apoptosis. Cellular proliferation is an increase in cell numbers as a result of growth and division of cells. Differentiation is the change in phenotype of cells. Migration is the movement of cells across the arterial wall. Apoptosis is the process of programmed cell death.

Cell fate may be determined independently by exposing vascular cells to either cyclic strain or shear stress separately or simultaneously in mono or co-culture (Section 2.3.4). Morrow *et al*, [89] have shown that cyclic strain concurrently inhibited SMC proliferation while significantly promoting SMC apoptosis. Cappadona *et al*, [90] concluded that pulse pressure dictates SMC proliferation, which in turn is dependent on the phenotype (differentiation state) of SMC. In a

study by Von Offenberg Sweeney *et al* [91], it was shown that the migration of EC was reduced due to cyclic strain condition.

2.4 Biomaterials

There have been rapid advances in the development of vascular tissue substitute biomaterials over the past decade, which include the use of hydrogels for engineering three-dimensional tissue constructs [92]. Despite this, major challenges need to be addressed in order for these biomaterials to progress to clinical applications. In order to create functional tissue through engineering, a biomaterial that permits cell signalling is required [5]. For cells to function properly, proper signals are required, which may include chemical signals (growth factors) or mechanical signals (shear stress or hydrostatic pressure) [5]. In addition, the biomaterial should provide a binding surface for the cells. There are currently a broad range of both natural and synthetic biomaterials used to produce membranes for a range of applications (cardiovascular bioreactors, vascular grafts). There are advantages and disadvantages to using both natural and synthetic biomaterials. A variety of different biomaterial types, with different functions, are required for different tissue engineering applications. A choice selection of natural and synthetic biomaterials will be reviewed in the following sections, as motivation for the selection of PVA-chitosan hydrogels for investigation in this project.

2.4.1 Hydrogels

Hydrogels are water-swollen, cross-linked polymer structures that are produced by hydrogen bonds and interactions between polymer chains or by reactions between one or more monomers. They may be based on natural or synthetic polymers. Hydrogels are hydrophilic polymers that may absorb from 5 % up to thousands of times their dry weight in water. Some hydrogels are chemically stable (for example; PVA) while others may degrade and eventually disintegrate and dissolve [93,94]. These gels are called "reversible" gels as they can be returned to an aqueous solution following solidification.

The hydrogel three-dimensional network of polymer chains allows easy

exchange of nutrients and waste products with the surrounding environment. Pores are a feature of the hydrogel that are formed during the fabrication process. The mechanical properties and diffusion characteristics are affected by the average pore size, distribution and interconnection. However, these can be difficult to quantify. Therefore diffusion characteristics are often associated with the composition and crosslink density of the hydrogel [95].

The compatibility of hydrogels with cells is of great importance for biomedical applications. *In vitro* experiments present a convenient approach to study aspects of the compatibility of biomaterials with cells under controllable conditions [96]. Cell adhesion on hydrogels is difficult due to their hydrophilic properties [97]. Cells do not adhere directly to the biomaterial but rather bind through a number of adhesion proteins that are absorbed onto the biomaterial [98]. Hydrogels that promote cell attachment have been shown to strongly influence cell proliferation [99]. In order for such a protein to attach to the hydrogel, a crosslinking component is often required.

2.4.2 Naturally occurring Biomaterials

The main benefit of using natural biomaterials is that they are identical or similar to substances found in the body. Consequently, the probability of toxicity to biological cells or inflammation is significantly reduced. Natural biomaterials contain particular adhesive molecules, such as arginine-glycine-aspartic acid (RGD), on their surfaces that can facilitate cell adhesion and maintain cell differentiation [100]. It is also possible to control the degradation rate through chemical means as natural biomaterials produce enzymes that are innately biodegradable [5]. While natural biomaterials possess many beneficial characteristics, they are often immunogenic (capable of producing an immune response) [5]. The extraction process of natural biomaterials is often difficult and may alter their natural structure. The variability of the biomaterials derived from animal sources is also another major issue [100]. An essential requirement for biomaterials is consistent quality. Therefore batch to batch variation must be limited. To address this concern, genetically modified forms of human collagen and other natural materials have been engineered to avoid the use of animal products by expressing them in cell lines [100].

Extracellular matrix proteins (single proteins or combinations), polysaccharides and fibrin have been used to create natural substrate biomaterials.

Collagen is the most abundant protein in the body representing approximately 25 % of all protein. Collagen is the primary component of connective tissue and is associated with development, wound healing and regeneration [101]. Collagen acts as a scaffold for our bodies, protecting and supporting the softer tissues and connecting them with the skeleton. It also controls cell shape and differentiation, migration, and the synthesis of a number of proteins [101]. In order to create collagen derived tissue substrate material, collagen is typically extracted from tendon, skin and fascia. The advantages of using collagen as a tissue substrate include biocompatibility, ease of fabrication and low cost. Various different chemical (formaldehyde, glutaraldhyde) or physical (UV irradiation, freeze-drying) crosslinkers may be used to create membranes and enhance their mechanical properties [102-104]. Weinberg and Bell [105,106] investigated the collagen substrates for use in vascular constructs and noted that EC functioned as a permeability barrier. The mechanical integrity of the construct was controlled by multiple layers of collagen integrated with a Dacron mesh. Vascular cells have been shown to orientate circumferentially as they would *in vivo* when seeded onto collagen gels [107]. Wissink *et al* [108], incorporated a releasable growth factor (basic fibroblast growth factor) into the collagen matrix to improve EC growth on the vascular constructs.

Chitosan is derived from chitin, a polysaccharide that is present in the hard exoskeletons of shellfish like shrimp and crab [109]. Chitosan is composed of glucosamine linked with *N*-acetyl glucosamine. The glucosamine/*N*-acetyl glucosamine ratio refers as the degree of deacetylation. The molecular weight of chitosan ranges from 300-1000 kD and the degree of deacetylation from 30% to 95% [110]. In its crystalline form, chitosan is insoluble in an aqueous solution above pH 7. However, in dilute acids (pH<6.0), for example acetic acidic solubility is achieved [111]. The pH-dependent solubility provides a convenient mechanism for the processing of chitosan under mild conditions [112]. Crosslinking may be achieved by UV irradiation, thermal variations or glutaraldehyde. Chitosan is degraded *in vivo* by enzymatic hydrolysis [113]. Highly deacetylated forms of chitosan (for example

>85%) reveal the lowest degradation rates and may last several months *in vivo*, while chitosan with a lower percentage deacetylation degrade more rapidly [113]. The degradation rate of the material also inherently affects the mechanical and solubility properties of chitosan. Chitosan has the ability to be moulded into various forms [114]. Chitosan possesses excellent ability to be processed into porous structures [112]. Porous membranes are generated by freezing and lyophilizing chitosan solutions. Removal of the ice crystals by lyophilisation generates a porous material. The pore size and orientation can be controlled by variation of the freezing rate, the ice crystal size and the geometry of thermal gradients during the freezing process [112]. The mechanical properties of chitosan membranes are dependant on the pore size and orientation. Chitosan membranes hydrated in NaOH (sodium hydroxide) were soft, spongy and very flexible while minor shrinkage and distortion was also evident [111]. However, the overall mechanical strength was very low [111]. Tensile testing of hydrated chitosan membranes showed a significant reduction in the elastic moduli of porous chitosan membranes (0.1-0.5 MPa) compared to non-pourous membranes (5-7 MPa) [112]. Porous chiotsan membranes displayed a stress strain curve characteristic of a composite material with two distinctive regions, a low-modulus region at low strains and a change to a two-three fold higher modulus at higher strains. Chemically derivatisation [112] and blending of chitosan with both synthetic and natural biomaterials [96,97,115-118] promotes new biological activities and can modify the mechanical properties of chitosan. Howling *et al* [119], achieved fibroblast cell adhesion and growth on chitosan membranes. Chitosan has also been blended with gelatine [120], nylon composites [121] and polyvinyl alcohol (PVA) [96] for biomedical applications. Chitosan blended with PVA [96] has been shown to support fibroblast cell growth. Chuang *et al* [96] reported that the PVA-chitosan blended membrane was more favourable for fibroblast cell culture than pure PVA membranes. Cells cultured displayed good spreading, cytoplasm webbing and flattening. Koyano *et al* [97] showed fibroblast cell attachment and growth on a PVA hydrogel with 40 wt % chitosan exceeded collagen in both quality of cell attachment and cell growth. The death of bacteria in cells has been accelerated due to the presence of chitosan [122]. Chitosan is used in drug delivery combining its antibacterial property with antibiotics [122]. Chitosan has also been used to modify the surface properties of prosthetic materials to enhance the attachment of osteoblasts [123,124]. The combination of good compatibility, intrinsic antibacterial activity,

ability to bind to growth factors and to be processed in a different shapes, makes chitosan a promising candidate for tissue engineering applications.

Elastin is a structural protein that provides distensibility to our tissues and organs. It is predominantly found in tissues such as blood vessels, ligaments and the lungs [125]. Its structure enables tissue to stretch and recoil back to its original position. Although elastin has desirable mechanical properties, purification problems make it a difficult material to use as a tissue substrate material [5]. However, Heilshorna *et al* [126] applied genetic engineering techniques to produce a extracellular elastin and fibronectin matrix to support adhesion of vascular EC. They reported that EC attachment strength to the matrix was sufficient at physiological shear stress to retain more than 60 % of cells on the extracellular matrix.

2.4.3 Synthetic Biomaterials

Synthetic constituents can provide an alternative to natural materials and offer some advantages. They can be produced with excellent reproducibility and reliability through consistent protocols and a reliable materials source [100]. The mechanical properties of these constituents may be engineered for specific applications [127]. To promote tissue cell growth on a biomaterial for use as a scaffold, the material must be highly porous [128]. However, an optimum pore size is required, as small pores sizes may affect nutrition and waste exchange by cells whilst larger pores affect the stability of the scaffold and its ability to provide physical support for the seeded cells [92]. Synthetic constituents can also be customised to incorporate bioactive signals (examples include: fibronectin [127], chitosan [96] and peptides [129,130]) that evoke desirable cellular responses [5].

PVA hydrogels have been proposed in many biomedical applications [131], arterial phantoms [132], heart valves [133,134], corneal implants [135] and cartilage tissue substitutes [136]. In addition to desirable mechanical and swelling properties, PVA also displays a size exclusion phenomenon due to the presence of crystalline regions that render the network insoluble [137]. The solute diffusion coefficient of the PVA has been related to the crystalline volume fraction [137]. PVA hydrogels may be formed by physical crosslinking using freeze-thaw cycles [132,138],

chemical crosslinking with aldehydes [127], and ultraviolet radiation [129]. The crosslinking of the PVA, concentration of aqueous solution, and molecular weight of PVA can be manipulated to control properties such as the overall water content, mechanical strength, and diffusive properties of the hydrogel. PVA hydrogels have hydrophilic properties [127]. Therefore important cell adhesion proteins do not adsorb to PVA hydrogels, and as a result, cells are unable to adhere to the hydrogel. To improve the compatibility and cell adhesion characteristics of PVA, different biological macromolecules such as collagen, hyaluronic acid, chitosan, fibronectin and peptides have been blended with the PVA hydrogels [128]. Cascone *et al* [128] investigated the morphology and porosity characteristics of PVA containing different concentrations of biological materials. They concluded that when a natural macromolecule was added to PVA the internal structure and porosity of the hydrogel changed. Schmedlen *et al* [129], covalently incorporated the peptide RGDS (arginine-glycine-aspartic acid-serine) or RGES (arginine-glycine-glutamic acid-serine) to enhance cell adhesion of human dermal fibroblast cells. Fibronectin has also been covalently attached on the surface of the PVA hydrogel surface to promote fibroblast attachment and proliferation [127,139]. Drug delivery from PVA prepared by freezing and thawing techniques has been examined previously [140]. The inclusion and release of various drugs (human growth hormone), proteins (fibronectin, gelatin) and natural biomaterials (chitosan, dextran) with PVA have also been investigated. Oxprenolol release was affected by the number of freezing/thawing cycles [141] which suggests that drug release could be optimised by controlling freezing and thawing conditions. It has been demonstrated by Hassan *et al* [142] that as the number of freeze-thaw increased the rate and overall amount of dissolution of PVA decreased. It was also shown for PVA hydrogels that as the number of freeze-thaw cycles were increased enhanced stability during swelling at 37°C for a 6 month period was evident demonstrating their appropriateness for long term biomedical applications [142,143].

Polyethylene gylcol (PEG) hydrogels are also highly hydrophilic and intrinsically resistant to cell adhesion. PEG may be crosslinked via ultraviolet exposure [144]. A number of different techniques have been investigated to render PEG hydrogels degradable [5]. West and Hubbell [130] created a degradable PEG hydrogel which has shown promise for cardiovascular applications [145], by forming

a block co-polymer of PEG and a protease-sensitive peptide. Similar to PVA hydrogels, cell adhesion ligands (RGD) have been covalently bonded to PEG in order to support adhesion and growth of smooth muscle and fibroblast cells [146]. Almany *et al* [147], crosslinked fibrinogen with PEG and demonstrated that SMC could penetrate through the hydrogel material and form interconnecting networks of cells. PEG shows promise as a biomaterial and exhibits versatile physical characteristics based on its percentage weight, molecular weight and crosslinking density.

2.4.4 Biomaterial Selection

There are a number of other different naturally occurring and synthetic biomaterials that may potentially be used for cardiovascular tissue engineering applications. Naturally occurring or synthetic biomaterials or a combination of the two may be used to form tissue engineered biomaterials. Each biomaterial has both advantages and disadvantages to its use. Therefore in order to choose which biomaterial (or combination of biomaterials) is best suited for a given application, a comprehensive investigation into the effects on various aspects of cell behaviour of chemical and physical properties were required.

To develop a biomaterial for cardiovascular applications there are a number of desirable characteristics including tissue like elasticity, permeability, mechanical strength and biological compatibility that need to be considered. PVA blended with chitosan has been selected. PVA was chosen as the primary constituent as it has been shown to exhibit a similar mechanical response to porcine aortic tissue [132] and human carotid arteries [148]. PVA has also demonstrated stability during swelling at 37°C for a 6 month period which indicates its suitability for long term biomedical applications [142,143]. PVA has also been used *in vivo* to coat the arterial wall post injury to prevent thrombosis and isolate the arterial wall from blood contact [149]. Chitosan has excellent compatibility with living tissue and has been used to increase the healing times of wounds [150]. Chitosan has also been used to enhance cell adhesion and proliferation. Cascone *at al* [151] investigated the morphology of PVA combined with chitosan and concluded that a PVA chitosan blended hydrogel displayed promise tissue engineering applications and drug release systems. *In vitro*

studies have shown that PVA chitosan blended membranes can support vascular cell growth [96]. In addition, PVA and chitosan have less batch to batch variability compared to naturally occurring biomaterials for example collagen or elastin. This enables greater control over the structural properties of the PVA chitosan blended hydrogel. Chitosan is one of the most abundant biomaterials and is much less expensive compared to alternative adhesive proteins (for example fibronectin), that could also have been used. Furthermore, superior fibroblast cell attachment and growth quality was achieved on PVA chitosan blended membranes compared to collagen [97]. It is hoped that the proposed biomaterial will exhibit the structural characteristics of PVA with the biofunctionality of chitosan [152]. It is hypothesised that PVA combined with chitosan contains the characteristics required to fabricate a biomaterial to mimic the mechanical, structural and physical properties of vascular tissue and provide the biological signals required to support vascular cell growth *in vitro.*

2.5 Objectives and Proposed Approach

Clearly there are numerous factors that need to be considered in the development, synthesis and characterisation of a biomaterial for use in *in vitro* or *in vivo* studies. Current experimental bioartificial systems for studying vascular cell response to mechanical stimuli do not adequately reproduce the mechanical stress and strain environment combined with the oxygen and nutrient transport processes experienced *in vivo.* PVA and chitosan have been identified with the potential to support cell viability and initial experiments have shown promising results. The control over mechanical properties offered by PVA and its ability to be blended with biological macromolecules is very promising for tissue engineering applications.

Although cell adhesion and growth on a biomaterial are of primary importance, biomechanical factors must also be considered in order to study the effect of vascular cell responses in an appropriate mechanical environment. The mechanical properties of most materials can be varied through processing techniques, although the effect on the biological compatibility may vary from one material to another. With a view to assessing potential biomaterial properties, the structure and

mechanical properties of the artery were reviewed. The challenge is to investigate the suitability of PVA-chitosan hydrogels to meet the following criteria:

- Macroscopic constitutive behaviour similar to arterial tissue within the normal physiological range.
- Structural properties similar to arterial blood vessels when fabricated into tubular structures.
- Compatibility and attachment of EC and SMC to the biomaterial, and effect of the biomaterial on cell fate.
- Reproducible properties based on constituent materials with consistent quality and morphology, and a well controlled processing procedure.

The proposed approach is:

- Structural modelling of arterial vessels to simulate the effect of constitutive parameters, vessel geometry and residual stresses on vessel behaviour using finite element analysis.
- Cellular activity experiments for different blends of hydrogel using phase contrast microscopy, immunocytochemistry staining (DAPI, F-actin, α-actin, Von Willebrand Factor) and FACS analysis (cell proliferation and apoptosis assays).
- Mechanical and morphological investigations using uniaxial tensions tests, biaxial inflations tests and SEM analysis.

The layout of the thesis, and the way in which this investigation is organised, is summarised in Figure 2.14.

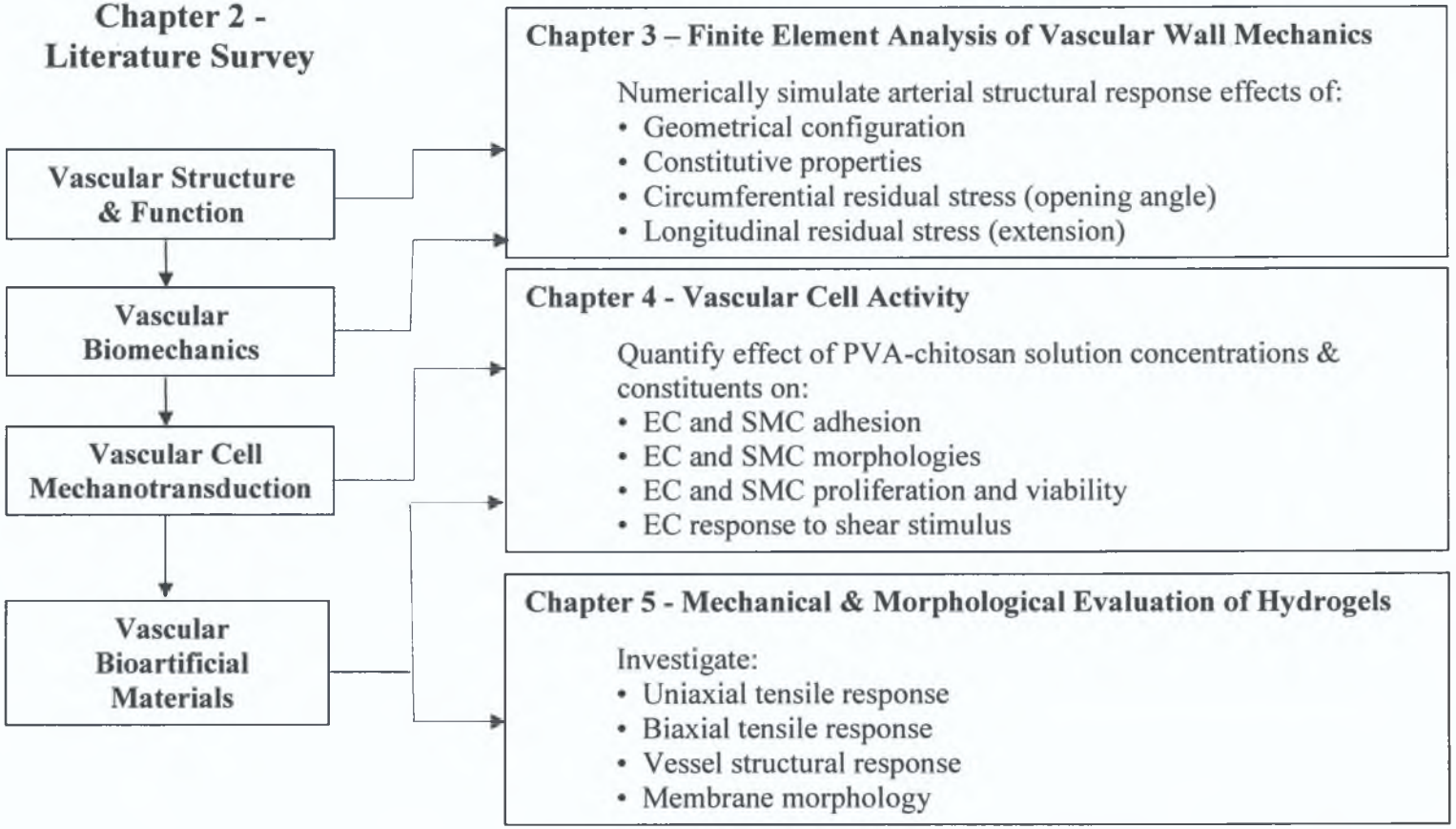

Figure 2.14 Schematic detailing the layout of the thesis.

Chapter 3

Finite Element Analysis Of Vascular Wall Mechanics

The arterial wall responds to alterations in its environment by changing its composition and morphology. The modifications that occur, which may be inducted by, for example, pathological changes in pressure or flow, have a major influence on both microscopic and macroscopic properties of the artery. An increase in shear stress on EC can affect the signal transduction of shear stress and adapt the smooth muscle cell regulation in the vessel, which in turn alters the dilation or constriction characteristics of a blood vessel. Therefore, in order to develop a biomaterial with suitable intrinsic material properties that may be used to fabricate a bioartificial vessel with appropriate structural properties, vascular wall mechanics must be considered. Numerical modelling approaches were utilised to identify the effect of vessel geometry, material properties and residual stresses on the structural response of an arterial segment. Pressure versus diameter response curves were employed to characterise the static structural response of the artery.

3.1 Geometric Description of Stress Free State

The arterial wall is considered as a cylindrical vessel with homogeneous material properties. Under the assumption that there are no external loads in the stress free state (Figure 3.1), the (residual) stress required to re-form the unloaded configuration has been calculated by Chuong and Fung [51], Fung and Liu [52] and Delfino *et al.* [153]. Residual stresses affect the overall response of the artery and the

stress and strain distributions through the arterial wall (for example [45]). It has been hypothesised that the circumferential stress in each component of its wall [45] and the strain distribution through the wall are essentially constant [154]. A number of constitutive models have been proposed to describe the behaviour of the arterial wall which includes residual stresses [15,51,153,155,156]. Holzapfel *et al* [15] developed an anisotropic model in which each layer of the artery was modelled with a separate strain energy function.

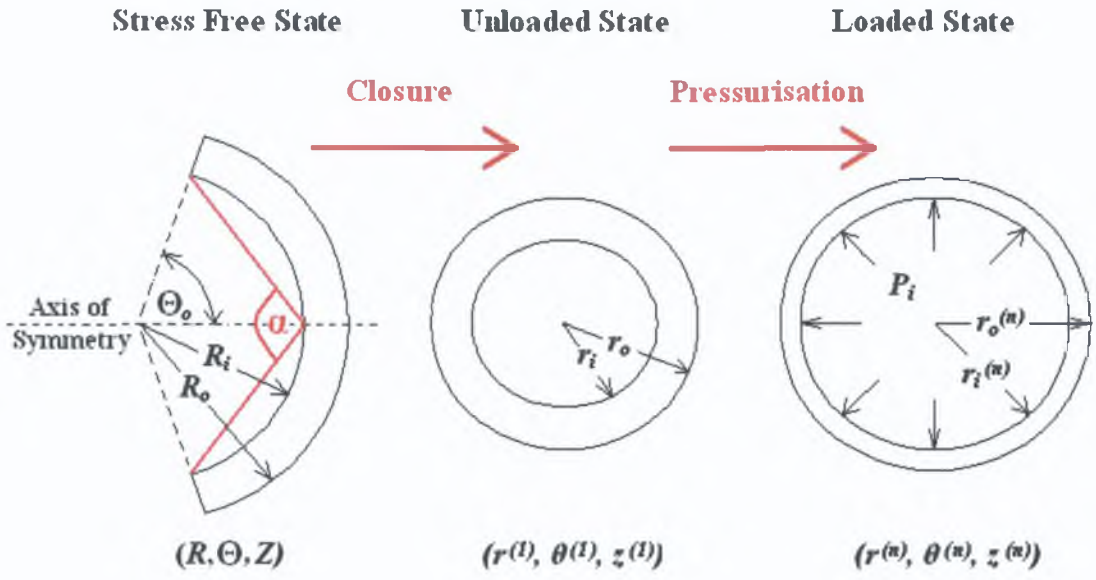

Figure 3.1 **Cross sectional representation of an artery at the stress free state, the unloaded state and the loaded state [51].** When an unloaded arterial ring is cut along its radial axis, the ring springs open (assumed stress free state) and the opening angle (α), R_i and R_o may be measured. The radial cut reduces the residual stresses in the arterial ring because there is a reduction in the strain energy stored.

In the present study an idealised model of the artery, based on analytical development by Chuong and Fung [51], was used to study the effect of overall structural behaviour of the artery. In order to analyse the response in an artery, it was assumed that a circumferential stress free state existed when an arterial ring was cut radially. Each layer of the artery was considered to be a cylindrical thick walled cylindrical vessel whose material was homogenous and anisotropic. Therefore, under this hypothesis, the vessel should become a sector of constant curvature and thickness.

3.2 Finite Element Analysis

3.2.1 Geometry

A three-dimensional finite element model was used to reproduce two independent stress free configurations of the intima/media and adventitia. It was decided to model the intima/media as one entity due to the fact that very limited data is available on the opening angles of the intima alone. The geometric input data was taken from published data for two examples of non-diseased aged human external iliac arteries [59].

Sample 1 was taken from a 75 year old male whereas Sample 2 was from an 81 year old female (Table 3.1). These two samples were selected as they represent two extremes of the range of values for the opening angles, Sample 1 having much smaller opening angles for the intima/media and adventitia layers compared to Sample 2. The unloaded radius of Sample 1 was 5.47 mm which was greater than that of Sample 2 at 4.4 mm. The intima/media opening angle of Sample 1 was 39 ^{o} however the corresponding opening angle for Sample 2 was significantly higher at 122 ^{o}. There was also a considerable difference in the opening angle of the adventitia between Sample 1 and Sample 2, 107 ^{o} and 172 ^{o} respectively. Finally, total thickness of Sample 1 was 1.38 mm compared to the 1.06 mm for Sample 2. This increase in the thickness was mostly attributed to the difference in the measured thickness of the intima, which was 0.39 mm for Sample 1 and 0.15 mm for Sample 2.

Figure 3.1 shows the reference configuration (assumed stress free state) of one arterial layer, which corresponds to a circular cylindrical section with an opening angle α. Due to the symmetry of the geometry and the loading conditions of the problem, only half of the artery cross section was modelled. The modelled segment was associated with the closed (unloaded but stressed) configuration. Using the data from Table 3.1, the stress free internal radius (R_i), external radius (R_o) and the polar angle (Θ_0) of the arterial specimens were calculated. Θ_0 represents half of the angle of the arterial segment at the stress free state (Figure 3.1). Θ_0 is related to the opening angle (α) by the following equation (3.1):

	Sample 1 (75 Year Old Male)	Sample 2 (81 Year Old Female)
Unloaded r_0 (mm)	5.47	4.4
Opening Angles (α)		
Intima/Media	39 °	122 °
Adventitia	107 °	172 °
Thickness (mm)		
Intima	0.39	0.15
Media	0.59	0.59
Adventitia	0.40	0.32
Total Thickness (mm)	**1.38**	**1.06**

Table 3.1 **Geometric input data from different arterial specimens.** Sample 1 and Sample 2 are related to Specimen IV and V from Schulze-Bauer *et al*, Table 2 [59].

$$\tan(\alpha/2) = \frac{\sin\Theta_0}{1-\cos\Theta_0} \tag{3.1}$$

Table 3.2 shows the associated geometrical data of Sample 1 and 2 for the intima, media and adventita, calculated using the data from Table 3.1 (See Appendix A).

3.2.2 Uniaxial Tensile Response

The material properties for the intima, media and adventitia used in the present analysis are based on uniaxial test data reported for non-diseased tissue of a diseased external iliac artery, excised from a 68 year old male within 24 hr after death [33]. The stress versus strain data reported for each layer was acquired from uniaxial extension tests from samples of the tissue cut in the longitudinal and circumferential directions (Figures 3.2-3.4). The stress versus strain responses for the different layers of the artery showed nonlinearity and anisotropy. For all layers the longitudinal response was stiffer. The intima is the stiffest layer, the media the softest layer and the adventitia demonstrates the most prominent stiffening behaviour at larger strains.

	Sample 1	Sample 2
Intima		
R_i (mm)	5.18	10.37
R_o (mm)	5.57	10.52
θ_0	141	58
Media		
R_i (mm)	5.57	10.52
R_o (mm)	6.16	11.11
θ_0	141	58
Adventitia		
R_i (mm)	10.50	91.80
R_o (mm)	12.90	92.12
θ_0	73	8

Table 3.2 **Calculated polar angle, internal and external radii for stress free configuration of the arterial layers of Sample 1 and 2.**

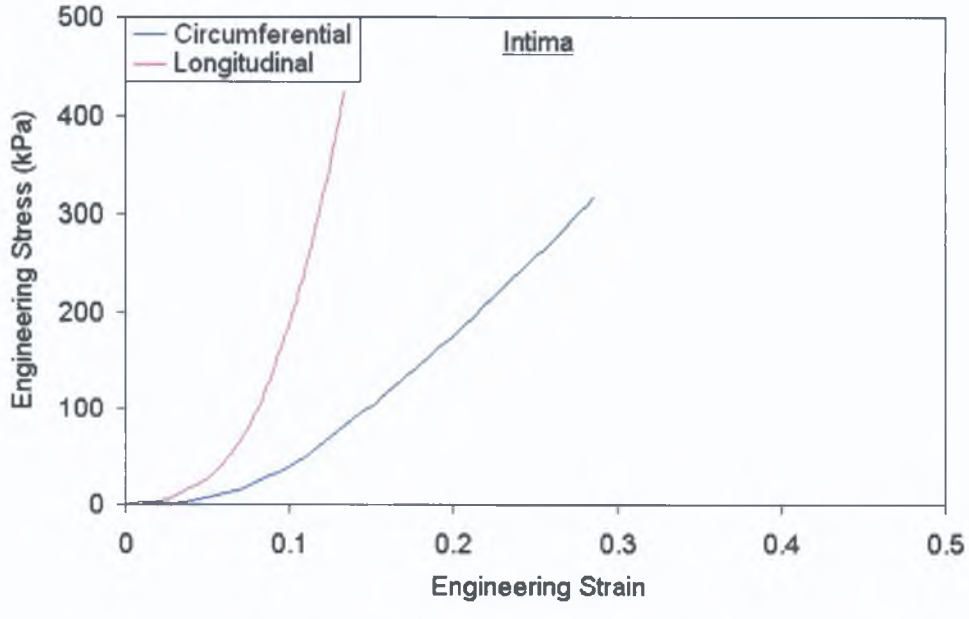

Figure 3.2 **Experimental stress versus strain response of intima [33].** Tissue specimens were cut in both circumferential and longitudinal directions. Samples underwent uniaxial extension tests. Data digitised from Holzapfel *et al* [33] using digitising software (xyextract©) and converted to engineering stress and stretch Appendix B defines engineering stress and strain.

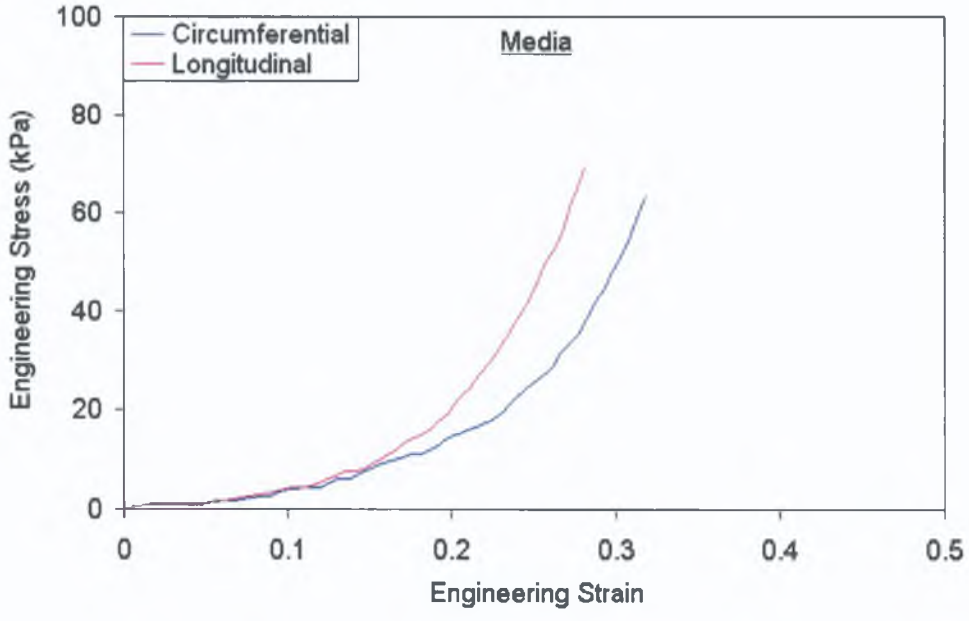

Figure 3.3 **Experimental stress versus strain response of media [33].** Tissue specimens were cut in both circumferential and longitudinal directions. Samples underwent uniaxial extension tests. Data digitised from Holzapfel *et al* [33] using digitising software (xyextract©) and converted to engineering stress and stretch.

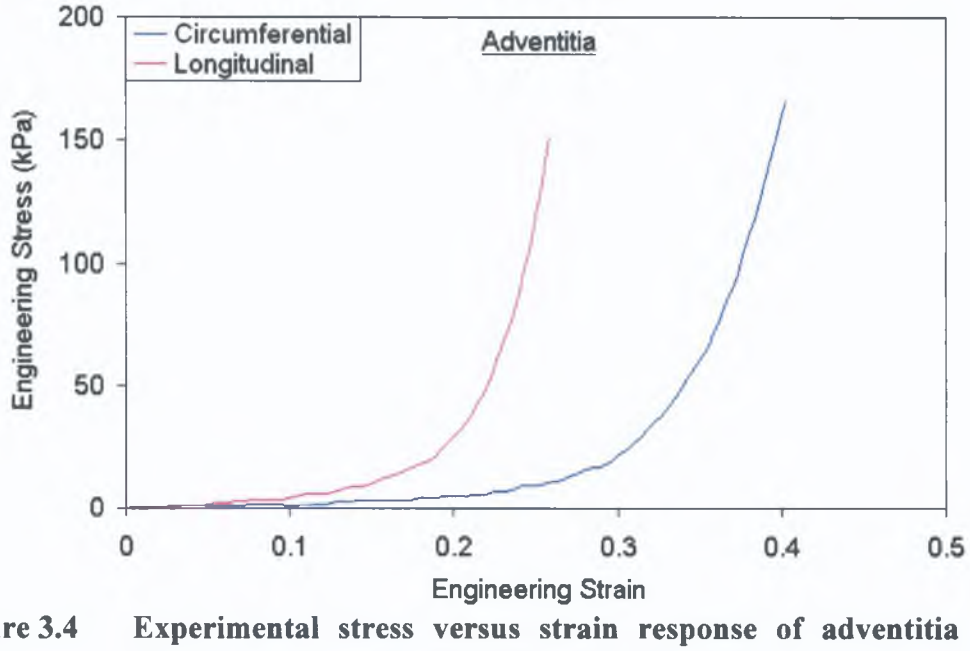

Figure 3.4 **Experimental stress versus strain response of adventitia [33].** Tissue specimens were cut in both circumferential and longitudinal directions. Samples underwent uniaxial extension tests. Data digitised from Holzapfel *et al* [33] using digitising software (xyextract©) and converted to engineering stress and stretch.

3.2.3 Constitutive Model

The mechanical behaviour of the arterial wall is very complex. In modelling the artery, it was important to use a material model which included the key features

of arterial tissue, including its stiffening non-linearity and the capability to represent large deformations.

Tickner and Sacks [157] theory for the study of arterial elasticity based on finite deformations of rubber-like incompressible materials assumed the existence of a strain energy density function, W, for the material that is a function of the principal stretches (λ_1, λ_2, λ_3) or the stretch invariants (I_1, I_2, I_3). A constitutive model based on defining a strain energy density function is termed a hyperelastic model. For a hyperelastic material:

$$S_{ij} = \frac{\partial W}{\partial E_{ij}} = 2\frac{\partial W}{\partial C_{ij}} \tag{3.2}$$

where:

S_{ij} = components of the second Piola-Kirchoff stress tensor

E_{ij} = components of Green-Lagrangian strain tensor

C_{ij} = components of the right Cauchy-Green deformation tensor

In terms of displacements, the general expression for E_{ij} is:

$$E_{ij} = \frac{1}{2}\left[\frac{\partial u_i}{\partial X_j} + \frac{\partial u_j}{\partial X_i} + \frac{\partial u_k}{\partial X_i}\frac{\partial u_k}{\partial X_j}\right] \tag{3.3}$$

Several forms of strain energy functions, in terms of the principal strain or stretches, have been proposed to fit experimental data from tests on arterial tissue. Most constitutive models have been established to describe the passive properties of arterial tissue [43,158-160]. However, Rachev and Hayashi [161] developed a constitutive model for arterial tissue which includes the contribution of the smooth muscle of the artery in its active state. More recently, Holzapfel *et al* [15] developed a three dimensional anisotropic multi-layer strain energy density function to describe arterial tissue.

For this study, the Ogden model for isotropic, incompressible, hyperelastic materials has been selected, in order to permit a study of the effects of the intima,

media and adventitia geometry, compliance and residual stresses on the overall structural behaviour of blood vessels.

The Ogden model has been formulated to model incompressible hyperelastic materials [158]. The Ogden form of strain energy potential is based on the principal stretches which have the form:

$$W = \sum_{k=1}^{N} \frac{\mu_k}{\alpha_k} (\lambda_1^{-\alpha_k} + \lambda_2^{-\alpha_k} + \lambda_3^{-\alpha_k} - 3) \qquad (3.4)$$

where: $\lambda_i^{-\alpha_k} = J^{-\frac{\alpha_k}{3}} \lambda_i^{\alpha_k}$ are the deviatoric principal stretches

μ_k and α_k are material constants established from experimental data fit.

$J = \lambda_1 \lambda_2 \lambda_3$

In order to apply this model, and many similar ones, to the study of arterial tissue the material constants have to be obtained from experimental tests (uniaxial and biaxial) on arterial tissue. An artery *in vivo* primarily experiences uniaxial and biaxial tension and uniaxial compression. Therefore an appropriate accurate model for arterial tissue would be a constitutive equation based on experimental data from uniaxial tension and equibiaxial tension tests, or data from inflation tests of arteries, which combine arterial lumen pressure with axial tension. Although these tests have been reported for different arterial types from different species, layer specific data for human arteries is very limited.

To determine the hyperelastic constants, μ_k and α_k of a 2-parameter Ogden model, a non-linear regression routine that is available in Marc/Mentat (MscSoftware, Santa Ana, CA, USA) was used to obtain the model that best fits the uniaxial data. During the data fitting, the least squares error to be minimised was based on absolute errors. The absolute error is defined as follows [162]:

$$\text{Absolute error} = \sum_i [\text{data measured}(i) - \text{data calculated}(i)]^2 \qquad (3.5)$$

Using the uniaxial experimental data shown in Figures 3.2-3.4 [33] the constitutive models to describe each layer of the artery were determined. The

material constants to define the Ogden strain energy density function of the material models are given in Table 3.3.

Circumferential Material Coefficients (kPa)

Layer	μ_1	μ_2	α_1	α_2	*error*
Intima	31.49	1.46×10^{-4}	10462	2453	1.13×10^{-2}
Media	2.68×10^{-1}	4.75×10^{-1}	17952	16286	4.68×10^{-5}
Adventita	1.02×10^{-5}	3.22×10^{-5}	8924	26234	4.31×10^{-4}

Longitudinal Material Coefficients (kPa)

Layer	μ_1	μ_2	α_1	α_2	*error*
Intima	11.98	3.59×10^{-5}	29713	13821	4.48×10^{-3}
Media	1.44×10^{-6}	1.59	14914	15917	3.52×10^{-4}
Adventita	1.21×10^{-1}	7.46×10^{-8}	31898	31174	7.59×10^{-4}

Table 3.3 **Hyperelastic material constants to describe the human external iliac arterial tissue for the intima, media and adventitia based on experimental data from circumferential and longitudinal uniaxial tension tests [33].** The parameters describe a 2 parameter Ogden model.

3.2.4 Finite Element Model

To construct a finite element model, details of the geometry (Table 3.2), constitutive properties of the artery (Table 3.3), and appropriate loading conditions were required. The geometry of each layer was discretised in the following manner. Fourteen and twelve elements were employed through the wall thicknesses (radial direction) of Sample 1 and Sample 2 respectively. In Sample 1, ten elements were used for the intima/media layer and four elements were used for the adventitia. The intima/media layer of Sample 2 was divided into eight elements and the adventitia into four elements. Each layer of the artery was discretised into 240 elements in the circumferential direction and had a thickness of 2 elements in the longitudinal direction (Figure 3.5). Sample 1 had a mesh with 6720 elements (12291 nodes) while Sample 2 had 5760 elements (10845 nodes). The element type used for the arterial tissue was a three-dimensional eight-node isoparametric with an additional ninth

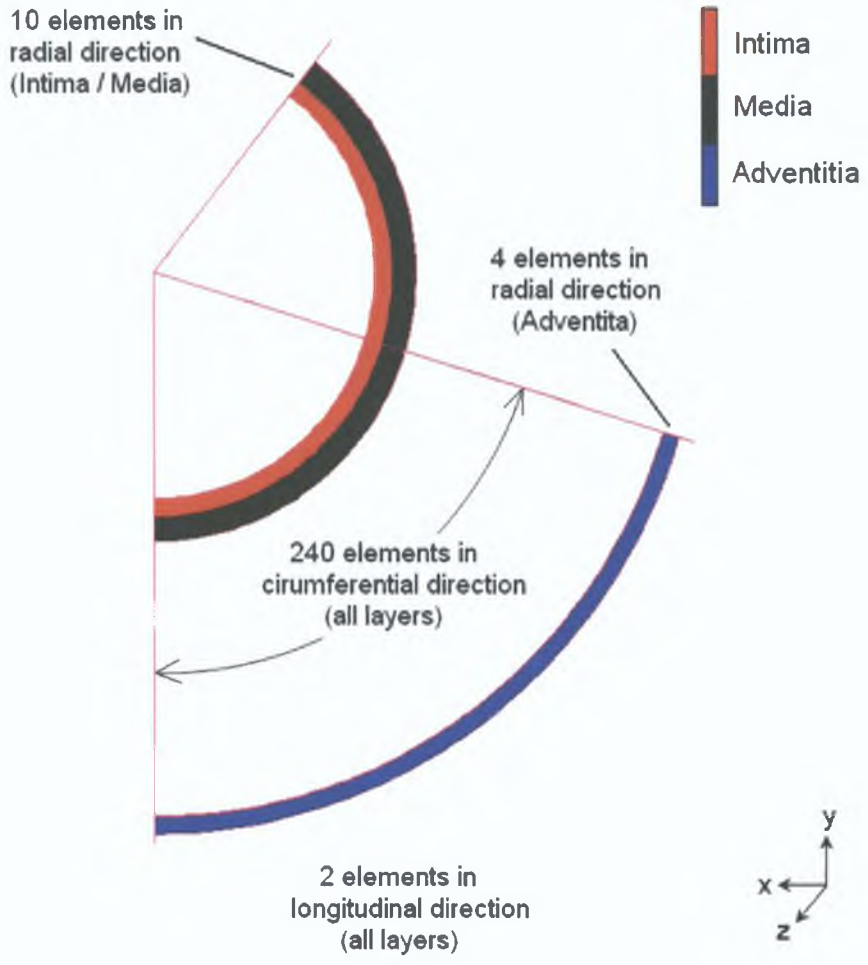

Figure 3.5 Element divisions in circumferential, radial and longitudinal directions for Sample 1.

node for pressure (Element 84 in Marc/Mendat) [162]. To model large deformation hyperelastic materials using this element, the updated Lagrange framework in Marc/Mentat was required to solve for true (Cauchy) stresses and logarithmic strains in the updated configuration. In an updated Lagrangian formulation, element quantities are determined in the current configuration and are updated during the analysis by the current displacements. This prevents premature termination of the analysis due to excessive element distortions. To enforce the incompressibility condition necessary for an Ogden material, a series of parameters (LARGE DISP, FOLLOW FOR, UPDATE, CONSTANT DILATION and ASSUMED STRAIN) must be activated within the updated Lagrangian method. The direct constraint contact algorithm was implemented to define contact conditions between the intima, media and adventitia. Appendix C contains a more detailed description on the contact and boundary conditions and Appendix D gives details on the loading process.

3.3 Results

The pressure versus diameter response at the outer layer of the artery associated with the stress free state was analysed for physiologically loaded configurations at different longitudinal stretches (λ_z). These were examined for and compared to arterial models where the effects of opening angles (α) were not modelled. Finally the circumferential strain at the outer layer of the artery and the circumferential stress distribution through the arterial layers were also examined.

The geometric data of the arterial segment was chosen such that an initial bending (closure) deformation, when applied to the stress free configurations of the layers of the artery, generated the dimensions of the arterial cross section for two samples of human external iliac arteries. The results for all models in the unloaded and loaded states were taken along centre line on the x-axis (Figure 3.6).

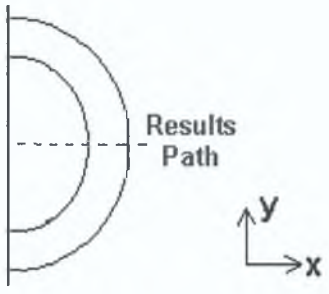

Figure 3.6 The circumferential data was extracted from the nodes along the X axis.

3.3.1 Effect of Constitutive Properties

The pressure versus diameter response for Sample 1 with and without the residual stresses (opening angles and longitudinal stretch) effects were computed for models based on the longitudinal and circumferential uniaxial tensile experimental data (Figures 3.2-3.4). Figure 3.7 and 3.8 illustrate the difference in the pressure versus diameter response of Sample 1 due to the different constitutive model parameters. The uniaxial stress versus strain curves for all layers of the artery were stiffer in the longitudinal direction in comparison to the circumferential direction. This was clearly evident in the pressure versus diameter responses for Sample 1 without opening angles or longitudinal stretches as shown in Figure 3.7. The addition

of opening angles and a longitudinal stretch of 1.2 also showed that the dramatic reduction in the outer diameter for the longitudinal uniaxial input data. The material input properties have a significant affect on the overall pressure versus diameter response of the arterial wall. All future models will be modelled using the longitudinal uniaxial input data.

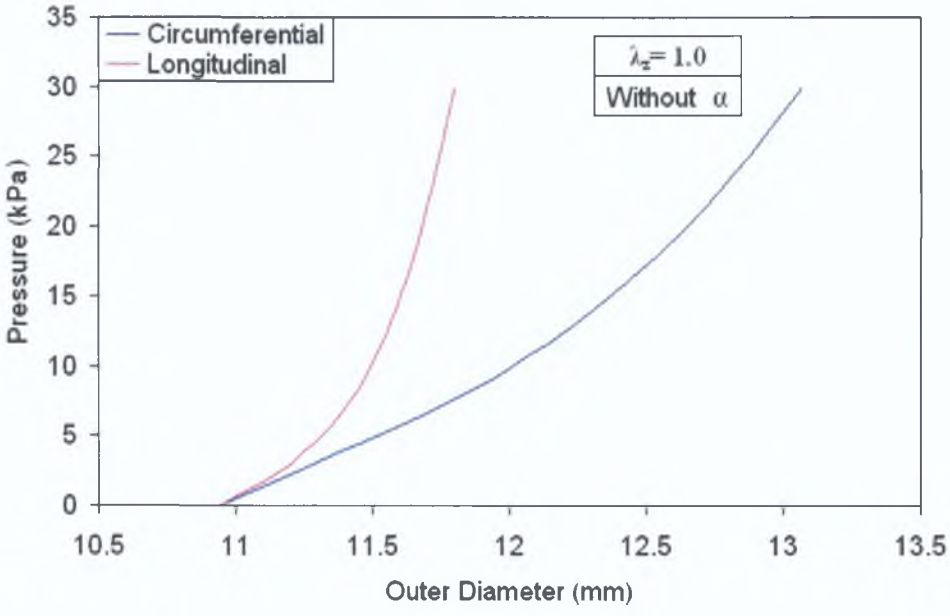

Figure 3.7 **Pressure versus diameter plot of Sample 1 with no opening angles and a longitudinal stretch of λz = 1.0.** Sample 1 was simulated with the experimental data obtained from the longitudinal and circumferential uniaxial tensile tests [33].

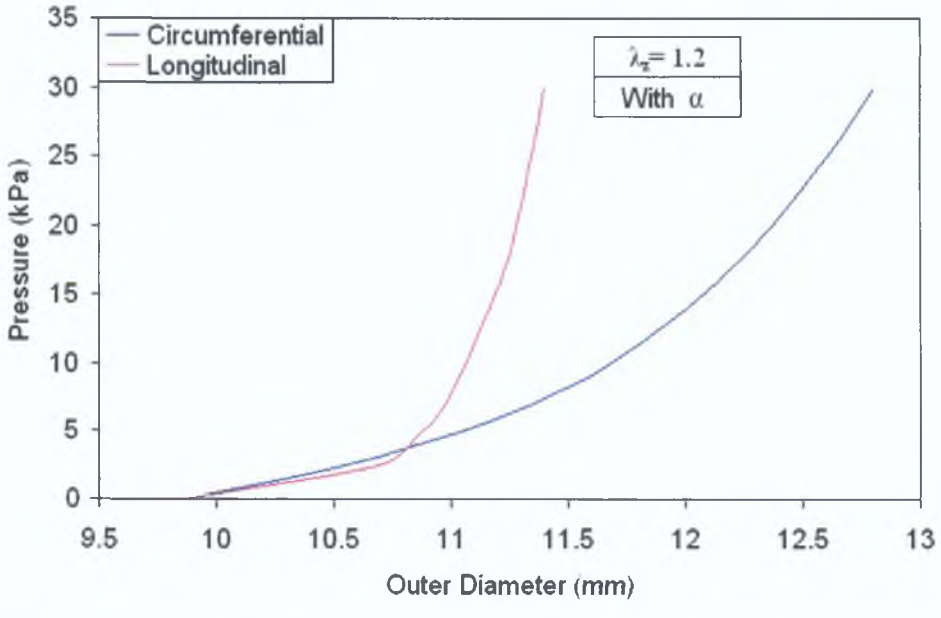

Figure 3.8 **Pressure versus diameter plot of Sample 1 based with opening angles and a longitudinal stretch of λz = 1.2.** Sample 1 was simulated with the experimental data obtained from the longitudinal and circumferential uniaxial tensile tests [33].

3.3.2 Effect of Residual Stresses

Sample 1 was modelled to determine the effect of increasing longitudinal stretch on the pressure versus diameter response of the artery modelled using longitudinal constitutive data. Figure 3.9 illustrates the pressure versus diameter response when opening angles are not included while Figure 3.10 plots the equivalent response when the effects of the opening angles are incorporated into the model. On both cases a change in the pressure versus diameter response was evident. As the longitudinal stretch was increased there was a stiffening effect. Figure 3.11 shows the pressure versus diameter plot of Sample 1 with and without opening angles with a longitudinal stretch of $\lambda_z = 1.1$. In general, the effect of opening angle and longitudinal residual stress appears to be less critical than the effect of constitutive properties, within the ranges reported by Schulze Bauer *et al* [59].

Similar characteristics were also evident for Sample 2 (See Appendix D, Figures D1-D3), and similar conclusions can be drawn.

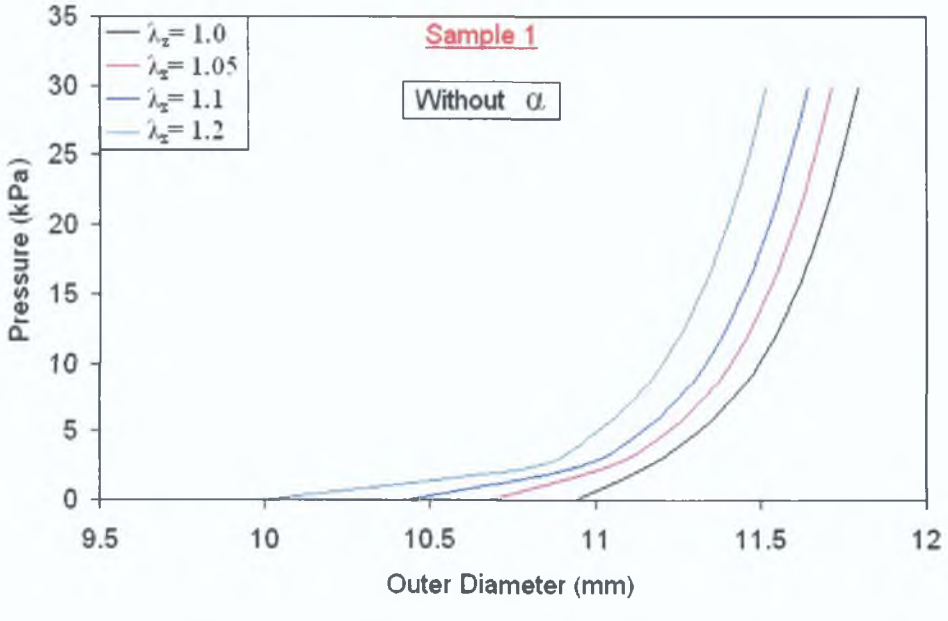

Figure 3.9 **Pressure versus diameter plot of Sample 1 with no opening angles (α) and longitudinal stretches of λz = 1.0, 1.05, 1.1 and 1.2 respectively.** Sample 1 was simulated with the experimental data obtained from the longitudinal uniaxial tensile tests [33].

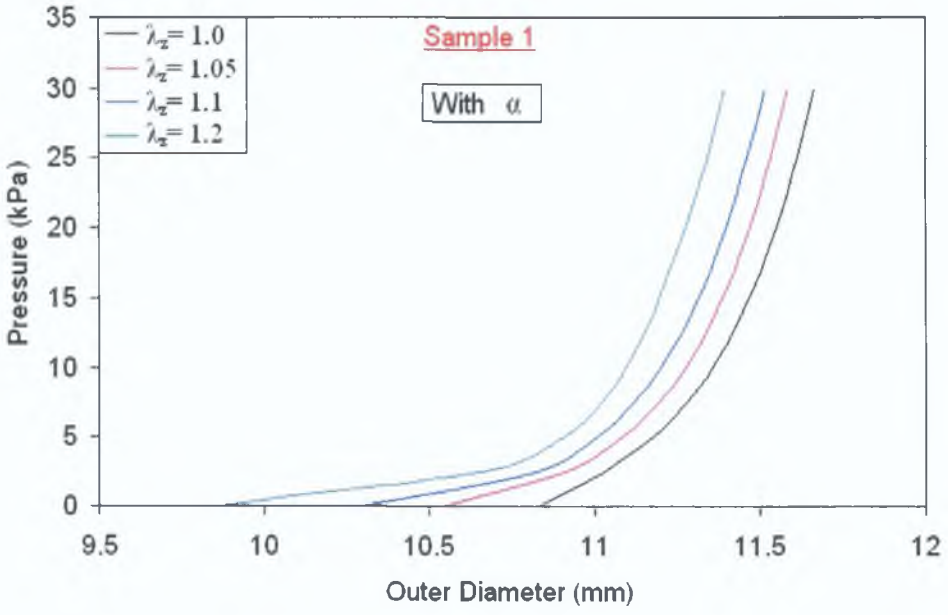

Figure 3.10 Pressure versus diameter plot of Sample 1 with opening angles (α) and longitudinal stretches of λz = 1.0, 1.05, 1.1 and 1.2 respectively. Sample 1 was simulated with the experimental data obtained from the longitudinal uniaxial tensile tests.

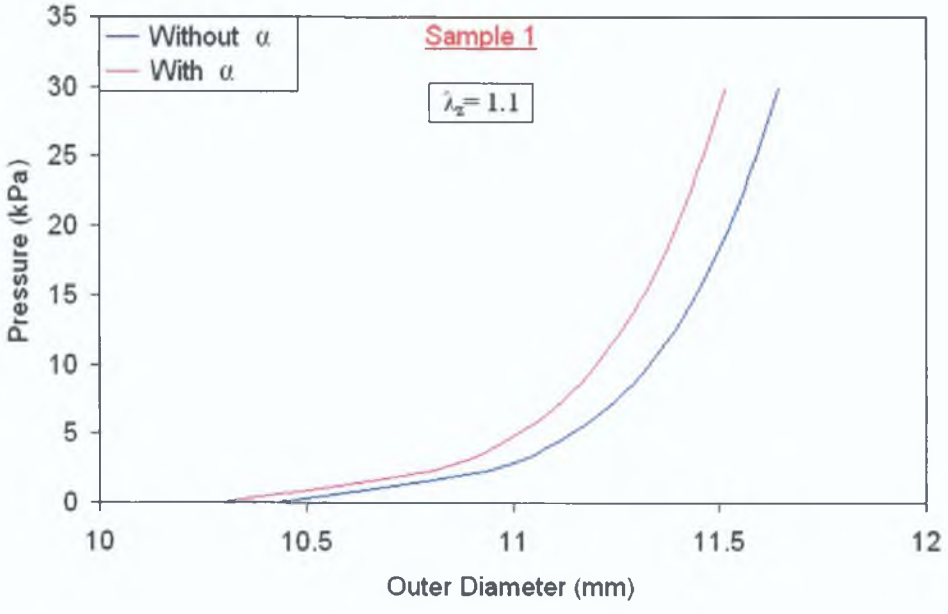

Figure 3.11 Pressure versus diameter plot of Sample 1 with and without opening angles (α) and a longitudinal stretch of λz = 1.1. Sample 1 was simulated with the experimental data obtained from the longitudinal uniaxial tensile tests.

3.3.3 Comparison of Sample 1 and Sample 2

The pressure versus circumferential stretch plot shown in Figure 3.12 illustrates the difference in the Samples 1 and 2. Sample 1 displays significantly

lower circumferential stretch compared to Sample 2. Since plot samples are simulated with the same constitutive properties, the differences can be attributed to the differences in the stress free configurations and the geometries (initial outer diameter and wall thickness). However, as previously shown in Figure 3.11, the opening angle did not have a significant effect on the pressure versus diameter response. Therefore the circumferential stretch increase for Sample 2 can be attributed to a smaller unloaded radius and total wall thickness.

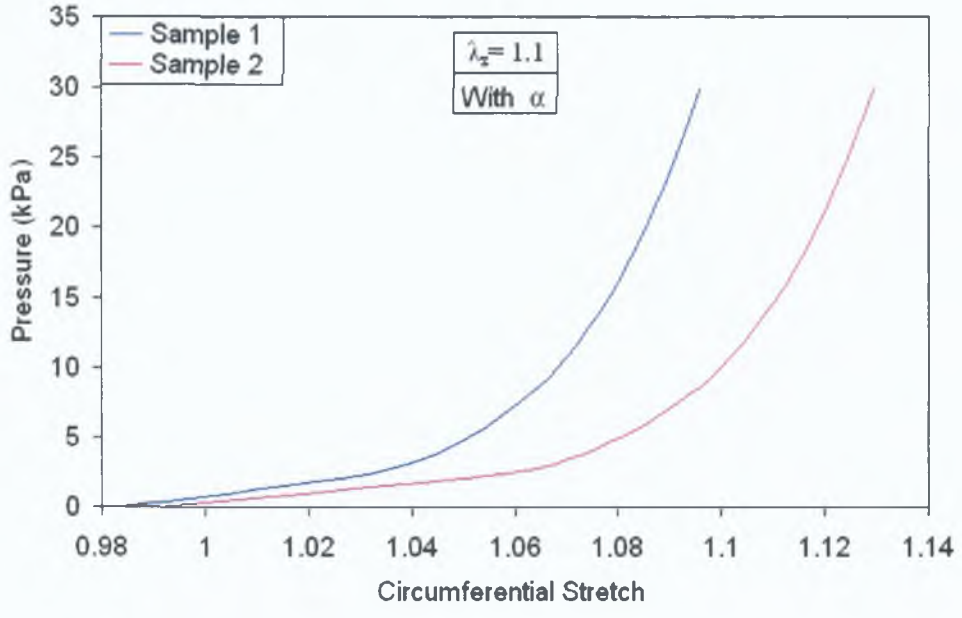

Figure 3.12 Pressure versus circumferential stretch plot of Sample 1 and Sample 2 with opening angle effects and a longitudinal stretch of λz = 1.1. Both samples were simulated with the same experimental data obtained from the longitudinal uniaxial tensile tests.

3.3.4 Comparison of Sample 1 and Equivalent Experimental Data

Schulze Bauer *et al* [59] reported passive biaxial inflation experiments on intact iliac arterial vessels, including Sample 1 and Sample 2 described above. The results they obtained can be compared to the predictions of the finite element models, with the caveat that the constitutive properties used in the model are based on data from different specimens. A significant difference was identified between the predicted and experimental pressure versus circumferential stretch responses of Sample 1 for longitudinal stretches of 1.0 and 1.1 (Figure 3.13). While exact matching of the responses was not expected because the constitutive data was based on different subjects, similar overall characteristic behaviour was not evident. The

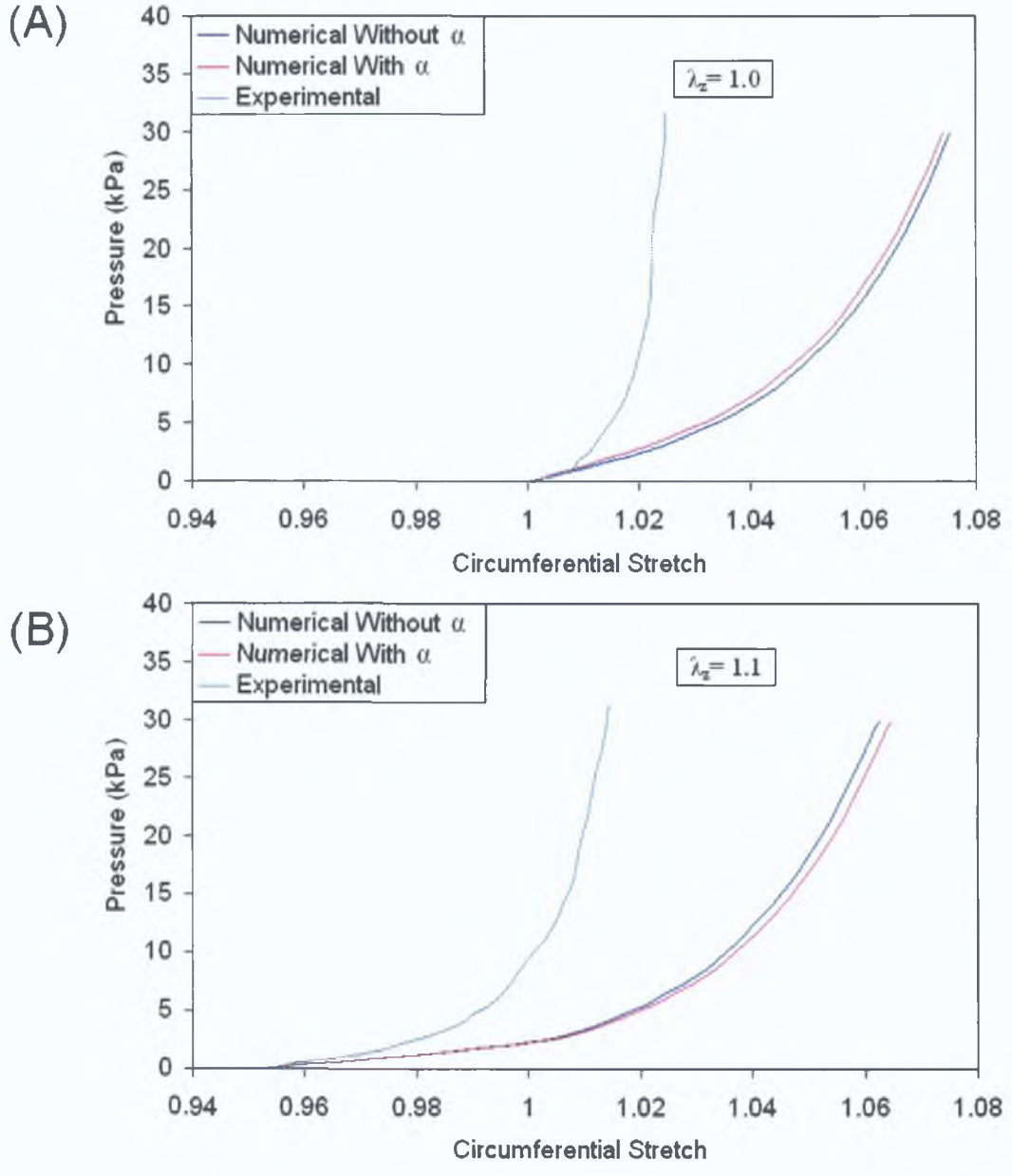

Figure 3.13 Experimental and numerical pressure versus circumferential stretch plots of Sample 1 with longitudinal stretches of: (A) λ_z = 1.0 and (B) λ_z = 1.1. Sample 1 was simulated with the experimental data obtained from the longitudinal uniaxial tensile tests [33]. Numerical simulation with and without opening angle effects were compared to the experimental data for corresponding sample. Experimental data digitised from Schulze-Bauer *et al* [59] (using xyextract© digitising software).

plots for the numerical data with opening angles were adjusted as the experimental data assumed that the initial unloaded circumferential stretch (Stretch = 1) represented the closed vessel configuration. Both plots illustrated the complex nonlinear deformation behaviour for Sample 1. The circumferential stretch decreases with higher longitudinal stretches for both the experimental and numerical results. A

stiffening effect at higher transmural pressures was evident in the experimental data, which is typical for all arteries. A less pronounced stiffening response was observed for the numerical models of Sample 1, with or without opening angles. The model does not show good agreement with the published experimental data, but it should be remembered that the model is based on constitutive data from a different subject.

3.4 Discussion

The effect on the structural response of arteries with and without residual stresses (opening angles and longitudinal stretches) was investigated based on published mechanical properties. The results indicated that circumferential stretch decreases with higher longitudinal stretch under internal pressurisation. However, the stiffening effect that is apparent for all artery types [59] at higher transmural pressures was not evident in the models. Arterial models that incorporated opening angles displayed a similar response to those where the opening angles were not included, despite the fact that literature shows that residual stresses have a significant affect on the stress and strain distribution through the thickness of the arterial wall [51]. The constitutive properties and the geometry were the two most significant parameters affecting the pressure versus diameter and pressure versus circumferential responses in the arterial models.

Three possible reasons why the overall response of the arterial models did not conform to the typical behaviour expected for arterial specimens; the use of an isotropic constitutive model, the fact that the uniaxial data used to determine the model coefficients was from a different subject and the mesh density. The isotropic hyperelastic material was based on uniaxial data alone, due to the fact that biaxial data was not available for the different layers of the artery. Ideally both uniaxial and biaxial constitutive responses would have been used when determining the constants used in the Ogden model.

Least squares curve fitting of uniaxial experimental data also implied that the other strain states (biaxial) were described by the model. However, these predicted states could have had a significantly different response to experimental data. A more appropriate isotropic model for arterial tissue would be a constitutive equation based

on experimental data from uniaxial and biaxial tension tests or data from inflation experiments with arteries, which combine arterial lumen pressure with longitudinal tension. Inclusion of constitutive models based on experimental biaxial data for each layer of the artery would be expected to lead to a less compliant vessel response.

Although a number of element sizes and aspect ratios were investigated to validate the model, an increase in the length of the artery in the longitudinal direction and in the overall mesh density would also be expected to improve the accuracy of the finite element model.

3.5 Conclusions

This chapter presented an exploratory investigation of the effect of different vessel geometries, longitudinal and tangential residual stresses and constitutive properties on the mechanical response of an arterial vessel to transmural pressures. The modelling approach incorporates the individual constitutive properties and opening angles of the intima, media and adventitia components of the iliac arterial wall, but does not account for anisotropy, fluid dynamics or three dimensional geometric effects.

The conclusions from this study are as follows:

- The effect of constitutive (stress versus strain) properties on the response of the arterial vessel is significant.
- The effect of opening angle (related to tangential residual stress) on the structural response of the iliac artery to internal pressurisation may be considered relatively small, in the range of constitutive and geometric properties considered here.
- The effect of longitudinal stretch (related to longitudinal residual stretches) is also small by comparison with the effects of constitutive response.

Based on these observations, the critical importance of replicating the constitutive properties of arterial tissue for the model vessel is clear.

Chapter 4

Vascular Cell Activity

PVA hydrogels and other hydrogels have been considered for applications in the field of tissue engineering for a wide variety of tissues and organs [5]. Individually PVA and chitosan hydrogels possess many attractive characteristics for use in tissue engineering applications. Combining PVA and chitosan to form a new biomaterial combines the structural properties of PVA with the biological properties of chitosan. The purpose of this aspect of the study was to biologically evaluate vascular cell activity on membranes of polyvinyl alcohol hydrogels (PVA) blended with chitosan. The attachment and growth of bovine aortic endothelial (BAEC) and smooth muscle cells (BASMC) on the PVA-chitosan modified hydrogels was studied to determine the effect of membrane composition on cell activity by comparison to cells cultured under control conditions. Successful adhesion of both cell types is a prerequisite to the use of PVA-chitosan blended hydrogels as a tissue mimicking biomaterial for *in vitro* cell culture experiments. Cell adhesion on the surface of the membranes was examined by phase contrast microscopy and scanning electron microscopy (SEM). Cell morphologies were studied using immunocytochemistry techniques to establish whether the fabricated membranes had any detrimental effects on the structure and composition of the cultured cells. Fluorescent activated cell sorter (FACS) analysis was used to determine cell proliferation and viability under static and shear culture conditions. Figure 4.1 illustrates the tests conducted to biologically evaluate the use of PVA-chitosan hydrogel as a potential biomaterial.

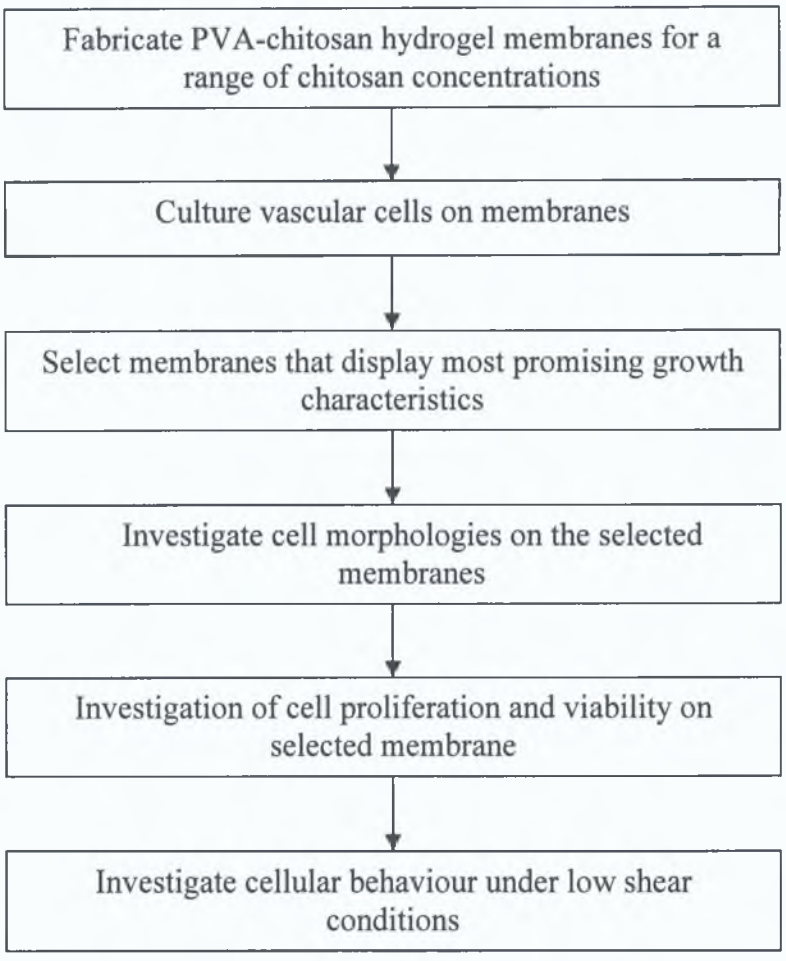

Figure 4.1 Schematic detailing the series of tests conducted to biologically evaluate the PVA-chitosan membranes.

4.1 Materials

PVA crystals with an average molecular weight of 78400 g/mol were purchased from Vassar Brothers Medical Center, New York, US. Water-insoluble chitosan powder with a molecular weight of 810000 g/mol and 85 % degree of de-acetylation was supplied by Sigma Aldrich, Poole Dorset, UK. In its most common form, chitosan does not dissolve in water, therefore a solvent is required to dissolve the chitosan. However, the non-physiological pH level of the solvent inhibits cell adhesion and growth. In order to promote cell adhesion, the substrate must have a pH level in the range of 7.4. Water-soluble chitosan with a de-acetylation degree of 85 % was purchased from Jinan Haidebi Marine Bioengineering Co. Ltd, China. The PVA crystals and chitosan powders were used as supplied without further purification. The chemical structure of the PVA and chitosan is shown in Figure 4.2.

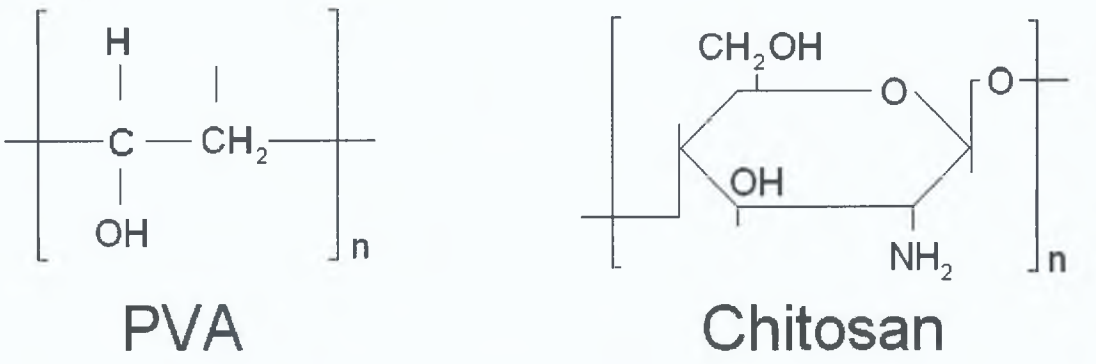

Figure 4.2 Chemical structure of PVA and chitosan.

All general purpose chemicals and reagents used in the biological experimental work were of analytical grade, and were purchased from the companies indicated in section 4.2.2. All cell culture plastic-ware was purchased from Sarstedt (Drinagh, Wexford, Ireland).

4.1.1 Biological Materials

Cell Lines

Bovine aortic smooth muscle cells (BASMC, Product No. B355-25) and endothelial cells (BAEC, B305-25) were purchased from Cell Applications Inc. (CA, USA). Bovine aortic SMC and EC were chosen as they closely mimic human vascular cells in size and behaviour and are more commonly commercially available than human vascular cells.

Stains and Antibodies

4'-6-Diamidino-2-phenylindole (DAPI) and the monoclonal anti-α smooth muscle cell actin were purchased from Sigma Aldrich Chemical Company (Poole, Dorset, England). The polyclonal rabbit anti-human Von Willebrand factor were purchased from Dakocytomation (Galway, Ireland). The Alexa-fluor phalloidin and conjugated secondary antibodies were purchased from Molecular Probes (Dublin, Ireland).

4.1.2 Commercial Kits

The following commercial kits were used:

Molecular Probes (Dublin, Ireland)
VybrantTM CFDA SE Cell Tracer Kit
VybrantTM Apoptosis Assay Kit #2

4.1.3 Chemical & Biological Reagents

The following commercial kits were used:

PALL Corporation (Dun Laoghaire, Ireland)
Acrodisc 32 mm 0.2 μm syringe filters

Sigma Chemical Company (Poole, Dorset, England)
4'-6-Diamidino-2-phenylindole (DAPI)
Acetic Acid
Bovine Serum Albumin (BSA)
Dimethlysulphoxide (DMSO)
Foetal Bovine Serum (FBS)
Formaldehyde
Hanks Balanced Salt Solution (HBSS)
Penicillin-Streptomycin (100x) (P/S)
Potassium Chloride
Potassium Hydroxide
Potassium Phosphate
RPMI-1640 Medium
Sodium Chloride
Sodium Phosphate
Sodium Sulphate
Triton X-100
Trypsin-Ethlyenediamine Tetracetic Acid (EDTA) solution (10x)

4.2 Membrane Fabrication Methods

4.2.1 Hydrogel Preparation

A 10 % PVA solution and a number of water-soluble and insoluble chitosan solutions were prepared and stored in autoclave bottles. The PVA was then blended with the chitosan solutions at various weight per volume ratios (Table 4.1). Each hydrogel was abbreviated as PVA-chitosan WS-X and PVA-chitosan IS-X (X referring to the percentage weight per volume ratio of the chitosan solution, WS to water soluble and IS meaning insoluble in water, eg: PVA-chitosan IS-0.5, a 10 % PVA solution blended with a 0.5 % water-insoluble chitosan solution). A pure hydrogel membrane containing no chitosan was also prepared. Table 4.1 shows the % concentrations of PVA and chitosan used in each solution.

Solution Name	Water (%)	PVA (%)	Acetic Acid (%)	Chitosan IS (%)	Chitosan WS (%)
PVA	90	10			
PVA-Chitosan IS-0.5	54	6	39.8	0.2	
PVA-Chitosan IS-1	54	6	39.6	0.4	
PVA-Chitosan IS-2	54	6	39.2	0.8	
PVA-Chitosan WS-0.5	93.8	6			0.2
PVA-Chitosan WS-1	93.6	6			0.4
PVA-Chitosan WS-2	93.2	6			0.8
PVA-Chitosan WS-6	91.6	6			2.4

Table 4.1 Percentage weight per volume ratios of PVA-chitosan solutions.

The 10 % PVA solution was prepared as follows: 100 g PVA crystals were added to an autoclave flask containing 900 ml distilled water and stirred for 30 min using a magnetic stirrer. The flask was then covered and weighed prior to autoclaving for 1 hr at 121 ^{o}C, and then re-weighed. The weight of the evaporated distilled water was added to the PVA solution until the flask was back to its pre-autoclave weight. The solution was immediately placed onto a magnetic stirrer for 2 hr to complete mixing. A sterile, homogeneous, clear solution was formed and stored in a sealed sterile container at room temperature until casting.

The water-insoluble chitosan powder was dissolved in an aqueous solution of 0.2 M acetic acid. The solution was stirred with a magnetic stirrer for 24 hr to ensure full chitosan dissolution and 0.5 %, 1.0 % and 2.0 % water-insoluble chitosan stock solutions were subsequently prepared.

The water-soluble chitosan was dissolved in distilled water until complete dissolution was achieved. Water-soluble chitosan solutions of 0.5 %, 1.0 %, 2.0 % and 6.0 % concentrations were also primed. Both water-soluble and -insoluble chitosan solutions were found to be stable at high temperature which permitted sterilisation by autoclaving on a liquid setting at a temperature of 121 ^{o}C for 30 min (Cited from [96]).

4.2.2 Blending Techniques

The mechanical properties of the PVA-water-insoluble chitosan membranes are controlled by two polymerisation processes; freeze-thaw cycles and submersion in a coagulation bath. The coagulation bath consists of distilled water with 7.5 % Potassium Hydroxide (KOH) concentration. Sodium disulphate (Na_2SO_4) was stirred in, until saturated.

Polymerisation of the PVA in the PVA-chitosan solution occurs during the freeze-thaw cycles. Hydrogen bonding between hydrophilic and polar groups provides some crosslinking. Freezing generates crystal nuclei, which grow into crystals upon thawing and act as crosslinking sites for the polymer. Further freezing produces areas of pure ice crystals forcing polymer molecules to come into closer proximity. During the thawing process the molecules that are in close proximity realign and bond to form crystallites [132]. As these crystallites grow in number and size, a rubber-like gel is formed.

Polymerisation in the coagulation bath is known as "phase inversion-immersion precipitation". Phase inversion-immersion precipitation was used to polymerise the water-insoluble chitosan in the PVA-water-soluble chitosan solution after the freeze-thaw cycles in addition to promoting PVA crosslinking [163]. The non-solvent (coagulation bath solution) begins to diffuse into the PVA-chitosan

matrix and the solvent in the PVA-water-insoluble solution (water and acetic acid) begins to diffuse into the coagulation bath. The mechanical properties of the PVA-chitosan membranes can be influenced by the PVA and chitosan concentrations, the ratio of the PVA-chitosan blends, the number of freeze-thaw cycles, the rate at which these cycles are completed in addition to the choice of solvent (water and acetic acid) and the nonsolvent (the coagulation bath) [132].

In order to polymerise the PVA-water-soluble chitosan membranes, the solution was subjected to freeze-thaw cycles. The PVA-water-soluble and insoluble chitosan solutions were frozen at -20 °C for a set time and allowed to thaw. Following this, the PVA-water-insoluble chitosan structures were placed in a coagulation bath. It was noted however, that the water soluble chitosan did not polymerise during the freeze-thaw process. Therefore after the freeze-thaw cycle the membranes were placed in the coagulation bath to polymerise the chitosan in a similar manner as the PVA-water-insoluble membranes.

4.2.3 Fabrication of Hydrogel Membranes

The 10 % w/v aqueous PVA solution was heated in a 100 °C water bath for 30 min, to decrease its viscosity and improve its ability to be poured. It was necessary to slightly loosen the autoclave bottle lid to prevent over pressurising this container. The container was removed from the boiling water, the lid tightened and slowly rotated to ensure thorough mixing of the PVA. The water-insoluble chitosan solutions (0.5 %, 1.0 % and 2.0 %) were each blended into a 10 % PVA solution at ratios of 3:2. This was repeated for 0.5 %, 1.0 %, 2.0 % and 6.0 % water-soluble solutions (Table 4.1).

A perspex mould was manufactured to fabricate the PVA-chitosan blended membranes for the cell culture experiments (Figure 4.3). The mould consists of a base plate and top plate, screwed together with 6 screws and was capable of fabricating membranes with a diameter of 34 mm and thickness of 0.5 mm. The hydrogel filled moulds was placed in a freezer at -20 °C and frozen for 12 hr and subsequently thawed at room temperature for a further 12 hr. After the freeze-thaw cycle had been completed the PVA-chitosan membranes were placed into a sterile

coagulation bath solution for 60 min which had been sterilised using acrodisc™ 32 mm diameter with 0.2 μm syringe filters to polyermise the chitosan in the PVA-chitosan solution. Finally the membranes were stored in distilled water at room temperature in order to retain moisture and prevent dehydration for up to 1 week. Forty eight membranes of PVA-chitosan solution were fabricated. Figure 4.4 details a summary of the PVA-chitosan hydrogel membrane preparation process.

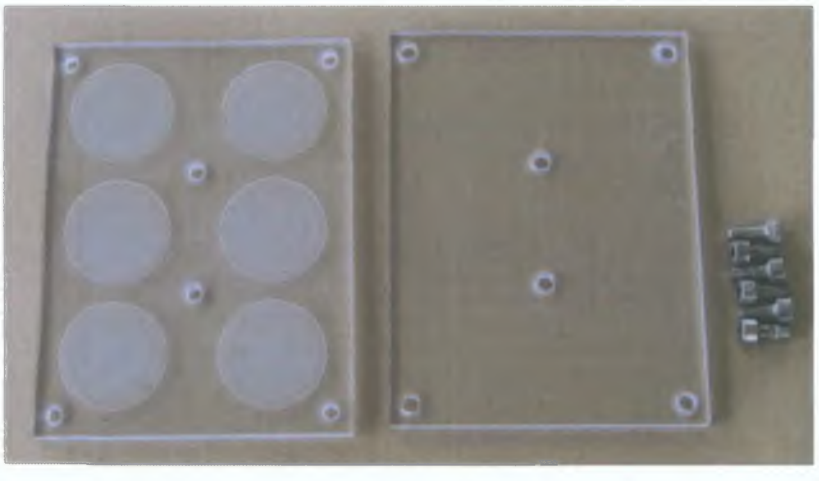

Figure 4.3 **Mould for manufacturing PVA-chitosan membranes for cell culture experiments.** Membranes had a diameter of 34 mm and depth of 0.5 mm.

4.3 Vascular Cell Culture Methods

All cell culture procedures were performed using aseptic techniques in a sterile environment created by an Aura 2000 m.a.c. laminar airflow cabinet (Bioair Instruments, Italy). Cells were visualised using an Olympus BX51 (Olympus, Japan) phase contrast microscope and the images were taken with an Olympus DP50 camera Olympus (Olympus, Japan), which was attached to the microscope. A *Becton Dickinson* FACSalibur instrument (Becton Dickinson UK, Oxford, UK) was used to determine the proliferative activity and apoptotic behaviour of the vascular cells.

4.3.1 Culture of Vascular Cells

The BASMC and BAEC were seeded on 175 cm^2 sterile polystyrene flasks with an initial cell seeding density of 3000 cells / cm^2. The cells were cultured in RPMI-1640 medium supplemented with 10 % foetal bovine serum (FBS), 1 % penicillin-streptomycin (P/S) in a Hera water jacketed cell culture incubator (an

apparatus in which environmental conditions, such as temperature and humidity are controlled). A humidified atmosphere of 5 % CO_2, 95 % air and a temperature of 37 °C was maintained.

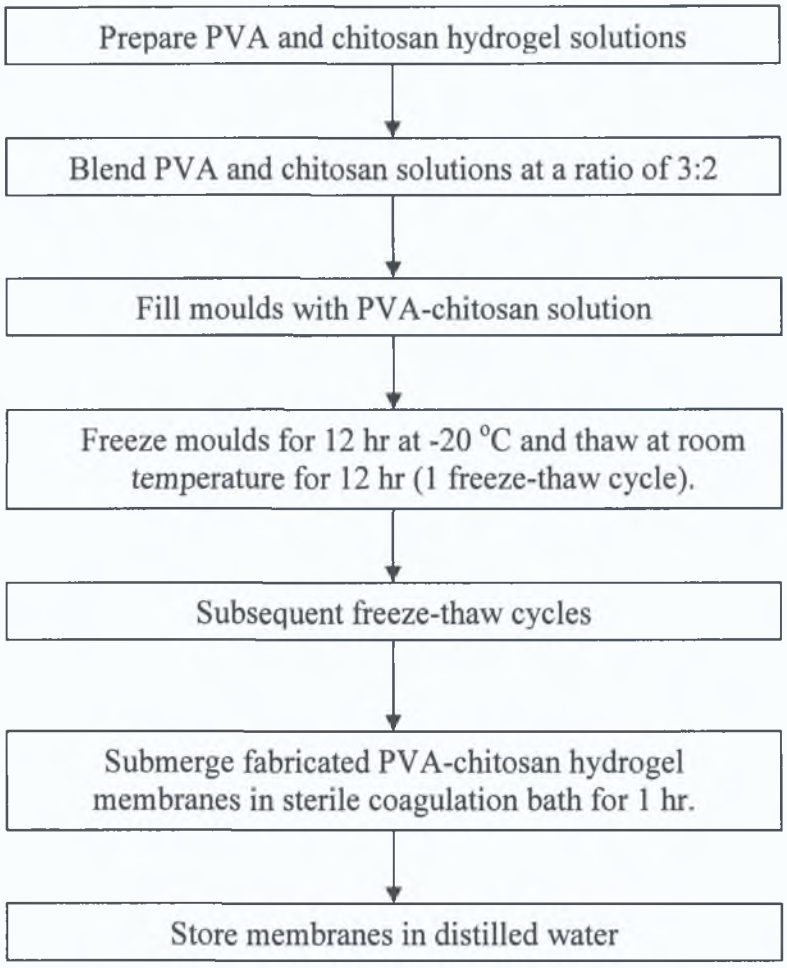

Figure 4.4 Schematic detailing the PVA-chitosan hydrogel membrane preparation process.

After the culture reached full confluency, the cells were routinely sub-cultured using a trypsinisation method. Tryspin is an enzyme that degrades adhesion proteins that allow cells to attach to the flask thus facilitating safe removal and transfer of cells. This method involved removal of the RPMI-1640 growth media from the cells, and two subsequent washes of the cells with Hanks Balanced Salt Solution (HBSS). The cells were then incubated with 1 X Trypsin/Ethlyenediamine Tetracetic Acid (EDTA), diluted from the 10 X stock solution with HBSS. Typically 1 ml of 1 X Trysin/EDTA was used per 25 cm^2 tissue culture flask area. The cells were then incubated at 37 °C for 5 min, or until the cells had detached from the flask. RPMI-1640 growth media was then added to the flask to neutralize the

trypsin/EDTA (an equal volume of RPMI-1640 growth media to trypsin/EDTA was typically added). The cell suspension was then removed from the flask, and centrifuged at 3,500 rpm for 5 min. The supernatant was subsequently removed, and the cells were re-suspended in fresh growth medium. Cells were fed every 2-3 days with RPMI-1640 growth media, and routinely sub-cultured at 90-100 % confluency. The cells were used up to eighteen passages of subculture after the primary culture. Smooth muscle cells displayed typical spindle shaped morphology and hill and valley pattern of growth in culture, while endothelial cells exhibited circular shaped morphology and grew on monolayers only.

4.3.2 Cell Counting

Prior to cell seeding, the density of the EC or SMC suspension was measured using a Sigma bright line haemocytometer, in order to determine the approximate number of cells that were seeded onto the PVA-chitosan membranes. The haemocytometer (EC or SMC counting chamber) was first carefully cleaned with lens tissue paper and ethanol. Then a homogenous cell suspension of the culture to be counted was prepared and a drop of cell suspension was used to fill the haemocytometer counting chamber. Cell suspensions were diluted enough so that the cells did not overlap each other on the grid and were uniformly distributed. Following visualization under 10 X magnification, the number of cells were counted in each of the four outer quadrants of the haemocytometer (Figure 4.5). The average of these four counts was equal to the number of cells x 10^4 / ml of cell suspension.

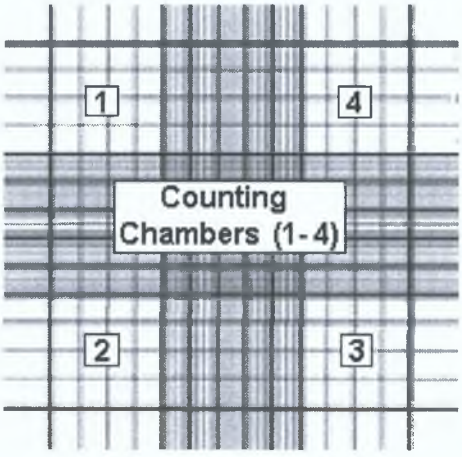

Figure 4.5 Haemocytometer counting grid.

4.3.3 Cell Storage and Recovery

For long-term storage of cells, freshly trypsinised and pelleted cells, as described in section 4.4.1, were re-suspended in freezing down media (RPMI-1640, 20 % FBS, 1 % P/S and 10 % DMSO) and transferred to sterile cryovials. Typically cells from a 175 cm^2 tissue culture flask were re-suspended in 3 ml freezing down media, and stored in 1 ml aliquots. The cryovials were then placed in a Nalgene cryofreezing container, and placed in the -80 ^{o}C freezer overnight. This allows for gradual freezing of the cells at a rate of -1 ^{o}C/min. Cells were then transferred to the Thermoylen locater junior cryostorage system for long-term storage in liquid nitrogen, the levels of which were monitored regularly.

Recovery of cells from liquid nitrogen storage involves rapid thawing of a 1 ml aliquot, and the immediate addition of the aliquot to 9 ml of RPMI-1640 growth medium when thawing occurs. Cells were then centrifuged at 3,500 rpm for 5 min, resuspended in 1 ml of RPMI growth medium, and added to 14 ml of medium in a 75 cm^2 tissue culture flask. Media was changed the following day, and cells were routinely sub-cultured before being used in an experiment to ensure complete recovery.

4.3.4 Cell Seeding onto PVA-chitosan Blended Hydrogels

PVA-chitosan membranes were opaque, making it difficult to visualise EC or SMC adherence and to perform immunocytochemistry staining techniques (See section 4.6). Therefore, prior to cell seeding, the membranes were baked in an oven at 60 ^{o}C for 24 hr. The membranes became transparent allowing phase contrast microscopic images to be obtained. Oven baking the membranes, while changing the mechanical properties, did not change the chemical structure of the material as both PVA and chitosan are stable at high temperatures (Cited from [96]). Following this, the 34 mm diameter PVA-chitosan membranes (Figure 4.6, A) were rinsed extensively in distilled water and soaked for 12 h in sterile RPMI-1640 medium to equilibrate membranes to pH 7.4. The prepared membranes were then placed in the base of a 6-well tissue culture polystyrene plate. A sterilised nylon ring (Figure 4.6 B) with an outer diameter of 34 mm and an inner diameter of 20 mm was placed on

top of each of the membranes in the wells to prevent them from floating (Figure 4.7). Aliquots (1 ml) containing 1.3 x 10^4 EC or 6.8 x 10^3 SMC were applied to the surface of each membrane or control wells (wells without membranes), as calculated using a haemocytometer as previously described. The cells were routinely fed with fresh media every 48 hr. All samples (PVA-chitosan membranes and control wells) were then cultured for 24-96 h prior to analysis.

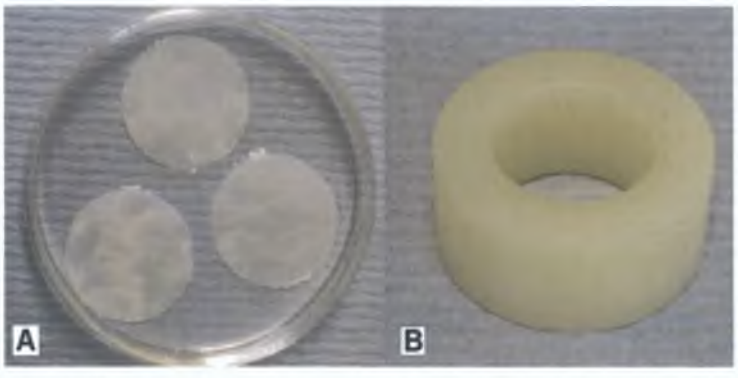

Figure 4.6 **(A) Three PVA-chitosan membranes prior to baking, (B) Nylon Insert**

Figure 4.7 **6-well culture plate with membranes and nylon inserts.**

4.4 Vascular Cell Morphology

For morphological observation, the PVA-chitosan membranes seeded with cells were washed with 1 ml 3 % formaldehyde in PBS for 15 min at room temperature. This functions as a fixative, fixing the cells to the surface of the membrane. The cells were then washed twice with 1 ml PBS for 3 min. Phase contrast microscopy and SEM were used to analyse cell adherence on the PVA-chitosan membranes. In addition DAPI (4'-6-Diamidino-2-phenylindole) staining was performed on the PVA-chitosan membranes in order to determine cell viability.

These dyes bind with deoxyribonucleic acid (DNA) inside the cell and readily fluoresce.

4.4.1 Scanning Electron Microscopy

Cell adherence on the PVA-chitosan blended membranes were analysed by a Hitachi S 300N scanning electron microscopy (SEM) (Hitachi Science Systems Ltd, Japan). The SEM is a microscope that uses electrons rather than light to form an image and provides nanometer resolution of a sample. Samples must always be viewed under vacuum. This technique permits images of samples at great resolution (0-180kX magnification) and depth of field. In order to examine the PVA-chitosan hydrogel membranes, the cells were first fixed to the surface of the membranes using 3 % formaldehyde in PBS for 15 min. They were frozen overnight at -80 ^{o}C and then freeze-dried in a Labconco Freeze Dry Freezone System (Labconco Corporation, USA) for 6 hr. Prior to examination, the hydrogel specimens were mounted on aluminium stubs. Images were acquired using a Hitachi S 300N SEM and analysed with SEM Image Analysis software (Oxford Instruments, Microanalysis Group, Halifax Road, High Wycombe, Bucks HP12 3SE, UK).

4.4.2 4'-6-Diamidino-2-phenylindole (DAPI) Staining

To assess cell viability and adherence of EC and SMC to the PVA-chitosan membranes the blue fluorescent dye, DAPI was utilised to stain the nuclei of the living cells. Cells are considered to be healthy when homogenously glowing bright blue [164].

After fixing the cells to the membrane in 3 % formaldehyde, permeabilising the cells in 0.2 % Triton X for 15 min, DAPI stock (1mg/ml) was diluted in distilled water at a ratio of 1:2000 and added to the membranes for a maximum of 3 min. DAPI is light sensitive so it was necessary to cover the wells with tin foil. The cells were washed with 1 ml PBS twice. The cells were viewed under an Olympus BX51 microscope and the images were taken with an Olympus DP50 camera, which was attached to the microscope. DAPI was visualised using a filter with an excitation and emission wavelength of 370 nm and 420 nm. The viable nuclei present stained blue.

4.5 Immunocytochemistry

Immunocytochemistry is a technique used in molecular biology to characterise the structure and function of proteins and their role in cell replication and the transmission of genetic information and allows for visualisation of the presence and subcellular localisation of proteins within a cell. Immunocytochemistry is based on antigen-antibody interactions, an antibody X being specific to an antigen X. Primary monoclonal antibodies bind specifically to the proteins of interest in the cells and secondary antibodies, specific to the primary monoclonals, containing a fluorescent tag, bind to the primary antibodies. The addition of an ultraviolet light source causes fluorescence specific to the secondary antibody tag, which in turn allows quantification of protein of interest (Figure 4.8).

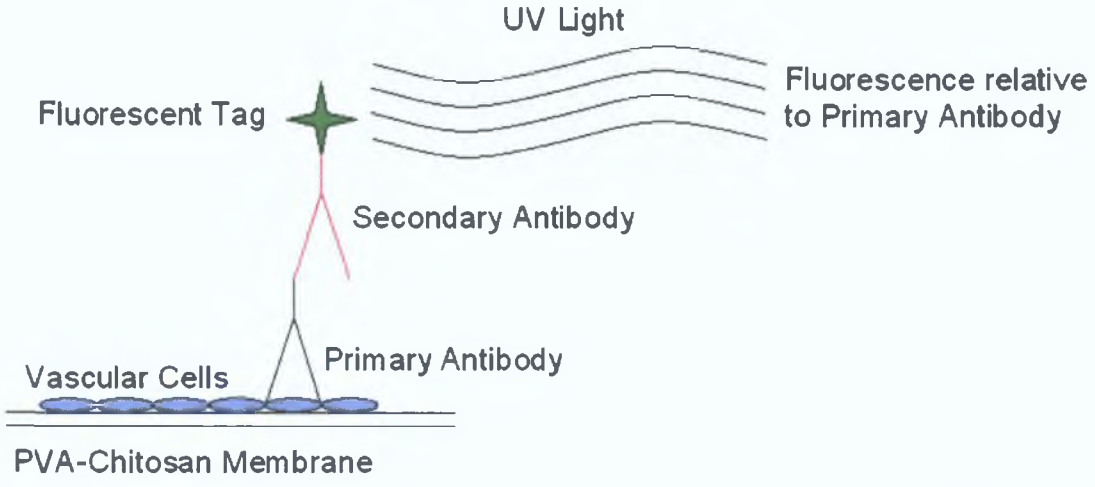

Figure 4.8 Schematic diagrams depicting the immunocytochemistry detection process.

4.5.1 Actin

Actin is a contractile protein that is abundantly expressed in vascular cells. The shape, structure and motions of cells are largely supported by microfilaments of actin. Intertwined actin microfilaments fill the cytoplasm of cells forming a "cytoskeleton". This gives the cell shape and form as well as providing a scaffold for organisation. Actin microfilaments lie in parallel to the thick filaments of myosin in muscle cells. In muscle contraction, actin microfilaments alternately chemically link and unlink with thick myosin filaments in a sliding action. Actin also functions in the

motility of non-muscle cells and for cell contraction during cell division [165,166]. In order to identify the presence of actin and investigate the morphology of the vascular cells on the PVA-chitosan membranes, two forms of actin were examined, filamentous actin (F-actin) specific to EC and α-actin specific to SMC. α-Smooth muscle cell actin recognises the α-smooth muscle isoform of actin.

F-Actin Staining - EC

The EC were fixed to the PVA-chitosan membranes with 3 % formaldehyde in PBS solution, as previously described in section 4.5. The cells were then washed twice with 1 ml PBS. To permeabilise the cells, a 0.1 % Triton X-100 in PBS solution was added to the cells for 5 min at room temperature. The cells were washed three times with PBS for 3 min. In order to ensure that non-specific background staining was at a minimum, the fixed cells were pre-incubated in PBS containing 1 % bovine serum albumin (BSA) for 30 min at room temperature. The cells were then washed twice with 1 ml PBS for 12 min.

Alexa Fluor 546 phalloidin was used to detect F-actin in EC. Samples were incubated in fluorescent phallotoxin at a concentration of 200 units/ml for 20 min at room temperature while being gently agitated on an orbital shaker. The cells and membranes were washed three more times for 3 min and then viewed under an Olympus BX51 microscope using a fluorescent filter with an emission wavelength of 590 nm and an excitation of 530-550 nm. The presence of F-actin in endothelial cells was indicated by red stained filaments and images were captured with an Olympus DP50 camera. Analysis of the orientation of the F-actin filaments in the BAEC, enables the morphological changes of the cells as they adhere to the PVA-chitosan membranes to be determined.

α-Smooth Muscle Cell Actin - SMC

The structure and orientation of anti α-smooth muscle actin fibres was examined in order to determine whether there was a significant change in the structure and composition of the BASMC that adhered to the PVA-chitosan membranes compared to the those cultured on control wells.

The SMC were fixed to the PVA-chitosan membranes as previously

described in section 4.5. The cells were then washed twice with 1 ml PBS for 3 min and then permeabilised with 1 ml 0.2 % Triton X-100 diluted in PBS at room temperature for 5 min. Cells were again washed twice for 3 min with 1 ml PBS per well. After the fixation and permeabilisation steps, the cells were blocked with 1 % BSA in PBS for 30 min in order to prevent non-specific protein interactions between the membrane and the primary antibody. The cells were washed twice with 1 ml PBS for 12 min.

The cells were then incubated with the primary antibody solution for 2 hr. The primary antibody used was monoclonal anti-α-smooth muscle cell actin which was diluted in blocking solution (1 % BSA) at a ratio of 1:300 and added to each well. The 6-well culture plate was placed on an orbital shaker and gently agitated during incubation. The cells were then washed with 1 ml PBS three times, for 3 min each time.

Anti-mouse Alexa Fluor 488 was the secondary antibody used and was diluted at a ratio of 1:800 in blocking solution. This antibody is light sensitive so it was necessary to cover the 6-well culture plates with tin foil. Plates were gently agitated on an orbital shaker and incubated at room temperature for 1 hr. A negative control was also conducted where a well of the plate was incubated with the secondary antibody in order to access fluorescence due to background signal. Finally the cells were washed twice in 1 ml PBS and then viewed under an Olympus BX51 microscope using a fluorescent filter with an emission wavelength of 515 nm and an excitation of 460-490 nm. The presence of anti- α-smooth muscle actin in SMC was indicated by intense fluorescent green stained filaments throughout the cell and images were captured with an Olympus DP50 camera.

4.5.2 Von Willebrand Factor

The expression of Von Willebrand Factor, a clotting protein, is confined to EC. Von Willebrand Factor acts like a glue that helps platelets stick together at the site of blood vessel injuries [167]. If this clotting factor is not present in EC, it would cause prolonged bleeding after an accident or injury. Von Willebrand Factor also carries clotting factor VIII, another protein that helps blood to clot [167]. Therefore

this factor was used in order to identify BAEC on the PVA-chitosan blended membranes.

Before incubation of the primary and secondary antibodies, the cells on membranes were fixed with 3 % formaldehyde in PBS, permeabilised with a 0.1 % Triton X-100 in PBS and blocked with a 1 % BSA-PBS solution as described in section 4.6.21 The procedure used was as previously described for anti-α-smooth muscle cell actin, however appropriate antibodies and dilutions were chosen to determine the presence of the Von Willebrand Factor. The primary antibody, polyclonal rabbit Anti-Human Von Willebrand Factor was diluted in the blocking solution at a ratio of 1:400. The secondary antibody, anti-rabbit Alexa Fluor 488 was diluted at a ratio 1:600 in blocking solution. Negative controls were also incorporated. The Von Willebrand stain was visualised with a filter that had an excitation of 460-490 nm and emission wavelength 515 nm. The presence of Von Willebrand in the EC was indicated by an intense fluorescent green stain scattered throughout the cell.

Table 4.2 lists the immunocytochemistry antibodies (primary and secondary) and the dilutions that were employed to determine various growth characteristics of the BAEC and BASMC.

4.6 Cell Fate

Numerous factors including mechanical forces, vasoactive substances and interactions between cells can affect vascular cell physiology and behaviour. Vascular cell fate defines the change in a cellular response to various stimuli. Cell fate may be divided into four main categories; proliferation, differentiation, migration and apoptosis. An increase in the number of cells as a result of growth and division of cells is known as cell proliferation. Differentiation is the change in phenotype (change in function due to change in environment) of cells. Movement of cells across and along the arterial wall is known as migration, while apoptosis is the process of programmed cell death. In this study cell proliferation and apoptosis in both vascular BAEC and BASMC on a selected PVA-chitosan membrane was examined. A fluorescence-activated cell sorter (FACS) was used to determine the

Stain Type	Cell Type	Primary Antibody / Stain	Dilution	Secondary Antibody	Dilution
DAPI	EC, SMC	DAPI Reagent	1mg/2000 µl		
F-actin	EC	Alexa Fluor 546 phalloidin	1:40		
α-Actin	SMC	Monoclonal Anti-α-Smooth Muscle Actin Clone 1A4	1:300	Anti-mouse Alexa Fluor 488	1:800
Von Willebrand	EC	Polyclonal Rabbit Anti-Human Von Willebrand Factor	1:400	Anti-rabbit Alexa Fluor 488	1:600

Table 4.2 Summary Table of Immunocytochemistry Antibodies and Stains

proliferative activity and apoptotic behaviour of vascular EC and SMC on selected unbaked membranes compared to the control samples.

FACS is a method of measuring specific physical and chemical characteristics of cells as they travel single file in suspension medium past a sensing point [168]. It is capable of rapidly separating cells (viable or non-viable) in a suspension on the basis of size and the colour of their fluorescence. The FACS measures the fluorescent intensity produced by the fluorescent labelled antibodies that bind to the specific cell proteins of interest. A *Becton Dickinson* FACSalibur was used to determine the proliferation and apoptotic profiles of the both vascular cells types grown on the PVA-chitosan WS-1 membrane.

4.6.1 Proliferation - Cell Proliferation Assay

A proliferation study was performed to compare the proliferative activity of BAEC and BASMC cultured on a selected PVA-chitosan membrane in comparison to corresponding control wells (6-well culture plates without membranes). A Vybrant® CFDA SE Cell Tracer Kit was used to conduct this experiment. Cells were pre-labelled with the fluorescent marker CFDA SE which is incorporated into the nucleus of the cells. Upon cell division, the label is inherited by daughter cell causing sequential halving of the CFDA SE fluorescence, resulting in a cellular fluorescence histogram in which the peaks represent successive generations.

The cells were seeded onto the membranes and control well at a cell density of 1 x 10^5 cells (approximately 50 % confluency per well) and were allowed to adhere to the membranes for 24 hr. A 10 mM CFDA SE stock solution was prepared by dissolving the contents of one vial in 90 µl DMSO and mixed thoroughly by gentle pipetting. The CFDS SE stock (dye) was diluted at a ratio of 1:2000 in pre-warmed (37 ^{o}C) 1X PBS. The media was removed from the cells and they were washed once in HBSS. The membranes and cells were then incubated at 37 ^{o}C for 30 min in the PBS-CFDA SE solution. The PBS-CFDA SE solution was replaced with fresh, pre-warmed RPMI-1640 medium and incubated at 37 ^{o}C for 5 hr. The cells were washed with RPMI-1640 medium supplemented with 0.2 % BSA and then

added to each well and incubated at 37 °C overnight to quiesce the cells.

At this point, the proliferative activity of the cells on Day 2 was analysed. The cells were washed in HBSS and 0.5 ml 1X Trysin/EDTA was added to each well. The area of one control well was approximately equal to the area of three wells with the membranes and nylon weights (Figure 4.9). The 6-well culture plates were incubated at 37 °C for 5 min to allow cells to trypsinise, following which, 1 ml of RPMI-1640 media supplemented with 10 % FBS and 1 % P/S was added to each well. The media and cells were removed from the wells (tube 1 - control well cell suspension, tube 2 - cell suspension from three wells with membranes) and pipetted in 15 ml tubes and immediately placed on ice. The proliferative activity was also examined at Day 7. Therefore, on Day 2 the 0.2 % BSA RPMI-1640 medium was replaced with RPMI-1640 medium supplemented with 10 % FBS and 1 % P/S then incubated at 37 °C for 5 days. The medium was replaced with fresh RPMI-1640 supplemented medium on Days 4 and 6 respectively. The cells were harvested from the wells as previously described.

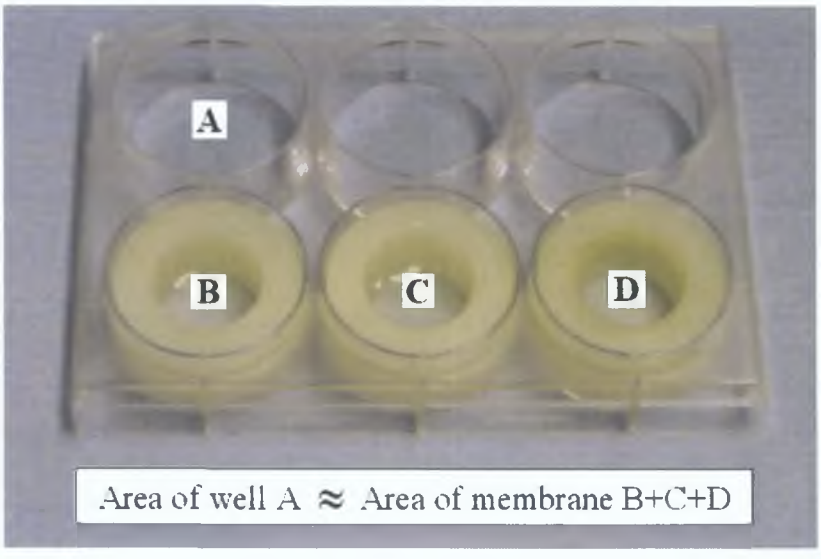

Figure 4.9 Area of well A ~ Area of membranes B+C+D.

The cells suspensions were then prepared for FACS analysis during which time they were kept on ice. The 15 ml tubes were centrifuged at 1500 rpm for 5 min at 4 °C to pellet the cells and the media was removed from each tube on ice without disturbing the cell pellet. 500 µl 1X PBS containing 0.1 % BSA was gently pipetted into each 15 ml tube and the contents were transferred into eppendorf tubes which

were centrifuged under the same conditions as previously stated. The tubes were again placed on ice and the 1X PBS-0.1 % BSA solution was carefully removed from each tube without disturbing the cell pellet. The cell pellets were gently re-suspended in 200 µl 1X PBS-0.1 % BSA and placed into FACS tubes and analysed.

4.6.2 Apoptosis - Cell Apoptosis Assay

The apoptosis levels of the vascular cells on a selected PVA-chitosan membrane was determined and compared to the apoptosis levels on control wells to determine whether the PVA or the chitosan was inducing abnormal levels of cell death. Effects of BAEC and BASMC apoptosis were determined using the Vybrant® Apoptosis Assay Kit #2. This kit provides a sensitive two-colour assay that employs a green fluorescent Alexa Fluor 488-conjugated annexin V and a red-fluorescent propidium iodide (PI) nucleic acid stain. Annexin V binds to phosphatidylserine located on the extracellular surface of apoptotic cells while PI is impermeable to live cells and apoptotic cells but satins necrotic cells with red fluorescence. Populations of cells are distinguished as viable, apoptotic or necrotic.

The cells were seeded onto the membranes and control well at a cell density of 1 x 10^5 cells (approximately 50 % confluency per well) and incubated at 37 °C for 24 hr to enable cell adherence to the membranes. The cells were washed once with RPMI-1640 medium supplemented with 0.2 % BSA. The 0.2 % BSA RPMI-1640 media was replaced with fresh, pre-warmed 0.2 % BSA RPMI-1640 medium and incubated at 37 °C overnight to allow the cells to quiesce. The apoptotic behaviour of the EC and SMC was analysed at Day 2. The cells were harvested from the membranes as previously described in Section 4.7.1. The cell suspension to be analysed was pippetted in 15 ml tubes and immediately placed on ice. The apoptotic activity of the vascular EC and SMC was also observed at Day 7. The 0.2 % BSA RPMI-1640 medium was replaced with RPMI-1640 medium supplemented with 10 % FBS and 1 % P/S on Day 0 and incubated at 37 °C for 5 days. The medium was replaced with fresh RPMI-1640 supplemented medium on Days 4 and 6 respectively. The cells were harvested as previously described in Section 4.7.1.

The cell suspensions were kept on ice during the preparatory phases for FACS analysis. The 5X annexin V binding buffer was diluted in 1X PBS and 0.1 % BSA and added to each sample. A PI working solution was prepared by diluting PI stock in 1X annexin-binding buffer at a ratio of 1:10. The 15 ml tubes were centrifuged at 1500 rpm for 5 min at 4 °C to pellet the cells. The cells were placed on ice and the media was removed from each tube without disturbing the cell pellet. 500 µl 1X PBS-0.1 % BSA solution was gently pipetted into each 15 tube and the contents were transferred to 1.5 ml eppendorf tubes. The tubes were then centrifuged at 1500 rpm for 5 min at 4 °C. The eppendorf tubes were placed on ice and the 1X PBS-0.1 % BSA solution was carefully pipetted off each tube without disturbing the cell pellet. The cell pellets were gently re-suspended in 100 µl 1X annexin-binding buffer. 1 µl annexin V and 0.4 µl PI was added to each 100 µl volume of cell suspension. The eppendorf tubes, complete with cell suspension, were then incubated at room temperature for 15 min. Following the incubation period, a further 100 µl 1X annexin-binding buffer was added to the cells. Finally the cell suspension was transferred from the eppendorf tubes into FACS tubes and placed on ice and analysed.

4.7 Shear Stress

The effects of shear stress on the proliferative and apoptotic behaviour of BAEC was also determined and compared to corresponding static samples that were cultured for the same period of time. FACS analysis, as previously described (section 4.7), was used to analyse the effect of shear stress on vascular BAEC proliferation and apoptosis and to determine whether the BAEC obtained sufficient adhesion to the PVA-chitosan membranes to withstand low levels of physiological shear stress [169]. The BAEC were analysed by flow cytometry on Day 2 and Day 3. An orbital shaker was used to apply low levels of physiological shear stress of 0.38 N/m^2 (3.8 dyn/cm^2) for 24 hr to the BAEC seeded on the PVA-chitosan WS-1 membranes. Despite the mean wall shear stress in large arteries generally being between 2-4 N/m^2 (20-40 $dynes/cm^2$) [64], this test gave an indication as to whether cells cultured on the membranes could withstand exposure to pathological shear stress. The 6-well culture plate was secured to the orbital shaker as shown in Figure 4.10. The rotation

speed on the orbital shaker was set to 1.25 rps (75 rpm) in order to obtain the desired shear stress on the PVA-chitosan specimens based on the following equation [170].

$$Shear\ stress = \alpha\sqrt{\rho n(2\pi f)^3} \qquad (4.1)$$

where:

α = *radius of rotation* = 0.02 *m*

ρ = *density of fluid* = 1000 kg/m^3

n = *buffer viscosity at* 37 °C = 7.5x10 $^{-4}$ *Pa.s*

π = 3.14159

$$f = rotation\ per\ sec = \frac{75rpm}{60\sec} = 1.25\ \text{rps}$$

$$Shear\ stress = 0.02\sqrt{(1000)(7.5\times10^{-4})[(2)(3.14159)(1.25)]^3}$$

$$= 0.02\sqrt{363.35}$$

$$= 0.38\ N/m^2\ \ (3.8\ dynes/cm^2)$$

Figure 4.10 6-well culture plate was secured to the orbital shaker.

4.8 Results

EC and SMC cellular behaviour on the PVA-chitosan combined hydrogels is an important factor in determining the biocompatibility of the biomaterial. After cell contact with the biomaterial, cells usually undergo morphological changes in order to stabilise the cell-material interaction. Therefore the processes of vascular adhesion, cell spreading and proliferation on the fabricated membranes have been investigated.

4.8.1 Cell Morphology

Phase contrast microscopy was used to demonstrate the presence of vascular cell on the surface of the fabricated membranes. In order to assess the viability of cells on the selected PVA-chitosan membranes, the membranes were stained with the nuclear stain DAPI which stains the nuclei of living cells. To ensure that the DAPI stain was not sticking to the pores in the PVA-chitosan blended membranes, negative controls were also conducted, where the membranes without cells were stained with DAPI.

BAEC on PVA-chitosan membranes

Initial results showed that BAEC readily adhered to the PVA-chitosan water-soluble and -insoluble membranes. Low magnification (4X) images not presented illustrated that cells successfully adhered to the membranes following a 96 hr culture. A negative control was also conducted which proved that the DAPI was specific to BAEC and there was no background staining/fluorescence (not presented). The phase contrast images (Figures 4.11 and 4.12) demonstrate that the BAEC adhered on all membranes solution types (Table 4.1), while the corresponding DAPI images (Figures 4.11 and 4.12) show that the BAEC remained viable after 96 hr. The phase contrast images illustrate that a confluent layer of BAEC was evident on the control well (Figure 4.11 A) and on the PVA-chitosan IS-1 and WS-1 membranes (Figures 4.11 C, 4.12 B). Webbing of the BAEC was noted on both the control well and all PVA-chitosan blends of membrane (Figures 4.11, 4.12). Clumps of BAEC were evident on the PVA-chitosan WS-2 (Figure 4.12 C) rather than the preferred even distribution of cells as seen on the control well and the PVA-chitosan IS-0.5, -1 and WS-0.5, -1 membranes.

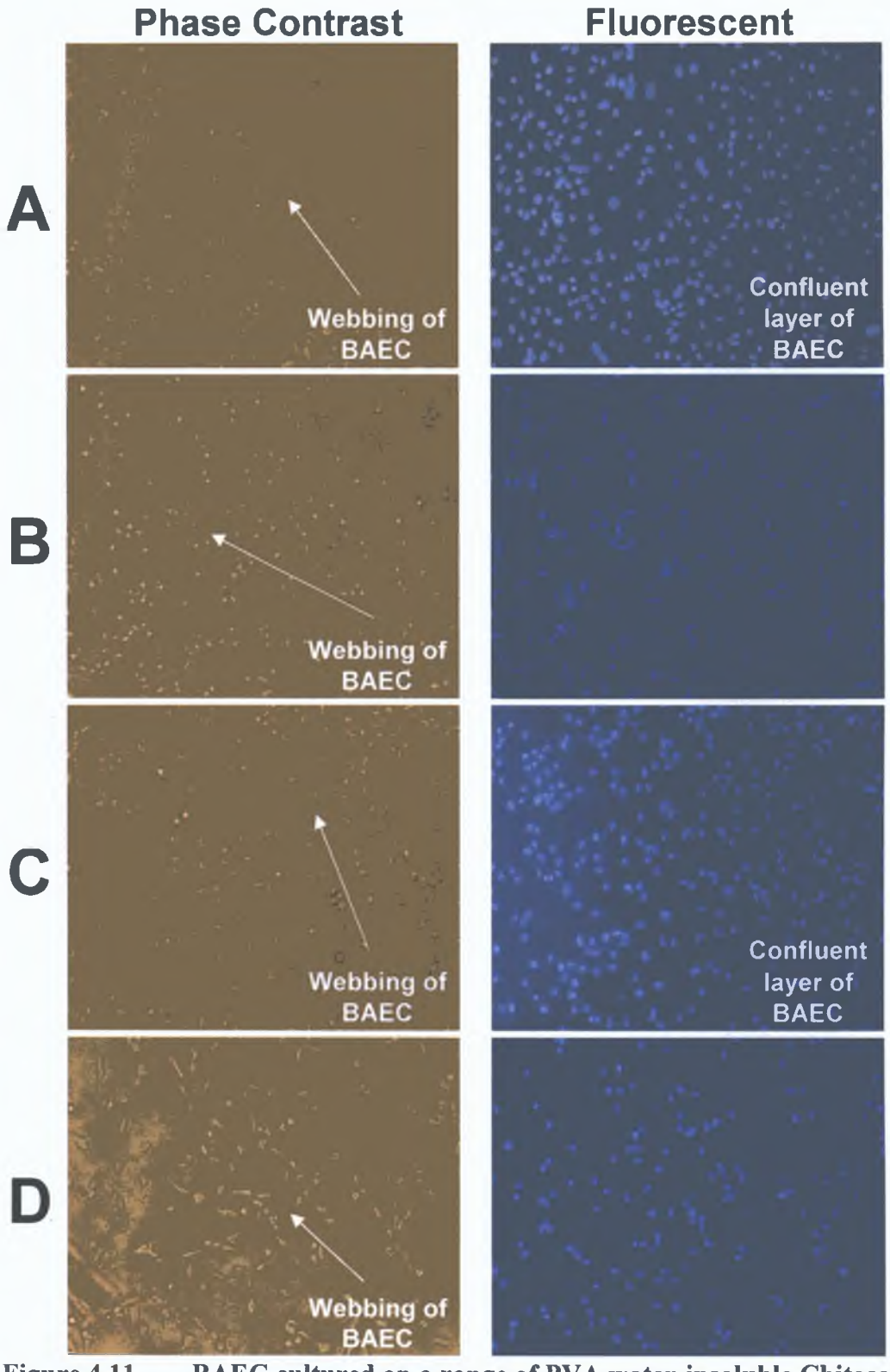

Figure 4.11 **BAEC cultured on a range of PVA water-insoluble Chitosan membranes.** Following a 96 hr growth period, cells were fixed to the membranes with 3% formaldehyde in PBS, stained with DAPI and viewed under a phase contrast and fluorescent microscopes. (A) Control well, (B) PVA-Chitosan IS-0.5, (C) PVA-Chitosan IS-1 and (D) PVA-Chitosan IS-2. Magnification 10X. Representative photographs, n = 3.

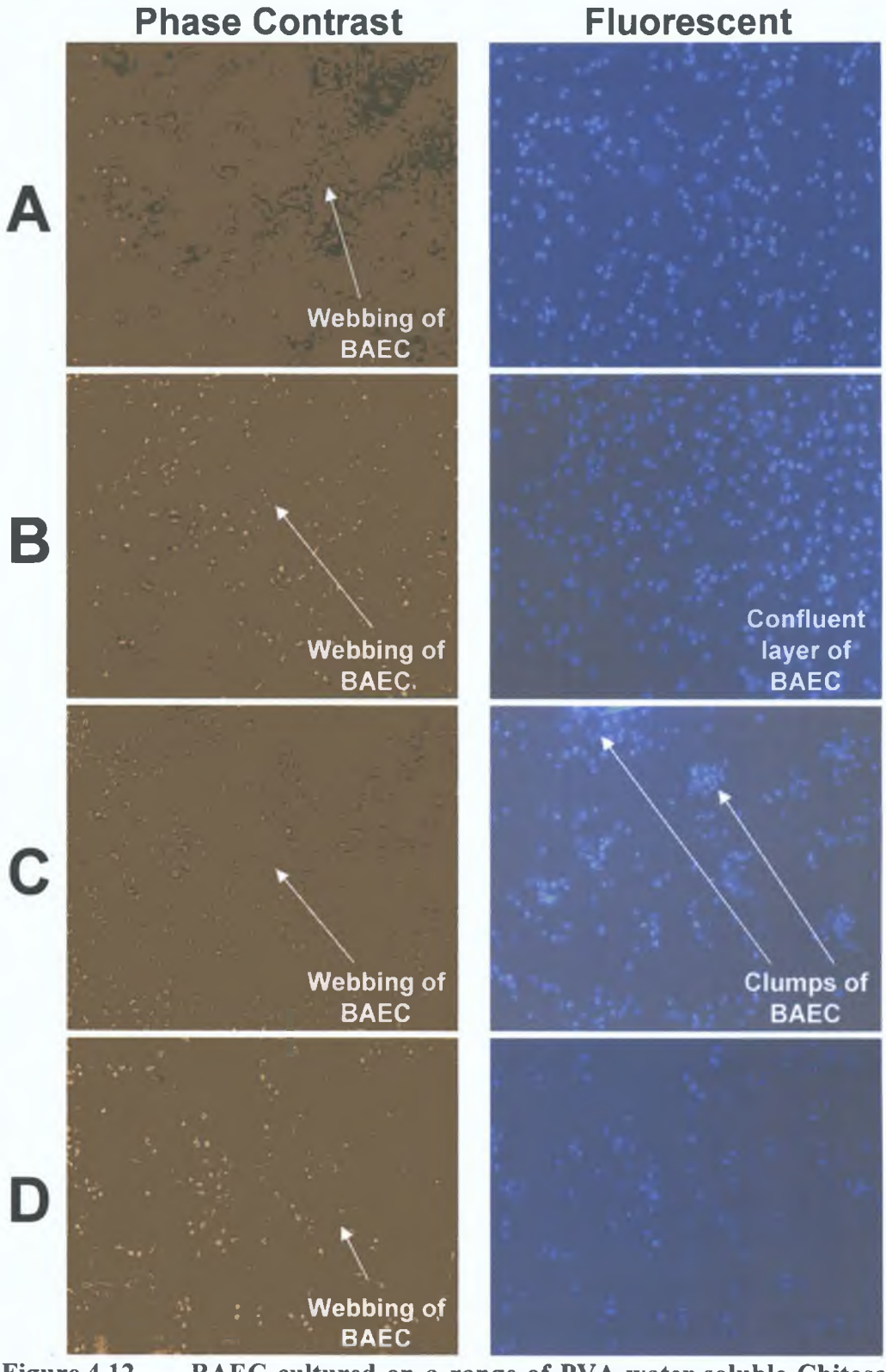

Figure 4.12 **BAEC cultured on a range of PVA water-soluble Chitosan membranes.** Following a 96 hr growth period, cells were fixed to membranes with 3% formaldehyde in PBS, stained with DAPI and viewed under a phase contrast and fluorescent microscopes. (A) PVA-Chitosan WS-0.5, (B) PVA-Chitosan WS-1, (C) PVA-Chitosan WS-2 and (C) PVA-Chitosan WS-6. Magnification 10X. Representative images, n = 3.

A bar chart was generated to compare the cell numbers of three 10X magnification images from each membrane to the control well (Figure 4.13). It can be seen from the histogram that the PVA-chitosan IS-0.5, -1, WS-0.5 and -1 have the closest resemblance to the control well in terms of providing a growth matrix. There was a significant reduction of 0.885 ± 0.022 in the fold change of cell numbers on the PVA-chitosan IS-0.5. A highly significant reduction of 0.525 ± 0.015, 0.708 ± 0.030 and 0.378 ± 0.009 was noted in the fold change of cell numbers compared to the control well on the PVA-chitosan IS-2, WS-2 and WS-6 membranes respectively. A significant fold increase of 1.150 ± 0.026 was evident on the PVA-chitosan WS-1 membrane. No significant difference was apparent in the fold change of the PVA-chitosan IS-1 (1.121 ± 0.037) or PVA-chitosan WS-0.5 (0.949 ± 0.0168) compared to the control well. In addition, there was no significant difference in the fold change of the PVA-chitosan soluble membranes compared to the corresponding PVA-chitosan insoluble membranes (eg: PVA-chitosan IS-0.5 and WS-0.5) which suggests that the adhesion and growth properties of BAEC were not adversely affected by the incorporation of water-soluble or insoluble chitosan.

Preliminary results proved that BAEC did successfully adhere to the PVA-chitosan membranes. There was no significant difference in the cell adhesion profiles or cell counts of the corresponding PVA-chitosan water-insoluble and -soluble membranes. Optimum growth of BAEC compared to the control well was achieved on the PVA-chitosan 0.5 % and 1 % water-soluble and insoluble membranes.

BASMC on PVA-chitosan Membranes

Cell adhesion and cell spreading of the BASMC was also achieved on both PVA-water-soluble and -insoluble chitosan membranes. The BASMC were cultured on all membranes for 96 hr. The phase contrast images on Figures 4.14 and 4.15 illustrate that the BASMC adhered to the control well and all of the different blends of PVA-water-soluble and insoluble chitosan membranes (See Table 4.1). Cell webbing was also evident on all samples. The equivalent DAPI images (Figures 4.14 and 4.15) show that the BASMC remained viable after 96 hr. It was also evident from the DAPI images that cell adhesion and growth was not uniform on all samples. A confluent layer of cells was evident on the control well (Figure 4.14, A) and PVA-chitosan IS-1 and WS-1 membranes (Figure 4.14, C and Figure 4.14, B). It was also

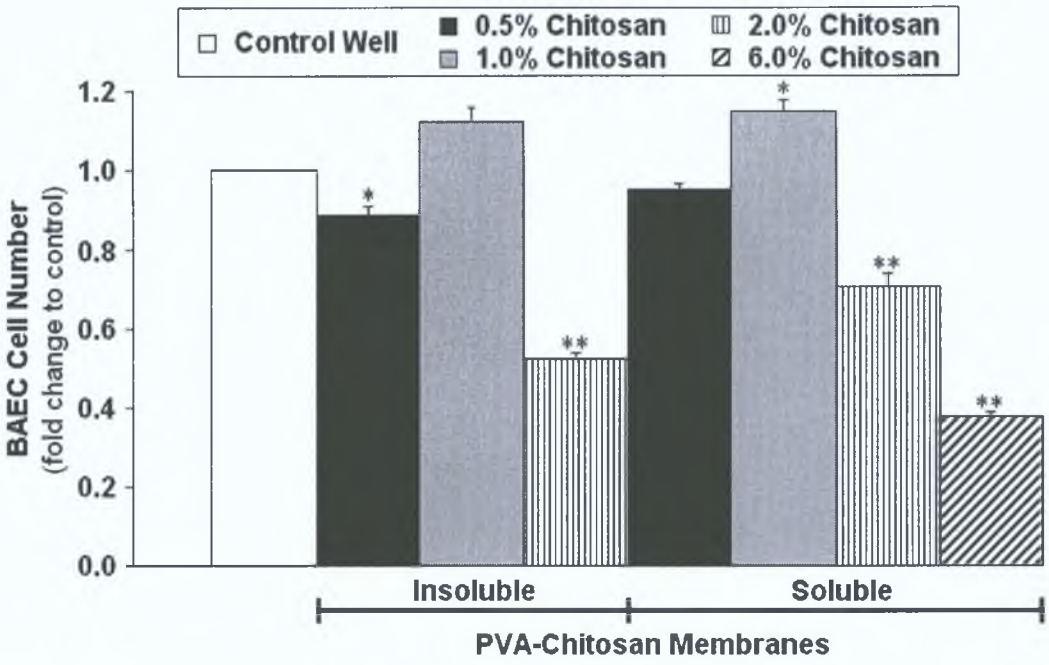

Figure 4.13 BAEC were seeded onto a range of PVA-chitosan membranes and control wells. Following a 96 hr growth period (n = 3), cells were fixed to the membranes with 3 % formaldehyde in PBS, stained with DAPI and viewed under a fluorescent microscope. The cell numbers on three 10X magnification images from each membrane were compared to the control well. * $p<0.05$, ** $p<0.005$ as compared to control well (student's t test).

apparent from the DAPI images that clusters of BASMC were evident on the PVA-chitosan IS-0.5 (Figure 4.14, B) and the PVA-chitosan WS-0.5 and WS-2 (Figure 4.15, A & C) membranes which is in contrast to the control well and PVA-chitosan IS-1 and WS-1 membranes where the cells were more evenly distributed. BASMC were more sparsely distributed on the PVA-chitosan IS-2 and WS-6 membranes.

In order to determine which PVA-chitosan membrane provided the optimum adhesion and growth characteristics, a bar chart was created from cell counts on images from three 10X images (Figure 4.16). Again the BASMC were cultured for 96 hr. There was no significant difference in the fold change of cell numbers on the PVA-chitosan IS-0.5 (0.989 ± 0.033) and WS-0.5 (1.059 ± 0.036) membranes in comparison to the control well. As with the BAEC, the PVA-chitosan IS-1 and WS-1 showed the greatest cell numbers. A significant fold increase of 1.196 ± 0.025 was evident for the PVA-chitosan IS-1 membrane while the PVA-chitosan WS-1 membrane showed a highly significant fold increase of 1.236 ± 0.026 in cell numbers compared to the control well. Highly significant reductions of 0.6 ± 0.044, 0.759 ±

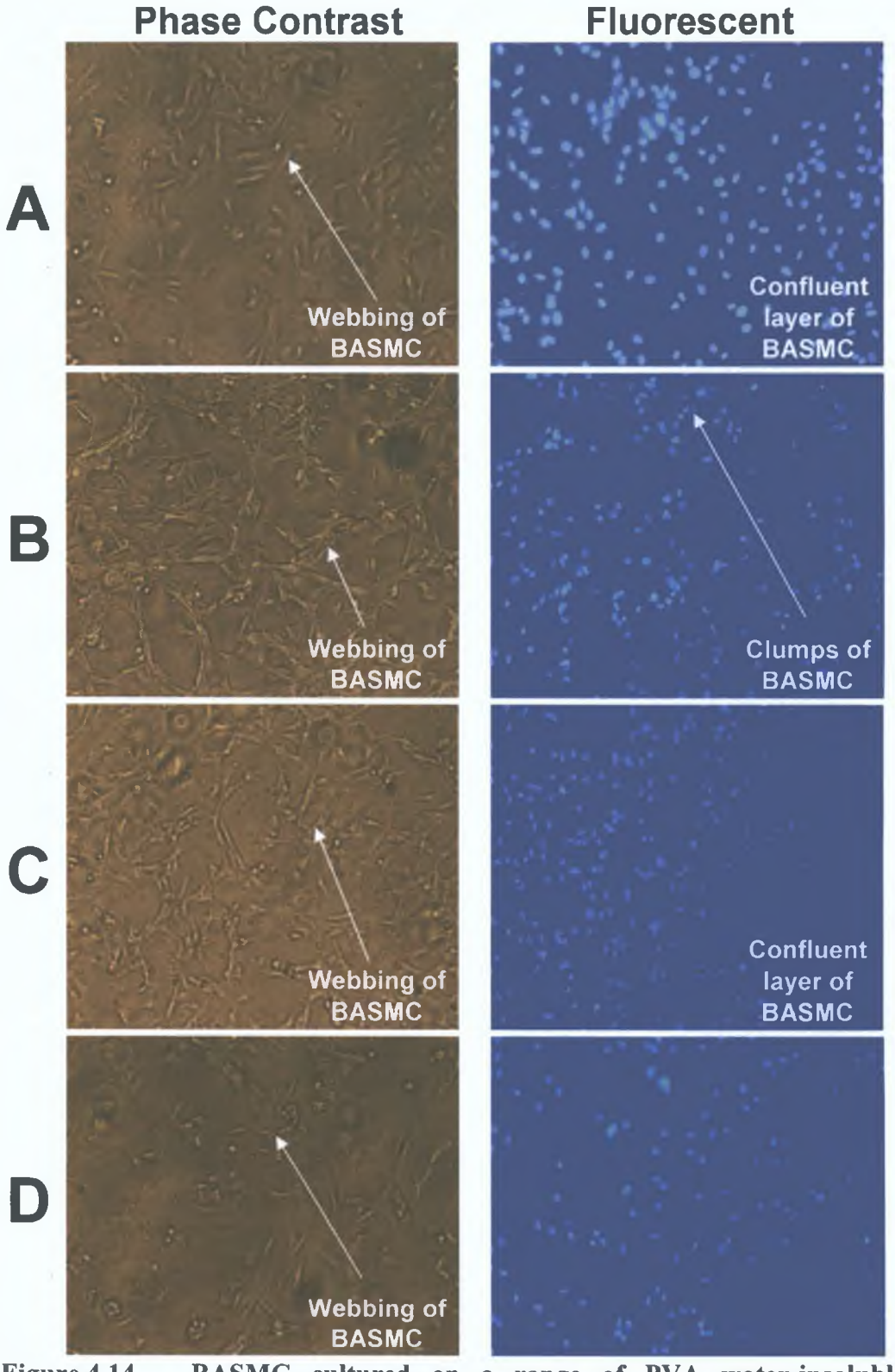

Figure 4.14 **BASMC cultured on a range of PVA water-insoluble Chitosan membranes.** Following a 96 hr growth period, cells were fixed to the membranes with 3% formaldehyde in PBS, stained with DAPI and viewed under a phase contrast and fluorescent microscopes. (A) Control well, (B) PVA-Chitosan IS-0.5, (C) PVA-Chitosan IS-1 and (D) PVA-Chitosan IS-2. Magnification 10X. Representative photographs, n = 3.

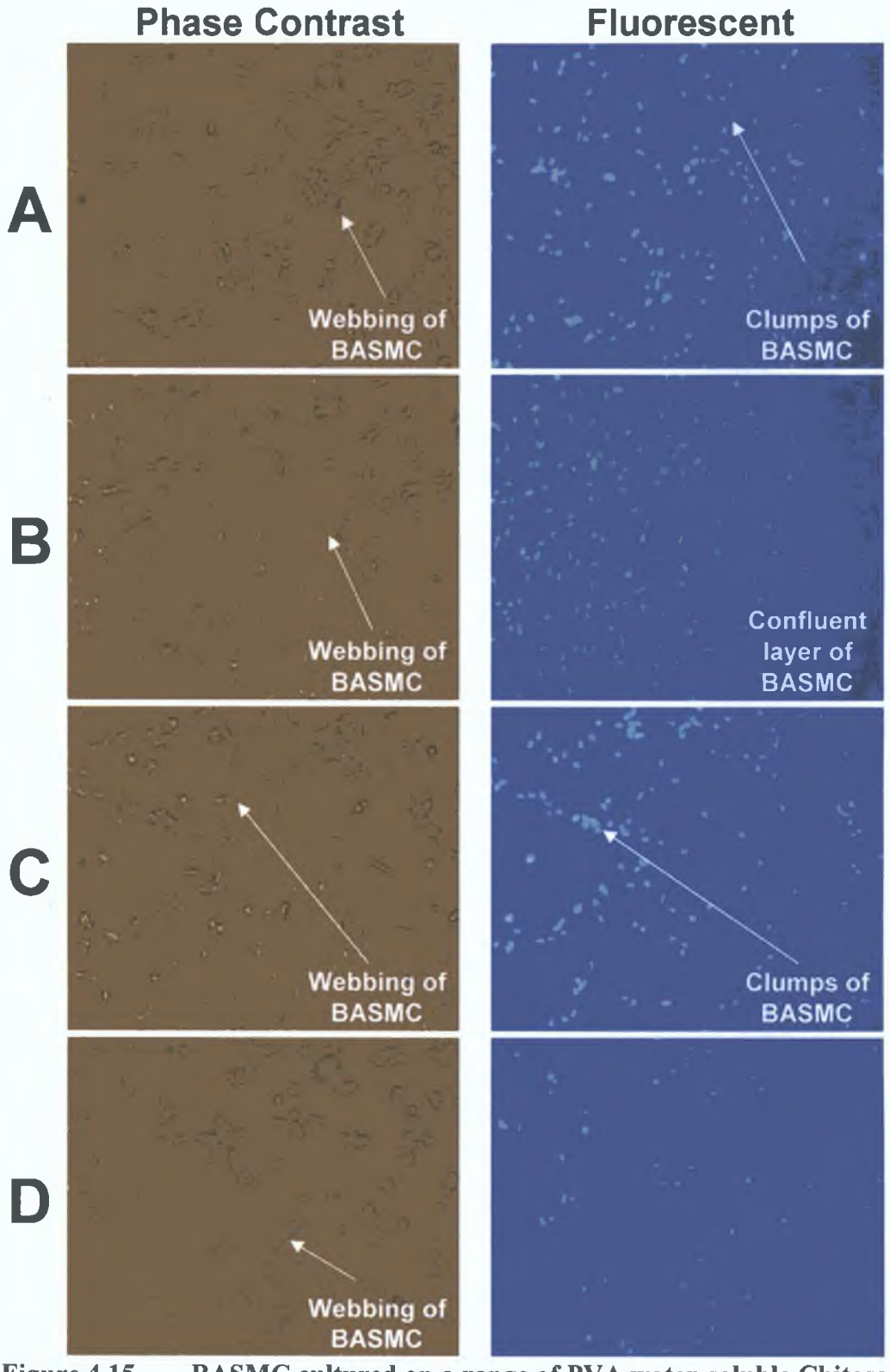

Figure 4.15 **BASMC cultured on a range of PVA water-soluble Chitosan membranes.** Following a 96 hr growth period, cells were fixed to membranes with 3% formaldehyde in PBS, stained with DAPI and viewed under a phase contrast and fluorescent microscopes. (A) PVA-Chitosan WS-0.5, (B) PVA-Chitosan WS-1, (C) PVA-Chitosan WS-2 and (C) PVA-Chitosan WS-6. Magnification 10X. Representative images, n = 3.

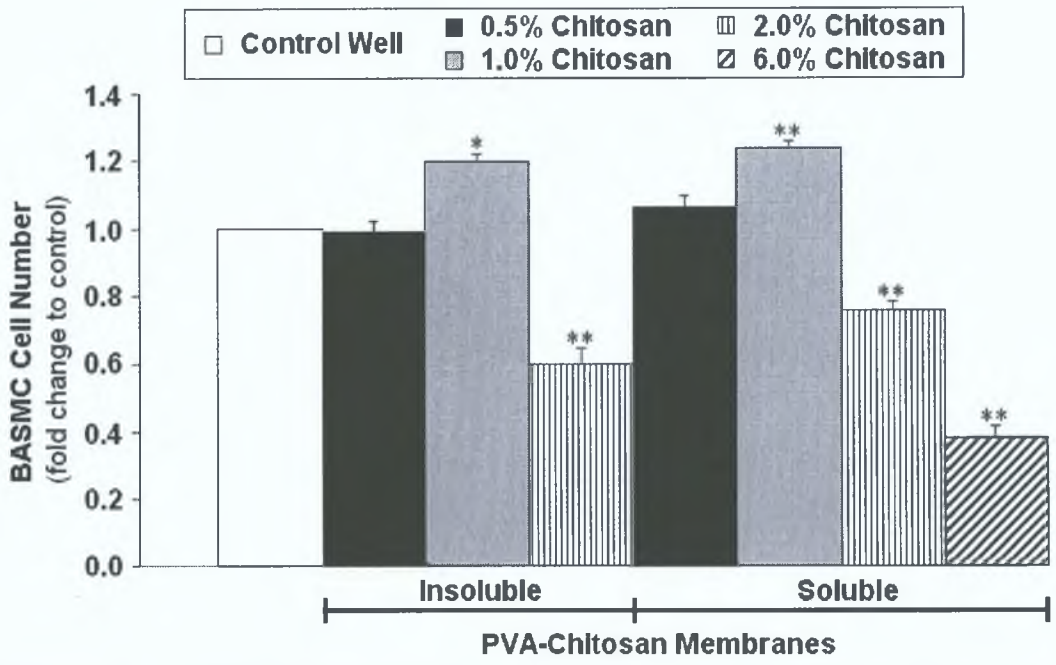

Figure 4.16 BASMC were seeded onto a range of PVA-chitosan membranes and control wells. Following a 96 hr growth period (n = 3), cells were fixed to the membranes with 3 % formaldehyde in PBS, stained with DAPI and viewed under a fluorescent microscope. The cell numbers on three 10X magnification images from each membrane were compared to the control well. * $p<0.05$, ** $p<0.005$ as compared to control well (student's t test).

0.025 and 0.382 ± 0.034 in the fold change of BASMC were noted on the PVA-chitosan IS-2, WS-2 and WS-6 membranes respectively. An increase in the concentration of the water-soluble chitosan to 6 % did not increase BASMC adhesion and proliferation, in fact there was a further reduction in the number of cells on the membrane.

Initial results have shown that BASMC did adhere and spread on the surface of both the PVA-chitosan water-soluble and -insoluble membranes. Comparing cell numbers on the control well to those on the PVA-chitosan blended membranes yielded similar results for BAEC and BASMC (Figure 4.16). There was no significant variation in the cell adhesion and cell counts on matching PVA-chitosan water-insoluble and -soluble membranes. The most prominent growth of BASMC compared to the control well was achieved on the PVA-chitosan WS-1 membrane. It was also evident that the vascular cells, once adhered, proliferated and spread across the surface of the membrane. While vascular cell adhesion and proliferation were evident, it was necessary to determine whether the cells that adhered to the surface of

the PVA-chitosan membranes behaved similarly to the cells cultured in the control conditions.

Various immunocytochemistry staining techniques were performed on the PVA-chitosan IS-1 and PVA-chitosan WS-1 membranes (See Table 4.1) due to the fact that cell adhesion and growth on both of the membranes most closely resembled that of the control sample. It was decided to concentrate on these two membrane compositions and assess cell behaviour accordingly. SEM analysis was conducted to assess cell adhesion on the selected PVA-chitosan blended membranes. DAPI was also used in conjunction with other various immunochemistry techniques, including actin and Von Willebrand Factor staining.

SEM Analysis

The morphology of BASMC cultured on the PVA-chitosan IS-1 and WS-1 membranes can be seen in Figure 4.17. The SEM examination shows the BASMC on both the PVA-chitosan IS-1 and WS-1 membranes are completely flattened and well spread (Figure 4.17, A & B,). Furthermore, cell fusion of the BASMC was also evident on both membrane blends.

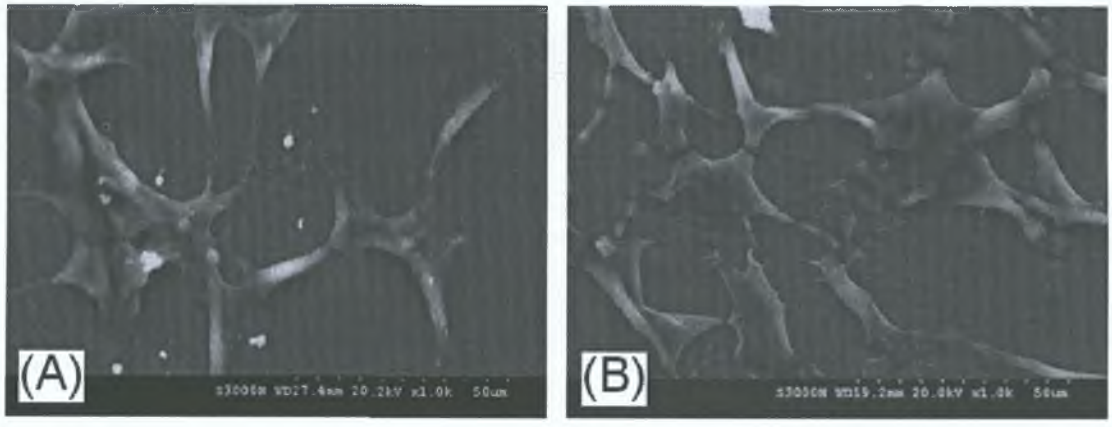

Figure 4.17 SEM images of BASMC cultured on PVA-chitosan membranes. Following a 96 hr growth period, cells were fixed to the membranes with 3 % formaldehyde in PBS, frozen overnight at -80°C, freeze-dried for 6 hrs and viewed under SEM. (A) PVA-chitosan IS-1, (B) PVA-chitosan WS-1. Magnification 1000X. Representative photographs, n = 3

4.8.2 Immunocytochemistry

F-actin - EC

To corroborate the presence of BAEC on the PVA-chitosan blended membranes, the presence of the EC-specific antigen, F-actin, was examined. To facilitate interruption of the fluorescent F-actin stain, DAPI was also used so that the nuclei relative to the F-actin filaments could be identified. Viable BAEC were evident from the DAPI images (Figure 4.18), whereas the corresponding F-actin images (Figure 4.18) validate that the vascular cells on the PVA-chitosan blended membranes were indeed BAEC. The actin fibres from individual cells are illustrated in Figure 4.19. There does not appear to be any perceptible difference in the structure and orientation between the actin fibres on the control well or the PVA-chitosan water-insoluble and -soluble membranes (Figure 4.19). This suggests that while some morphological changes most probably occur as the BAEC adhered to the PVA-chitosan blended membranes, they do not have a significant effect on the structure and composition of the cells.

α-*Smooth Muscle Cell Actin - SMC*

In order to verify the presence of BASMC on the PVA-chitosan blended membranes, the presence of α-actin was investigated. DAPI was also used to assist the interpretation of the fluorescent α-actin stain. The DAPI images in Figure 4.20 illustrate the presence of viable cells, while the equivalent α-actin images confirm that the vascular cells on the samples were definitely BASMC. Analysing of α-actin fibres orientation indicated if the BASMC were changing morphology. Figure 4.21 revealed the actin fibres that were present in BASMC. It was noticeable that the actin fibres were more pronounced on the control well (Figure 4.21, C), compared to the BASMC on the membranes (Figure 4.21, A & B), thus suggesting that there were changes in the morphology of the BASMC as they adhered to the PVA-chitosan blended membranes. The BASMC that were not adhered to the membranes but on top of the first layer of cells had more visible actin fibres, implying that the morphological changes encountered did not adversely effect the composition and behaviour of the cells. A closer look at the actin fibres of the BASMC in Figure 4.22 revealed that while the fibres were more prominent on the control well, a structured

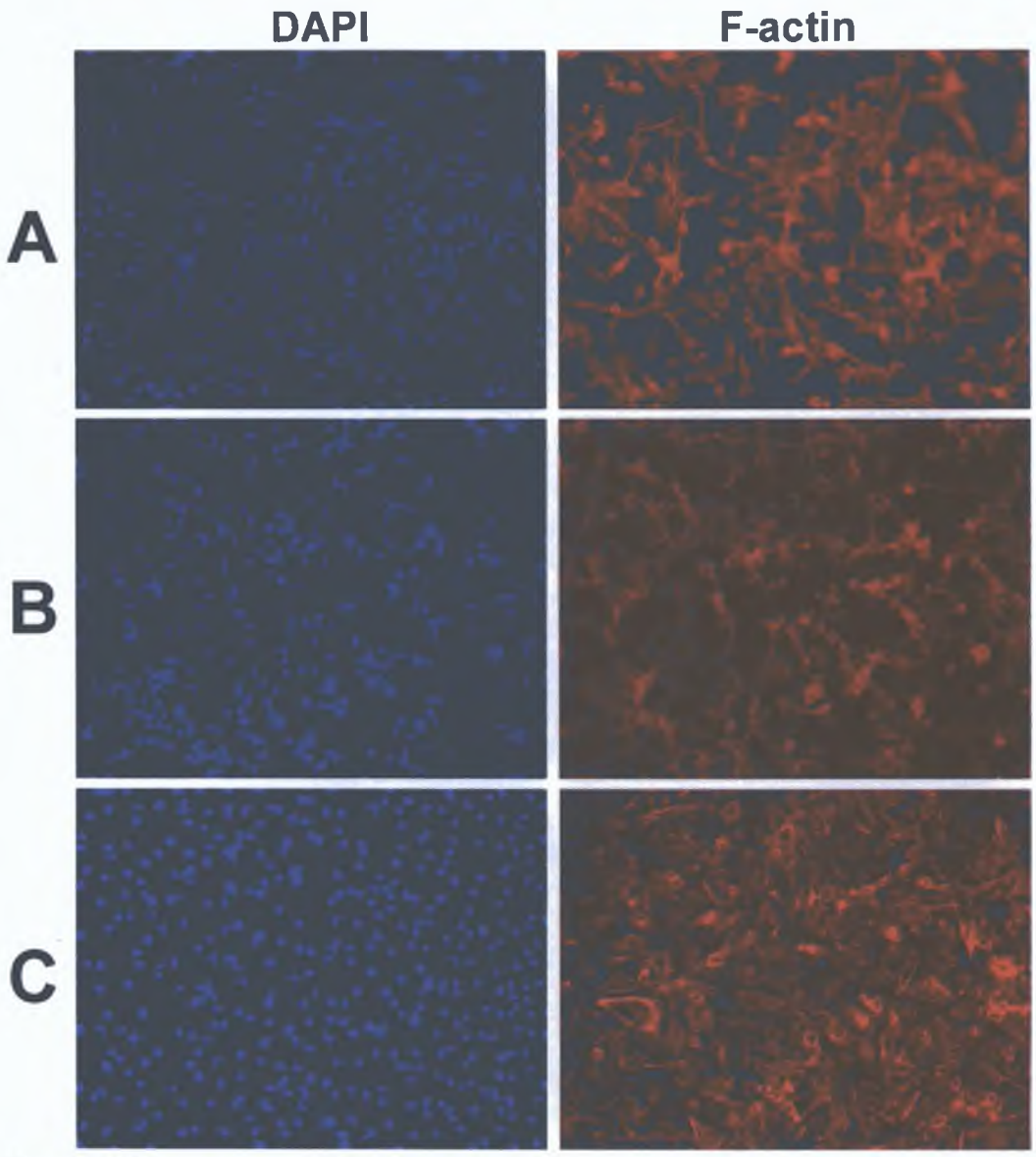

Figure 4.18 **F-actin staining of BAEC cultured on PVA-Chitosan membranes and control wells.** Following a 96 hr growth period, cells were fixed to the membranes with 3% formaldehyde in PBS, stained with Alexa Fluor 546 phalloidin and DAPI and viewed under a fluorescent microscope. Representative F-actin and corresponding DAPI images of BAEC on: (A) PVA-Chitosan IS-1, (B) PVA-Chitosan WS-1 and (C) control well. Magnification 20X, n = 3.

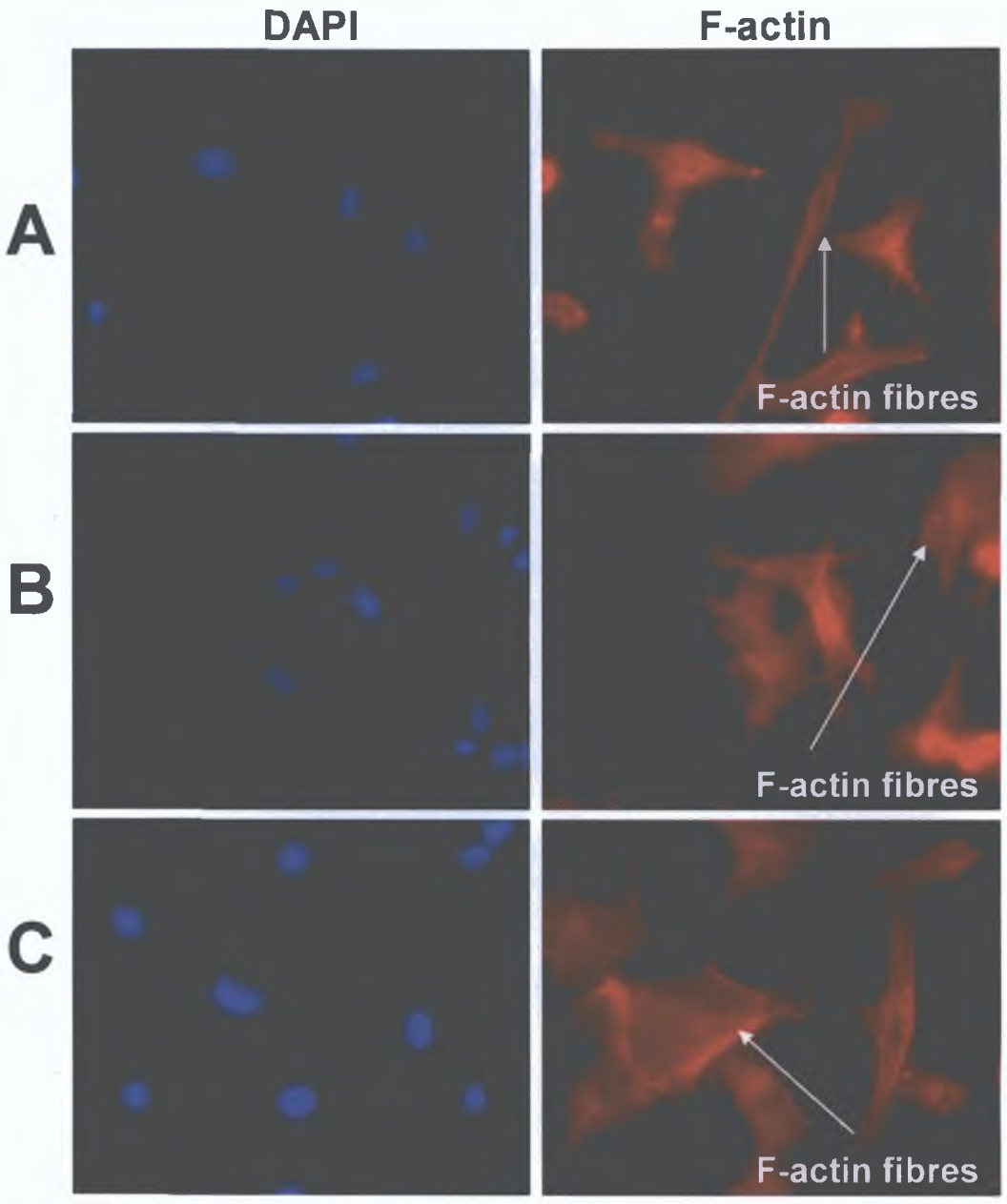

Figure 4.19 **F-actin staining of BAEC cultured on PVA-Chitosan membranes and control wells.** Following a 96 hr growth period, cells were fixed to the membranes with 3% formaldehyde in PBS, stained with Alexa Fluor 546 phalloidin and DAPI and viewed under a fluorescent microscope. Representative F-actin and corresponding DAPI images of BAEC on: (A) PVA-Chitosan IS-1, (B) PVA-Chitosan WS-1 and (C) control well. Magnification 60X, n =3.

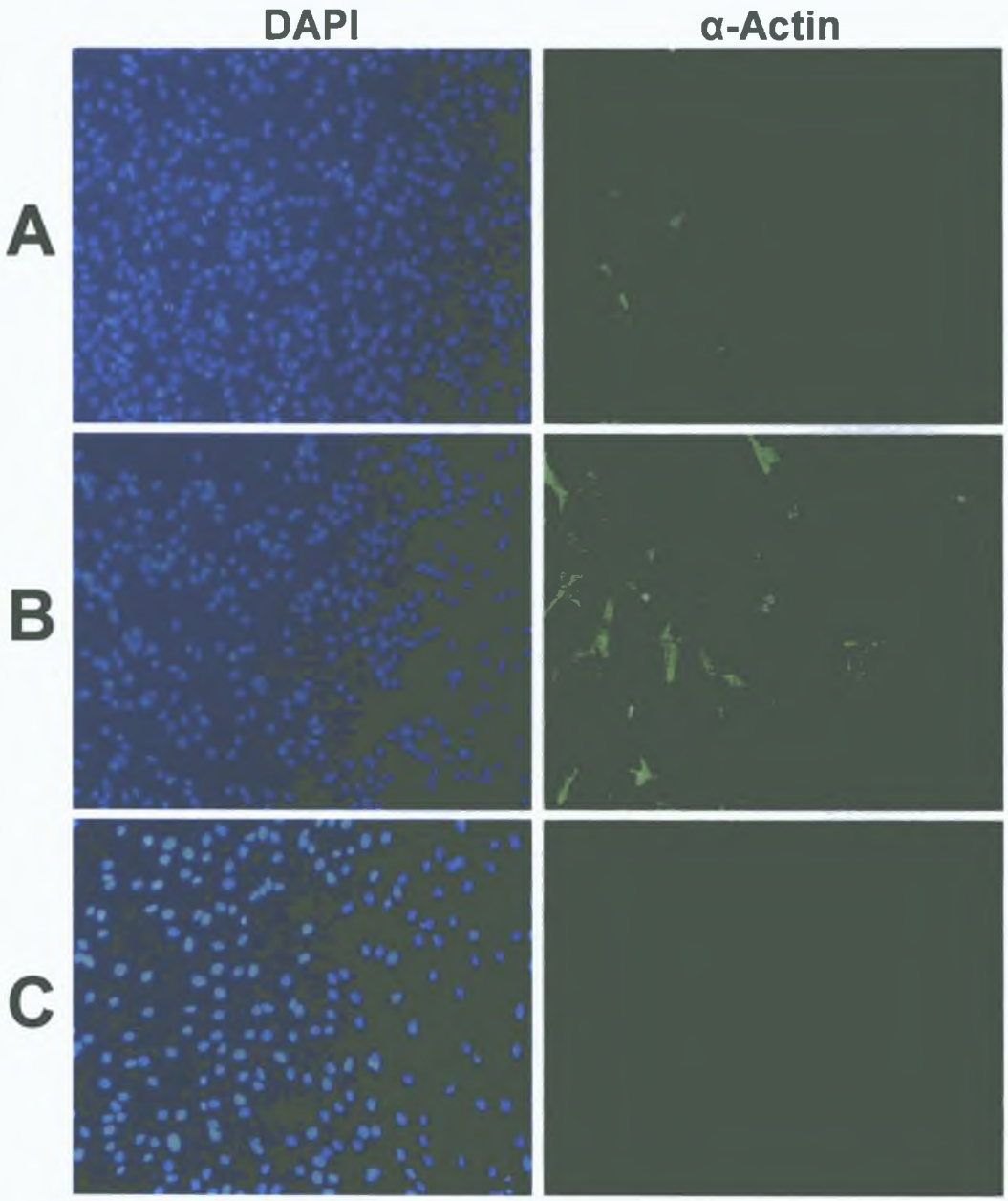

Figure 4.20 **α-Actin stain of BAEC cultured on PVA-Chitosan membranes and control wells.** Following a 96 hr growth period, cells were fixed to the membranes with 3% formaldehyde in PBS, stained with the primary antibody "monoclonal anti-α-smooth muscle cell actin", the secondary antibody "anti-mouse Alexa Fluor 488" and DAPI. Finally cells were viewed under a fluorescent microscope. Representative α-actin and corresponding DAPI images of BASMC on: (A) PVA-Chitosan IS-1, (B) PVA-Chitosan WS-1 and (C) control well. Magnification 10X, n = 3.

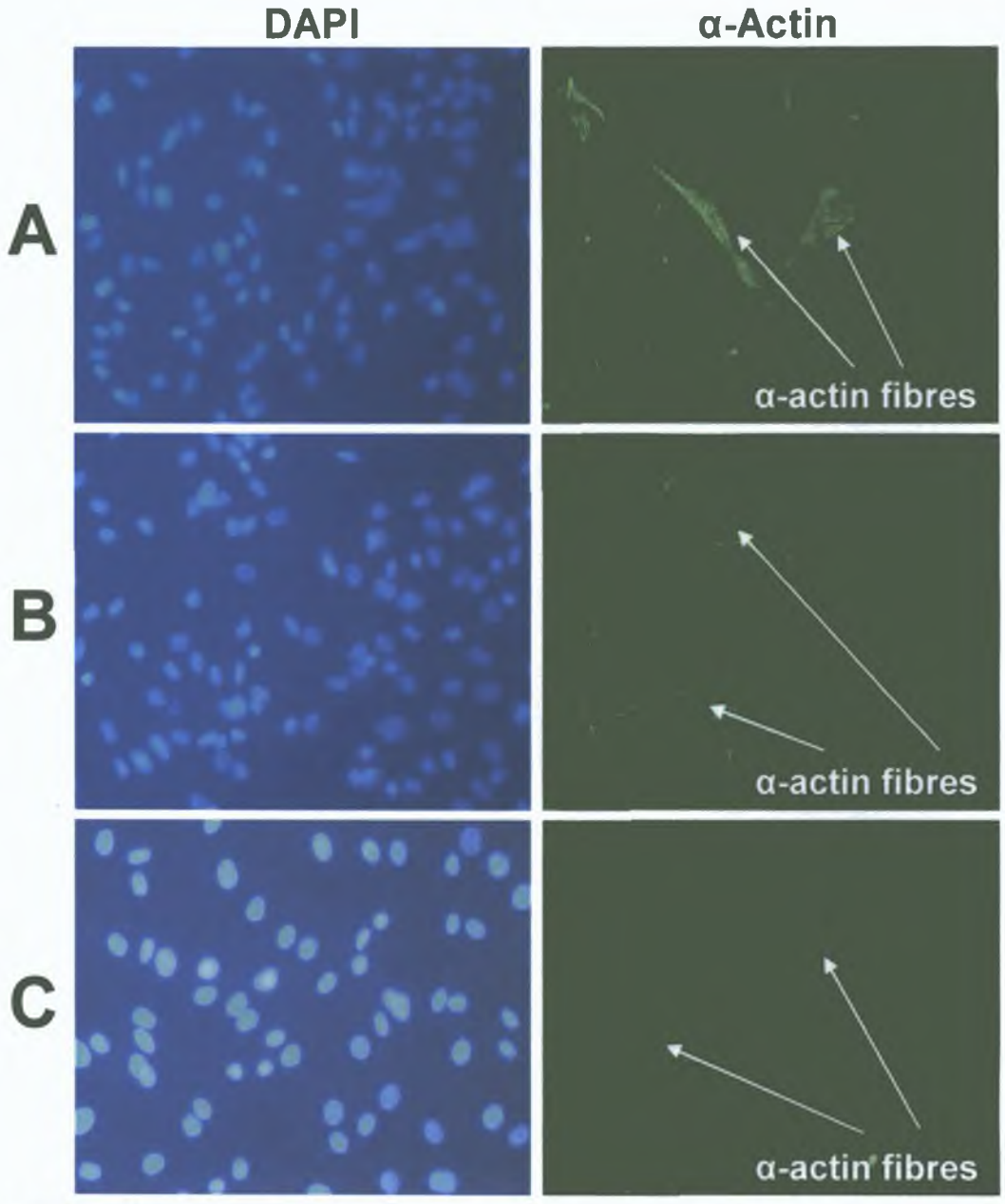

Figure 4.21 **α-Actin stain of BAEC cultured on PVA-Chitosan membranes and control wells.** Following a 96 hr growth period, cells were fixed to the membranes with 3% formaldehyde in PBS, stained with the primary antibody "monoclonal anti-α-smooth muscle cell actin", the secondary antibody "anti-mouse Alexa Fluor 488" and DAPI. Finally cells were viewed under a fluorescent microscope. Representative α-actin and corresponding DAPI images of BASMC on: (A) PVA-Chitosan IS-1, (B) PVA-Chitosan WS-1 and (C) control well. Magnification 20X, n = 3.

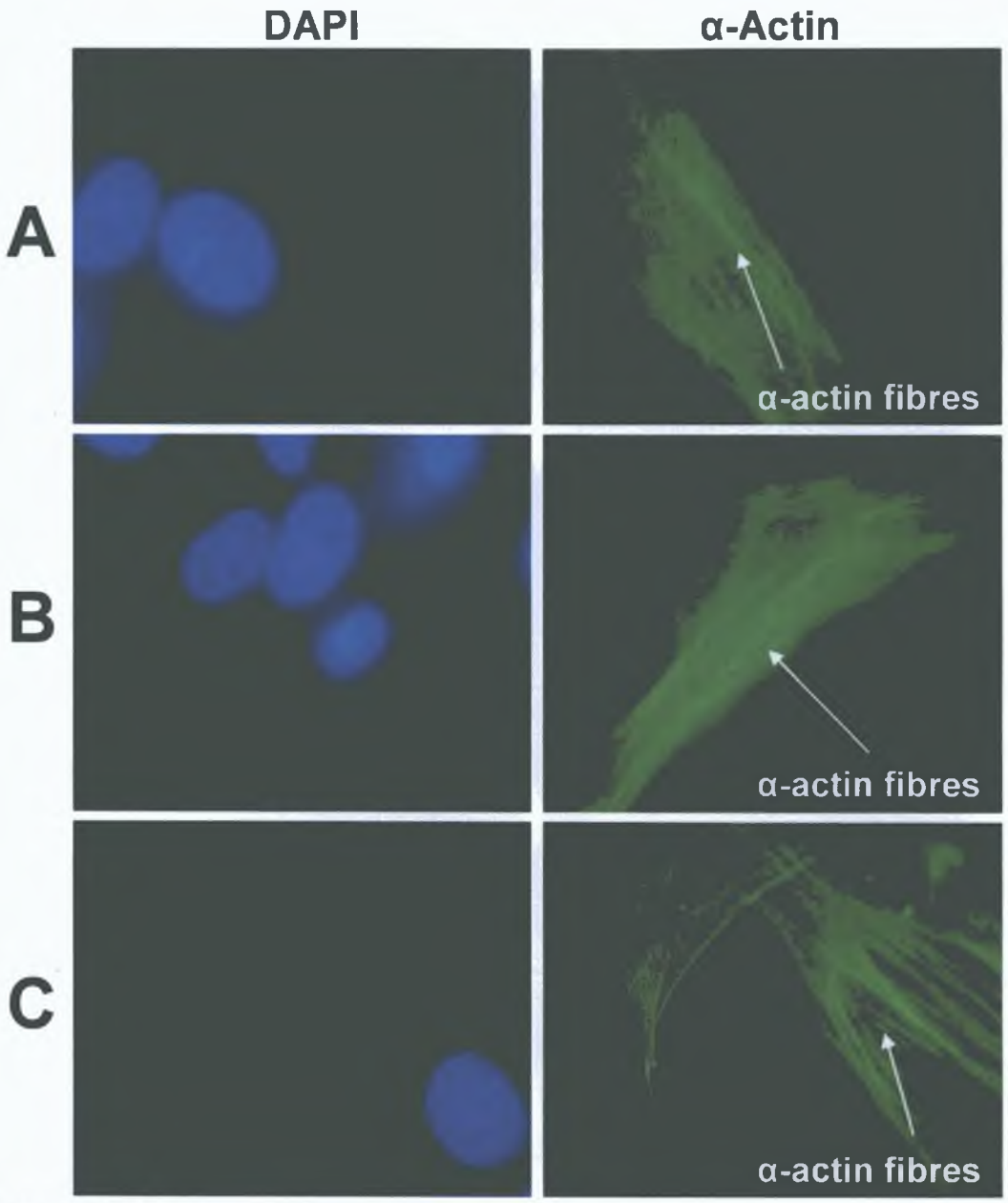

Figure 4.22 **α-Actin stain of BAEC cultured on PVA-Chitosan membranes and control wells.** Following a 96 hr growth period, cells were fixed to the membranes with 3% formaldehyde in PBS, stained with the primary antibody "monoclonal anti-α-smooth muscle cell actin", the secondary antibody "anti-mouse Alexa Fluor 488" and DAPI. Finally cells were viewed under a fluorescent microscope. Representative α-actin and corresponding DAPI images of BASMC on: (A) PVA-Chitosan IS-1, (B) PVA-Chitosan WS-1 and (C) control well. Magnification 100X, n = 3.

orientation of the fibres was evident on the PVA-chitosan IS-1 and WS-1 membranes as well as the control well. These findings suggest that despite the fact that there were some BASMC morphological changes on the membranes, the BASMC on the PVA-chitosan blended membranes had similar fibrous characteristics to the cells on the control sample.

Von Willebrand Factor

Von Willebrand Factor was also used to verify the presence of healthy BAEC on the PVA-chitosan fabricated membranes. Figure 4.23 shows the DAPI and corresponding Von Willebrand Factor images. The green fluorescence dispersed throughout the cell signifying that the cells were indeed BAEC. A confluent layer of cells was apparent on the control well and PVA-chitosan WS-1 membrane. An absence of Von Willebrand Factor in BAEC on the PVA-chitosan membranes would indicate that the morphological changes that the cells underwent after contact with the biomaterial was having a detrimental effect on the BAEC.

4.8.3 Cell Fate

Cell Proliferation Assay

In light of the previous findings, a cell proliferation assay was conducted to determine how proliferation of the vascular cells on the PVA-chitosan WS-1 compared to the control well. The PVA-chitosan WS-1 membrane was chosen (instead of the PVA-chitosan IS-1 membrane) due to the fact cell adhesion and distribution on this membrane most closely resembled that of the control well. To determine the proliferation characteristics of BAEC and BASMC on the PVA-chitosan WS-1 membrane, the cells were analysed on Day 2 and again on Day 7. To obtain the proliferation data from the cell suspension, a scatter graph of the cells was obtained (Figure 4.24).The x and y axis represent forward scatter (approximate cell size) and side scatter (cell complexity) respectively. The primary cell population representing viable cells was selected and the proliferation activity of these cells only was analysed. In some cases a second cell population was evident which if included in the analysis could have a different proliferative rate. The proliferation of the cell population was determined by the relative fluorescence intensity of the cells. For illustration purposes, the inverse of the relative fluorescence intensity on a

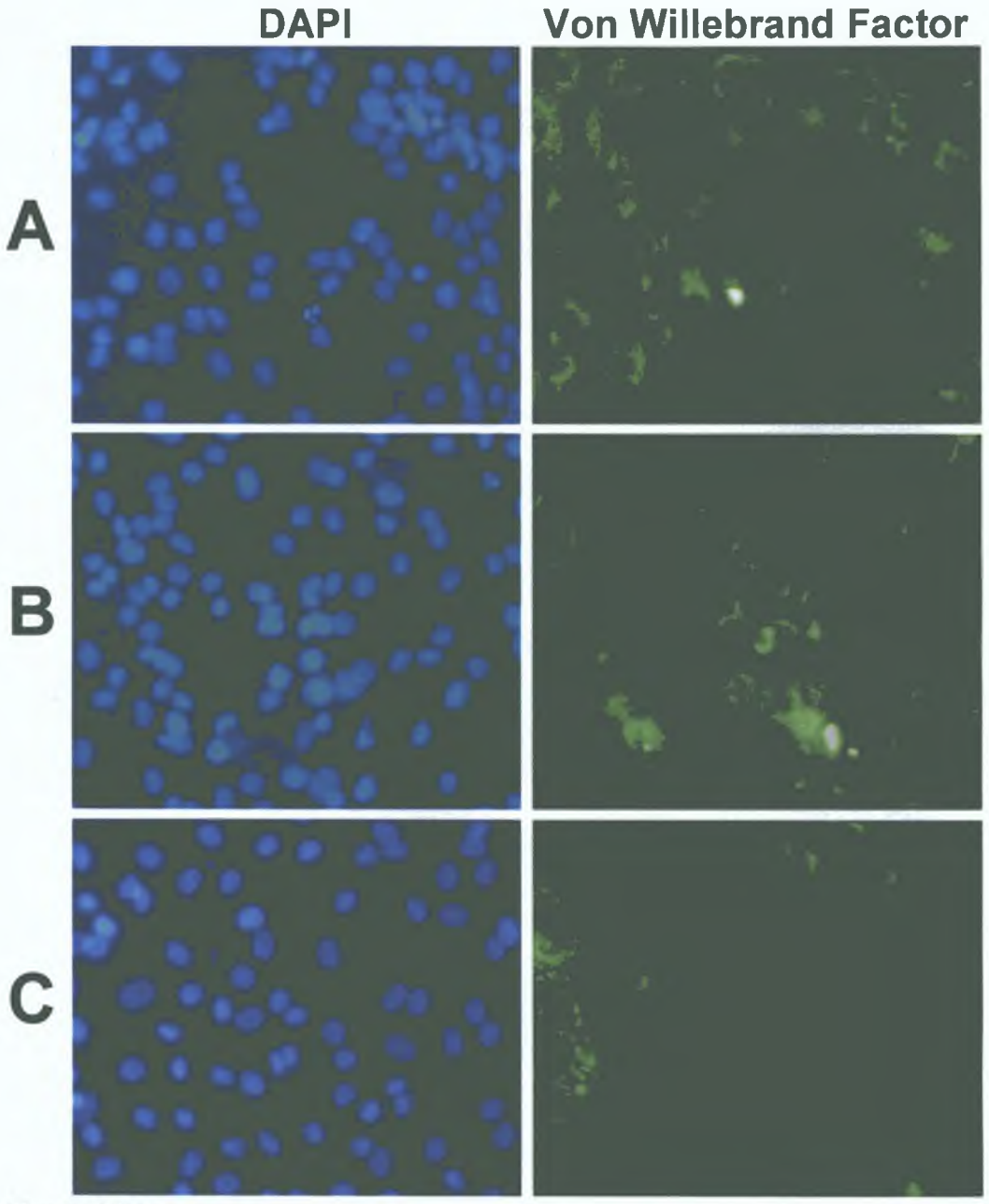

Figure 4.23 **Von Willebrand Factor staining of BAEC cultured on PVA-Chitosan membranes and control wells.** Following a 96 hr growth period, cells were fixed to the membranes with 3% formaldehyde in PBS, stained with the primary antibody "Polyclonal rabbit anti-human Von Willebrand Factor", the secondary antibody "anti-rabbit Alexa Fluor 488" and DAPI. Finally cells were viewed under a fluorescent microscope. Representative Von Willebrand Factor and corresponding DAPI images of BAEC on: (A) PVA-Chitosan IS-1, (B) PVA-Chitosan WS-1 and (C) control well. Magnification 20X, n = 3.

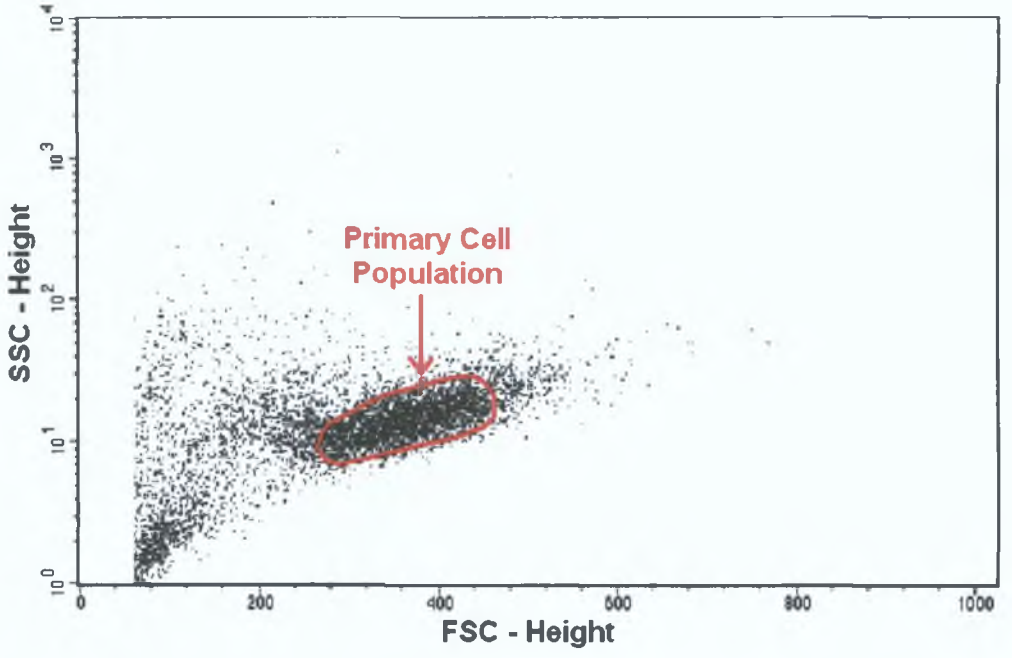

Figure 4.24 Flow cytometry scatter plot of BASMC (Control well - Day 0) stained with fluorescent marker CFDA SE.

logarithmic scaled graph was used to demonstrate proliferation of cells on samples.

Following quiescence of BAEC, similar proliferative activity was evident on the PVA-chitosan WS-1 membrane ($3.7 \times 10^{-4} \pm 8.6 \times 10^{-5}$) and the control well ($4.6 \times 10^{-4} \pm 6.7 \times 10^{-5}$) on Day 2 (Figure 4.25, A). There was also comparable proliferative activity for BAEC on the control well ($1.7 \times 10^{-2} \pm 4.58 \times 10^{-3}$) and PVA-chitosan WS-1 membrane ($1.92 \times 10^{-2} \pm 6.15 \times 10^{-3}$) Day 7. Figure 4.25 (B) shows a representative time-dependent analysis of the proliferative activity of BAEC seeded onto PVA-chitosan WS-1 membranes and control wells where proliferation was a measure of the relative fluorescence intensity. An increase in the proliferation on Day 7 from Day 2 was determined by a reduction in the relative fluorescence intensity (left shift of the curve on the graph), the greater the reduction in the fluorescence intensity the greater the proliferation of the cells. The analysis also suggests that there were some BAEC on the membranes which had different proliferation rates implying BAEC from a secondary cell population were analysed. This may have been due to the fact the BAEC were harvested from three membranes compared to one control well.

The proliferation study of BASMC illustrated some interesting findings (Figure 4.26, A). Comparable to the BAEC, proliferation of BASMC on the PVA-

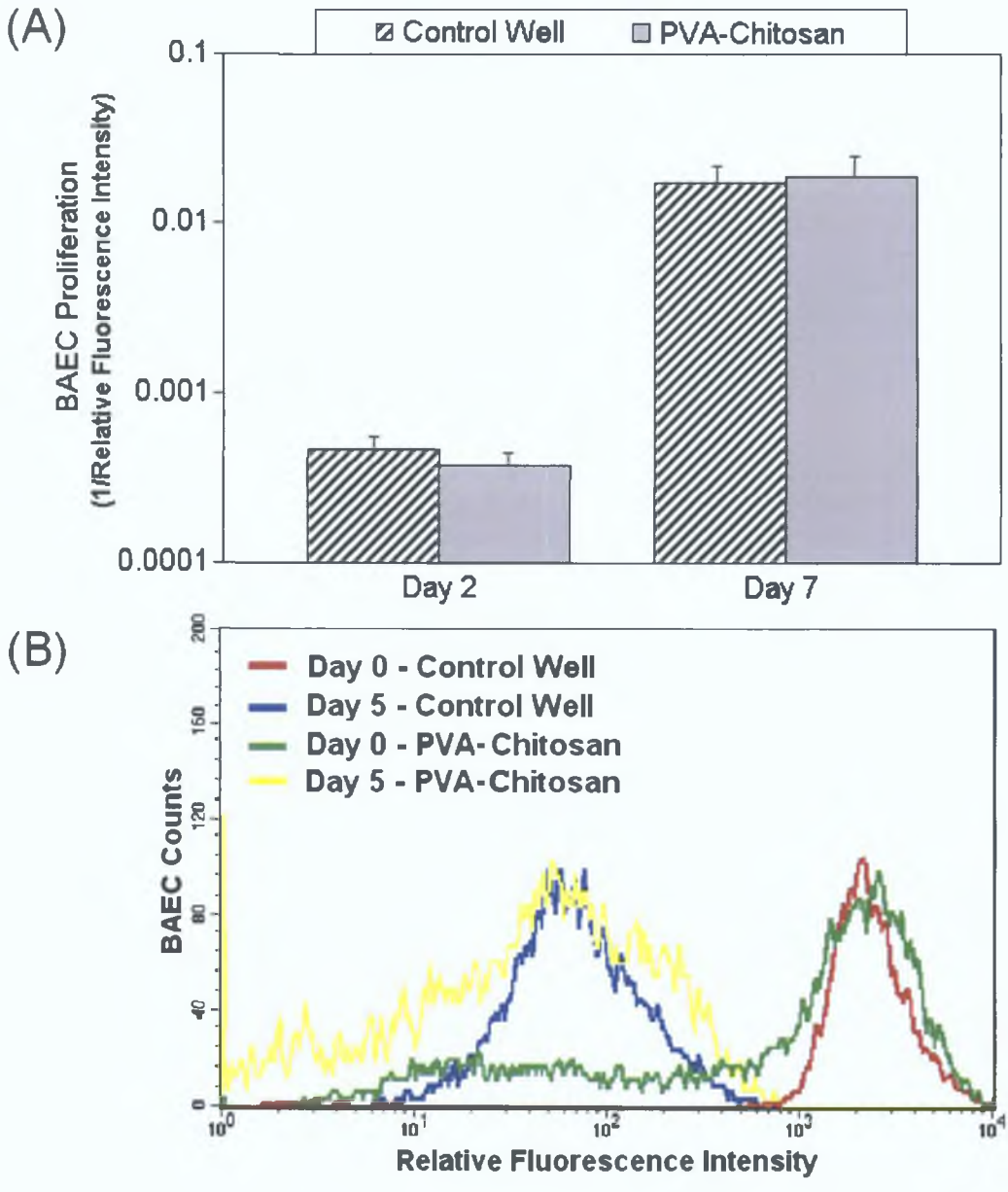

Figure 4.25 **Proliferative activity of BAEC cultured on PVA-Chitosan membranes and control wells.** Following a 24 hr adhesion period, the BAEC were pre-labeled with the fluorescent marker CFDA SE and quiesced for 24 hr (Day 2) and cultured for a further five days (Day 7). Cell suspensions were harvested and analysed by FACS on Day 2 and Day 7. (A) A time-dependent analysis of the proliferative activity of BAEC seeded onto PVA-chitosan WS-1 membranes and control wells. Graph showing BAEC proliferation (1/Relative Fluorescence Intensity) on control well and PVA-chitosan WS-1 membrane on Day 2 and Day 7 (n = 3). (B) A representative time-dependent analysis of the proliferative activity of BAEC seeded onto PVA-chitosan WS-1 membranes and control wells. Graph showing a representative analysis of BAEC division on control well and PVA-chitosan WS-1 membrane on Day 2 and Day 7.

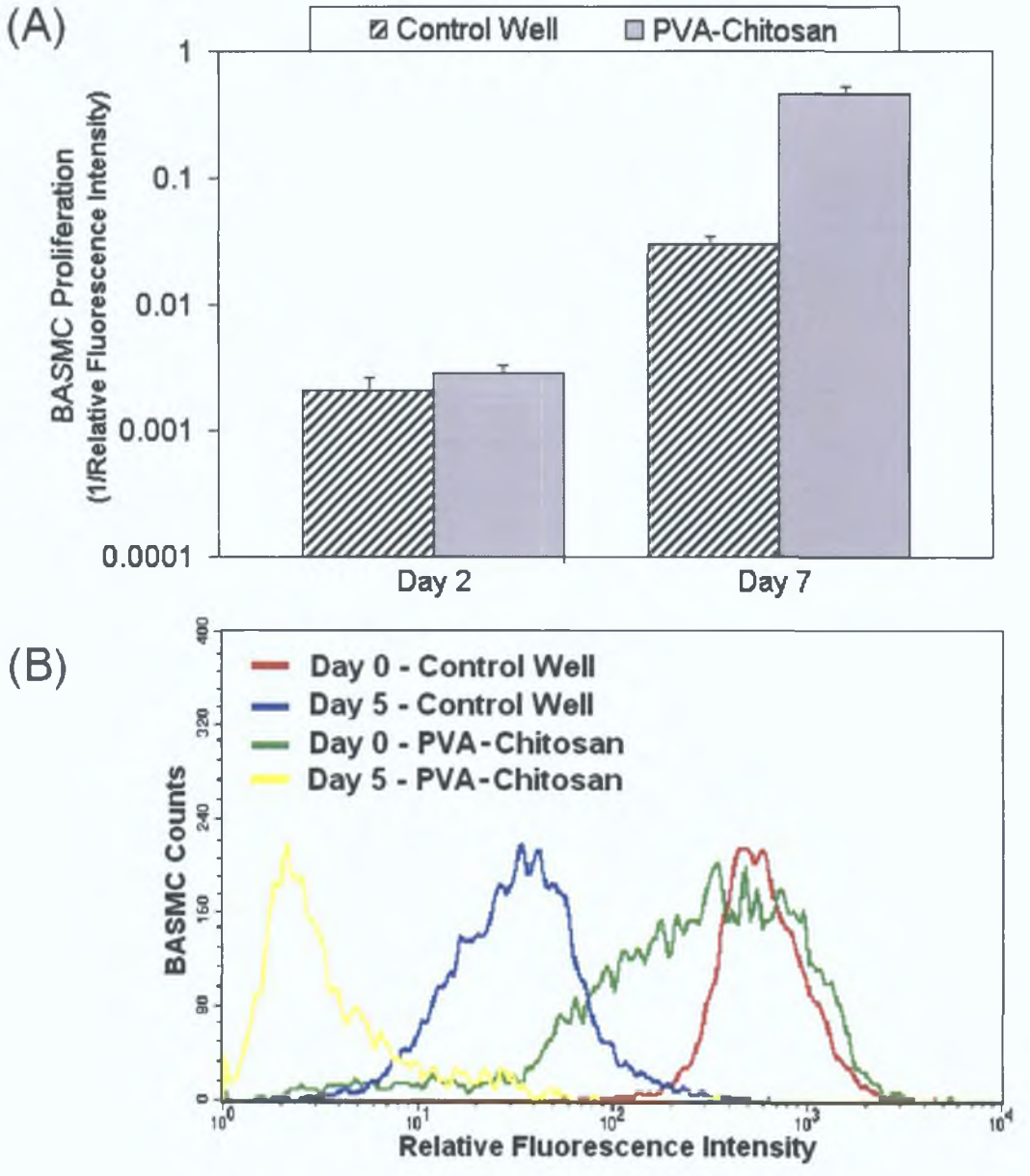

Figure 4.26 Proliferative activity of BASMC cultured on PVA-Chitosan membranes and control wells. Following a 24 hr adhesion period, the BASMC were pre-labeled with the fluorescent marker CFDA SE and quiesced for 24 hr (Day 2) and cultured for a further five days (Day 7). Cell suspensions were harvested and analysed by FACS on Day 2 and Day 7. (A) A time-dependent analysis of the proliferative activity of BAEC seeded onto PVA-chitosan WS-1 membranes and control wells. Graph showing BASMC proliferation (1/Relative Fluorescence Intensity) on control well and PVA-chitosan WS-1 membrane on Day 2 and Day 7 (n = 3). (B) A representative time-dependent analysis of the proliferative activity of BASMC seeded onto PVA-chitosan WS-1 membranes and control wells. Graph showing a representative analysis of BASMCC division on control well and PVA-chitosan WS-1 membrane on Day 2 and Day 7.

chitosan WS-1 membrane showed similar characteristics to the control well on Day 2. After Day 7, it was noted that there was significantly greater proliferation activity on the PVA-chitosan WS-1 membrane compared to the control well. A representative time-dependent analysis of the proliferative activity of BASMC seeded onto PVA-chitosan WS-1 membranes and control wells where proliferation was a measure of the relative fluorescence intensity is shown in Figure 4.26 (B). It is clear from this representation that a small number of BASMC on the PVA-chitosan WS-1 membrane on Day 2 were not in equivalent proliferative states or sufficiently quiesced.

Cell Apoptosis Assay

While it is evident that the vascular cells adhere and proliferate it was equally important to establish whether the PVA-chitosan blended membranes adversely influenced cell viability. As previously described (Section 4.9.3), the viable cell population was selected to be analysed by FACS. Viable, apoptotic and necrotic cells were detected as shown in Figure 4.27. The percentage of apoptotic cells could then be obtained.

To investigate the apoptotic response of BAEC on the PVA-chitosan WS-1 membrane, the state and activity of the cells were analysed on Day 2 and again on Day 7 and compared to equivalent control wells (Figure 4.28). The flow cytometry analysis indicated that on Day 2, greater apoptosis occurred in BAEC plated on the PVA-chitosan WS-1 membrane compared to control (15.5 ± 3.5 % versus 12.5 ± 3 % respectively, n = 3). On Day 7, there was a small but non-significant reduction on the apoptotic levels of the BAEC on the PVA-chitosan WS-1 membrane and the control well (12.8 ± 2.5 % and 10.1 ± 1.5 % respectively, n = 3). While the apoptotic levels of the BAEC on the PVA-chitosan WS-1 membrane were greater than the control well, they were not significantly higher as to suggest that the PVA-chitosan blended membranes were directly responsible for the apoptotic behaviour of the BAEC. Also the level of reduction in the apoptosis from Day 2 to Day 7 was comparable for the control well and PVA-chitosan blended membranes.

With respect to the apoptotic behaviour of BASMC, a non-significant increase in apoptosis was observed in cells plated on the PVA-chitosan WS-1

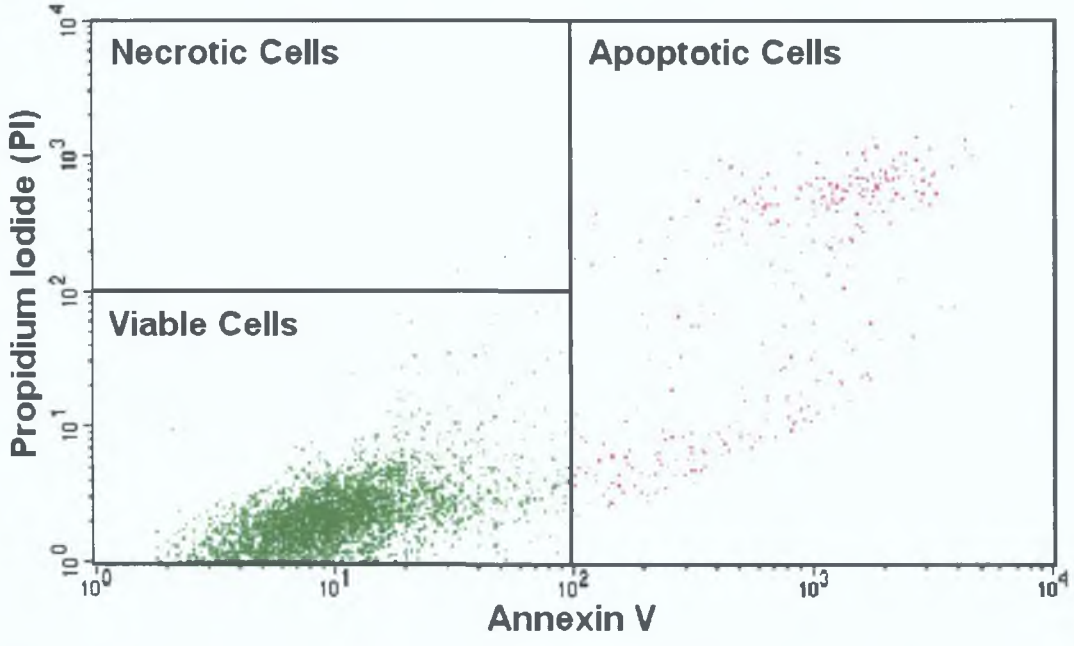

Figure 4.27 **Flow cytometry patterns of BASMC (Control well - Day 2) stained with annexin V and PI.**

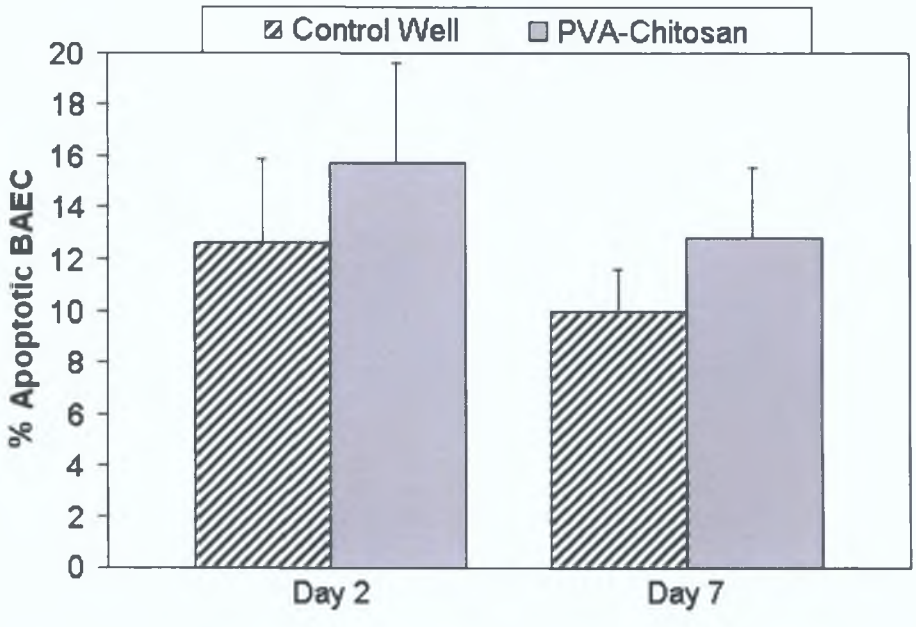

Figure 4.28 **Time-dependent apoptotic profile of BAEC seeded onto PVA-chitosan WS-1 membranes and control wells.** Following a 24 hr adhesion period, the cells were quiesced for 12 hr (Day 2) and cultured for a further five days (Day 7). Cell suspensions were harvested and analysed on Day 2 and Day 7 and stained with Alexa Fluor 488-conjugated annexin V and propidium iodide nucleic acid stains before being analysed by FACS. Graph showing percentage apoptotic of BAEC on control well and PVA-chitosan WS-1 membrane on Day 2 and Day 7 (n = 3).

membrane compared to control (12 ± 2.3 % versus 10.5 ± 1.8 % respectively, n = 3; Figure 4.29) at Day 2. A significant reduction in the apoptotic levels of the BASMC on both the control well and the PVA-chitosan WS-1 membrane was evident on Day 7 (2.8 ± 1.2 % and 5.5 ± 1.3 % respectively, n = 3). In terms of the apoptotic behaviour of the BASMC on the control well versus the PVA-chitosan WS-1 membrane, there was greater apoptosis on the PVA-chitosan WS-1 membrane, however it was not significantly greater than the control well. In addition, the difference in the ratios of apoptosis on the PVA-chitosan WS-1 membrane did not dramatically increase from Day 2 to Day 7 suggesting that the BASMC can remain viable on the PVA-chitosan membranes for long term cell culture studies.

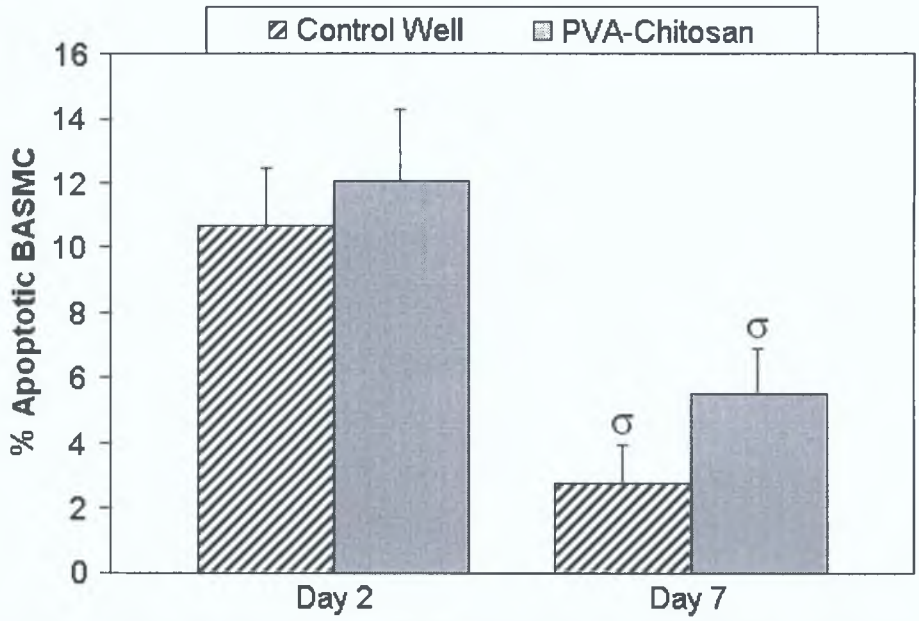

Figure 4.29 **Time-dependent apoptotic activity of BASMC seeded onto PVA-chitosan WS-1 membranes and control wells.** Following a 24 hr adhesion period, the cells were quiesced for 12 hr (Day 2) and cultured for a further five days (Day 7). Cell suspensions were harvested and analysed on Day 2 and Day 7 and stained with Alexa Fluor 488-conjugated annexin V and propidium iodide nucleic acid stains before being analysed by FACS. Graph showing percentage apoptotic of BASMC on control well and PVA-chitosan WS-1 membrane on Day 2 and Day 7 (n = 3). σ, $p<0.05$ as compared to control well (student's t test).

4.8.4 Shear Stress

The effect of low level physiological shear stress on the proliferative and apoptotic behaviour of BAEC was analysed using flow cytometry, as previously

described in section 4.7. There was no significant difference between the proliferative activity of the BAEC cultured on the control wells or the PVA-chitosan membrane on Day 2 (Figure 4.30). Increased proliferation of BAEC was evident on Day 3, however there was no significant difference in the proliferation of BAEC that were statically cultured and those that were subjected to shear stress. Comparable proliferative rates of BAEC were apparent on the control well and the PVA-chitosan membrane. In this 24 hr study, low level shear stress did not cause any increase in BAEC proliferation on either the control well or the PVA-chitosan WS-1 membrane. Therefore the BAEC behaved similarly under both static and shear conditions. A representative time-dependent analysis of the proliferative activity of BASMC seeded onto control wells and PVA-chitosan WS-1 membranes where proliferation was a measure of the relative fluorescence intensity is shown in Figure 4.31 (A & B).

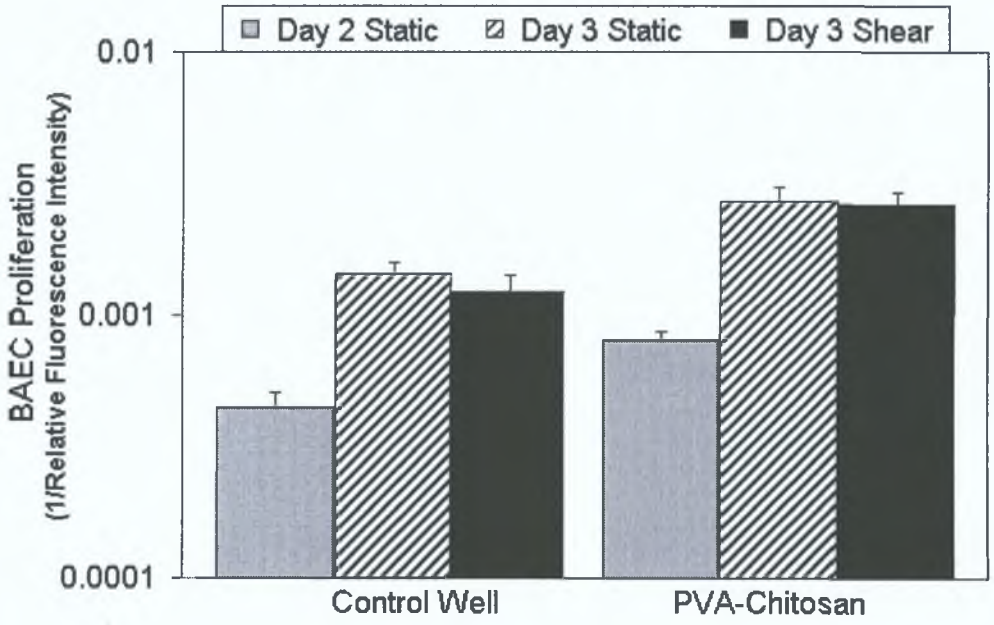

Figure 4.30 **A time-dependent analysis of the proliferative activity of BAEC seeded onto control wells under static and shear (shear stress = 0.38 N/m2) culture conditions.** Following a 24 hr adhesion period, the cells were pre-labeled with the fluorescent marker CFDA SE and quiesced for 12 hr (Day 2). Static or shear culture followed for 24 hr (Day 3). Cell suspensions were harvested and analysed by FACS on Day 2 and Day 3. Graph showing BAEC proliferation (1/Relative Fluorescence Intensity) on control well and PVA-chitosan WS-1 membrane under static and shear culture conditions on Day 2 and Day 3 (n = 3).

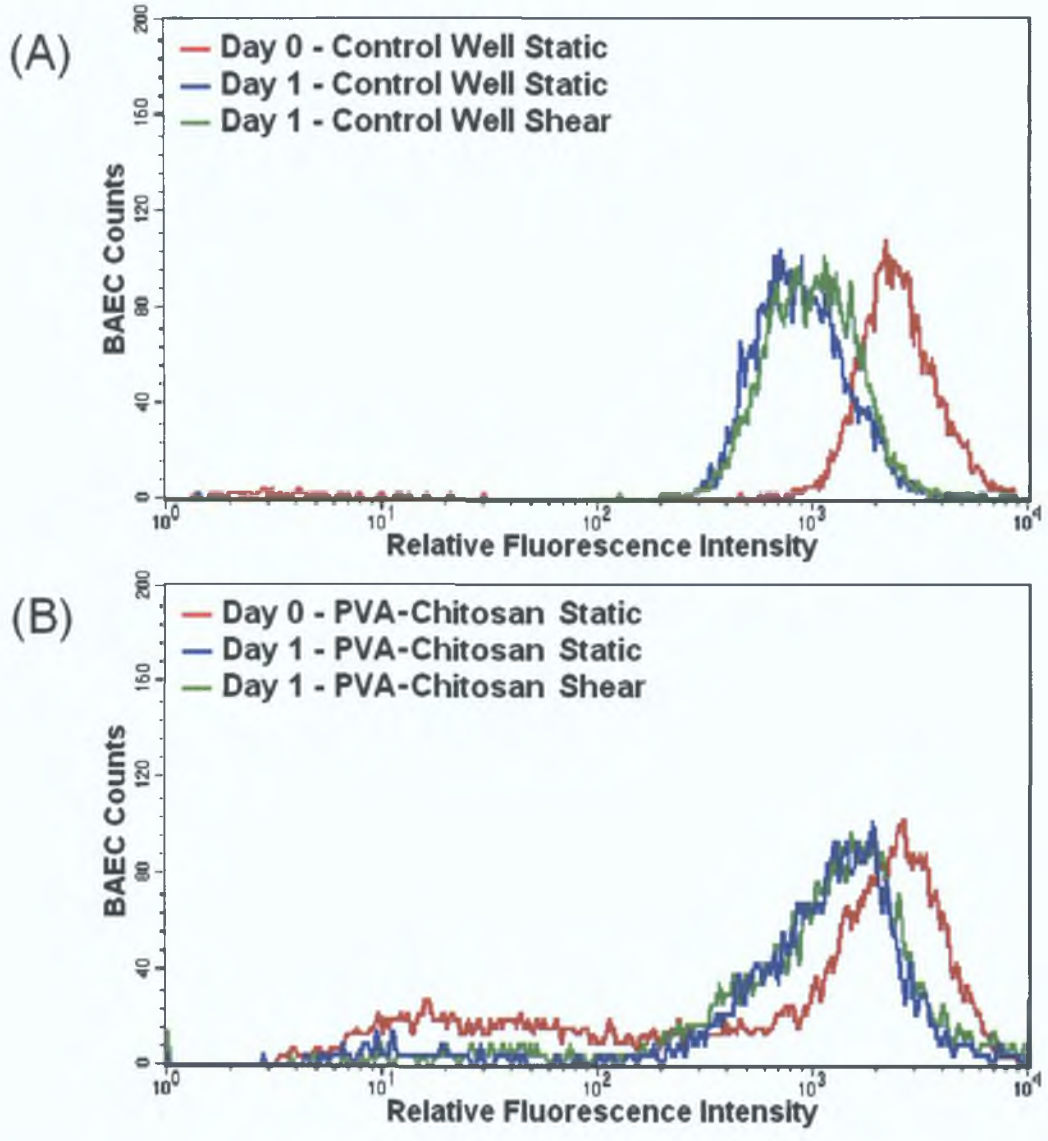

Figure 4.31 **Representative analyses of BAEC cultured onto PVA-chitosan membranes and control wells under static and shear culture conditions.** Following a 24 hr adhesion period, the cells were pre-labeled with the fluorescent marker CFDA SE and quiesced for 12 hr (Day 2). Static or shear (shear stress = 0.38 N/m^2) culture followed for 24 hr (Day 3). Cell suspensions were harvested and analysed by FACS on Day 2 and Day 3. Graphs showing representative analyses of BAEC division on control well and PVA-chitosan WS-1 membranes under static and shear culture conditions on Day 2 and Day 3 (A) A representative time-dependent analysis of the proliferative activity of BAEC seeded onto control wells under static and shear culture conditions (B) A representative time-dependent analysis of the proliferative activity of BAEC seeded onto PVA-chitosan WS-1 membranes under static and shear culture conditions.

The apoptotic behaviour of the BAEC was also studied and compared to control well (Figure 4.32). It was noted that the average apoptosis levels on the control well remained at ~12.5 ± 3 % on Day 2 and Day 3 under both static and shear

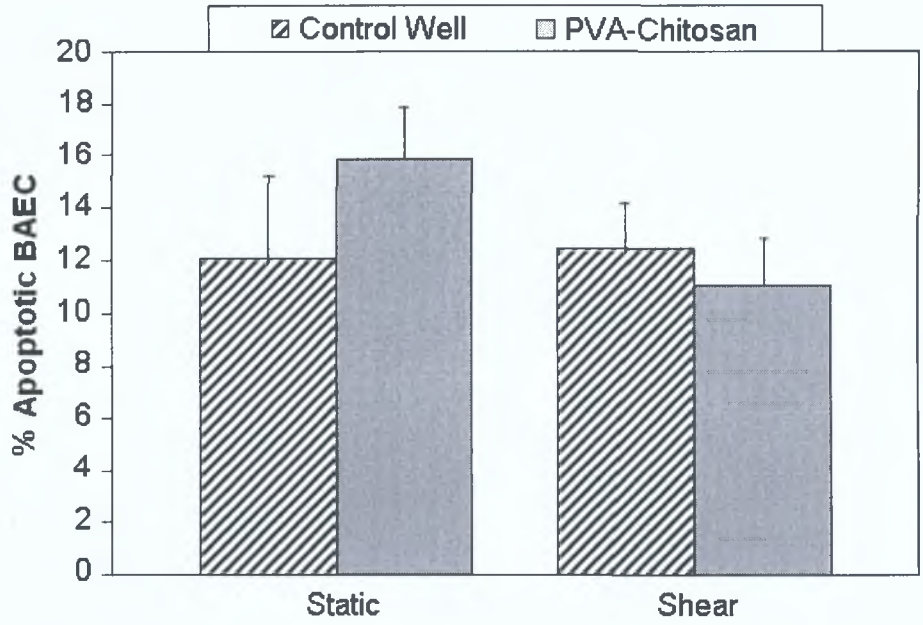

Figure 4.32 A time-dependent effect on the apoptotic activity of BAEC that were seeded onto PVA-chitosan WS-1 membranes and control wells under static and shear (shear stress = 0.38 N/m2) culture conditions. Following a 24 hr adhesion period, the cells were quiesced for 12 hr (Day 2) and cultured for a further 24 hr (Day 3) under static or shear conditions. Cell suspensions were harvested and analysed on Day 3 and stained with Alexa Fluor 488-conjugated annexin V and propidium iodide nucleic acid stains before being analysed by FACS. Graph showing percentage apoptotic of BAEC on control well and PVA-chitosan WS-1 membrane on Day 3 under static and shear culture conditions (n = 3).

culture conditions. However, while there was ~15 ± 2.5 % apoptosis on the PVA-chitosan WS-1 membrane on Day 2 and Day 3 under static culture conditions, the was a reduction of apoptosis of the BAEC subjected to shear stress to ~11.06 ± 1.75 % on the PVA-chitosan WS-1 membrane on Day 3. In support of this, it is well documented that shear stress inhibits apoptosis of endothelial cells [171]. Shear stress did not significantly affect the levels of apoptosis on the control well or the PVA-chitosan WS-1 membrane.

4.9 Discussion

The adhesion and growth of BAEC and BASMC on PVA-chitosan blended membranes were evaluated. Cell morphology and cell viability were investigated by immunocytochemical techniques and FACS analysis respectively. PVA has been used in many biomedical applications [127,131-136,144,172,173] however, different

biological macromolecules such as chitosan, collagen, fibronectin and peptides [171] have been used in conjunction with PVA to improve its cell compatibility. While initial results have proved promising [96,97,127,128,171], the fabrication techniques and biological macromolecules for all but chitosan are very expensive. Chitosan is a natural biocompatible product [139] which has been shown to enhance fibroblast cell attachment on PVA-chitosan blended membranes [96]. In this study, water-soluble and insoluble chitosan were blended with PVA. To the author's knowledge, water-soluble chitosan has not been used in any previous cell culture studies.

The results of the cell adhesion study show that BAEC and BASMC, like fibroblast cells [96], successfully adhered to the PVA-chitosan membranes for all chitosan percentages and for both solubility types. However, an optimum quantity and percentage of chitosan solution must be blended to the PVA in order to achieve similar vascular cell adhesion and growth activity on the membranes to that of cells cultured in control wells. The surfaces of the different PVA-chitosan blended membranes had different consequences for the vascular cells, PVA-chitosan WS-1 displaying the best cell adhesion and PVA-chitosan WS-6 the poorest. Both BAEC and BASMC displayed similar cell adhesion characteristics on the different membranes. BAEC and BASMC growth on all PVA-chitosan membranes displayed webbing characteristics. Cells were most evenly distributed on PVA-chitosan IS-1 and WS-1 membranes. Clumping of cells were apparent for both cell types as the percentage of the chitosan solution was increased to 2 % or reduced to 0.5 % while cells were sparsely distributed on the PVA-chitosan WS-6 membrane.

Although cellular adhesion to the PVA-chitosan membrane is important, the subsequent cell response to the biomaterial is imperative. The presence of Von Willebrand Factor confirmed that BAEC were growing and indicated that the BAEC were behaving similarly on the PVA-chitosan membranes and the control wells. The cells attached and spread on the PVA-chitosan WS-1 and IS-1 membranes without perceptible deterioration to cell morphology of BAEC or BASMC as identified by the examination of the F-actin and α-actin fibres. In addition, it was also concluded that the choice of water-soluble or -insoluble chitosan had no significant bearing on the vascular cell adhesion properties or morphologies. For this reason, coupled with the ease of solubilisation, the water-soluble chitosan was selected for FACS and

shear studies.

A quantitative assay to investigate the function and behaviour of BAEC and BASMC on PVA-chitosan membranes over the typical time period of *in vitro* cell culture studies was also conducted. The flow cytometry studies revealed that the proliferative activity of the BAEC on the selected PVA-chitosan blended hydrogel membrane compared favourably to cells cultured on control wells. Additionally, the BASMC cultured on the selected PVA-chitosan membrane illustrated increased proliferation compared to the control. Moreover, it was also shown by FACS analysis that the vascular cells remained viable on the PVA-chitosan blended membranes for up to 7 days (7 days in total: cell seeded for 1 day, serum starved for 1 day, cultured for 5 days). While apoptosis was greater on the membranes compared to the control it was not significantly higher as to suggest that the increase was directly related to the composition of the membranes. Interestingly, on Day 7, greater proliferation and apoptosis levels on the membranes compared to the control were apparent. This is not surprising as apoptosis can play a positive role in cell culture. Cell death is crucial in tissue regeneration: the number of cells making up tissue in adults must be kept constant whilst assuring cell renewal and regulation of the balance between cellular proliferation and death [174]. Thus the link between cell proliferation and death is that the tendency of cells to undergo apoptosis is a normal consequence of the engagement of the cell's proliferative pathways [175]. To the authors knowledge, the quantitative assays to investigate the function and behaviour of BAEC and BASMC on PVA-chitosan membranes have not been previously reported.

In addition it has been demonstrated that BAEC adhered to these fabricated membranes and can endure low levels of shear stress (0.38 N/m^2 for 24 hr). This is an important characteristic as it suggests that more realistic *in vivo* situations may now be simulated using PVA-chitosan blended membranes for *in vitro* dynamic vascular cell culture studies. In a study by Elshazly [10], PVA coated with a layer of Type 1 purified collagen has been shown permit BAEC adhesion with an adhesion strength to the material surface *in vitro* withstand physiologic flow (2 N/m^2 or 20 dynes/cm^2).

In light of the findings in this study it seems that the chitosan content on the surface of the membranes acts like an attachment protein for BAEC and BASMC, such as fibronectin, and subsequently could create an integral connection with the receptors on the cellular surface [176]. For cells that have receptors for chitosan, the amount of chitosan on the surface of the PVA-chitosan membranes appears to be a critical factor in controlling cell interactions within the biomaterial [177]. It is also necessary for the membrane to have a degree of rigidity to support the stress caused by the deformation and flattening of cells [176]. The cellular size in relation to the porosity of the membranes is another critical factor controlling cell adhesion and growth [178].

4.10 Conclusion

The findings of this study demonstrate that BAEC and BASMC adhere to the surface of a PVA-chitosan blended hydrogels and suggest that this material can provide a support scaffold for various bioreactor and tissue-engineering applications. The addition of chitosan to the PVA enhanced both BAEC and BASMC attachment and growth on the membranes.

The conclusions from this section are as follows:

- The concentration of the chitosan solutions blended with the PVA solution effects cell adhesion on the surface of the fabricated membranes.
- The use of water-soluble or insoluble chitosan showed no significant difference in the cell adhesion characteristics or cell morphologies.
- PVA-chitosan WS-1 and IS-1 displayed the best cell adhesion and growth (webbing) characteristics in comparison to control samples.
- Proliferation and apoptosis characteristics of vascular cells cultured on the PVA-chitosan WS-1 were favourable in comparison to cells cultured on control samples under static (BAEC and BASMC) and low level shear conditions (BAEC).

In conclusion, PVA-chitosan WS-1 and IS-1 membranes were selected to

study the mechanical and morphological properties. These mechanical and morphological test conditions and results which were based on the vascular cell growth and activity characteristics are presented in Chapter 5.

Chapter 5

Mechanical and Morphological Evaluation of Hydrogels

PVA-chitosan WS-1 and IS-1 membranes showed the best adhesion and growth characteristics, from the results presented in Chapter 4. These two membrane compositions were therefore selected for more detailed mechanical and morphological testing. The mechanical testing of these two membrane compositions are described and the results presented in this chapter.

The necessary mechanical properties of a vascular tissue substitute material include mechanical integrity, compliance properties similar to vascular tissue and ease of manufacture. Hydrogels possess many characteristics, such as tissue-like elasticity, permeability and mechanical strength that can be engineered for the application of choice [127] and the appearance and feel of PVA hydrogels are similar to native arterial tissue. Chu and Rutt [132] and O'Flynn *et al* [148] have developed PVA arterial vessels with similar mechanical properties to that of porcine aortas and human carotid arteries respectively.

In this study, mechanical testing of PVA, PVA-chitosan WS-1 and IS-1 hydrogels was conducted. PVA-chitosan WS-1 and IS-1 were selected for the mechanical and morphological evaluation study as they displayed similar cell adhesion, cell growth characteristics and cell morphologies in comparison to biological control samples (Chapter 4). To determine the effect of chitosan on the

mechanical and morphological characteristics of the PVA, pure PVA hydrogel membranes were also fabricated.

Uniaxial extension tests, bi-axial inflation tests, vessel inflation tests and opening angle observations were used to mechanically characterise the PVA, PVA-chitosan WS-1 and IS-1 blended hydrogels. The morphological characteristics of fabricated hydrogels were investigated by scanning electron microscopy (SEM).

5.1 Fabrication of Hydrogel Test Specimens

The hydrogel solutions were prepared and crosslinked as previously described in Section 4.3 (Figure 5.1 details a summary of the preparation process, as previously shown in Figure 4.3). The number of freeze-thaw cycles was varied in order to adapt the mechanical properties of the hydrogel solutions.

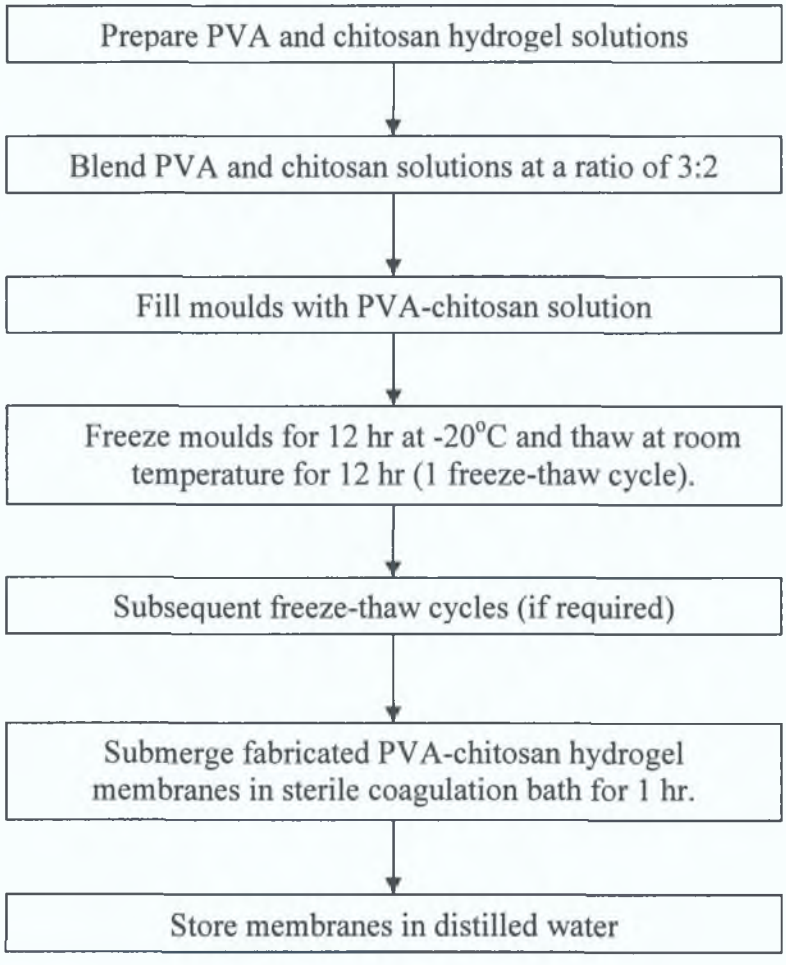

Figure 5.1 Schematic detailing the PVA-chitosan hydrogel membrane preparation process.

5.1.1 Uniaxial Tensile Specimens

A mould was manufactured from perspex to produce sheets of hydrogel 2.5mm in thickness. The mould was filled with the PVA-chitosan solution, frozen for 12 hr at -20 ^{o}C and thawed for 12 hr respectively (1 freeze-thaw cycle). Tests were conducted on the PVA, PVA-chitosan IS-1 and PVA-chitosan WS-1 hydrogels. The properties of the three blends of hydrogels were determined for 1, 2, 3 and 4 freeze-thaw cycles. The sheets of hydrogels were removed from the mould then submerged in a coagulation bath for 60 min after the final freeze-thaw cycle as previously described (Section 4.3).

In order to ensure consistent shape and dimensions for all test specimens a dogbone-shaped cutting device was designed and manufactured from stainless steel (Figure 5.2). The overall specimen size was 80 mm x 14 mm overall. The standard dogbone shape design was implemented to minimise the effects of stress concentrations in the grip contacting regions of the material and to control the location of fracture, i.e. to the middle of the test specimen. The filleted corners of the dogbone shaped samples enabled any stress concentrations at the end of the grips to be dissipated through these fillets at the end of each grip face providing gradual relief. Before testing the specimens, the thickness of each piece was measured using a depth micrometer. The middle segment of the specimen had a uniform cross-sectional area, and was assumed to undergo uniform reduction when the sample was subjected to tension. A ratio of 4:1 for the gauge length (12 mm): gauge width (4 mm) was incorporated in the design. The hydrogel tensile specimens were placed in distilled water at room temperature prior to use for up to 1 week. Uniaxial tensile specimens were fabricated for PVA, PVA-chitosan WS-1 and PVA-chitosan IS-1.

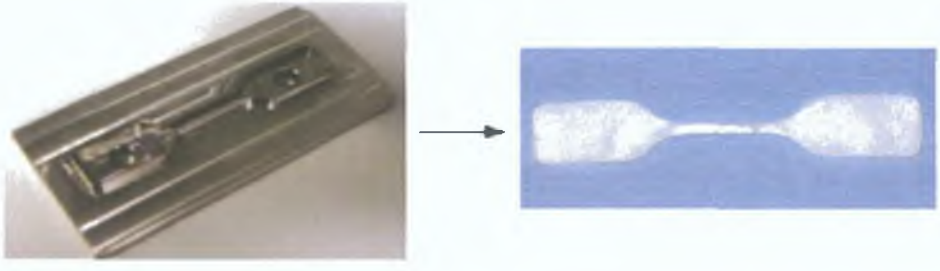

Figure 5.2 Stainless steel cutting device and dog-boned shaped PVA sample.

5.1.2 Biaxial Test Specimens

The PVA-chitosan solution was poured into a perspex mould capable of manufacturing 2 bi-axial membranes (Figure 5.3). The membranes were 45 mm in diameter and fabricated with a thickness of 1.5 mm. The mould consists of a base plate and top plate, screwed together with 6 screws. The mould was placed in a freezer at -20° C and frozen for 12 hr. Samples were thawed at room temperature for a further 12 hr. Specimens were made-up with 1, 2, 3 and 4 freeze-thaw samples. The top plate was taken off the mould and the base plate was placed in a coagulation bath for 30 min to polyermise the chitosan in the PVA-chitosan solution after the final freeze-thaw cycle. Finally the membranes were stored in distilled water at room temperature in order to retain moisture and prevent dehydration for up to 1 week.

Figure 5.3 Mould for manufacturing PVA-chitosan bi-axial membranes.

5.1.3 PVA-Chitosan Hydrogel Vessels

To fabricate the PVA-chitosan hydrogel vessels (dimensions; length = 100 mm, outer diameter = 13.5 mm, thickness 1.5 mm), a mould was designed and manufactured from perspex (Figure 5.4). Its consists of two outer sections that slot into one another, two end pieces and a perspex mandrel, held together with plastic screws. In order to minimise evaporation of water the PVA-chitosan solution was minimally exposed to air and the mould was sealed immediately after filling. It was stored vertically at room temperature for 1 hr to allow the air bubbles to rise out of the solution. Following this, the PVA-chitosan hydrogel solution was polymerised as previously described while manufacturing the unaxial tensile and bi-axial specimens. The vessels were stored in a bath of distilled water at room temperature to prevent dehydration prior to use for up to 1 week. Figure 5.5 shows an example of a PVA-chitosan vessel that was produced.

Figure 5.4 Perspex mould used in the fabrication of arterial vessels.

Figure 5.5 Sample PVA-chitosan hydrogel vessel. The vessel was fabricated from PVA and chitosan solutions blended at a ratio of 3:2, then crosslinked using a combination of freeze-thaw cycles and submersion into a potassium sulphate coagulation bath.

5.2 Mechanical Characterisation of Hydrogels

5.2.1 Uniaxial Tensile Test

The uniaxial tensile tests were performed on a Zwick Z005 displacement controlled tensile testing machine. Stainless steel grips, the gripping faces of which were covered with emery paper to prevent slippage during loading, were mounted onto the tensile testing machine. Extension of the specimen was taken to be the crosshead displacement. All tests in this study were loaded until failure of the hydrogel specimen occurred. However, preconditioning of selected specimens was conducted to a predefined load at a strain rate of 60 % min^{-1}.

Two preconditioning cycles were performed and equilibrium was reached where no further change occurred in the material stress versus strain curve after two cycles. A strain rate of 60 % min^{-1} was used to test the specimens to failure after the

preconditioning. Tests were also conducted on samples loaded to failure at a strain rate of 60 % min^{-1} without preconditioning. In addition, specimens cut in both the horizontal and vertical directions were tested to verify the isotropic behaviour of the material (Figure 5.6).

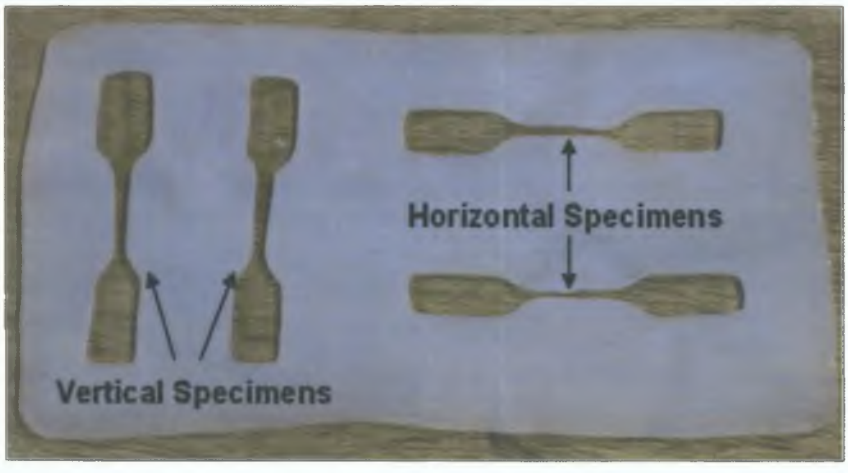

Figure 5.6 Uniaxial stress versus strain specimens cut in the vertical and horizontal directions from a PVA-chitosan WS hydrogel sheet that underwent 3 freeze-thaw cycles.

At the start of each test, the load was calibrated and balanced to zero to ensure accurate results. The gauge length was also set to zero at the beginning of each test. The tests were stopped when tearing began at either the grips or along the length of the specimen. Load, displacement, gauge length and cross sectional area were recorded for each specimen. The engineering stress was obtained by dividing the instantaneous load by the original cross sectional area. The engineering strain was determined by dividing the change in length by the original length. The original length of each specimen was taken as the distance between the custom made stainless steel grips. Finally the engineering stress and strain values were converted to true stress and true strain values using the following equations:

$$\sigma_T = \sigma_E (1 + \varepsilon_E) \quad (1)$$

and

$$\varepsilon_T = \ln(1 + \varepsilon_E) \quad (2)$$

where,

σ_E = Engineering Stress $\quad$ ε_T = True Strain

ε_E = Engineering Strain $\quad$ σ_T = True Stress

For a more comprehensive explanation on the conversion of engineering stress and strain to true stress and strain see Appendix B.

5.2.2 Biaxial Testing

Biaxial testing was performed on a static custom made bubble inflation apparatus (Figure 5.7, A). The circular hydrogel samples were clamped in position by 4 screws to prevent air leakage during inflation with an aluminium ring of internal diameter 30 mm. The thickness of the hydrogel specimens was measured using a depth micrometer and slip gauges (Figure 5.7, B) at several places on the specimen and the average value was recorded. The apparatus consisted of a fabricated PVA-chitosan WS-1 hydrogel circular specimens that had undergone 2 freeze-thaw cycles, additional tubing, a low pressure transducer (Jofra Calibrators, 3520 Farum, Denmark), a valve and a pressure inflation device (Medtronic, Ireland) used to apply an internal pressure. The pressure applied to the membrane was measured by the pressure transducer. The specimen was inflated by a hand operated high pressure inflation device that is normally using to inflate the balloon during balloon angioplasty and stenting procedures. Samples were inflated until rupture or until maximum extension of the pressure inflation device had been achieved. The deformation of the specimen was recorded using a depth micrometer and slips gauges at various pressure increments as shown in Figure 5.8.

5.2.3 Residual Stress Measurement

The existence of opening angles in the PVA-chitosan vessels was investigated. Rings of 3 mm in length, were cut from the vessels. They were then cut along the radial direction and images were taken immediately and after 5 min. Opening angles were measured from photographs according to a common definition with angle sides running from each end of the sector to its centre [179] (Also see Section 3.2).

5.2.4 Vessel Inflation Testing

A PVA-chitosan hydrogel vessel maintained at a constant length with a pre-defined axial strain was inflated by applying an internal pressure. The apparatus consisted of a fabricated PVA-chitosan WS-1 hydrogel tubular sample that had undergone 3 freeze-thaw cycles, additional tubing, a low pressure transducer

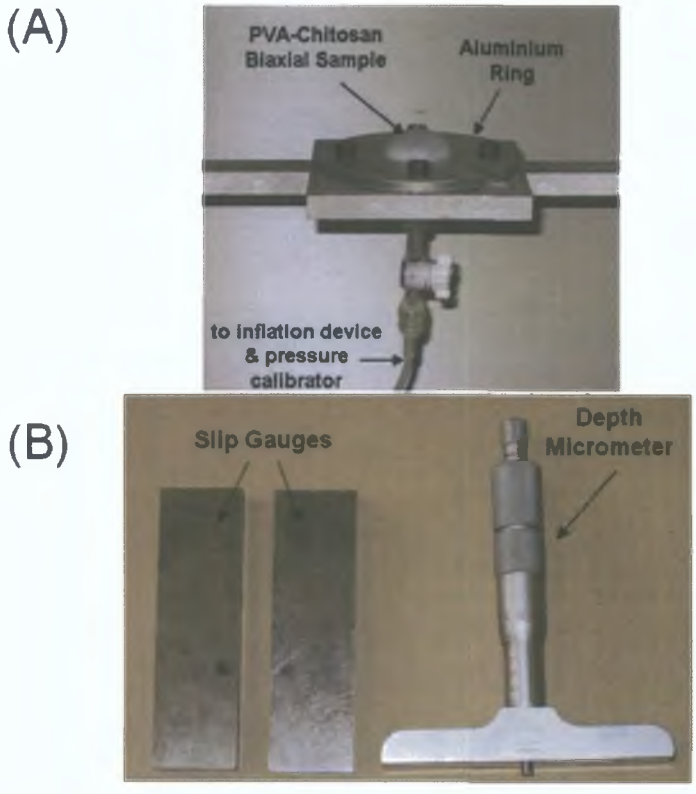

Figure 5.7 **Bubble inflation testing apparatus setup and depth micrometer.** (A) The hydrogel sample was clamped with an aluminium ring. The sample was then inflated by applying an internal pressure. (B) A depth micrometer and slip gauges used to measure thickness of samples and deformation of the hydrogel samples during inflation.

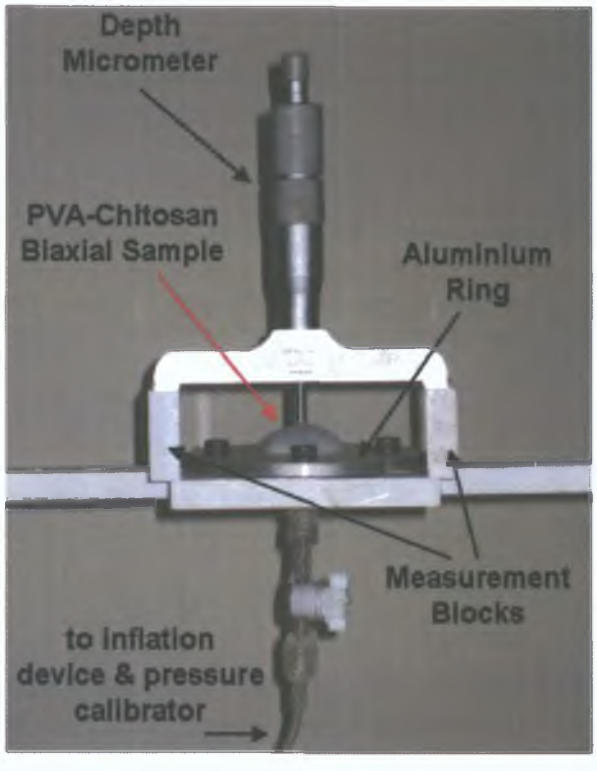

Figure 5.8 **Bubble inflation measurement configuration.**

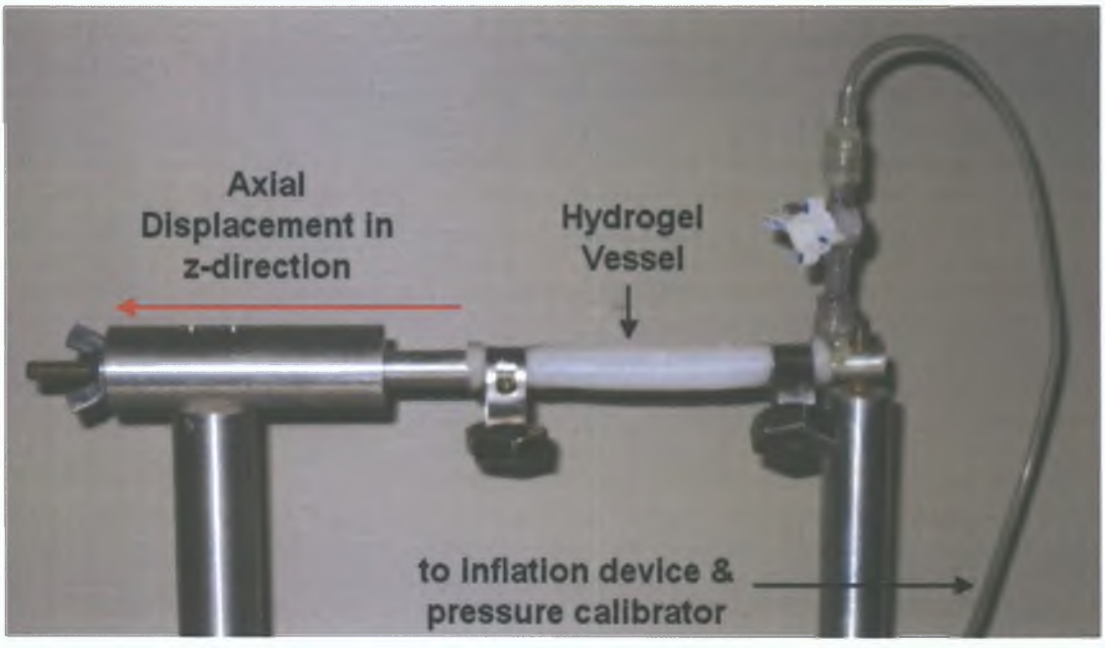

Figure 5.9 **Apparatus used to inflate the PVA-chitosan WS hydrogel vessels.** Axial strains of 0 %, 10 %, 20 % and 30 % were applied to the vessels which were inflated at internal pressures ranging from 0-16 kPa. The internal pressures and corresponding external diameters of the vessels were recorded.

(Jofra, Denmark), a valve and a pressure inflation device (Medtronic, Ireland) used to apply an internal pressure (Figure 5.9). The internal pressure was measured by the pressure transducer. Digital vernier callipers were used to measure the external diameter of the hydrogel vessel at internal pressures ranging from 0-16 kPa. Pressure versus diameter data was recorded for PVA-chitosan WS-1 hydrogel tubes, which were subjected to an axial strain of 0 %, 5 %, 10 % and 20 % respectively.

Internal pressurisation of the hydrogel vessel represents a three-dimensional stress and strain state. The pressure versus diameter data acquired from this experimental setup was compared to the pressure versus diameter response of a finite element model of the hydrogel vessel simulated using the uniaxial data for the PVA-chitosan WS-1 hydrogel subjected to 3 freeze-thaw cycles.

The effective use of the one-dimensional data to predict a three-dimensional response aims to validate the use of uniaxial data when simulating this PVA-chitosan fabricated hydrogel.

5.2.5 Scanning Electron Microscopy

Scanning electron microscopy (SEM) is a powerful method for analysing the physical properties of hydrogels. The SEM is a microscope that uses electrons rather than light to form an image and provides nanometer resolution of a sample. The use of this technique allows for observation of the polymeric network of the PVA hydrogel. Such observations may increase the understanding of molecular interactions of the PVA-chitosan hydrogels and may lead to improved sample preparation. The cross-sectional structure of the PVA-chitosan blended hydrogels were examined using a Hitachi S 300N scanning electron microscopy (SEM). Images were analysed with SEM Image Analysis software (Oxford Instruments, UK).

A morphological characterisation of the networks may increase understanding of the molecular interactions that define the physical and mechanical properties of the PVA-chitosan hydrogel. Prior to SEM examination, the hydrated hydrogel samples were cut into squares (15 mm x 15 mm), frozen overnight at -80 °C and then freeze-dried in a Labconco Freeze Dry Freezone System for 10 hr. The dehydrated hydrogel specimens were placed in a mini vice in order to examine the cross section structure of the hydrogel. Samples were analysed under vacuum and with an operating voltage of 20 kV. The effects of blending PVA with water-soluble and -insoluble chitosan were investigated.

5.3 Results

5.3.1 Uniaxial Tensile Tests

Repeatability of Experiments

In order to determine whether the PVA-chitosan experiments showed repeatability, a number of specimens for each hydrogel were tested. Figure 5.10 shows the repeatability of the PVA-chitosan WS-1 hydrogel with 4 freeze-thaw cycles. Clearly, good repeatability of the experiments has been achieved, especially within the strain range of 0 to 0.4. Appendix E contains repeatability test results for PVA, PVA-chitosan IS-1 and PVA-chitosan WS-1 hydrogels specimens.

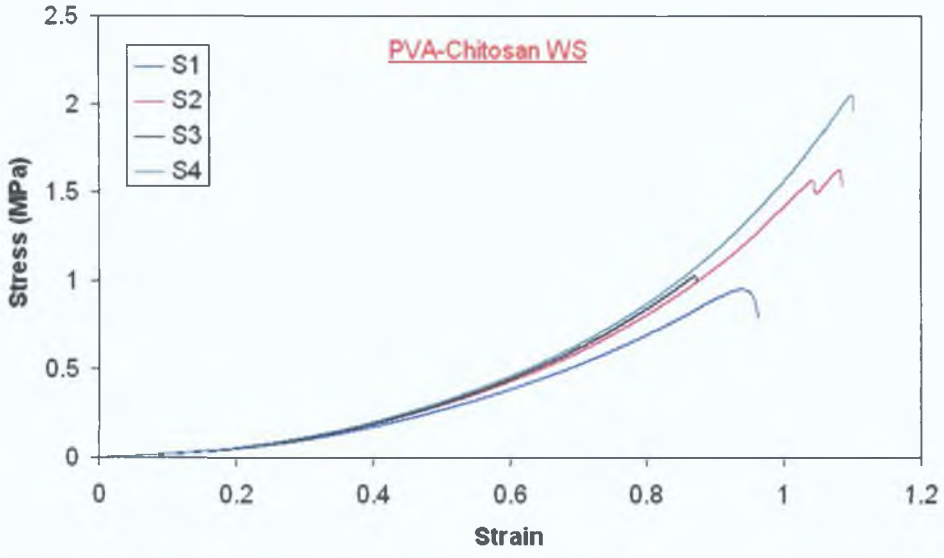

Figure 5.10 Uniaxial stress versus strain data for PVA-chitosan WS hydrogel samples that underwent 4 freeze-thaw cycles. (S = Specimen).

Effect of Number of Freeze-Thaw Cycles

The number of freeze-thaw cycles that the PVA, PVA-chitosan IS and PVA-chitosan WS hydrogels was varied to determine the effect on the stress versus strain behaviour of the hydrogel. For the PVA-chitosan IS, PVA-chitosan WS and PVA (Figure 5.11, 5.12, 5.13) hydrogels it was evident that there was a definite variation in the elastic behaviour of the various samples for 1, 2, 3 and 4 freeze-thaw cycles. The stiffness of each hydrogel increased as the number of freeze-thaw cycles increased.

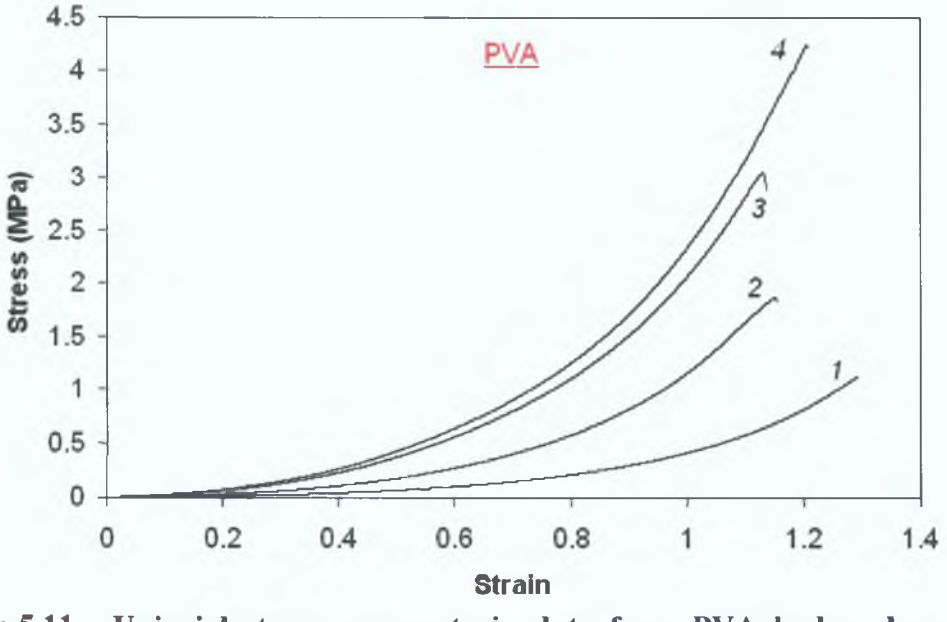

Figure 5.11 Uniaxial stress versus strain data from PVA hydrogel samples that underwent 1, 2, 3 and 4 freeze-thaw cycles.

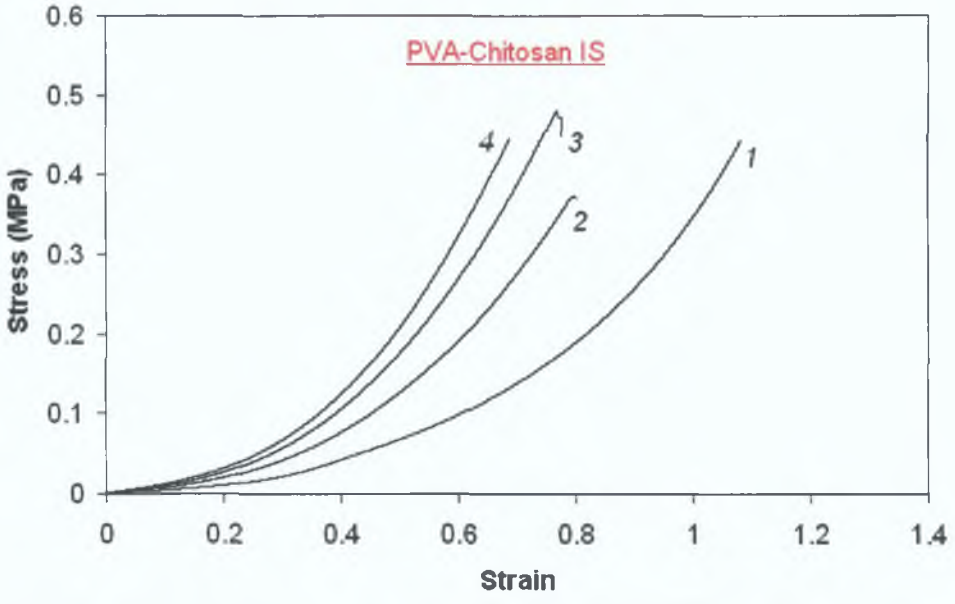

Figure 5.12 Uniaxial stress versus strain data from PVA-chitosan IS hydrogel samples that underwent 1, 2, 3 and 4 freeze-thaw cycles.

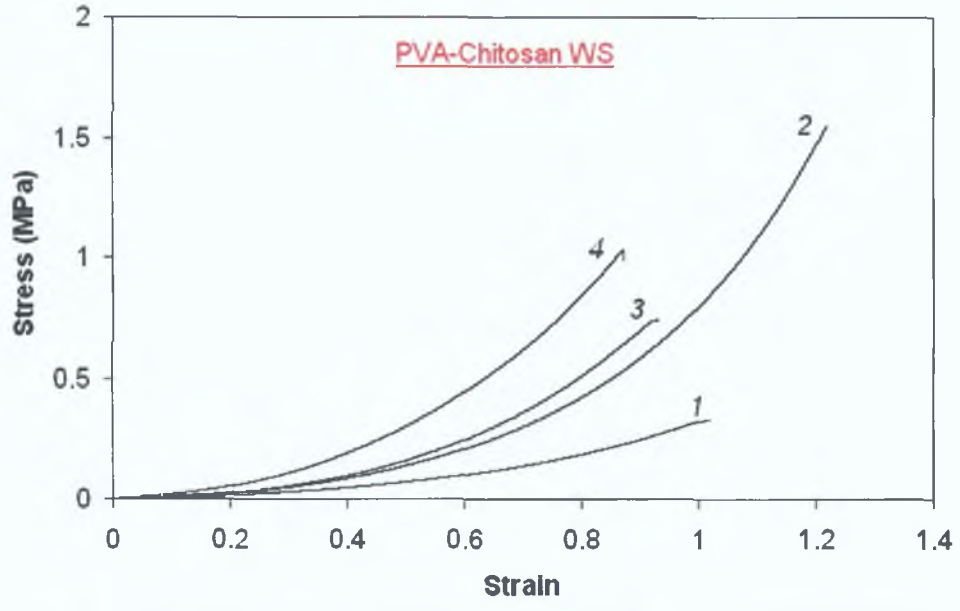

Figure 5.13 Uniaxial stress versus strain data from PVA-chitosan WS hydrogel samples that underwent 1, 2, 3 and 4 freeze-thaw cycles.

Comparison of Hydrogels

All hydrogels were fabricated in the same manner, in terms of the number of freeze-thaw cycles and submersion into a coagulation bath. Therefore it was necessary to examine the effect the water-soluble and -insoluble chitosan had on the properties of the hydrogels (PVA-chitosan IS, PVA-chitosan WS) compared to the PVA hydrogel without chitosan.

In Figure 5.14 (1 freeze-thaw cycle), the PVA, the PVA-chitosan IS and PVA-chitosan WS hydrogels displayed similar elastic behaviour. A change in the elastic behaviour of the PVA-chitosan IS and PVA-chitosan WS hydrogels compared to the PVA was evident for in Figure 5.15 (2 freeze-thaw cycles). However, the stress versus strain behaviour of the PVA-chitosan IS and PVA-chitosan WS remained very similar (Figure 5.14-5.17). There was a greater change in the elastic response of the PVA-chitosan IS and PVA-chitosan WS in comparison to the PVA hydrogel as shown in Figure 5.16 (3 freeze-thaw cycles). Finally Figure 5.17 (4 freeze-thaw cycles), also showed a significant difference in the stress versus strain behaviour of the PVA-chitosan IS and PVA-chitosan WS compared to the PVA hydrogel specimen.

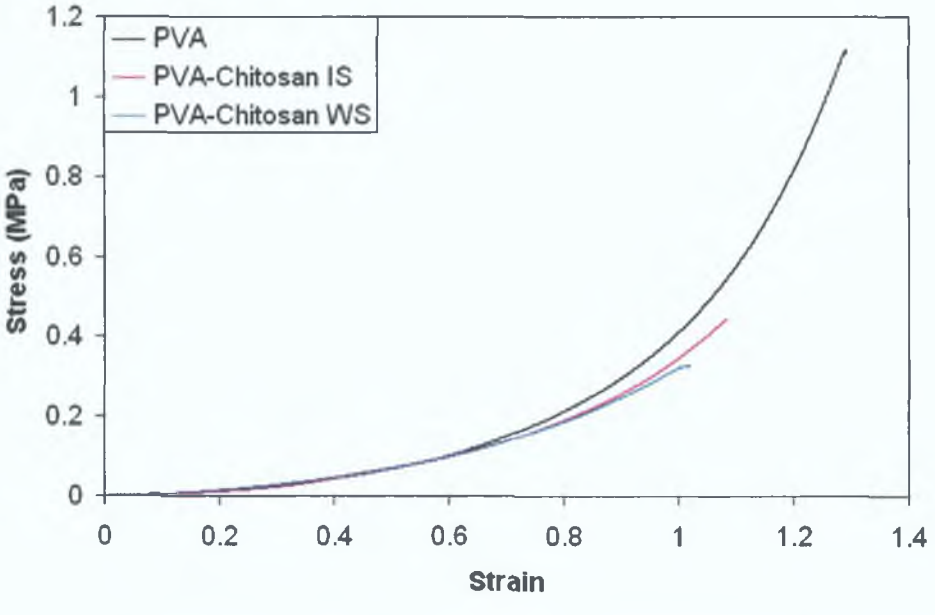

Figure 5.14 Comparison of the uniaxial stress versus strain data from PVA, PVA-chitosan IS and WS hydrogel specimens (1 freeze-thaw cycle).

This interesting finding can be explained by close examination of the polymerisation of the hydrogels. It has been shown by Chu and Rutt [132] that PVA stiffens as the number of freeze-thaw cycles is increased as has already been shown in Figure 5.11 This characteristic was also evident for the PVA-chitosan IS and PVA-chitosan WS hydrogels. However comparing the three blends of hydrogels it was evident that there was a greater rate of stiffening of the PVA than the PVA-chitosan IS and PVA-chitosan WS hydrogels. During the freeze-thaw cycles the PVA was polymerised and as the number of freeze-thaw cycles increased the

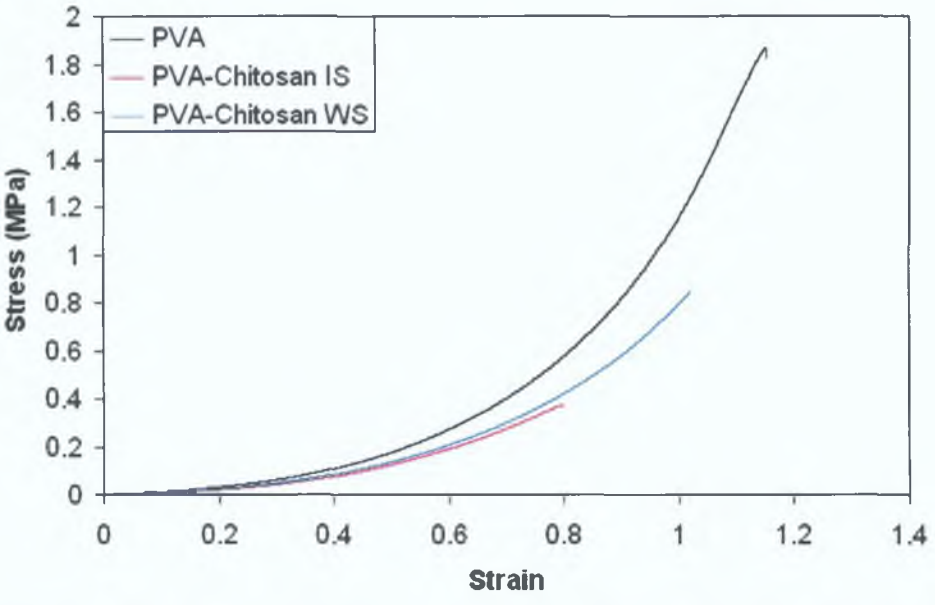

Figure 5.15 Comparison of the uniaxial stress versus strain data from PVA, PVA-chitosan IS and WS hydrogel specimens (2 freeze-thaw cycles).

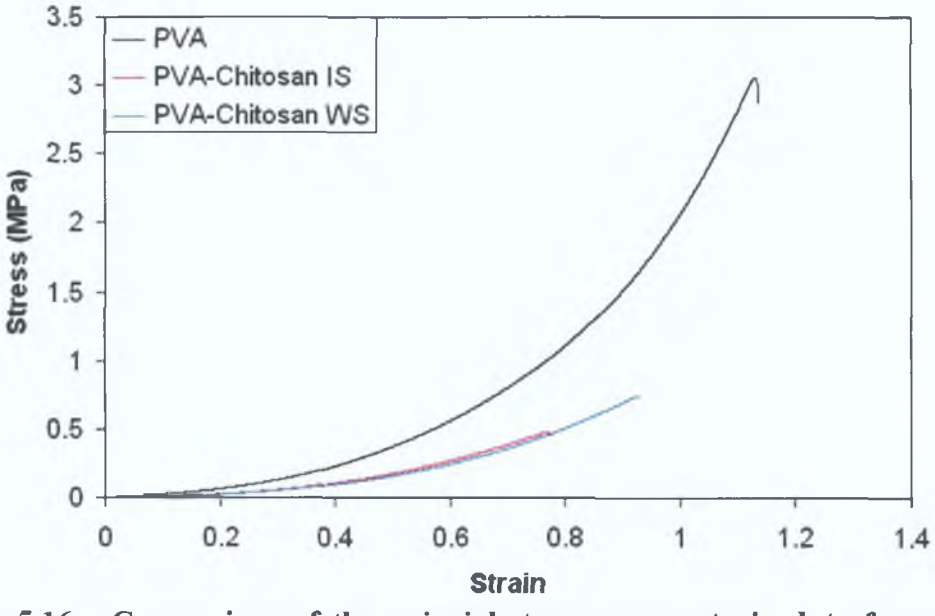

Figure 5.16 Comparison of the uniaxial stress versus strain data from PVA, PVA-chitosan IS and WS hydrogel specimens (3 freeze-thaw cycles).

stiffness of the PVA increased (Figure 5.11). For the PVA-chitosan IS and WS hydrogels the PVA was again polymerised during the freeze-thaw cycles. While the chitosan was encapsulated in the PVA matrix, it was not polyermised during the freeze-thaw cycles. The hydrogels were submerged in the coagulation bath to polymerise the chitosan and neutralise the pH of the hydrogel. In regard to determining the mechanical properties of the materials, the PVA was certainly the more mechanically significant material. While the chitosan did contribute to the

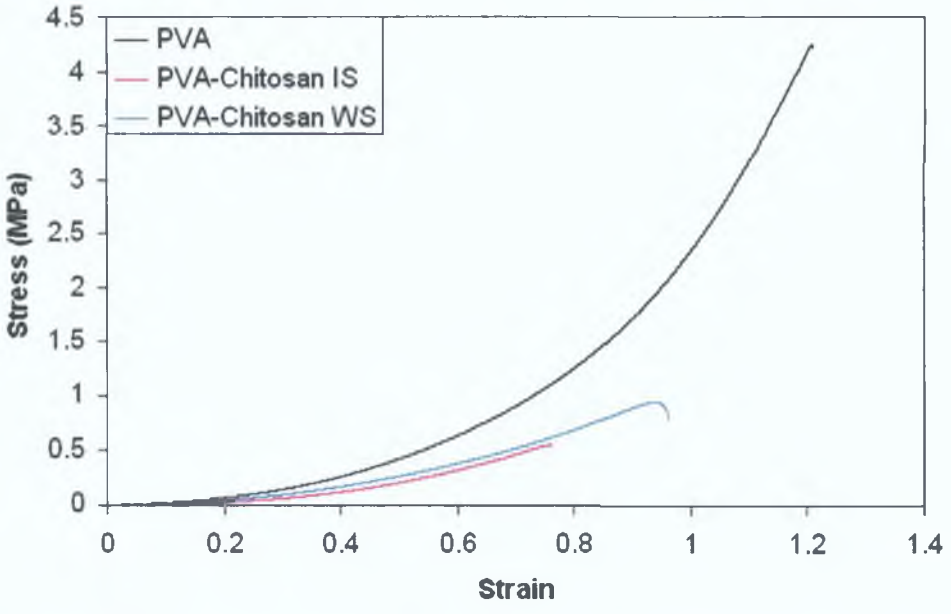

Figure 5.17 Comparison of the uniaxial stress versus strain data from PVA, PVA-chitosan IS and WS hydrogel specimens (4 freeze-thaw cycles).

mechanical properties, it was the freeze-thaw cycles that significantly affected the elastic behaviour of the hydrogels. Therefore the difference in the stiffness of the PVA compared to the PVA-chitosan IS and PVA-chitosan WS hydrogels is due to the fact the PVA was composed of the 10 % PVA solution only while the PVA-chitosan hydrogels were composed of the 10 % PVA and 1 % chitosan solutions blended at a ratio of 3:2. Comparing the PVA-chitosan IS and PVA-chitosan WS hydrogels showed that the use of water-soluble or insoluble chitosan was insignificant for 1, 2, 3 and 4 freeze-thaw cycles. In light of this finding, it may be concluded that as the number of freeze-thaw cycles increases, the PVA stiffens at a greater rate than the PVA-chitosan IS and PVA-chitosan WS hydrogels.

Comparison of Vertical and Horizontal Unidirectional Specimens

In order to exemplify the homogeneous nature of the PVA-chitosan membrane, samples were cut out of a PVA-chitosan hydrogel sheet in both the vertical and horizontal directions (Figure 5.6). The uniaxial stress versus strain characteristics shown in Figure 5.18 showed as expected that PVA-chitosan specimens cut in both directions have a similar stress versus strain relationship.

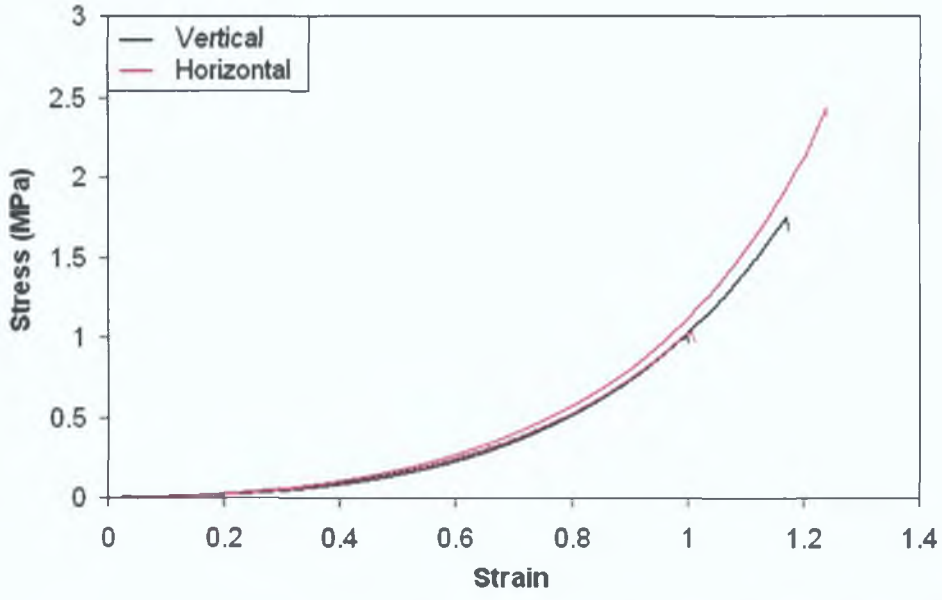

Figure 5.18 Uniaxial stress versus strain data for two PVA-chitosan WS hydrogel specimens cut out in vertical and horizontal directions from the same hydrogel sheet that underwent 3 freeze-thaw cycles.

Comparison of PVA-chitosan WS to Porcine Aorta

The uniaxial stress versus strain curves for PVA-chitosan WS specimens for 1, 2, 3 and 4 freeze-thaw cycles were compared to five uniaxial stress versus strain curves for porcine aortic tissue [180]. Clearly, the PVA-chitosan WS samples bear a close resemblance to the porcine aortic tissue especially within the strain range of interest (Figure 5.19). The PVA-chitosan WS specimens that experienced 1, 2 and 3 freeze-thaw cycles had similar stress strain characteristics within the strain range of 0-0.6. The hydrogel fabricated with 4 freeze-thaw cycles was stiffer compared to the uniaxial stress versus strain curves for all five porcine aortic samples. These results indicate that the uniaxial stress versus strain characteristics for PVA-chitosan WS specimens fabricated with 1, 2 and 3 freeze-thaw cycles closely resembled the uniaxial stress versus strain curves for porcine aortic tissue, with 1 freeze-thaw and 3 freeze-thaw cycles representing the softer and stiffer porcine aortic specimens respectively.

Effect of Preconditioning

The hydrogel specimens were preconditioned to determine whether there was any variation in the elastic behaviour of the hydrogels during cyclic loading. Specimens of PVA, PVA-chitosan IS and WS hydrogel specimens that underwent 1 and 4

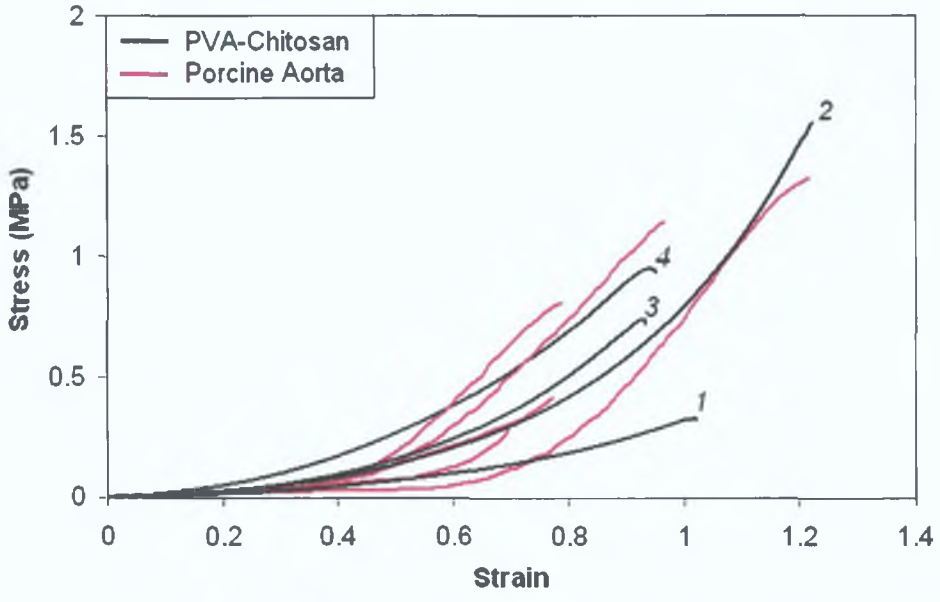

Figure 5.19 Uniaxial stress versus strain data from PVA-chitosan WS hydrogel samples that underwent 1, 2, 3 and 4 freeze-thaw cycles compared to five uniaxial stress versus strain curves for porcine aortic tissue. Porcine data digitised from Prendergast *et al* [180] (using xyextract© digitising software).

freeze-thaw cycles (plus coagulation bath) were preconditioned twice. Due to the variation in the stress versus strain relationships of the hydrogels subjected to 1 or 4 freeze-thaw cycles, the specimens that underwent 1 freeze-thaw cycle were preconditioned to a maximum load of 0.3N while specimens that underwent 4 freeze-thaw cycle to a maximum load of 1N at a strain rate of 60 % min^{-1}. Cyclic loading was performed to the specified loads for two consecutive cycles and then finally loaded to failure. In Figures 5.20 and 5.21, it can clearly be seen that the response becomes more compliant after the initial cycle. For the PVA specimens (Figure 5.22), the effect of the preconditioning was not as prominent as for the PVA-chitosan IS and WS hydrogel specimens. For all hydrogel specimens in the third cycle, it was evident that the response of the loading was very similar to the cyclic loading (loading/unloading) in the second cycle. In addition, all hydrogel specimens dissipate most energy in the first cycle. By preconditioning the hydrogel specimens, the material tends to become less stiff. The preconditioning of the hydrogels shows hysteresis where the loading and unloading of the specimen causes a change in the response to future loads. When the hydrogel specimens were subjected to cyclic loading, the stress versus strain curves for unloading fall below that for loading, forming this hysteresis loop. The area enclosed by this hysteresis loop represents the strain energy lost in each cycle. Appendix F contains results of PVA, PVA-chitosan

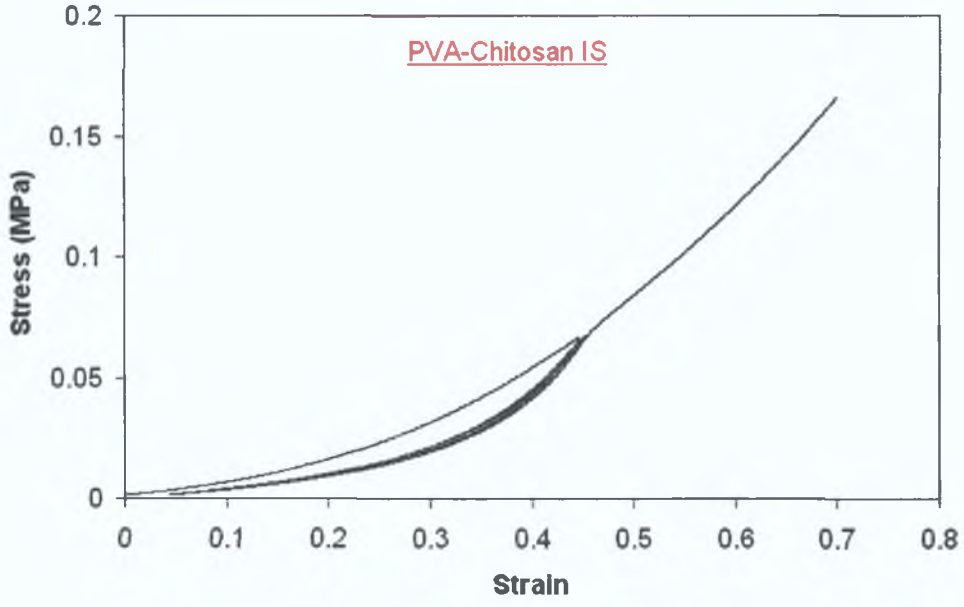

Figure 5.20 Two preconditioning cycles of PVA-chitosan IS to a load of 0.3N which was then loaded to failure (1 freeze-thaw cycle).

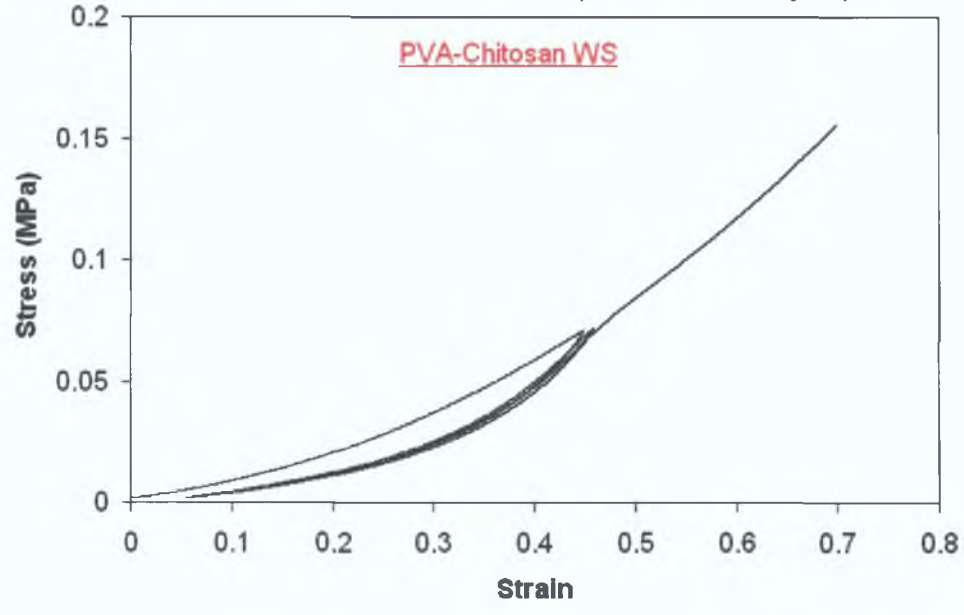

Figure 5.21 Two preconditioning cycles of PVA-chitosan WS to a load of 0.3N which was then loaded to failure (1 freeze-thaw cycle).

IS-1 and PVA-chitosan WS-1 hydrogels specimens that were preconditioned to a maximum load of 1N. Similar characteristics were evident under the increased preconditioned load.

5.3.2 Biaxial Inflation Tests

A static bubble inflation test apparatus was used to illustrate the difference in biaxial properties between the PVA and the PVA-chitosan hydrogel specimens. The

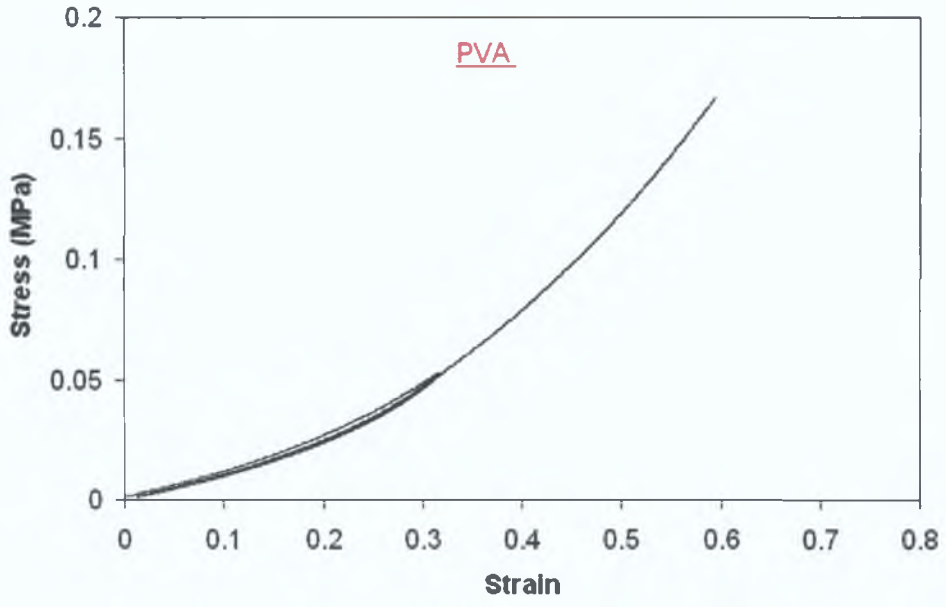

Figure 5.22 Two preconditioning cycles of PVA to a load of 0.3N which was then loaded to failure (1 freeze-thaw cycle).

pressure and the height of the bubble were recorded for increasing pressure. The bubble height versus pressure response for PVA-chitosan IS-1, PVA-chitosan WS-1 and PVA again display good experimental repeatability (Figure 5.23-5.25). Comparison of the biaxial specimens (2 freeze-thaw cycles) illustrate that both PVA-chitosan compositions have similar inflation properties (Figure 5.26). There was a significant reduction in the bubble height of PVA, reiterating what has been already shown, that as the number of freeze-thaw cycles was increased the greater the difference in the stress versus strain response of PVA in comparison to the PVA-chitosan samples. Figure 5.27 illustrated the reduction in the bubble height of PVA-chitosan membranes for a given input pressure as the number of freeze-thaw cycles was increased.

5.3.3 Opening Angle Measurements

To determine whether opening angles existed in the PVA-chitosan hydrogel vessels, rings were cut in the radial direction. The opening angles were measured from photographs. For all vessels, no opening angles were present (eg: Figure 5.28). This finding suggests that there are no significant residual stress in the PVA-chitosan hydrogel vessels.

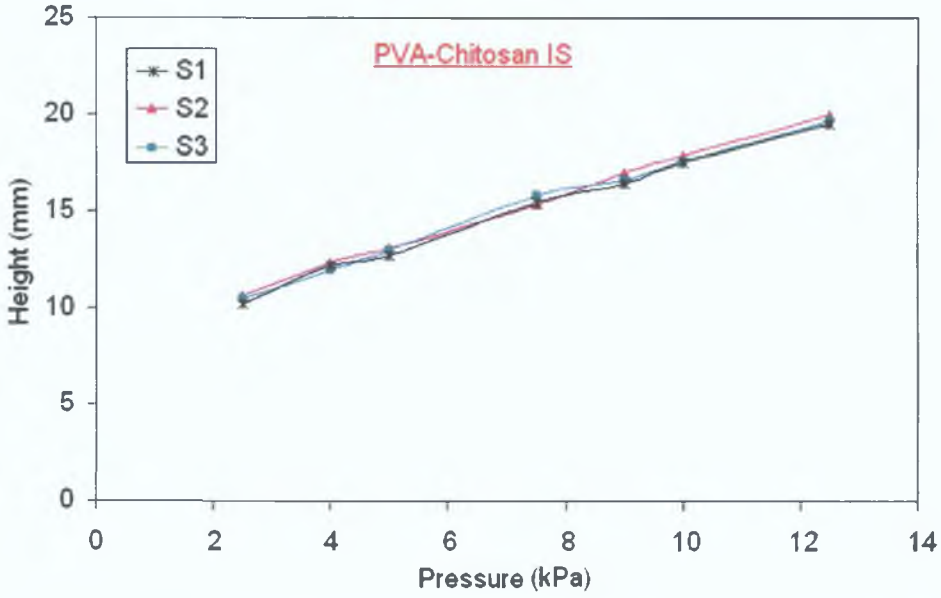

Figure 5.23 Bubble height versus pressure response for PVA-chitosan IS hydrogel samples that underwent 2 freeze-thaw cycles. (S = Specimen)

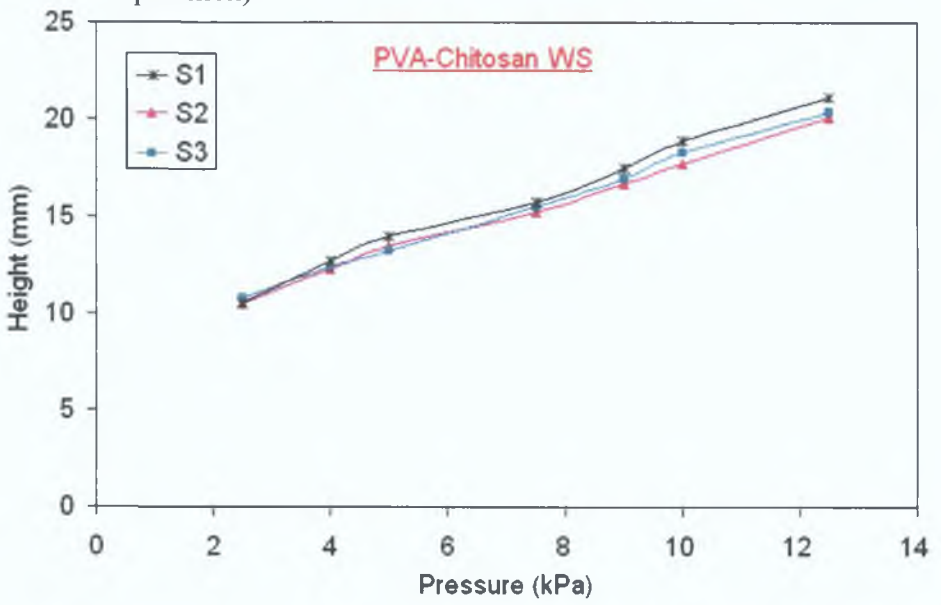

Figure 5.24 Bubble height versus pressure response for PVA-chitosan WS hydrogel samples that underwent 2 freeze-thaw cycles. (S = Specimen).

5.3.4 Vessel Inflation Tests

Internal inflation of thick-walled tubes was used to determine the structural response of PVA-chitosan WS-1 hydrogel vessels. The external diameter of the vessels with axial strains of 0 %, 5 %, 10 % and 20 % respectively was plotted at stepped increases of internal pressure. For comparison purposes, a finite element model of this experiment was constructed using the methods described in Chapter 3.

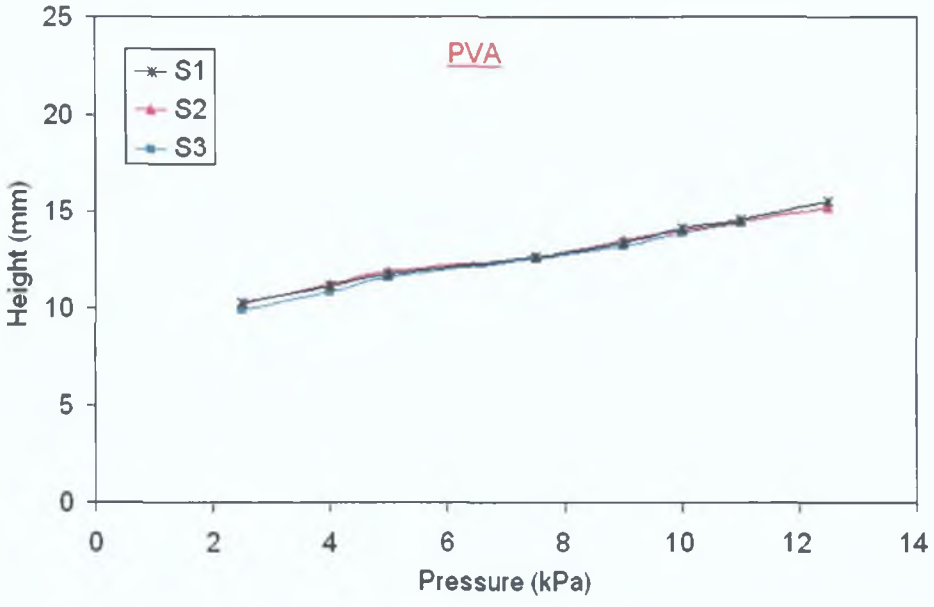

Figure 5.25 Bubble height versus pressure response for PVA hydrogel WS samples that underwent 2 freeze-thaw cycles. (S = Specimen).

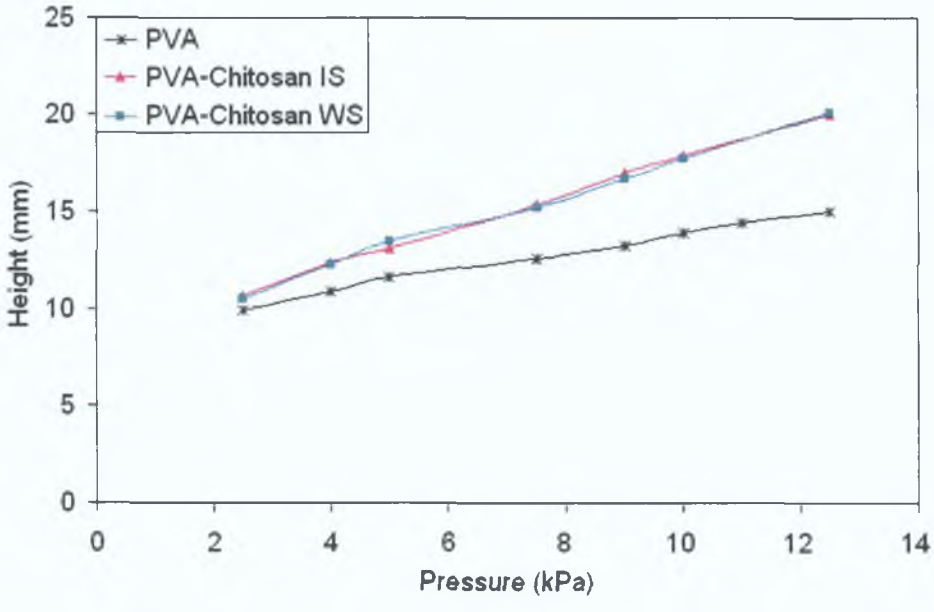

Figure 5.26 Comparison of bubble height versus pressure response from PVA, PVA-chitosan IS and WS hydrogel specimens (2 freeze-thaw cycles).

The uniaxial data for PVA-chitosan WS-1 that had undergone 1, 2, 3 and 4 freeze-cycles previously presented in this chapter (Figure 5.13) was used to determine coefficients for the Ogden 2 parameter constitutive model (Table 5.1). The structural response of the numerical model was compared to the experimental measurements for the PVA-chitosan hydrogel vessels that had undergone 3 freeze-thaw cycles, as shown in Figure 5.29. Examination of the overall experimental response of the vessels associated with specific axial strains (Figure 5.29, A) illustrated that as the

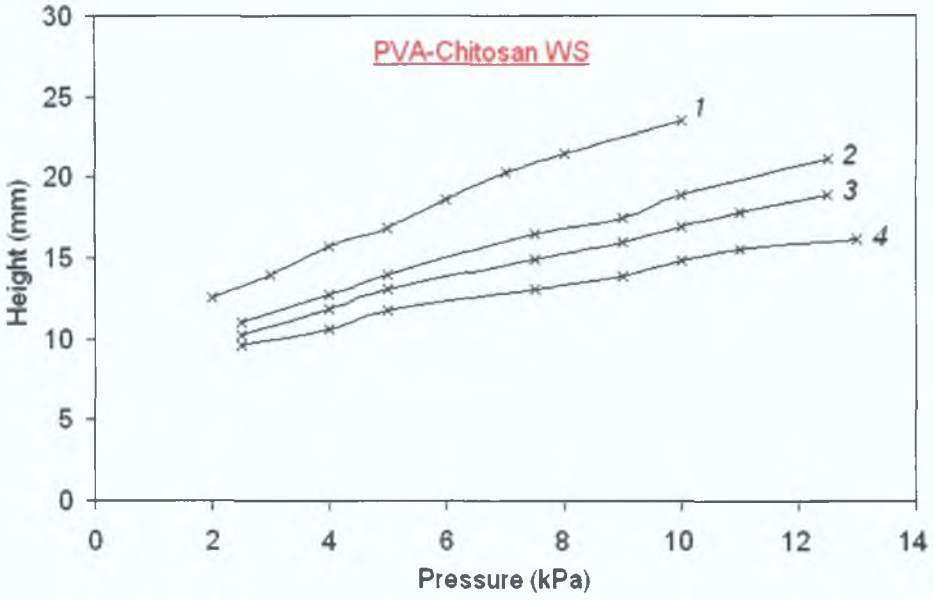

Figure 5.27 **Bubble height versus pressure response from PVA-chitosan WS hydrogel samples that underwent 1, 2, 3 and 4 freeze-thaw cycles.**

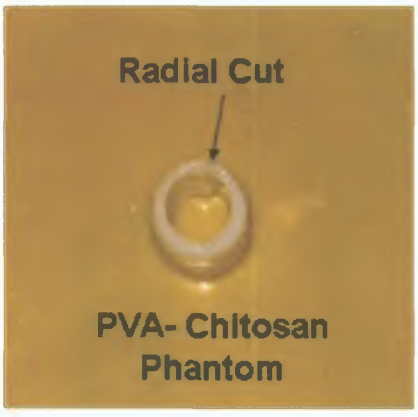

Figure 5.28 **A radial cut was made in a ring from a PVA-chitosan WS vessel. (3 freeze-thaw cycles)**

PVA-chitosan WS-1 Material Coefficients (kPa)

Freeze-thaw cycles	μ_1	μ_2	α_1	α_2	*error*
1	8.90	4.31×10^{-5}	6162.6	1716.9	5.63×10^{-4}
2	4.54	14.71	8075.1	4604.8	4.89×10^{-3}
3	13.97	8.65×10^{-8}	7076.4	5100.5	4.70×10^{-3}
4	3.42×10^{-5}	31.09	2633.1	6599.3	9.79×10^{-3}

Table 5.1 **Hyperelastic material constants to describe PVA-chitosan WS-1 for 1, 2, 3 and 4 freeze-thaw cycles based on experimental data from uniaxial tension tests (Figure 5.11).** The parameters describe a 2 parameter Ogden model.

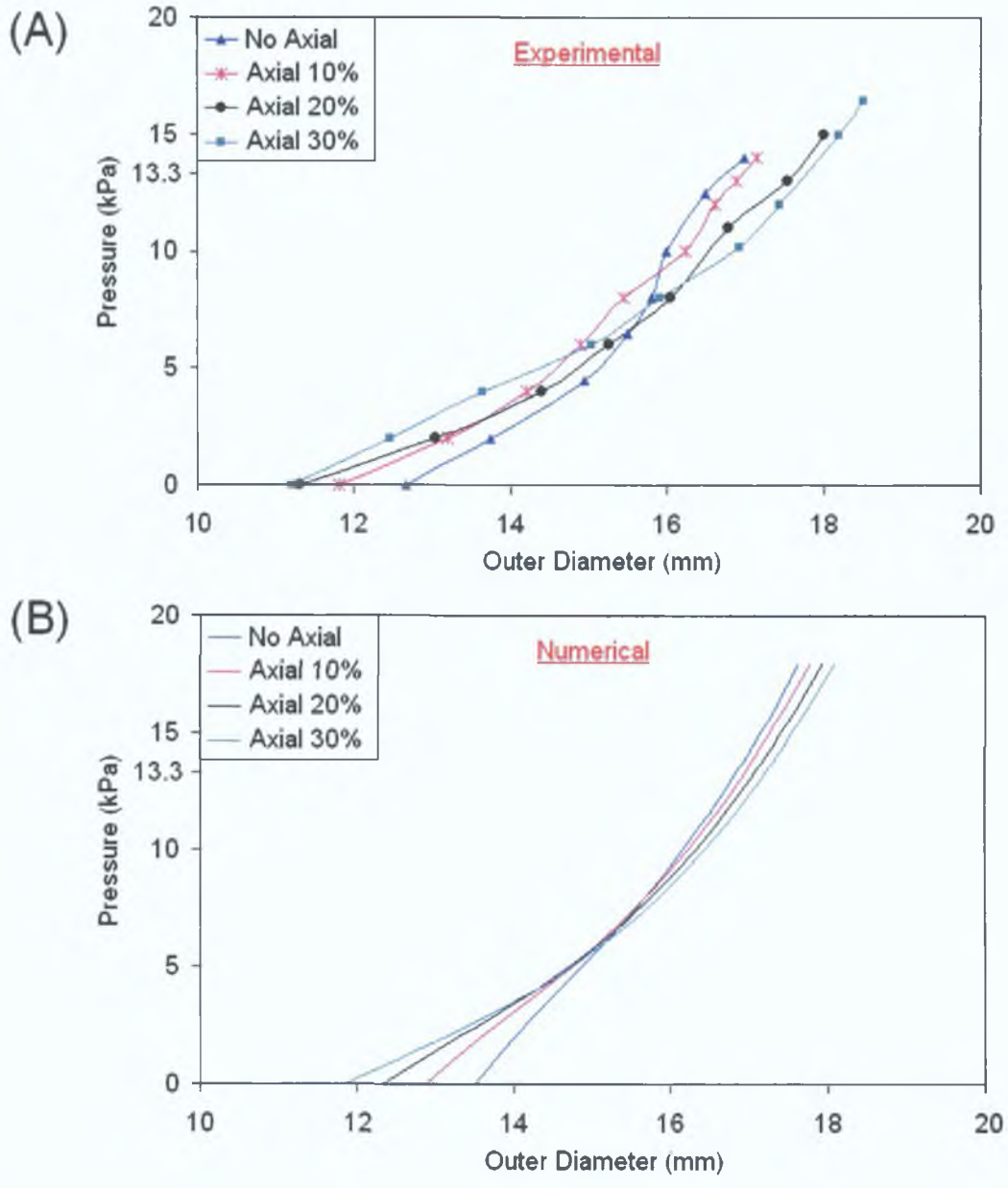

Figure 5.29 Comparison of the experimental and numerical inflations of a PVA-chitosan WS-1 hydrogel vessel (3 freeze-thaw cycles). (A) Experimental pressure versus diameter relationship plot of the hydrogel vessel with no axial, 10 %, 20 % and 30 % axial strains, n = 3. (B) Numerical pressure versus diameter relationship of the hydrogel vessel with no axial, 10 %, 20 % and 30 % axial strains.

axial strain increased the un-pressurised outer diameter of the vessel decreased. As the pressure was increased (above ~8 kPa), a change in the response of the vessels was noted. Similar characteristics were also evident in the numerical model predictions (Figure 5.29, B).

Figures 5.30 to 5.33 show the pressure versus outer diameter plots comparing

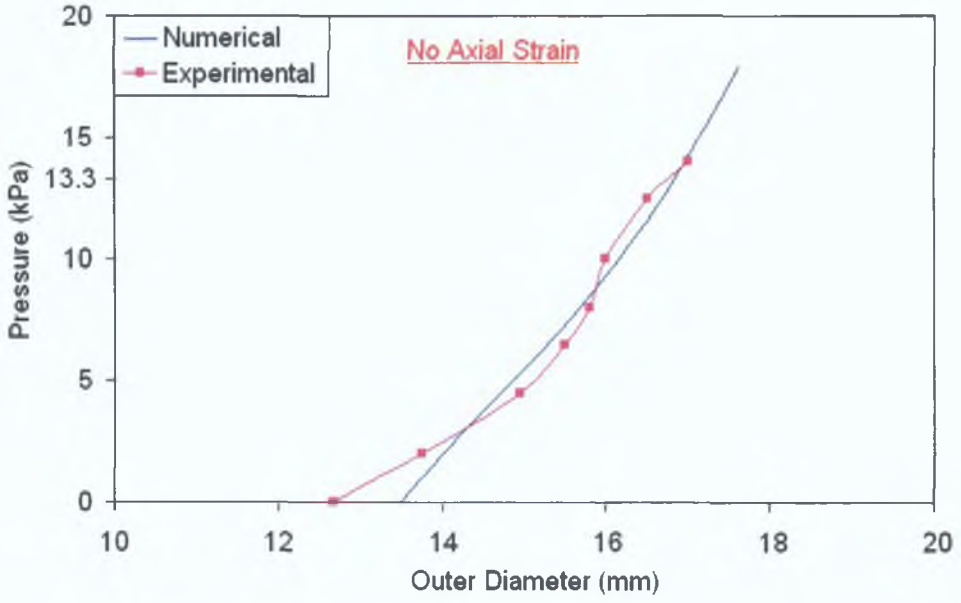

Figure 5.30 Pressure versus diameter plots comparing the experimental and numerical inflations of PVA-chitosan WS-1 hydrogel vessels with no axial strain. (3 freeze-thaw cycles)

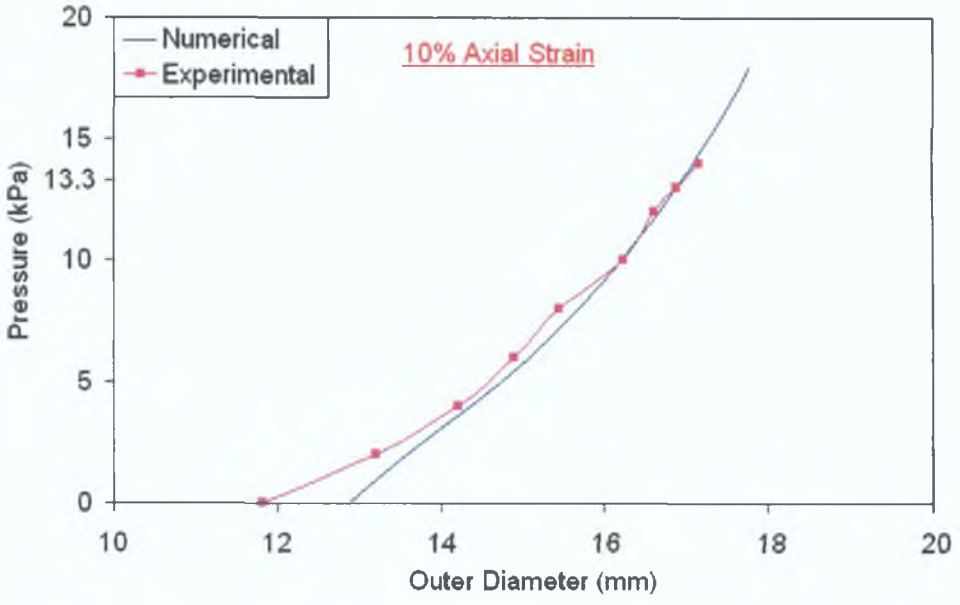

Figure 5.31 Pressure versus diameter plots comparing the experimental and numerical inflations of PVA-chitosan WS-1 hydrogel vessels with axial strain of 10 %. (3 freeze-thaw cycles)

the experimental and numerical inflations of PVA-chitosan WS-1 hydrogel vessels with 0 %, 10 %, 20 % and 30 % axial strains respectively. Good agreement can be seen between the numerical and experimental results for all axial strains, indicating that constitutive models based on uniaxial data predict the vessel structural behaviour quite well for static internal pressurisation.

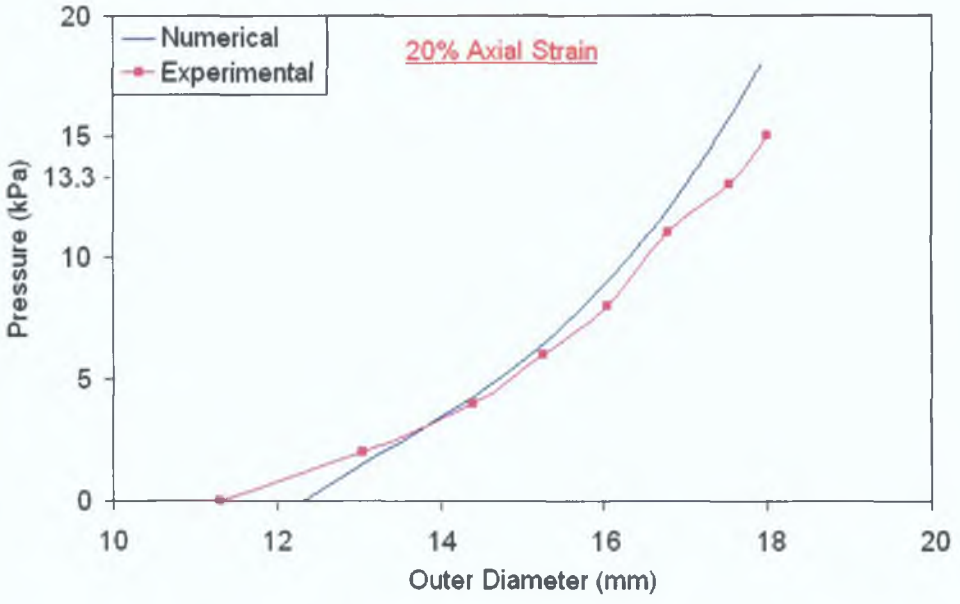

Figure 5.32 Pressure versus diameter plots comparing the experimental and numerical inflations of PVA-chitosan WS-1 hydrogel vessels with axial strain of 20 %. (3 freeze-thaw cycles)

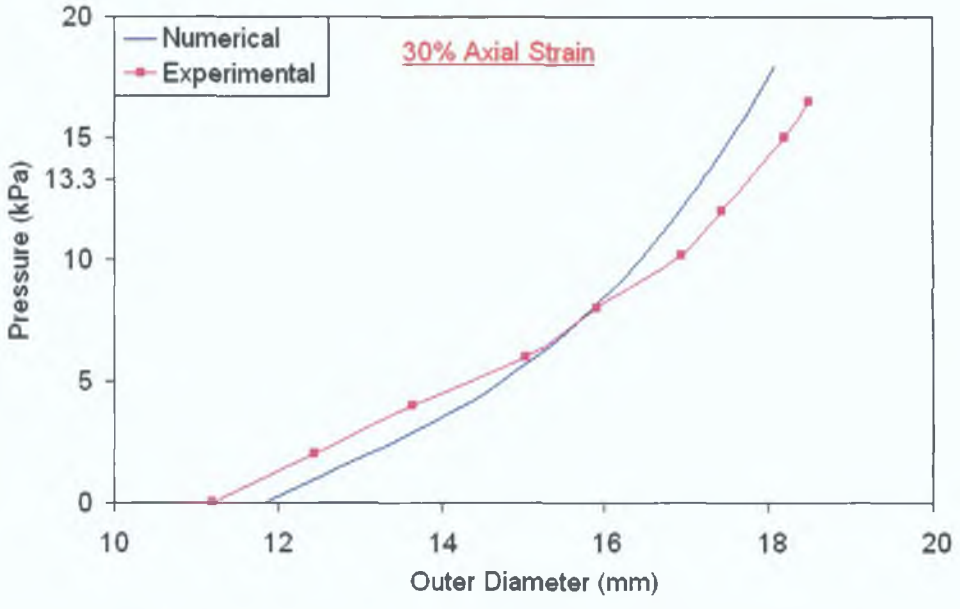

Figure 5.33 Pressure versus diameter plots comparing the experimental and numerical inflations of PVA-chitosan WS-1 hydrogel vessels with axial strain of 30 %. (3 freeze-thaw cycles)

5.3.5 Scanning Electron Microscopy

Macroporous hydrogels, based on the various blends of PVA with chitosan, were dehydrated by freeze drying prior to investigation. The effects of blending PVA with water-soluble and -insoluble chitosan on the morphology and pore distribution

were investigated by SEM. The SEM images of three hydrogel compositions, namely PVA, PVA-chitosan WS and PVA-chitosan IS provide high magnification images of cross-sections of the materials. Macroscopically, all membranes appear opaque. The microscopic analyses of the membranes displayed distinct differences in the composition of the each dehydrated hydrogels for 1, 2 and 4 freeze-thaw cycles.

Figure 5.34 displays a porous morphology for 1, 2 and 4 freeze-thaw cycles of a pure PVA hydrogel. Larger pores were evident for 1 freeze-thaw cycle of PVA (Figure 5.34, A) in comparison to 2 freeze-thaw cycles (Figure 5.34, B). No significant visual differences are apparent in the cross-sectional structure of the PVA for 2 and 4 freeze-thaw cycles. For all freeze-thaw cycles of PVA, an ordered structure was evident, suggesting a homogenous structure. When water-soluble or insoluble chitosan was added to the PVA, significant changes were apparent in the internal structure of the hydrogel compositions (Figures 5.35 and 5.36). A similar structural morphology for both water-soluble and insoluble chitosan was evident for 1, 2 and 4 freeze-thaw cycles. The PVA-chitosan WS and IS hydrogel that underwent 1 freeze-thaw cycle, had a sponge like cross-sectional structure (Figures 5.35, A and 5.36, A). After 2 freeze-thaw cycles, larger pores were evident for both hydrogel compositions (Figures 5.35, B and 5.36, B). Finally, following 4 freeze-thaw cycles, the pores were of similar size to the pores after 2 freeze-thaw cycles but were much more clearly defined (Figures 5.35 (C) and 5.36, C). A histogram of the average pore diameters was generated (Figure 5.37) from three 1000X cross sectional SEM images (n = 3) of the dehydrated PVA, PVA-chitosan IS and PVA-chitosan WS hydrogel membranes following 1, 2 and 4 freeze-thaw cycles. There were approximately 40 ± 15 pores per image. Only one (representative image) of these images is shown in Figure 5.34-5.36. The histogram illustrates that there was no significant difference in the average pore diameter for PVA following 1, 2 and 4 freeze-thaw cycles (2.24, 2.44 and 2.47μm respectively – See Table 5.2). There was a significant increase in the average pore diameter following 2 freeze-thaw cycles for PVA-chitosan WS and IS membranes in comparison to average pore diameter following 1 freeze-thaw cycle. Another increase in the pore diameter of the PVA-chitosan WS and IS membranes was evident following 4 freeze-thaw cycles in comparison to 2 freeze-thaw cycles.

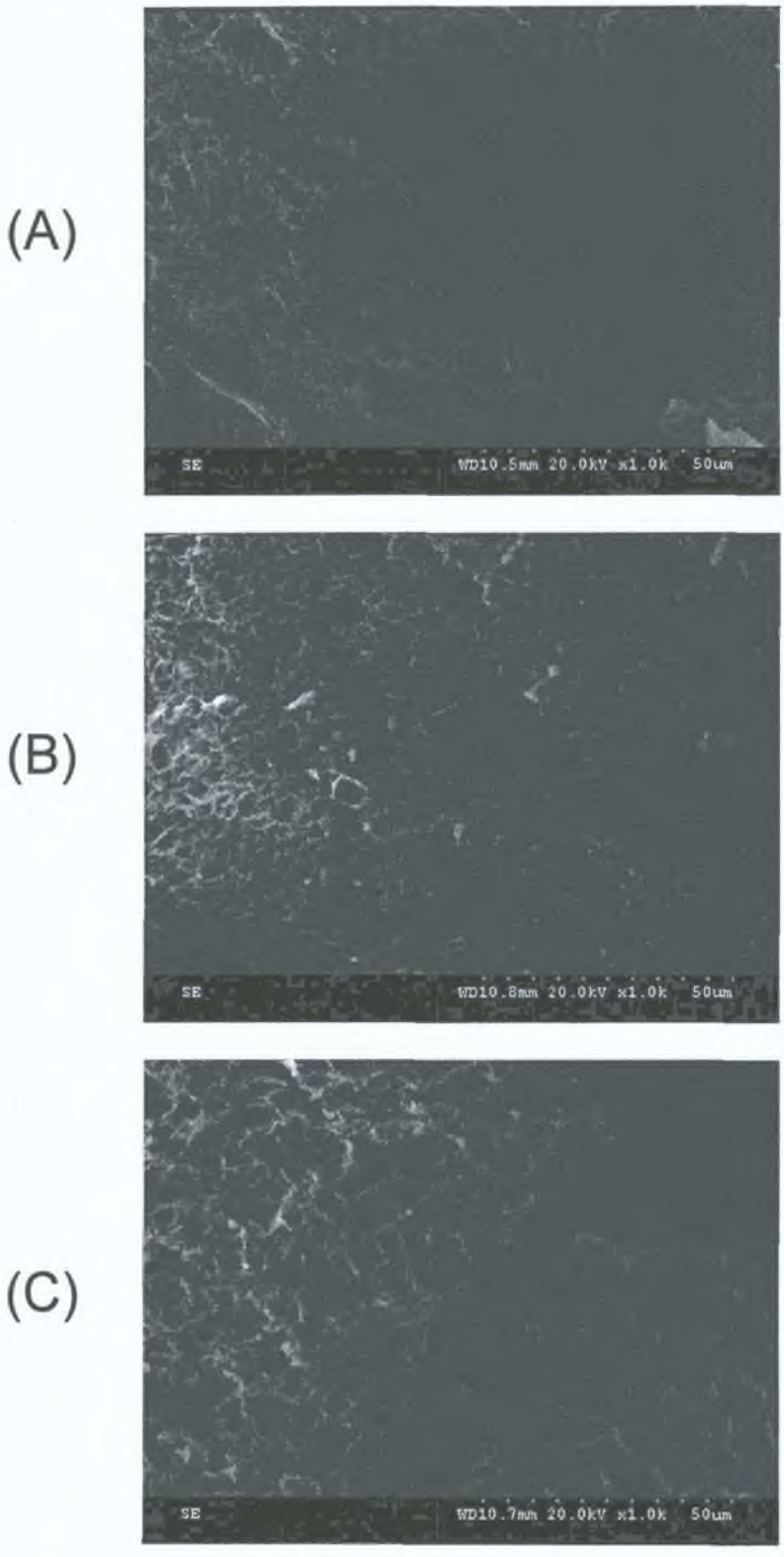

Figure 5.34 Cross-section SEM images of dehydrated PVA membranes. (A) 1 freeze-thaw cycle, (B) 2 freeze-thaw cycles and (C) 4 freeze-thaw cycles. Representative images, n =3. Magnification 1000x.

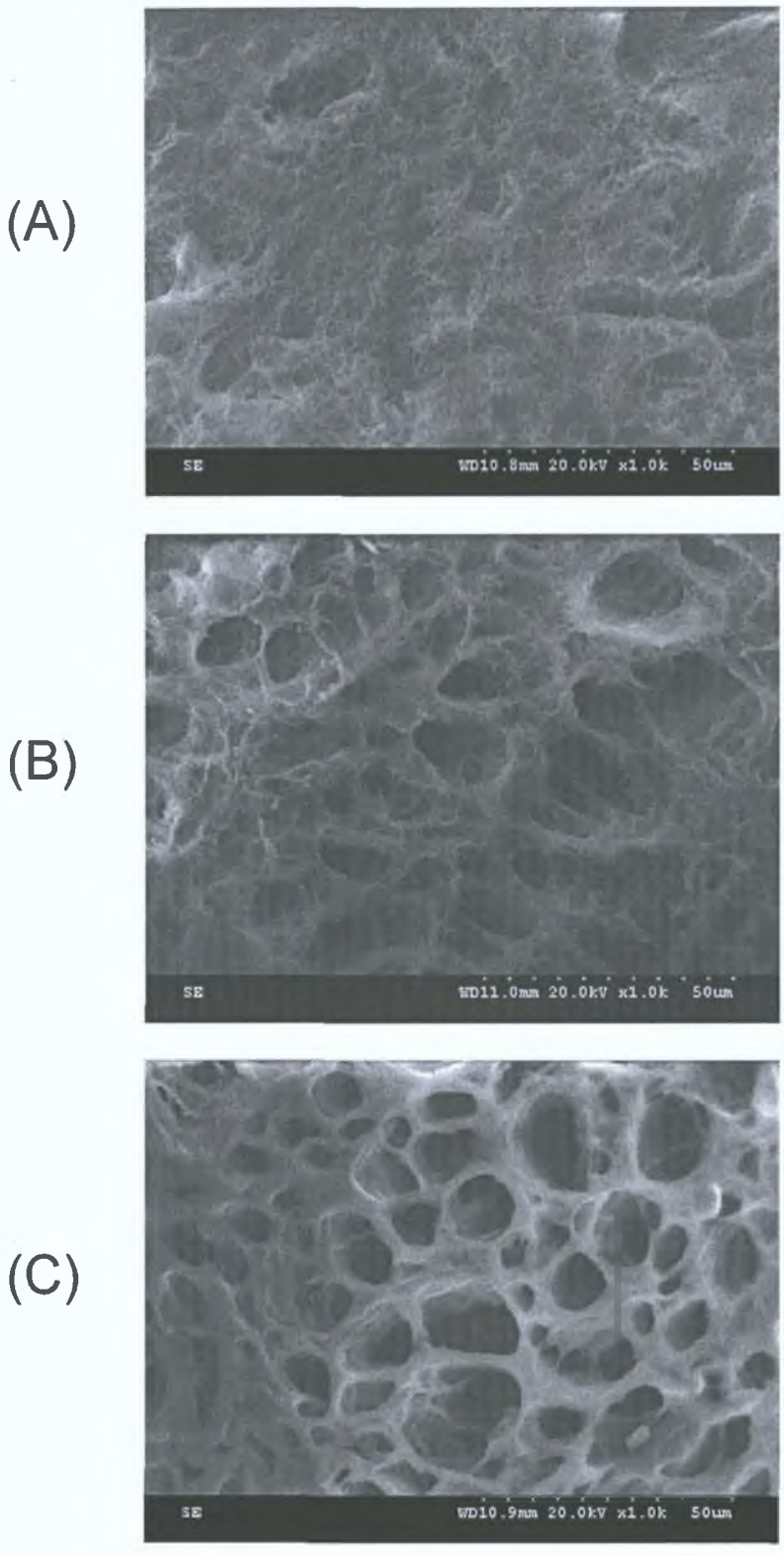

Figure 5.35 Cross-section SEM images of dehydrated PVA-chitosan WS membranes. (A) 1 freeze-thaw cycle, (B) 2 freeze-thaw cycles and (C) 4 freeze-thaw cycles. Representative images, n =3. Magnification 1000x.

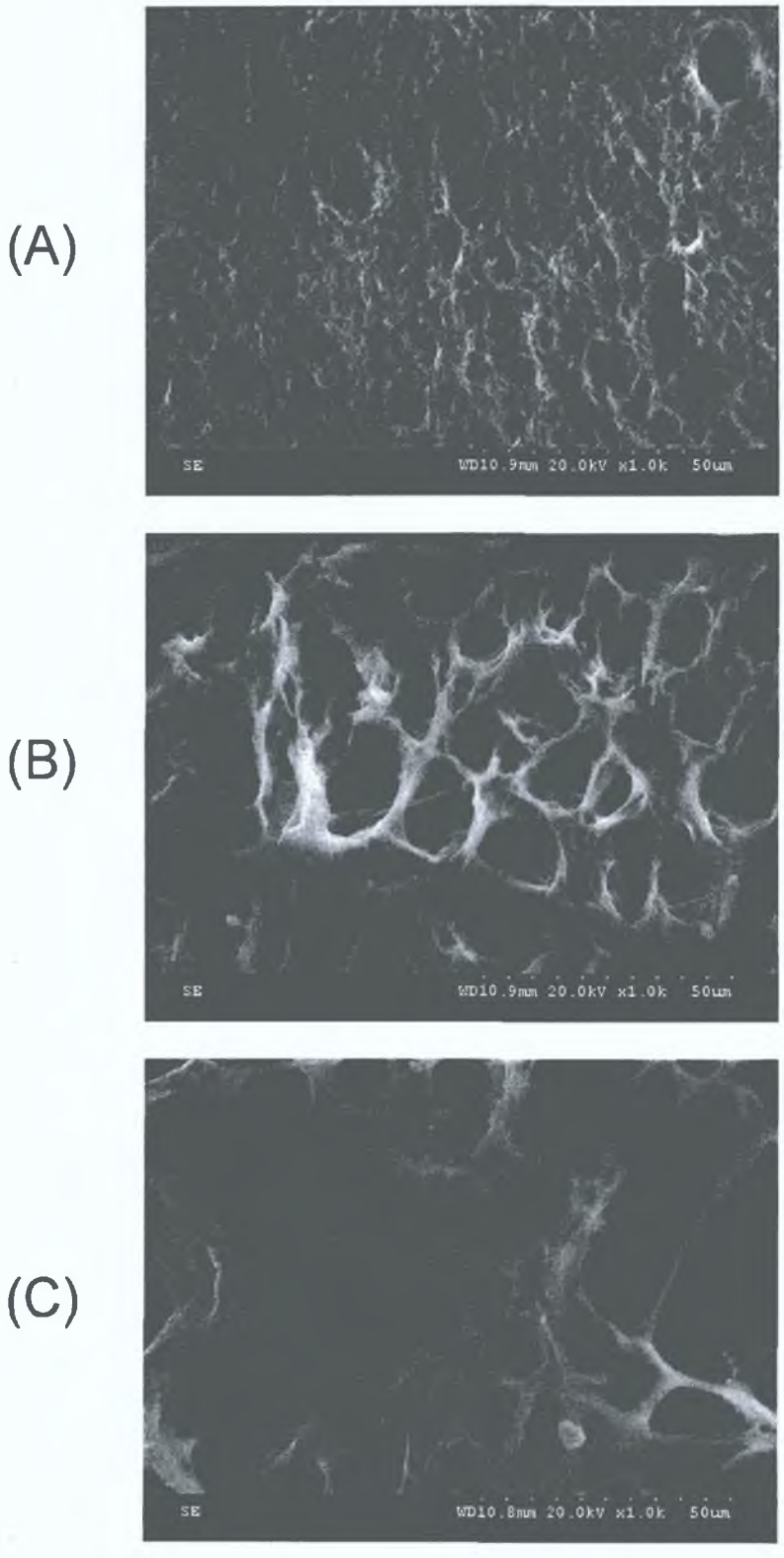

Figure 5.36 Cross-section SEM images of dehydrated PVA-chitosan IS membranes. (A) 1 freeze-thaw cycle, (B) 2 freeze-thaw cycles and (C) 4 freeze-thaw cycles. Representative images, n =3. Magnification 1000x.

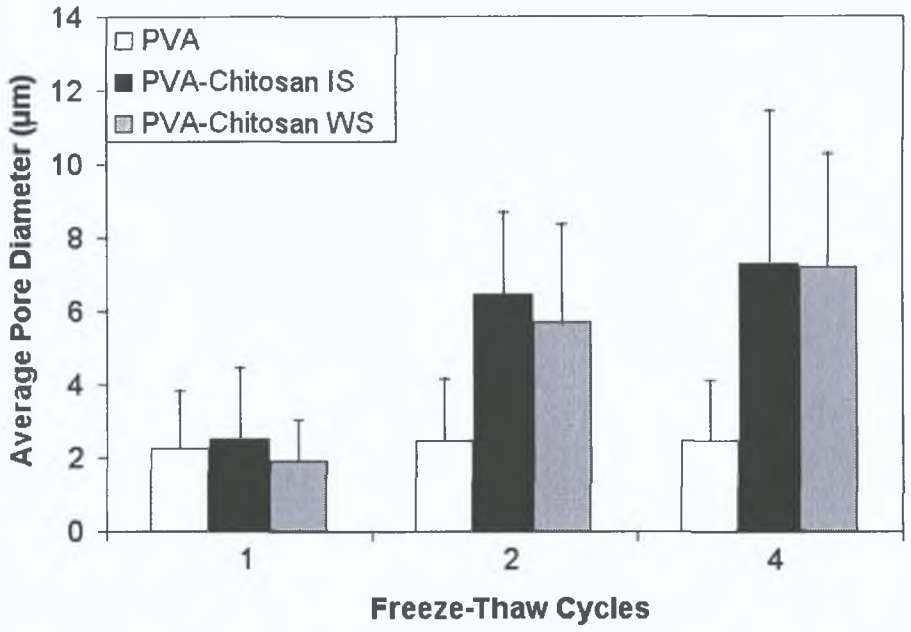

Figure 5.37 Average pore diameter of PVA, PVA-chitosan IS and PVA-chitosan WS. (Determined from the cross-section SEM images of dehydrated hydrogel membranes using LabVIEW software, n = 3)

It can be concluded that both water-soluble and insoluble chitosan have a similar affect on the morphological structure of the material when blended with PVA. SEM images of the internal PVA, PVA-chitosan WS and PVA-chitosan IS structure show a porous filamentous membrane which could allow the transport of additives through the membrane. As previously shown in Chapter 4, PVA-chitosan WS and PVA-chitosan IS support vascular cell culture which indicates that the pore sizes in these hydrogels provide a suitable membrane for all cell growth. However, there was a marked difference on the maximum and minimum pore diameters of the PVA-chitosan WS and IS membranes (See Table 5.2). Ideally a biomaterial for this application would have uniform pore architecture [181] that allows quantification of the nutrient transport through the membrane.

5.4 Discussion

The mechanical and morphological properties of PVA and PVA-chitosan WS-1 and IS-1 blended membranes were evaluated. The mechanical behaviour of the hydrogels was investigated by uniaxial tensile testing, biaxial experiments (bubble inflation technique and vessel inflation) and opening angle measurements. SEM

PVA Pore Diameters (μm)

Freeze-thaw cycles	Maximum	Minimum	Average
1	3.68	1.61	2.24
2	3.76	1.73	2.44
4	3.80	1.67	2.47

PVA-chitosan IS Pore Diameters (μm)

Freeze-thaw cycles	Maximum	Minimum	Average
1	3.71	1.95	2.50
2	11.19	2.26	6.44
4	15.19	4.16	7.29

PVA-chitosan WS Pore Diameters (μm)

Freeze-thaw cycles	Maximum	Minimum	Average
1	2.69	1.15	1.90
2	11.97	2.66	5.72
4	13.75	3.12	7.19

Table 5.2 Maximum, minimum and average pore diameters of PVA, PVA-chitosan IS and PVA-chitosan WS following 1, 2 and 4 freeze-thaw cycles.

analysis of the cross-section of hydrogel specimens was used to assess the changes in the pore diameter of the blended hydrogels for 1, 2 and 4 freeze-thaw cycles. Mechanical and morphological characterisation of the hydrogels aims to increase knowledge of the material and thus facilitate future structural design and analysis of hydrogels.

The results of the uniaxial tests showed that the PVA and PVA-chitosan WS-1 and IS-1 blended hydrogels can be manufactured reliably with excellent repeatability, which is an important characteristic in the search for potential biomaterials [5]. It was also noted in the elastic responses for all hydrogel compositions that the materials (PVA, PVA-chitosan WS-1 and PVA-chitosan IS-1) stiffened as the number of freeze-thaw cycles increased. Comparing PVA and PVA-chitosan (water-soluble and -insoluble) for a given number of freeze-thaw cycles

showed that the PVA was the more mechanically dominant constituent. The use of water-soluble or -insoluble chitosan had no influence on the stress versus strain characteristics of the PVA-chitosan blended samples. A preconditioning effect was apparent for all samples. However, it was more prominent for the PVA-chitosan blended specimens. After the initial preconditioning, all hydrogel displayed a similar loading and unloading response for subsequent loading cycles. Similar to PVA, which has been fabricated to match the constitutive response of porcine aortic tissue [132] and a human carotid artery [148], PVA-chitosan WS samples also closely resembled the response of porcine aortic tissue.

In order to mechanically characterise hydrogel vessels, biaxial tests were also required. Whilst the fabricated hydrogels had isotropic material properties it was necessary to evaluate their response in 2 or 3-dimensional scenarios (bubble and vessel inflation). The bubble inflation results from these studies demonstrated that the PVA-chitosan WS-1 response stiffens as the number of freeze-thaw cycles was increased. The addition of an axial strain to the vessel had the opposite effect to the pressure versus diameter response compared to arterial tissue. Instead of the axial strain stiffening the pressure versus diameter response as with arterial tissue [59], the PVA-chitosan actually soften. As expected, no opening angles were evident in the PVA-chitosan vessels.

The SEM analysis of the different hydrogel compositions that had undergone 1, 2 and 4 freeze-thaw cycles illustrated a significant difference in cross-sectional analysis of the PVA due to the addition of either water-soluble or -insoluble chitosan after 2 or more freeze-thaw cycles. A "sponge-like" structure was evident for the PVA after all freeze-thaw cycles. The significant change in the pore structure of the PVA-chitosan membranes indicated that adding chitosan into the PVA solution dramatically changes the structure during the membrane formation. However, the pore structure was not regular, and a uniform pore size was not evident. A consistent porous hydrogel could be achieved using the overrun process [182], which is the process utilised in the manufacture of soft ice cream. In this process, injected gas bubbles and ice crystals are used to create porous structures.

5.5 Conclusion

This series of experiments indicate that the addition of chitosan to the PVA affects the mechanical behaviour and morphological structure of the fabricated membrane. Therefore, these findings, coupled with those from the biological evaluation studies suggest that PVA-chitosan can be used to fabricate bioartificial vessels with appropriate mechanical and structural properties for *in vitro* vascular cell culture studies in a vascular bioreactor.

The conclusions from this study are as follows:

- The effect of freeze-thaw cycles on the uniaxial, biaxial and vessel structural properties of PVA-chitosan WS-1 and IS-1 have been determined. The effect of preconditioning has been shown to be significant. Uniaxial properties were within the range of porcine aortic tissue.
- Non-linear hyperelastic constitutive Ogden models have been used to describe the behaviour of each PVA-chitosan WS membrane for 1, 2, 3 and 4 freeze-thaw cycles.
- A numerical model of the vessel response to internal pressurisation agrees well with experimental measurements for the 3 freeze-thaw cycle PVA-chitosan WS-1 hydrogel vessel.
- The number of freeze-thaw cycles was shown to have a significant effect on the morphological characteristics of the PVA-chitosan WS-1 and IS-1 hydrogels membranes.

In conclusion, PVA-chitosan vessels can be fabricated whose behaviour can be modelled numerically and whose overall structural behaviour will be similar to porcine aortic vessels.

Chapter 6

Conclusions and Future Work

This study involved the development and evaluation of a biomaterial to simultaneously mimic the mechanical properties of vascular tissue while providing the biological cues required to support vascular cell growth. The findings of all three separate studies indicated the significant potential of PVA-chitosan for use in bioartificial vessels.

The finite element analysis of the iliac arteries highlighted the need for more experimental data (uniaxial and biaxial) on the intima, media and adventitia in order to replicate the constitutive properties of the arteries more appropriately. There was a limited effect of residual stresses on the structural response of the arterial models presented in this study. However, the wall stresses may be more significantly affected by the residual stress. Holzapfel *at al* [15] have developed the most advanced constitutive equation to date which accounts for the anisotropic behaviour of the material [35]. Therefore, ideally future finite element models of arterial tissue should use a constitutive equation that includes anisotropy to characterise the structural response and wall stresses of the artery, once models of this type are more widely available in finite element simulation software.

The material investigations presented uniaxial, biaxial and the structural response of the PVA-chitosan membranes. While previous studies have examined the PVA [132,148], the investigations of PVA blended with water-insoluble and -soluble

chitosan are novel. The proposed material (PVA-chitosan WS-1) displayed a mechanical response similar to porcine aortic tissue.

The findings of the biological experiments demonstrated that vascular cells adhered to the PVA-chitosan water-soluble and -insoluble membranes. PVA-chitosan WS-1 and IS-1 displayed favourable behaviour in terms of cell growth and morphology. BAEC and BASMC cultured on PVA-chitosan WS-1 exhibited comparable proliferation and apoptosis characteristics to control samples. Previous studies [96,97], investigated adhesion of fibroblast cells on PVA blended with water-insoluble chitosan. In addition, water-soluble chitosan was a new constituent for this kind of experiments and may have other applications.

6.1 Experimental Limitations

A description of the experimental limitations for each research discipline aims to facilitate the appropriate use of the results obtained.

6.1.1 Numerical Models

An idealised geometry of artery in the stress free states were assumed based on the strain-energy function developed by Chuong and Fung [51]. However, in most cases noncircular arterial segments (albeit, slightly noncircular) are evident [183]. The idealised geometries had the same opening angle, actual internal and external radii as the artery but an averaged wall thickness. In addition, this strain-energy function assumed that the artery had homogenous material properties. Also Raghavan *et al* [183], hypothesised that for an artery with a given residual stress, a short segment will reveal a different opening angle compared to a long segment of that artery. Therefore, based on the fact that the residual stress is lower in a short arterial segment for a given opening angle, they suggested that a shorter segment will reveal a smaller polar angle (2θ, see Figure 3.1) or a larger opening angle. Furthermore, they proposed that the length to thickness ratio of ten or more was desirable for consistency with *in vivo* conditions. In the case of the opening angles measurements in Schulze-Bauer *et al* [59], a length to thickness ratio of ten or more was not implemented for all layers of the arterial specimens.

The Ogden constitutive equation was used in the finite element representations of the artery. This model is an isotropic hyperelastic model and therefore does not fully represent the arterial tissue mechanical characteristics since the arterial tissue has been identified as being anisotropic [35]. It is important to examine the stress versus strain response of arterial tissue, in order to understand this limitation in relation to the calculation of stresses. The experimental data for each layer of the human external iliac artery used to define the Ogden model illustrates the key characteristics of the non-linear stress-strain behaviour of soft tissue. However, experimental testing has shown that there is a great deal of variability in the stress versus strain response of arterial tissue in the uniaxial deformation mode [44,180]. Whilst an anisotropic model would be more accurate it is clear that the variability in the tissue elasticity would necessitate a host-specific anisotropic model to accurately represent the arterial tissue. The Ogden model presented here for each layer of the artery was based on published data but limited to uniaxial data. Models were simulated for axial and circumferential uniaxial tensile tests to account for the variability in the tissue samples. Although this model was based on uniaxial data alone, it is proposed that the addition of biaxial stress versus stretch data to the current model would represent an appropriate compromise to a host specific anisotropic model. To represent the variability of tissue, it is possible to develop several isotropic models covering the range of arterial tissue elasticity, based on both uniaxial and biaxial stress versus stretch data [184].

Arterial tissue also exhibits viscoelastic properties such as strain rate dependency [30,31]. The Ogden hyperelastic model does not account for the viscoelasticity of arterial tissue. To minimise the affect of this, all uniaxial experiments were conducted at the same strain rate and the arterial tissue was preconditioned.

6.1.2 Biological Evaluation

The *in vitro* cell study's results are limited to the specific cell type utilised in the experiments (BAEC and BASMC). In determining membranes composition that displayed the most favourable growth for both BAEC and BASMC, cell counts on each membrane were taken from three 10X DAPI images which were often highly

subjective. Although unbiased means were used in this analysis, the subjective nature is an intrinsic limitation of the study. In addition, the hydrogel samples that were exposed to a dynamic environment demonstrated that BAEC adhesion could withstand low levels of shear stress but this does not prove that BAEC could withstand physiological shear stress. However, the results do show that this is possible. The strength of cell adhesion could be tested by developing a flow loop that exposes the cells culture on the hydrogel to physiological shear stress.

6.1.3 Mechanical Evaluation

Limitations were evident in experimental setups. Uniaxial elongation of the material sample was based on the grip separation of the mechanical tester (displacement-controlled testing) which is an indirect measurement. The biaxial inflation test was static test and deformation measurements were conducted with a depth micrometer. A dynamic test using a non-contact measurement device, for example a laser sensor, to measure the change in height of the bubble would provide more accurate data and enable controlled cyclic dynamic tests to be conducted. The phantom inflation testing presents some difficulties with respect to phantom placement. For accurate deformation measurements, the tube must be kept at constant length with a predefined axial displacement. In addition, no twisting can be induced in the tube. In practice, it was difficult to attach the phantom while strictly abiding by these guidelines. Although extreme care was taken for phantom placement, minor phantom deformations most probably occurred. Phantom deformations were conducted using digital vernier callipers. This contact measurement method was not ideal and while great care was taken in measuring the phantom deformation it was inevitable that this was a source of errors. Furthermore, as previously stated for the biaxial inflation test, more accurate data and greater flexibility in the tests protocols could be evaluated with the use of a non-contact measurement device.

SEM analysis of the cross sectional structure of the hydrogel provided an excellent characterisation of the material. However, some caution is warranted in interpreting the differences in the samples since these tests were conducted on dehydrated samples. To obtain a more accurate representation of the material

characteristics cryo-high resolution SEM could be utilised. This tool enables the observation of the polymer network of hydrogels in their hydrated state, which would be useful in determining the true pore size of the materials during biological studies.

6.2 Future Directions

Despite the results reported in this thesis, much work is still required to develop a bioartificial vessel for cell culture experiments and investigate vascular cell fate. In particular the following areas need to be investigated:

- Experimental Data

  Uniaxial and biaxial experimental data of the intima, media and adventitia are required to develop more complete numerical models and permit further understanding of the structural response of arterial vessels. In addition, mechanical testing of the collagen and elastin constituents of the artery wall would enable more complex finite element models to be developed.

- Preconditioning

  A preconditioning effect was evident for the PVA-chitosan hydrogel membranes. Further investigation is required to determine effects of various strain rates and preconditioning maximum loads on the stress versus strain characteristics of the biomaterial. Dynamic testing protocols would also enable evaluation of the stress versus strain behaviour of the PVA-chitosan blended hydrogel for stepped preconditioned loads and consecutive cyclic loading cycles.

- Vascular cell activity

  The vascular cell activity was assessed on PVA-chitosan following one freeze-thaw cycle. The mechanical properties and morphological

characteristics of the PVA-chitosan blended membranes were altered as the number of freeze-thaw cycles were increased. These changes to the surface texture of the biomaterial and cross-sectional pore structure will have a significant affect on the adhesion, growth, proliferation and apoptosis of the vascular cells [185].

- Anisotropic response of biomaterial - Fabrication methods to produce hydrogels with anisotropic material properties are required.

  One approach would be to fabricate the PVA-chitosan biomaterial from nanoscale hydrogel fibres. These fibres could in turn be incorporated into PVA-chitosan hydrogel tubular vessels creating a tube with an anisotropic respsone similar to arterial tissue. A number of manufacturing processes have been explored to fabricate micro or nanoscale fibrous matrices, including drawing [186], self-assembly [187], phase separation [188], and electrospinning [189-191]. Electrospinning has been generally accepted as the simplest and least expensive method to manufacture ultrafine fibrous biomaterials and offers many attractive attribute for tissue engineering applications. A high surface area-to volume and high porosity can be achieved which can enhance cell adhesion and perfusion. Electrospinning also allows for precise control of nano-, micro- and macro-scales for flexible biomaterial design. Multiple biomaterials and bioactive ingredients may be blended to product fibres [192]. The fibrous biomaterials can also enhance the mechanical properties compared to their solid equivalents [193]. Ohkawa *et al* and Ignatova *et al* [194,195] have successfully fabricated PVA-chitosan blended fibres via electrospinning.

- Porosity of biomaterial - Experimental investigations are required into the control of the pore size in the hydrogel in order to allow for communication between cells and appropriate diffusion of nutrients.

  An alternative to electrospinning to create pores is to prepare a PVA-chitosan hydrogel solution containing pores. Several methods such as the

porogen technique [99], the phase separation technique [196], the foaming technique [197], the overrun process [182] have been proposed to produce porous hydrogels. With the exception of the overrun process, most techniques require additives (for example organic solvents, foaming agents and porogen) to create pores. The overrun process (a process used in the manufacturing of soft ice cream) entraps injected air during the manufacturing process at low temperature because the entrapped air can produce pores in the hydrogel. The pore size and distribution can be easily controlled by adjusting several aspects of the process (impeller rate and operative temperature) and the concentration of the hydrogel [182].

- Micromesh patterning - Experimental studies to determine the optimum surface roughness for culture of different cell types.

The biomaterial surface plays an important role in cellular adhesion, proliferation, differentiation and apoptosis [185]. Micro or nanopatterns on the surface of the biomaterial, allows control and manipulation of the cell–biomaterial and cell–cell interactions in such a way to create patterns of cells that are highly oriented and differentiated [185]. Cells react to chemical and topographical stimuli through specific receptors. Therefore micro and nanopatterned biomaterials can be utilized to investigate the influence of surface morphology of biomaterials on the adhesion and growth of specific cells types. Numerous different techniques including microcontact printing, photolithography [198], photoimmobilisation process [198] have been developed to creating mircopatterns on the surface of biomaterials. It has been reported that nanoscale patterns increased both cell density and cell spreading during the initial cell culture stages [199] and enhanced adhesion and growth of EC [200].

- Fabrication processes - More efficient processes are required for fabricating PVA-chitosan hydrogels in short cycle times without sacrificing control over mechanical properties.

An attractive method of polymerisation of PVA-chitosan is photopolymerisation. Hydrogels can be photopolymerised in the presence of photoinitiators using ultraviolet UV light [201]. Photopolymerisation has several advantageous feature compared to other polymerization techniques including spatial and temporal control over polymerisation, fast curing rates (less than a second to a few minutes) at room/physiological temperatures, and minimal heat production [202]. A wide variety of biomedical applications have been suggested for photopolymerised hydrogels including prevention of thrombosis [149], post-operative adhesion formation [203], drug delivery [204] and tissue engineering scaffolds [201].

- **Bioreactor - Commission a bioreactor with bioartificial vessels to simultaneously expose vascular cells to cyclic strain and shear stress.**

  In order to develop the bioreactor a number of steps are required:
  - Co-culture EC and SMC on the PVA-chitosan membranes.
  - Physiological shear stress, pressure and cyclic strain.
  - Static versus dynamic culture experiments.

- **Bioreactor potential**

  Cellular functionality and behaviour for physiological and non-physiological conditions. Cellular response due to antibiotics and mechanical interventional procedures (for example drug-eluding stents) could also be evaluated.

References

[1] Thom, T., Haase, N., Rosamond, W., Howard, V.J., Rumsfeld, J., Manolio, T., Zheng, Z.J., Flegal, K., O'Donnell, C., Kittner, S., Lloyd-Jones, D., Goff, D.C., Jr., Hong, Y., Adams, R., Friday, G., Furie, K., Gorelick, P., Kissela, B., Marler, J., Meigs, J., Roger, V., Sidney, S., Sorlie, P., Steinberger, J., Wasserthiel-Smoller, S., Wilson, M. and Wolf, P., (2006), "Heart disease and stroke statistics--2006 update: a report from the American Heart Association Statistics Committee and Stroke Statistics Subcommittee", *Circulation*, Vol.113 (6), pp.e85-151.

[2] World Health Organisation, W., (2006), "The Atlas of Heart Disease and Stroke."

[3] Irish Heart Foundation, (2004), "Cardiovascular Disease Mortality Rates ".

[4] Gibbons, G. and Dzau, V., (1994), "The emerging concept of vascular remodelling." *New England Journal of Medicine*, Vol.330 (20), pp.1431-1438.

[5] Mann, B.K., (2003), "Biologic gels in tissue engineering", *Clin Plast Surg*, Vol.30 (4), pp.601-609.

[6] Amsden, B., (1998), "Solute Diffusion within Hydrogels. Mechanisms and Models." *Macromolecules*, Vol.31 (23), pp.8382 - 8395.

[7] Hern, D.L. and Hubbell, J.A., (1998), "Incorporation of adhesion peptides into nonadhesive hydrogels useful for tissue resurfacing", *J Biomed Mater Res*, Vol.39 (2), pp.266-276.

[8] Mazzucotelli, J.P., Moczar, M., Zede, L., Bambang, L.S. and Loisance, D., (1994), "Human vascular endothelial cells on expanded PTFE precoated with an engineered protein adhesion factor", *Int J Artif Organs*, Vol.17 (2), pp.112-117.

[9] Greisler, H.P., Gosselin, C., Ren, D., Kang, S.S. and Kim, D.U., (1996), "Biointeractive polymers and tissue engineered blood vessels", *Biomaterials*, Vol.17 (3), pp.329-336.

[10] Elshazly, T., (2004), "Characteristaion of PVA hydrogels with regards to vascular graft development." Masters Thesis, Georgia Institute of Technology.

[11] Hayashi, K., (2001), "In: Mechanical Properties of Arterial Wall", *International Centre for Mechanical Sciences, Italy.*

[12] Nichols, W., and O'Rourke, M.F. "McDonald's Blood flow in arteries : theoretic, experimental and clinical principles", *Hodder Arnold*, 5th Edition, London, 2005.

[13] University of Oulu, Finland, [online], http://herkules.oulu.fi/isbn951426973X/html/x840.html (last accessed 12th May 2006)

[14] Silver, F.H., Christiansen, D.L. and Buntin, C.M., (1989), "Mechanical properties of the aorta: a review", *Crit Rev Biomed Eng*, Vol.17 (4), pp.323-358.

[15] Holzapfel, G., Gasser, T. and Ogden, R., (2000), "A new constitutive framework for arterial wall mechanics and a comparative study of material models", *Journal of Elasticity*, Vol.61 (1-3), pp.1-48.

[16] Huttner, I., Kocher, O. and Gabbiani, G. (1989) Endothelial and Smooth-Muscle Cells., Springer-Verlag, London. pp. 10-39.

[17] Clark, J.M. and Glagov, S., (1979), "Structural integration of the arterial wall. I. Relationships and attachments of medial smooth muscle cells in normally distended and hyperdistended aortas", *Lab Invest*, Vol.40 (5), pp.587-602.

[18] Humphrey, J.D., (2002),*Cardiovascular Solid Mechanics: Cells, Tissues, and Organs.* , Springer-Verlag New York Inc., New York.

[19] Humphrey, J.D., (1995), "Mechanics of the arterial wall: review and directions", *Crit Rev Biomed Eng*, Vol.23 (1-2), pp.1-162.

[20] Martini, F., (2001), "Fundamentals of Anatomy and Physiology ", (Fifth Edition), pp.666.

[21] Xie, J., Zhou, J. and Fung, Y.C., (1995), "Bending of blood vessel wall: stress-strain laws of the intima-media and adventitial layers", *J Biomech Eng*, Vol.117 (1), pp.136-145.

[22] Holzapfel, G., Gasser, T. and Stadler, M., (2002), "A structural model for the viscoelastic behavior of arterial walls: Continuum formulation and finite

element analysis", *European Journal of mechanics A-solids*, Vol. 21 (3), pp.441-463.

[23] Wolinsky, H. and Glagov, S., (1964), "Structural Basis For The Static Mechanical Properties Of The Aortic Media", *Circ Res*, Vol.14 pp.400-413.

[24] Hayashi, K., (2003), "Mechanical Properties and Histological Structure of Soft Tissue. In: Biomechanics of Soft Tissue in Cardiovascular Systems International.

[25] Carew, T.E., Vaishnav, R.N. and Patel, D.J., (1968), "Compressibility of the arterial wall", *Circ Res*, Vol.23 (1), pp.61-68.

[26] Zhao, S.Z., Xu, X.Y. and Collins, M.W., (1998), "The numerical analysis of fluid-solid interactions for blood flow in arterial structures. Part 1: A review of models for arterial wall behaviour", *Proc Inst Mech Eng [H]*, Vol.212 (4), pp.229-240.

[27] Dobrin, P.B. and Rovick, A.A., (1969), "Influence of vascular smooth muscle on contractile mechanics and elasticity of arteries", *Am J Physiol*, Vol.217 (6), pp.1644-1651.

[28] Patel, D.J., Janicki, J.S. and Carew, T.E., (1969), "Static anisotropic elastic properties of the aorta in living dogs", *Circ Res*, Vol.25 (6), pp.765-779.

[29] Chuong, C.J. and Fung, Y.C., (1983), "Three-dimensional stress distribution in arteries", *J Biomech Eng*, Vol.105 (3), pp.268-274.

[30] von Maltzahn, W.W., Warriyar, R.G. and Keitzer, W.F., (1984), "Experimental measurements of elastic properties of media and adventitia of bovine carotid arteries", *J Biomech*, Vol.17 (11), pp.839-847.

[31] Wu, S.G. and Lee, G.C., (1984), "On nonlinear viscoelastic properties of arterial tissue", *J Biomech Eng*, Vol.106 (1), pp.42-47.

[32] Wu, S.G., Lee, G.C. and Tseng, N.T., (1984), "Nonlinear elastic analysis of blood vessels", *J Biomech Eng*, Vol.106 (4), pp.376-383.

[33] Holzapfel, G.A., Schulze-Bauer, C.A.J. and Stadler, M., (2000), "Mechanics of angioplasty: Wall, balloon and Stent", *Mechanics in Biology*, Vol.242 (46), pp.141-156.

[34] Sharma, M.G., (1974), "Viscoelastic behavior of conduit arteries", *Biorheology*, Vol.11 (4), pp.279-291.

[35] Patel, D.J. and Fry, D.L., (1969), "The elastic symmetry of arterial segments in dogs", *Circ Res*, Vol.24 (1), pp.1-8.

[36] Mohan, D. and Melvin, J.W., (1982), "Failure properties of passive human aortic tissue. I--uniaxial tension tests", *J Biomech*, Vol.15 (11), pp.887-902.

[37] Bergel, D.H., (1961), "The static elastic properties of the arterial wall." *J Physiol*, Vol.156 pp.445-457.

[38] Manak, J.J., (1980), "The two-dimensional in vitro passive stress-strain elasticity relationships for the steer thoracic aorta blood vessel tissue", *J Biomech*, Vol.13 (8), pp.637-646.

[39] Vito, R.P., (1980), "The mechanical properties of soft tissues--I: a mechanical system for bi-axial testing", *J Biomech*, Vol.13 (11), pp.947-950.

[40] Mohan, D. and Melvin, J.W., (1983), "Failure properties of passive human aortic tissue. II--Biaxial tension tests", *J Biomech*, Vol.16 (1), pp.31-44.

[41] Vaishnav, R.N., Young, J.T., Janicki, J.S. and Patel, D.J., (1973), "Nonlinear anisotropic elastic properties of the canine aorta." *Biophysical Journal*, Vol.12 pp.1008-1027.

[42] Sacks, M.S., (2000), "Biaxial Mehanical Evaluation of Planar Biological Materials." *J Elast*, Vol.61 pp.199-246.

[43] Fung, Y.C., Fronek, K. and Patitucci, P., (1979), "Pseudoelasticity of arteries and the choice of its mathematical expression", *Am J Physiol*, Vol.237 (5), pp.H620-631.

[44] van Andel, C.J., Pistecky, P.V. and Borst, C., (2003), "Mechanical properties of porcine and human arteries: implications for coronary anastomotic connectors", *Ann Thorac Surg*, Vol.76 (1), pp.58-64; discussion 64-55.

[45] Ogden, R.W. and Schulze-Bauer, C.A.J., (2000), "Phenomenological and structural aspects of the mechanical response of arteries." *Proceedings in Mechanics in Biology*, Vol.242 (46), pp.125-140.

[46] Cox, R.H., (1978), "Passive mechanics and connective tissue composition of canine arteries", *Am J Physiol*, Vol.234 (5), pp.H533-541.

[47] Speckmann, E.W. and Ringer, R.K., (1966), "Volume-pressure relationships of the turkey aorta", *Can J Physiol Pharmacol*, Vol.44 (6), pp.901-907.

[48] Toner, D., (2005), "The relationship between variations in the uniaxial tensile properties of porcine aortic tissue and distance form the heart." *Final Year Project, Dublin City University.*

[49] Rachev, A. and Greenwald, S.E., (2003), "Residual strains in conduit arteries", *J Biomech*, Vol.36 (5), pp.661-670.

[50] Vito, R.P. and Dixon, S.A., (2003), "Blood vessel constitutive models-1995-2002", *Annu Rev Biomed Eng*, Vol.5 pp.413-439.

[51] Chuong, C.J. and Fung, Y.C., (1986), "On residual stresses in arteries", *J Biomech Eng*, Vol.108 (2), pp.189-192.

[52] Fung, Y.C. and Liu, S.Q., (1989), "Change of residual strains in arteries due to hypertrophy caused by aortic constriction", *Circ Res*, Vol.65 (5), pp.1340-1349.

[53] Han, H.C. and Fung, Y.C., (1995), "Longitudinal strain of canine and porcine aortas", *J Biomech*, Vol.28 (5), pp.637-641.

[54] Greenwald, S.E., Moore, J.E., Jr., Rachev, A., Kane, T.P. and Meister, J.J., (1997), "Experimental investigation of the distribution of residual strains in the artery wall", *J Biomech Eng*, Vol.119 (4), pp.438-444.

[55] Vossoughi, J., Hedjazi, Z. and Borris, F.S., (1993), "Intimal residual stress and strain in large arteries." *ASME Advances in Bioengineering*pp.434-437.

[56] Saini, A., Berry, C. and Greenwald, S., (1995), "Effect of age and sex on residual stress in the aorta", *J Vasc Res*, Vol.32 (6), pp.398-405.

[57] Zeller, P.J. and Skalak, T.C., (1998), "Contribution of individual structural components in determining the zero-stress state in small arteries", *J Vasc Res*, Vol.35 (1), pp.8-17.

[58] Fung, Y.C. and Liu, S.Q., (1991), "Changes of zero-stress state of rat pulmonary arteries in hypoxic hypertension", *J Appl Physiol*, Vol.70 (6), pp.2455-2470.

[59] Schulze-Bauer, C., Morth, C. and Holzapfel, G., (2003), "Passive biaxial mechanical response of aged human iliac arteries." *J Biomech Eng-T ASME*, Vol.125 (3), pp.395-406.

[60] Fung, Y.C., (1991), "What are the residual stresses doing in our blood vessels?" *Ann Biomed Eng*, Vol.19 (3), pp.237-249.

[61] Traub, O. and Berk, B.C., (1998), "Laminar shear stress: mechanisms by which endothelial cells transduce an atheroprotective force", *Arterioscler Thromb Vasc Biol*, Vol.18 (5), pp.677-685.

[62] Zou, Y., Hu, Y., Metzler, B. and Xu, Q., (1998), "Signal transduction in arteriosclerosis: mechanical stress-activated MAP kinases in vascular smooth muscle cells (review)", *Int J Mol Med*, Vol.1 (5), pp.827-834.

[63] Xu, Q., (2000), "Biomechanical-stress-induced signaling and gene expression in the development of arteriosclerosis", *Trends Cardiovasc Med*, Vol. 10 (1), pp.35-41.

[64] Davies, P.F., (1995), "Flow-mediated endothelial mechanotransduction", *Physiol Rev*, Vol. 75 (3), pp.519-560.

[65] Patrick, C.W., Jr. and McIntire, L.V., (1995), "Shear stress and cyclic strain modulation of gene expression in vascular endothelial cells", *Blood Purif*, Vol. 13 (3-4), pp.112-124.

[66] Kamiya, A., Bukhari, R. and Togawa, T., (1984), "Adaptive regulation of wall shear stress optimizing vascular tree function", *Bull Math Biol*, Vol. 46 (1), pp.127-137.

[67] Diamond, S.L., Sharefkin, J.B., Dieffenbach, C., Frasier-Scott, K., McIntire, L.V. and Eskin, S.G., (1990), "Tissue plasminogen activator messenger RNA levels increase in cultured human endothelial cells exposed to laminar shear stress", *J Cell Physiol*, Vol.143 (2), pp.364-371.

[68] Gotlieb, A.I. and Langille, B.L., (1996), "The Role of Rheology in Atherosclerotic Coronary Artery Disease." pp.595-606.

[69] Cornhill, J.F., Herderick, E.E. and Stary, H.C., (1990), "Topography of human aortic sudanophilic lesions", *Monogr Atheroscler*, Vol.15 pp.13-19.

[70] Gimbrone, M.A., Jr., (1989), "Endothelial dysfunction and atherosclerosis", *J Card Surg*, Vol.4 (2), pp.180-183.

[71] Rao, R.S., Miano, J.M., Olson, E.N. and Seidel, C.L., (1997), "The A10 cell line: a model for neonatal, neointimal, or differentiated vascular smooth muscle cells?" *Cardiovasc Res*, Vol. 36 (1), pp.118-126.

[72] Shanahan, C.M., Weissberg, P.L. and Metcalfe, J.C., (1993), "Isolation of gene markers of differentiated and proliferating vascular smooth muscle cells", *Circ Res*, Vol. 73 (1), pp.193-204.

[73] Benditt, E.P., (1977), "The origin of atherosclerosis", *Sci Am*, Vol.236 (2), pp.74-85.

[74] Barron, V., Lyons, E., Stenson-Cox, C., McHugh, P.E. and Pandit, A., (2003), "Bioreactors for cardiovascular cell and tissue growth: a review", *Ann Biomed Eng*, Vol. 31 (9), pp.1017-1030.

[75] Moore, J.E., Jr., Burki, E., Suciu, A., Zhao, S., Burnier, M., Brunner, H.R. and Meister, J.J., (1994), "A device for subjecting vascular endothelial cells

to both fluid shear stress and circumferential cyclic stretch", *Ann Biomed Eng*, Vol.22 (4), pp.416-422.

[76] Redmond, E.M., Cahill, P.A. and Sitzmann, J.V., (1995), "Perfused transcapillary smooth muscle and endothelial cell co-culture--a novel in vitro model", *In Vitro Cell Dev Biol Anim*, Vol.31 (8), pp.601-609.

[77] Blackman, B.R., Garcia-Cardena, G. and Gimbrone, M.A., Jr., (2002), "A new in vitro model to evaluate differential responses of endothelial cells to simulated arterial shear stress waveforms", *J Biomech Eng*, Vol.124 (4), pp.397-407.

[78] Lawrence, M.B., McIntire, L.V. and Eskin, S.G., (1987), "Effect of flow on polymorphonuclear leukocyte/endothelial cell adhesion", *Blood*, Vol.70 (5), pp.1284-1290.

[79] Brown, D.C. and Larson, R.S., (2001), "Improvements to parallel plate flow chambers to reduce reagent and cellular requirements", *BMC Immunol*, Vol.2 pp.9.

[80] Banes, A.J., Link, G.W., Jr., Gilbert, J.W., Tran Son Tay, R. and Monbureau, O., (1990), "Culturing cells in a mechanically active environment", *Am Biotechnol Lab*, Vol.8 (7), pp.12-22.

[81] DiCorleto, P.E. and Gimbrone, M.A., Jr., (1996), "Vascular Endothelium", pp.387-399.

[82] Humphrey, J.D. and Delange, S.L., (2004), "An Introduction to Biomechanics - Solids and Fluids, Analysis and Design", Springer-Verlag New York, Inc .pp.7.

[83] Langille, B.L. and Adamson, S.L., (1981), "Relationship between blood flow direction and endothelial cell orientation at arterial branch sites in rabbits and mice", *Circ Res*, Vol.48 (4), pp.481-488.

[84] Flaherty, J.T., Pierce, J.E., Ferrans, V.J., Patel, D.J., Tucker, W.K. and Fry, D.L., (1972), "Endothelial nuclear patterns in the canine arterial tree with particular reference to hemodynamic events", *Circ Res*, Vol.30 (1), pp.23-33.

[85] Ziegler, T. and Nerem, R.M., (1994), "Effect of flow on the process of endothelial cell division", *Arterioscler Thromb*, Vol.14 (4), pp.636-643.

[86] Hsieh, H.J., Li, N.Q. and Frangos, J.A., (1991), "Shear stress increases endothelial platelet-derived growth factor mRNA levels", *Am J Physiol*, Vol.260 (2 Pt 2), pp.H642-646.

[87] Koller, A., Sun, D. and Kaley, G., (1993), "Role of shear stress and endothelial prostaglandins in flow- and viscosity-induced dilation of arterioles in vitro", *Circ Res*, Vol.72 (6), pp.1276-1284.

[88] Camillieri, J.P. Berry, C.L., Fiessinger, J., Bariety, J, (1989), "*Diseases of the Arterial Wall*", Springer.

[89] Morrow, D., Sweeney, C., Birney, Y.A., Cummins, P.M., Walls, D., Redmond, E.M. and Cahill, P.A., (2005), "Cyclic strain inhibits Notch receptor signaling in vascular smooth muscle cells in vitro", *Circ Res*, Vol.96 (5), pp.567-575.

[90] Cappadona, C., Redmond, E.M., Theodorakis, N.G., McKillop, I.H., Hendrickson, R., Chhabra, A., Sitzmann, J.V. and Cahill, P.A., (1999), "Phenotype dictates the growth response of vascular smooth muscle cells to pulse pressure in vitro", *Exp Cell Res*, Vol.250 (1), pp.174-186.

[91] von Offenberg Sweeney, N., Cummins, P.M., Birney, Y.A., Redmond, E.M. and Cahill, P.A., (2004), "Cyclic strain-induced endothelial MMP-2: role in vascular smooth muscle cell migration", *Biochem Biophys Res Commun*, Vol.320 (2), pp.325-333.

[92] Levenberg, S. and Langer, R., (2004), "Advances in tissue engineering", *Curr Top Dev Biol*, Vol.61 pp.113-134.

[93] Zhang, Y., Li, Y., Shen, W., Liu, D. and Chen, J., (2005), "A new strain, Streptomyces venezuelae GY1, producing a poly(vinyl alcohol)-degrading enzyme." *World Journal of Microbiology & Biotechnology.*

[94] Sakazawa, C., Shimao, M., Taniguchi, Y. and Kato, N., (1981), "Symbiotic utilization of polyvinyl alcohol by mixed cultures", *Appl Environ Microbiol*, Vol.41 (1), pp.261-267.

[95] Hoffman, A.S., (2002), "Hydrogels for biomedical applications", *Adv Drug Deliv Rev*, Vol.54 (1), pp.3-12.

[96] Chuang, W.Y., Young, T.H., Yao, C.H. and Chiu, W.Y., (1999), "Properties of the poly(vinyl alcohol)/chitosan blend and its effect on the culture of fibroblast in vitro. " *Biomaterials*, Vol.20 (16), pp.1479-1487.

[97] Koyano, T., Minoura, N., Nagura, M. and Kobayashi, K., (1998), "Attachment and growth of cultured fibroblast cells on PVA/chitosan-blended hydrogels", *J Biomed Mater Res*, Vol.39 (3), pp.486-490.

[98] Ratner, B.D., (1993), "New ideas in biomaterials science--a path to engineered biomaterials", *J Biomed Mater Res*, Vol.27 (7), pp.837-850.

[99] Oxley, H.R., Corkhill, P.H., Fitton, J.H. and Tighe, B.J., (1993), "Macroporous hydrogels for biomedical applications: methodology and morphology", *Biomaterials*, Vol.14 (14), pp.1064-1072.

[100] Shachar, M. and Cohen, S., (2003), "Cardiac tissue engineering, ex-vivo: design principles in biomaterials and bioreactors", *Heart Fail Rev*, Vol.8 (3), pp.271-276.

[101] Biospecifics Technologies Corporation, US, [online], http://www.biospecifics.com/collagendefined.html (last accessed 12th May 2006).

[102] Lee, C.R., Grodzinsky, A.J. and Spector, M., (2001), "The effects of cross-linking of collagen-glycosaminoglycan scaffolds on compressive stiffness, chondrocyte-mediated contraction, proliferation and biosynthesis", *Biomaterials*, Vol.22 (23), pp.3145-3154.

[103] Park, S.N., Park, J.C., Kim, H.O., Song, M.J. and Suh, H., (2002), "Characterization of porous collagen/hyaluronic acid scaffold modified by 1-ethyl-3-(3-dimethylaminopropyl)carbodiimide cross-linking", *Biomaterials*, Vol.23 (4), pp.1205-1212.

[104] Schoof, H., Apel, J., Heschel, I. and Rau, G., (2001), "Control of pore structure and size in freeze-dried collagen sponges", *J Biomed Mater Res*, Vol.58 (4), pp.352-357.

[105] Weinberg, C.B. and Bell, E., (1985), "Regulation of proliferation of bovine aortic endothelial cells, smooth muscle cells, and adventitial fibroblasts in collagen lattices", *J Cell Physiol*, Vol.122 (3), pp.410-414.

[106] Weinberg, C.B. and Bell, E., (1986), "A blood vessel model constructed from collagen and cultured vascular cells", *Science*, Vol.231 (4736), pp.397-400.

[107] Ziegler, T., Alexander, R.W. and Nerem, R.M., (1995), "An endothelial cell-smooth muscle cell co-culture model for use in the investigation of flow effects on vascular biology", *Ann Biomed Eng*, Vol.23 (3), pp.216-225.

[108] Wissink, M.J., Beernink, R., Poot, A.A., Engbers, G.H., Beugeling, T., van Aken, W.G. and Feijen, J., (2000), "Improved endothelialization of vascular grafts by local release of growth factor from heparinized collagen matrices", *J Control Release*, Vol.64 (1-3), pp.103-114.

[109] Chandy, T. and Sharma, C.P., (1990), "Chitosan--as a biomaterial", *Biomater Artif Cells Artif Organs*, Vol.18 (1), pp.1-24.

[110] Di Martino, A., Sittinger, M. and Risbud, M.V., (2005), "Chitosan: a versatile biopolymer for orthopaedic tissue-engineering", *Biomaterials*, Vol.26 (30), pp.5983-5990.

[111] Madihally, S.V. and Matthew, H.W., (1999), "Porous chitosan scaffolds for tissue engineering", *Biomaterials*, Vol.20 (12), pp.1133-1142.

[112] Suh, J.K. and Matthew, H.W., (2000), "Application of chitosan-based polysaccharide biomaterials in cartilage tissue engineering: a review", *Biomaterials*, Vol.21 (24), pp.2589-2598.

[113] Hirano, S., Tsuchida, H. and Nagao, N., (1989), "N-acetylation in chitosan and the rate of its enzymic hydrolysis", *Biomaterials*, Vol.10 (8), pp.574-576.

[114] Hu, Q., Li, B., Wang, M. and Shen, J., (2004), "Preparation and characterization of biodegradable chitosan/hydroxyapatite nanocomposite rods via in situ hybridization: a potential material as internal fixation of bone fracture", *Biomaterials*, Vol.25 (5), pp.779-785.

[115] Chenite, A., Chaput, C., Wang, D., Combes, C., Buschmann, M.D., Hoemann, C.D., Leroux, J.C., Atkinson, B.L., Binette, F. and Selmani, A., (2000), "Novel injectable neutral solutions of chitosan form biodegradable gels in situ", *Biomaterials*, Vol.21 (21), pp.2155-2161.

[116] Risbud, M., Ringe, J., Bhonde, R. and Sittinger, M., (2001), "In vitro expression of cartilage-specific markers by chondrocytes on a biocompatible hydrogel: implications for engineering cartilage tissue", *Cell Transplant*, Vol.10 (8), pp.755-763.

[117] Xia, W., Liu, W., Cui, L., Liu, Y., Zhong, W., Liu, D., Wu, J., Chua, K. and Cao, Y., (2004), "Tissue engineering of cartilage with the use of chitosan-gelatin complex scaffolds", *J Biomed Mater Res B Appl Biomater*, Vol.71 (2), pp.373-380.

[118] Hu, S.G., Jou, C.H. and Yang, M.C., (2003), "Protein adsorption, fibroblast activity and antibacterial properties of poly(3-hydroxybutyric acid-co-3-hydroxyvaleric acid) grafted with chitosan and chitooligosaccharide after immobilized with hyaluronic acid", *Biomaterials*, Vol.24 (16), pp.2685-2693.

[119] Howling, G.I., Dettmar, P.W., Goddard, P.A., Hampson, F.C., Dornish, M. and Wood, E.J., (2001), "The effect of chitin and chitosan on the proliferation of human skin fibroblasts and keratinocytes in vitro", *Biomaterials*, Vol.22 (22), pp.2959-2966.

[120] Risbud, M., Endres, M., Ringe, J., Bhonde, R. and Sittinger, M., (2001), "Biocompatible hydrogel supports the growth of respiratory epithelial cells: possibilities in tracheal tissue engineering", *J Biomed Mater Res*, Vol.56 (1), pp.120-127.

[121] Wang, J.H., Wei, C.W., Liu, H.C. and Young, T.H., (2003), "Behavior of MG-63 cells on nylon/chitosan-blended membranes", *J Biomed Mater Res A*, Vol.64 (4), pp.606-615.

[122] Aimin, C., Chunlin, H., Juliang, B., Tinyin, Z. and Zhichao, D., (1999), "Antibiotic loaded chitosan bar. An in vitro, in vivo study of a possible treatment for osteomyelitis", *Clin Orthop Relat Res* (366), pp.239-247.

[123] Lee, J.Y., Nam, S.H., Im, S.Y., Park, Y.J., Lee, Y.M., Seol, Y.J., Chung, C.P. and Lee, S.J., (2002), "Enhanced bone formation by controlled growth factor delivery from chitosan-based biomaterials", *J Control Release*, Vol.78 (1-3), pp.187-197.

[124] Bumgardner, J.D., Wiser, R., Gerard, P.D., Bergin, P., Chestnutt, B., Marin, M., Ramsey, V., Elder, S.H. and Gilbert, J.A., (2003), "Chitosan: potential use as a bioactive coating for orthopaedic and craniofacial/dental implants", *J Biomater Sci Polym Ed*, Vol.14 (5), pp.423-438.

[125] The Williams Syndrome Comprehensive Web Site, US, [online], http://www.wsf.org/medical/literature/layreader/elastin.htm (last accessed 12th May 2006)

[126] Heilshorn, S.C., DiZio, K.A., Welsh, E.R. and Tirrell, D.A., (2003), "Endothelial cell adhesion to the fibronectin CS5 domain in artificial extracellular matrix proteins", *Biomaterials*, Vol.24 (23), pp.4245-4252.

[127] Nuttelman, C.R., Mortisen, D.J., Henry, S.M. and Anseth, K.S., (2001), "Attachment of fibronectin to poly(vinyl alcohol) hydrogels promotes NIH3T3 cell adhesion, proliferation, and migration", *J Biomed Mater Res*, Vol.57 (2), pp.217-223.

[128] Cascone, M.G., Lazzeri, L., Sparvoli, E., Scatena, M., Serino, L.P. and Danti, S., (2004), "Morphological evaluation of bioartificial hydrogels as potential

tissue engineering scaffolds", *J Mater Sci Mater Med*, Vol.15 (12), pp.1309-1313.

[129] Schmedlen, R.H., Masters, K.S. and West, J.L., (2002), "Photocrosslinkable polyvinyl alcohol hydrogels that can be modified with cell adhesion peptides for use in tissue engineering", *Biomaterials*, Vol.23 (22), pp.4325-4332.

[130] West, J.L. and Hubbell, J.A., (1999), "Polymeric biomaterials with degradation sites for proteases involved in cell migration." *Macromolecules*, Vol.32 pp.241-244.

[131] Muller, B., (1996), "Photocrosslinked polymers", US5508317.

[132] Chu, K.C. and Rutt, B.K., (1997), "Polyvinyl alcohol cryogel: an ideal phantom material for MR studies of arterial flow and elasticity", *Magn Reson Med*, Vol.37 (2), pp.314-319.

[133] Wan, W.K., Campbell, G., Zhang, Z.F., Hui, A.J. and Boughner, D.R., (2002), "Optimizing the tensile properties of Polyvinyl Alcohol Hydrogel for the construction of a bioprosthetic heart valve stent. " *J Biomed Mater Res*, Vol.63 pp.854-861.

[134] Jiang, H., Campbell, G., Boughner, D., Wan, W.K. and Quantz, M., (2004), "Design and manufacture of a polyvinyl alcohol (PVA) cryogel tri-leaflet heart valve prosthesis." *Medical Engineering and Physics* Vol.26 pp.269-277.

[135] Vijayasekaran, S., Fitton, J.H., Hicks, C.R., Chirila, T.V., Crawford, G.J. and Constable, I.J., (1998), "Cell viability and inflammatory response in hydrogel sponges implanted in the rabbit cornea", *Biomaterials*, Vol.19 (24), pp.2255-2267.

[136] Stammen, J.A., Williams, S., Ku, D.N. and Guldberg, R.E., (2001), "Mechanical properties of a novel PVA hydrogel in shear and unconfined compression", *Biomaterials*, Vol.22 (8), pp.799-806.

[137] Hickey, A.S. and Peppas, N.A., (1995), "Mesh size and diffusive characteristics of semicrystalline poly(vinyl alcohol) membranes prepared by freezing/thawing techniques." *J. Membr. Sci*, Vol.107 pp.229–237.

[138] Cascone, M.G., Sim, B. and Downes, S., (1995), "Blends of synthetic and natural polymers as drug delivery systems for growth hormone", *Biomaterials*, Vol.16 (7), pp.569-574.

[139] Zajaczkowski, M.B., Cukierman, E., Galbraith, C.G. and Yamada, K.M., (2003), "Cell-matrix adhesions on poly(vinyl alcohol) hydrogels", *Tissue Eng*, Vol.9 (3), pp.525-533.

[140] Ficek, B.J. and Peppas, N.A., (1993), "Novel preparation of poly(vinyl alcohol) microparticles without crosslinking agent for controlled drug delivery of proteins." *J. Control. Rel.*, Vol.27 pp.259–264.

[141] Peppas, N.A. and Mongia, N.K., (1997), "Ultrapure poly(vinyl alcohol) hydrogels with mucoadhesive drug delivery characteristics." *Eur. J. Pharm. Biopharm.*, Vol.43 pp.51–58.

[142] Hassan, C.M., Stewart, J.E. and Peppas, N.A., (2000), "Diffusional characteristics of freeze/thawed poly(vinyl alcohol) hydrogels: applications to protein controlled release from multilaminate devices", *Eur J Pharm Biopharm*, Vol.49 (2), pp.161-165.

[143] Hassan, C.M. and Peppas, N.A., (2000), "Structure and Morphology of Freeze/Thawed PVA Hydrogels. " *Macromolecules*, Vol.33 pp.2472-2479

[144] Bryant, S.J. and Anseth, K.S., (2001), "The effects of scaffold thickness on tissue engineered cartilage in photocrosslinked poly(ethylene oxide) hydrogels", *Biomaterials*, Vol.22 (6), pp.619-626.

[145] Mann, B.K., Gobin, A.S., Tsai, A.T., Schmedlen, R.H. and West, J.L., (2001), "Smooth muscle cell growth in photopolymerized hydrogels with cell adhesive and proteolytically degradable domains: synthetic ECM analogs for tissue engineering", *Biomaterials*, Vol.22 (22), pp.3045-3051.

[146] Park, K.H., Kim, M.H., Park, S.H., Lee, H.J., Kim, I.K. and Chung, H.M., (2004), "Synthesis of Arg-Gly-Asp (RGD) sequence conjugated thermo-reversible gel via the PEG spacer arm as an extracellular matrix for a pheochromocytoma cell (PC12) culture", *Biosci Biotechnol Biochem*, Vol.68 (11), pp.2224-2229.

[147] Almany, L. and Seliktar, D., (2005), "Biosynthetic hydrogel scaffolds made from fibrinogen and polyethylene glycol for 3D cell cultures", *Biomaterials*, Vol.26 (15), pp.2467-2477.

[148] O'Flynn, P.M., Roche, E.T. and Pandit, A.S., (2005), "Generating an ex vivo vascular model", *Asaio J*, Vol.51 (4), pp.426-433.

[149] Hill-West, J.L., Chowdhury, S.M., Slepian, M.J. and Hubbell, J.A., (1994), "Inhibition of thrombosis and intimal thickening by in situ

photopolymerization of thin hydrogel barriers", *Proc Natl Acad Sci U S A*, Vol.91 (13), pp.5967-5971.

[150] Risbud, M., Hardikar, A. and Bhonde, R., (2000), "Growth modulation of fibroblasts by chitosan-polyvinyl pyrrolidone hydrogel: implications for wound management?" *J Biosci*, Vol.25 (1), pp.25-31.

[151] Cascone, M.G. and Maltinti, S., (1999), "Hydrogels based on chitosan and dextran as potential drug delivery systems", *J Mater Sci Mater Med*, Vol.10 (5), pp.301-307.

[152] Leach, J.B. and Schmidt, C.E., (2005), "Characterization of protein release from photocrosslinkable hyaluronic acid-polyethylene glycol hydrogel tissue engineering scaffolds", *Biomaterials*, Vol.26 (2), pp.125-135.

[153] Delfino, A., Stergiopulos, N., Moore, J.E., Jr. and Meister, J.J., (1997), "Residual strain effects on the stress field in a thick wall finite element model of the human carotid bifurcation", *J Biomech*, Vol.30 (8), pp.777-786.

[154] Takamizawa, K. and Hayashi, K., (1987), "Strain energy density function and uniform strain hypothesis for arterial mechanics", *J Biomech*, Vol.20 (1), pp.7-17.

[155] Rachev, A., (1997), "Theoretical study of the effect of stress-dependent remodeling on arterial geometry under hypertensive conditions", *J Biomech*, Vol.30 (8), pp.819-827.

[156] von Maltzahn, W.W., Besdo, D. and Wiemer, W., (1981), "Elastic properties of arteries: a nonlinear two-layer cylindrical model", *J Biomech*, Vol.14 (6), pp.389-397.

[157] Tickner, E.G. and Sacks, A.H., (1967), "A theory for the static elastic behavior of blood vessels", *Biorheology*, Vol.4 (4), pp.151-168.

[158] Ogden, R.W., (1984), "Nonlinear elastic deformations." *John Wiley and Sons, New York.*

[159] Mooney, M., (1940), "A theory of large elastic deformation." *Journal of Applied Physics*, Vol.11 pp.582-592.

[160] Vaishnav, R.N., Young, J.T., Janicki, J.S. and Patel, D.J., (1972), "Nonlinear anisotropic elastic properties of the canine aorta." *Biophysical Journal*, Vol.12 pp.1008-1027.

[161] Rachev, A. and Hayashi, K., (1999), "Theoretical study of the effects of vascular smooth muscle contraction on strain and stress distributions in arteries", *Ann Biomed Eng*, Vol.27 (4), pp.459-468.

[162] Marc/Mendat manuals, (2005), *MSC Software* Vol.Santa Ana, CA, USA.

[163] Zhou, B., (2003), "Simulation of Formation of Polymer Membrane by Immersion Precipitation", *Massachusetts Institute of Technology*.

[164] Wikipedia, US, [online], http://en.wikipedia.org/wiki/Staining#DAPI (last accessed 12th May 2006)

[165] Answers Corporation, US, http://www.answers.com/actin (last accessed 12th May 2006)

[166] HighBeam Research Incorporation (Encyclopedia.com), US, http://www.encyclopedia.com/html/a1/actin.asp (last accessed 12th May 2006)

[167] National Heart, Lung, and Blood Institute, US, [online], http://www.nhlbi.nih.gov/health/dci/Diseases/vWD/vWD_WhatIs.html (last accessed 12th May 2006)

[168] University of Massachusetts, US, [online], http://www.bio.umass.edu/mcbfacs/intro.htm (last accessed 12th May 2006)

[169] Tseng, H., Peterson, T.E. and Berk, B.C., (1995), "Fluid shear stress stimulates mitogen-activated protein kinase in endothelial cells", *Circ Res*, Vol.77 (5), pp.869-878.

[170] Ley, K., Lundgren, E., Berger, E. and Arfors, K.E., (1989), "Shear-dependent inhibition of granulocyte adhesion to cultured endothelium by dextran sulfate", *Blood*, Vol.73 (5), pp.1324-1330.

[171] Dimmeler, S., Haendeler, J., Rippmann, V., Nehls, M. and Zeiher, A.M., (1996), "Shear stress inhibits apoptosis of human endothelial cells." *FEBS Lett.*, Vol.9 (399(1-2)), pp.71-74.

[172] Jen, A.C., Wake, M.C. and Mikos, A.G., (1996), "Review: Hydrogels for cell immobilization." *Biotechnol Bioeng* Vol.50 pp.357-364.

[173] Mueller, B., (1996), "Photocrosslinked polymers." *US Patent No. 5508317.*

[174] Buemi, M., Marino, D., Di Pasquale, G., Floccari, F., Ruello, A., Aloisi, C., Corica, F., Senatore, M., Romeo, A. and Frisina, N., (2001), "Effects of homocysteine on proliferation, necrosis, and apoptosis of vascular smooth

muscle cells in culture and influence of folic acid", *Thromb Res*, Vol.104 (3), pp.207-213.

[175] Evan, G. and Littlewood, T., (1998), "A matter of life and cell death", *Science*, Vol.281 (5381), pp.1317-1322.

[176] Tharanathan, R.N. and Kittur, F.S., (2003), "Chitin--the undisputed biomolecule of great potential. " *Crit Rev Food Sci Nutr*, Vol.43 (1), pp.61-87.

[177] Nagaoka, S., Tanzawa, H. and Suzuki, J., (1990), "Cell proliferation on hydrogels." *In Vitro Cell Dev Biol*, Vol.26 (1), pp.51-56.

[178] Horbett, T.A. and Schway, M.B., (1988), "Correlations between mouse 3T3 cell spreading and serum fibronectin adsorption on glass and hydroxyethylmethacrylate-ethylmethacrylate copolymers. " *J Biomed Mater Res*, Vol.22 (9), pp.763-793.

[179] Liu, S.Q. and Fung, Y.C., (1988), "Zero-stress states of arteries", *J Biomech Eng*, Vol.110 (1), pp.82-84.

[180] Prendergast, P., Lally, C., Daly, S., Reid, A.J., Lee, T., Quinn, D. and Dolan, F., (2003), "Analysis of Prolapse in Cardiovascular Stents: A Constitutive Equation for Vascular Tissue and Finite-Element Modelling." *J Biomech. Eng*, Vol.125 pp.692-699.

[181] Hollister, S.J., Maddox, R.D. and Taboas, J.M., (2002), "Optimal design and fabrication of scaffolds to mimic tissue properties and satisfy biological constraints", *Biomaterials*, Vol.23 (20), pp.4095-4103.

[182] Kang, H.G., Lee, S.G. and Lee, Y.M., (2005), "Novel preparative method for porous hydrogels using overrun process." *Polymer international.* , Vol.54 (537-543.).

[183] Raghavan, M.L., Trivedi, S., Nagaraj, A., McPherson, D.D. and Chandran, K.B., (2004), "Three-dimensional finite element analysis of residual stress in arteries", *Ann Biomed Eng*, Vol.32 (2), pp.257-263.

[184] Lally, C., Reid, A.J. and Prendergast, P.J., (2004), "Elastic behavior of porcine coronary artery tissue under uniaxial and equibiaxial tension", *Ann Biomed Eng*, Vol.32 (10), pp.1355-1364.

[185] Barbucci, R., Lamponi, S., Magnani, A. and Pasqui, D., (2002), "Micropatterned surfaces for the control of endothelial cell behaviour", *Biomol Eng*, Vol.19 (2-6), pp.161-170.

[186] Jayaraman, K., Kotaki, M., Zhang, Y., Mo, X. and Ramakrishna, S., (2004), "Recent advances in polymer nanofibers", *J Nanosci Nanotechnol*, Vol.4 (1-2), pp.52-65.

[187] Hartgerink, J.D., Beniash, E. and Stupp, S.I., (2002), "Peptide-amphiphile nanofibers: a versatile scaffold for the preparation of self-assembling materials", *Proc Natl Acad Sci U S A*, Vol.99 (8), pp.5133-5138.

[188] Ma, P.X. and Zhang, R., (1999), "Synthetic nano-scale fibrous extracellular matrix", *J Biomed Mater Res*, Vol.46 (1), pp.60-72.

[189] Srinivasan, G. and Reneker, D.H., (1995), "Structure and morphology of small-diameter electrospun aramid fibers. " *Polym Int*, Vol.36 pp.195-201.

[190] Reneker, D.H. and Chun, I., (1996), "Nanometre diameter fibres of polymer, produced by electrospinning. " *Nanotechnology*, Vol.7 pp.216–223.

[191] Yarin, A.L., Koombhongse, S. and Reneker, D.H., (2001), "Bending instability in electrospinning of nanofibers. " *J Appl Phys*, Vol.89 pp.3018-3026.

[192] Luu, Y.K., Kim, K., Hsiao, B.S., Chu, B. and Hadjiargyrou, M., (2003), "Development of a nanostructured DNA delivery scaffold via electrospinning of PLGA and PLA–PEG block copolymers." *J Control Release*, Vol.89 (2), pp.341-353.

[193] Fang, X. and Reneker, D.H., (1997), "DNA fibers by electrospinning. " *J Macromol Sci Phys*, Vol.B36 (2), pp.169-173.

[194] Ignatova, M., Starbova, K., Markova, N., Manolova, N. and Rashkov, I., (2006), "Electrospun nano-fibre mats with antibacterial properties from quaternised chitosan and poly(vinyl alcohol)", *Carbohydr Res*.

[195] Ohkawa, K., Cha, D., H. Kim, H., Nishida, A. and Yamamoto, H., (2004), "Electrospinning of chitosan. " *Macrmol Rapid Commun*, Vol.25 pp.1600-1605.

[196] Crawford, G.J., Constable, I.J., Chirila, T.V., Vijayasekaran, S. and Thompson, D.E., (1993), "Tissue interaction with hydrogel sponges implanted in the rabbit cornea", *Cornea*, Vol.12 (4), pp.348-357.

[197] Chen, J., Park, H. and Park, K., (1999), "Synthesis of superporous hydrogels: hydrogels with fast swelling and superabsorbent properties", *J Biomed Mater Res*, Vol.44 (1), pp.53-62.

[198] Curtis, A. and Wilkinson, C., (1997), "Topographical control of cells", *Biomaterials*, Vol.18 (24), pp.1573-1583.

[199] Miller, D.C., Thapa, A., Haberstroh, K.M. and Webster, T.J., (2004), "Endothelial and vascular smooth muscle cell function on poly(lactic-co-glycolic acid) with nano-structured surface features", *Biomaterials*, Vol.25 (1), pp.53-61.

[200] Chung, T.W., Liu, D.Z., Wang, S.Y. and Wang, S.S., (2003), "Enhancement of the growth of human endothelial cells by surface roughness at nanometer scale", *Biomaterials*, Vol.24 (25), pp.4655-4661.

[201] Nguyen, K.T. and West, J.L., (2002), "Photopolymerizable hydrogels for tissue engineering applications", *Biomaterials*, Vol.23 (22), pp.4307-4314.

[202] Decker , D., (1987), "UV-curing chemistry: past, present, and future. " *J Coat Technol*, Vol.59 pp.97-106.

[203] Sawhney, A.S., Pathak, C.P., van Rensburg, J.J., Dunn, R.C. and Hubbell, J.A., (1994), "Optimization of photopolymerized bioerodible hydrogel properties for adhesion prevention", *J Biomed Mater Res*, Vol.28 (7), pp.831-838.

[204] Hill-West, J.L., Dunn, R.C. and Hubbell, J.A., (1995), "Local release of fibrinolytic agents for adhesion prevention", *J Surg Res*, Vol.59 (6), pp.759-763.

Appendix A

Residual Stress in Arteries

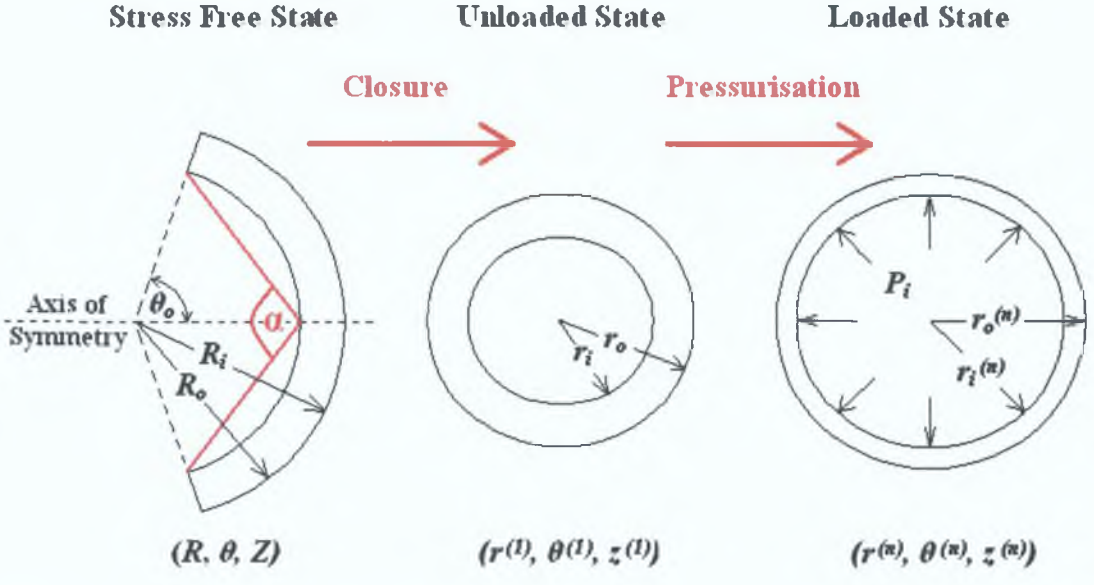

Figure A1 Cross sectional representations of an artery at the stress free state, the unloaded state and the loaded state [51].

Figure A1 shows the idealised arterial wall configurations at stress free, unloaded and loaded states [51]. Let:

Stress free state	=	state 0,
Unloaded state	=	state 1
Loaded states	=	states 2, 3, …N

A material point is denoted by (R, Θ , Z) for state 0 and (r, θ, z) in states 1, 2, …, N for cylindrical polar coordinate system. The subscripts i and e represent the inner and outer radii of the artery wall respectively. Θ_0 is related to the opening angle (α) by the following equation:

$$\tan(\alpha / 2) = \frac{\sin \Theta_0}{1 - \cos \Theta_0}$$

The incompressibility condition implies that:

Area stress free state = Area loaded states

$$\Theta\left(R_e^2 - R_i^2\right) = \pi\lambda_z(r_e^2 - r_i^2)$$

where λ_z is the axial stretch ratio. The deformation of the thick walled vessel under transmural pressure and axial tethering can be described by the following mathematical transformation:

$$r = r(R), \quad \theta = \left(\frac{\pi}{\Theta_0}\right)\Theta, \quad z = z(Z)$$

Hence the principal stretch ratios are:

$$\lambda_r = \frac{\partial r}{\partial R}, \quad \lambda_\theta = \left(\frac{\pi}{\Theta_0}\right)\frac{r}{R}, \quad \lambda_z = \frac{\partial z}{\partial Z}$$

The incompressibility condition states that $\lambda_r\lambda_\theta\lambda_z = 1$, therefore the internal radius of the artery can be calculated from:

$$r_i = \sqrt{r_e^2 - \frac{\theta_0}{\pi}\left(R_e^2 - R^2\right)}$$

Appendix B

Conversion of Engineering Stress and Strain to True Stress and Strain

Load, displacement, gauge length and cross sectional area was recorded for each specimen. All load and displacement data were converted to engineering stress and engineering strain.

Engineering Stress

$$\sigma_E = \frac{F}{A_o}$$

Engineering Strain

$$\varepsilon_E = \frac{\Delta l}{l_o}$$

where,

σ_E = Engineering Stress

F = load,

A_o = Original Cross Sectional Area,

ε_E = Engineering Strain

Δl = Change in gauge length,

l_o = Original gauge length,

As the hydrogel stretches along its longitudinal axis it subsequently contracts in the radial direction. The effect of this lateral contraction and associated decrease in cross sectional area gives rise to a difference between engineering stress and true stress. Under the assumption that the hydrogel is incompressible true stress can be related to engineering stress in the following way:

True Stress

True stress is defined as the ratio of the applied load (F) to the instantaneous cross-sectional area (A_i) of the material at the time of loading.

$$A_F \cdot l_F = A_o \cdot l_o$$

then,

$$\sigma_T = \frac{F}{A_F} = \frac{F}{A_o} \cdot \frac{l_F}{l_o}$$

since,

$$l_F = \Delta l + l_o$$

finally true stress is:

$$\sigma_T = \sigma_E(1 + \varepsilon_E)$$

where,

σ_T = True Stress

A_F = Final Area,

l_F = Final gauge length.

True Strain

True strain is defined as the sum of all the instantaneous engineering strains. Letting

$$d\varepsilon = \frac{dl}{l},$$

the true strain is,

$$\varepsilon_T = \int d\varepsilon = \int_{l_o}^{l_F} \frac{dl}{l} = \ln\left[\frac{l_F}{l_o}\right]$$

True strain can be related to engineering strain as follows:

$$\varepsilon_T = \ln\left[\frac{l_F}{l_o}\right] = \ln\left[\frac{l_o + \Delta l}{l_o}\right]$$

$$\varepsilon_T = \ln(1 + \varepsilon_E)$$

where,

ε_T = True Strain

Appendix C

Contact & Boundary Conditions

To define contact conditions between the layers of the artery the direct constraint contact algorithm was employed. The motion of the bodies are tracked in this algorithm and when contact occurs direct constraints are placed on the motion using boundary conditions (kinematic constraints on transformed degrees of freedom and nodal forces). Deformable-deformable contact was used to describe the contact between the layers of the artery. Contact between the artery and the rigid bodies was defined as deformable-rigid contact (Figure C.1). All contact bodies were mathematically defined as analytical surfaces where the normal to the contact surface was recalculated at each iteration based on the current surface position.

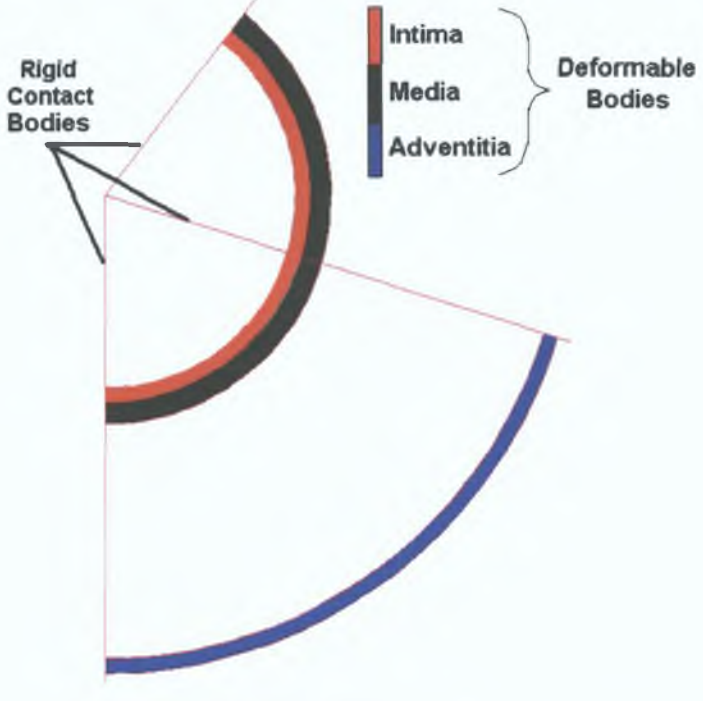

Figure C.1 **Contact algorithms used to describe the contact conditions of the finite element model.** Contact between intima, media and adventitia was defined as deformable-deformable contact, while contact between the artery and the rigid bodies was defined as deformable-rigid contact. Geometry configuration of Sample 1.

In the initial load step, the stress free arterial segments were subjected to an initial pure bending deformation (closure). Sliding contact was permitted between the three layers. Rigid contact bodies with sliding contact constrained the artery in the axial directions during all load steps (not shown). The initial boundary conditions were chosen as shown in Figure C.2 (A). The rigid contact bodies were rotated about the centre point of the stress free segment such that a 175 ° section was achieved after the bending deformation. Due to the sliding contact constraint between each layer of the artery (deformable bodies) and rigid contact bodies, and the fact that there were no boundary conditions in the Y direction, a 180 ° section could not be achieved in one load step. In order to completely close the arterial segment to become an 180° sector all the nodes at one end of each segment were displaced in the negative x direction (Close up Figure C.2 (B)). The cylindrical three layered structure was then used as the reference for subsequent deformation processes. Axial strains in the Z direction of 5, 10 and 20 % were applied to the three layers of the artery. Finally a range of internal pressures (P_i), both physiological and non-physiological pressures, were applied to the lumen of the arterial model (Figure C.2 (C)).

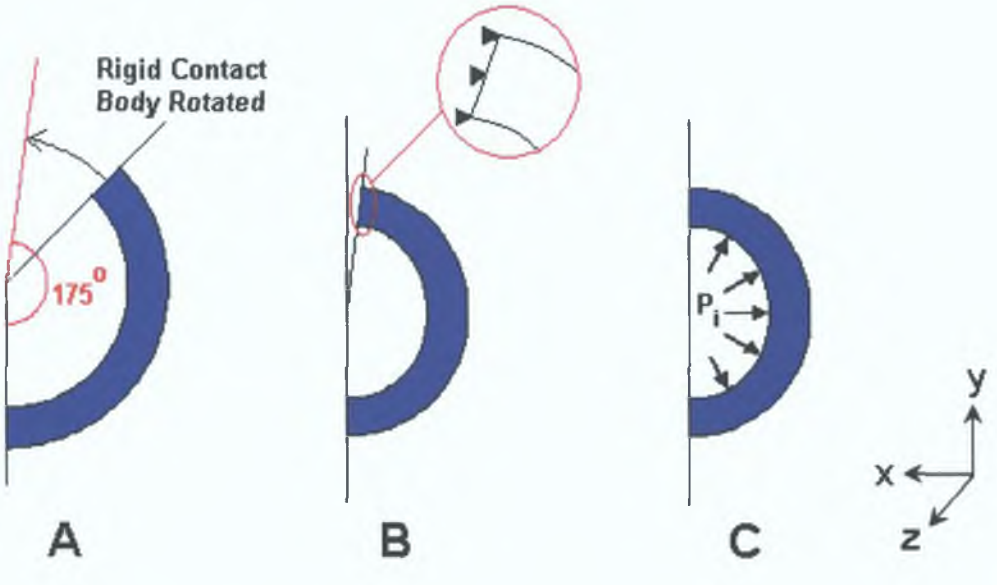

Figure C.2 **Loading Process: A:** Boundary conditions for initial load step for one layer of the artery. Sliding contact was permitted between the artery (deformable body) and the rigid contact body. The rigid contact body was rotated about the centre point such that a 175 ° segment was achieved. **B:** Nodes at one end of the arterial segment were enforced to move in the negative x-direction such that a 180 ° cylindrical specimen was achieved. **C:** Circular cylindrical arterial structure was inflated to a lumen pressure of P_i.

Appendix D

Pressure Versus Diameter Response - Sample 2

The pressure versus diameter responses for Sample 2 without and with the affect of opening angles for different longitudinal stretches are shown in Figures D.1 and D.2. Figure D.3 compares the pressure versus diameter plot of Sample 2 with and with no opening angles and an axial stretch of $\lambda_z = 1.1$.

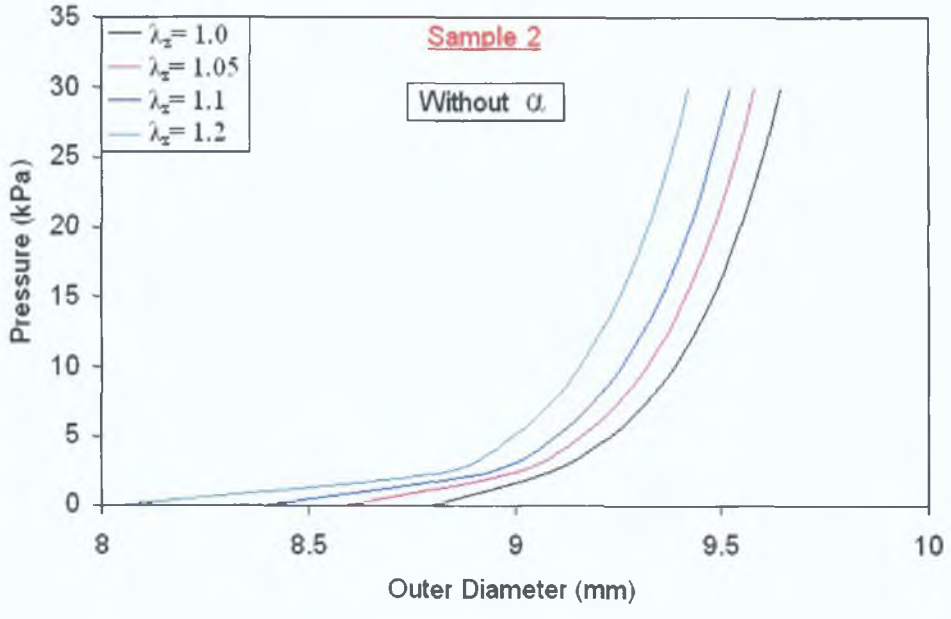

Figure D.1 **Pressure versus diameter plot of Sample 2 with no opening angles (α) and axial stretches of λz = 1.0, 1.05, 1.1 and 1.2 respectively.** Sample 2 was simulated with the experimental data obtained from the axial uniaxial tensile tests.

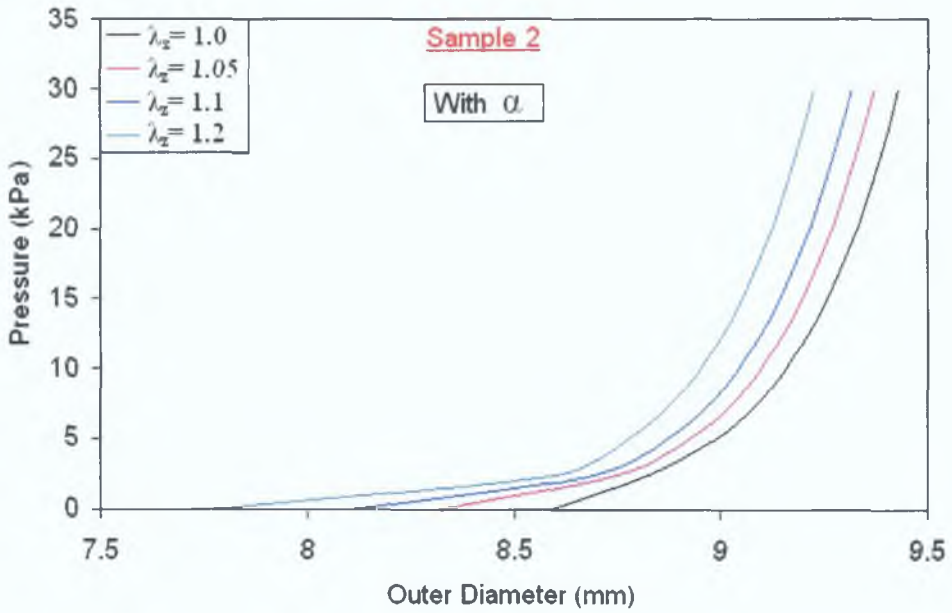

Figure D.2 **Pressure versus diameter plot of Sample 2 with opening angles (α) and axial stretches of λz = 1.0, 1.05, 1.1 and 1.2 respectively.** Sample 2 was simulated with the experimental data obtained from the axial uniaxial tensile tests.

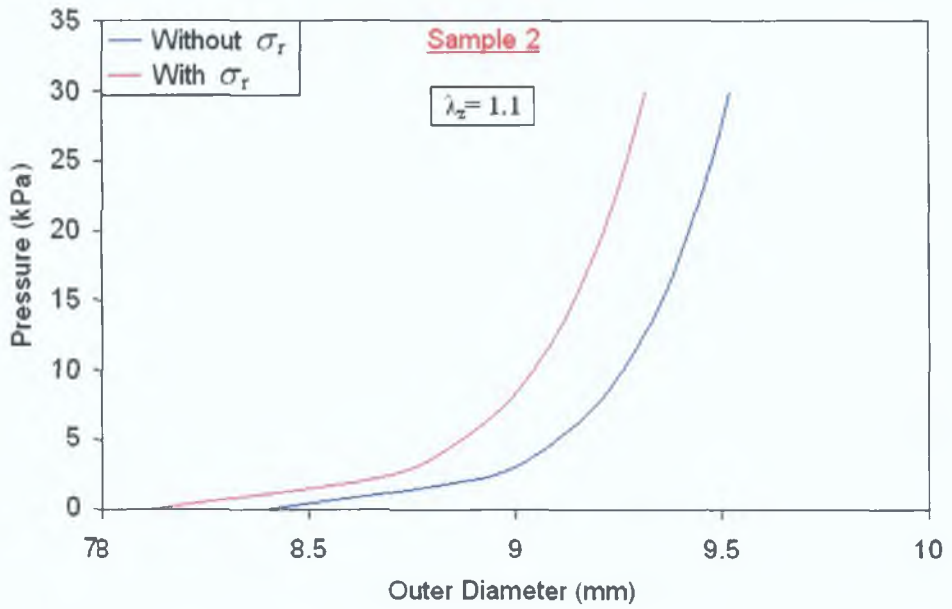

Figure D.3 **Pressure versus diameter plot of Sample 2 with and without opening angles (α) with an axial stretch of λz = 1.1.** Sample 2 was simulated with the experimental data obtained from the axial uniaxial tensile tests.

Appendix E

Repeatability Tests

The uniaxial stress versus strain data for PVA, PVA-chitosan IS-1 and PVA-chitosan WS-1 hydrogels specimens are shown in Figures E.1-E.12. Excellent repeatability of the all specimens was achieved.

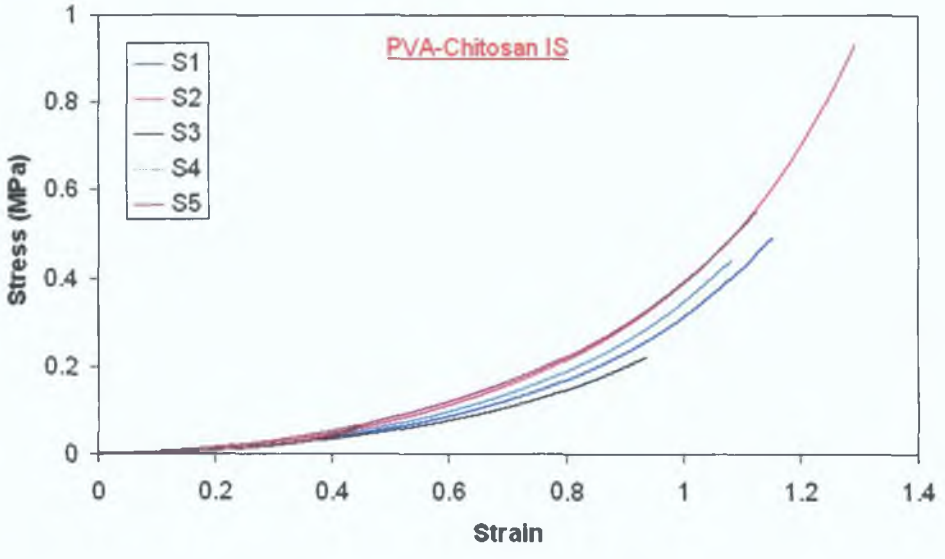

Figure E.1 **Uniaxial stress versus strain data for PVA-chitosan IS hydrogel samples that underwent 1 freeze-thaw cycle (S = Specimen).**

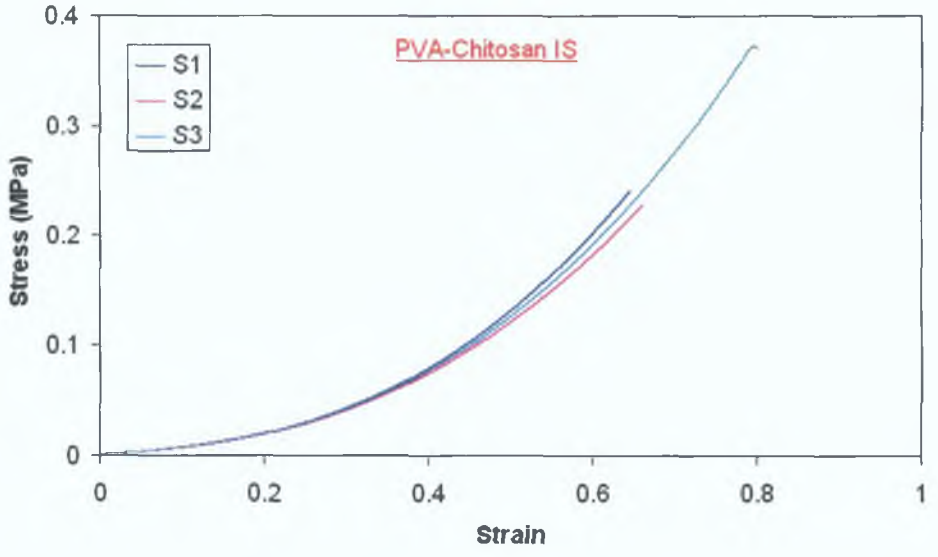

Figure E.2 **Uniaxial stress versus strain data for PVA-chitosan IS hydrogel samples that underwent 2 freeze-thaw cycles (S = Specimen).**

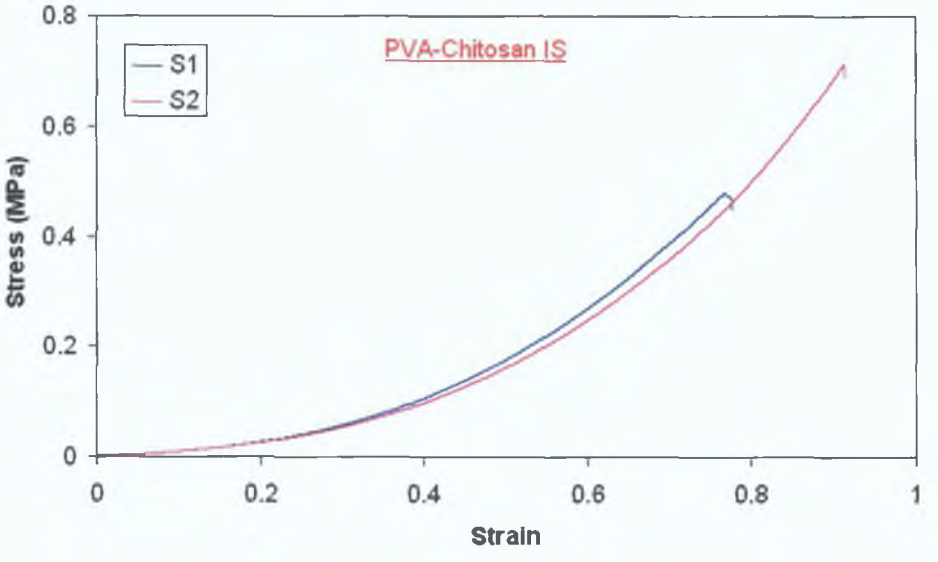

Figure E.3 **Uniaxial stress versus strain data for PVA-chitosan IS hydrogel samples that underwent 3 freeze-thaw cycles (S = Specimen).**

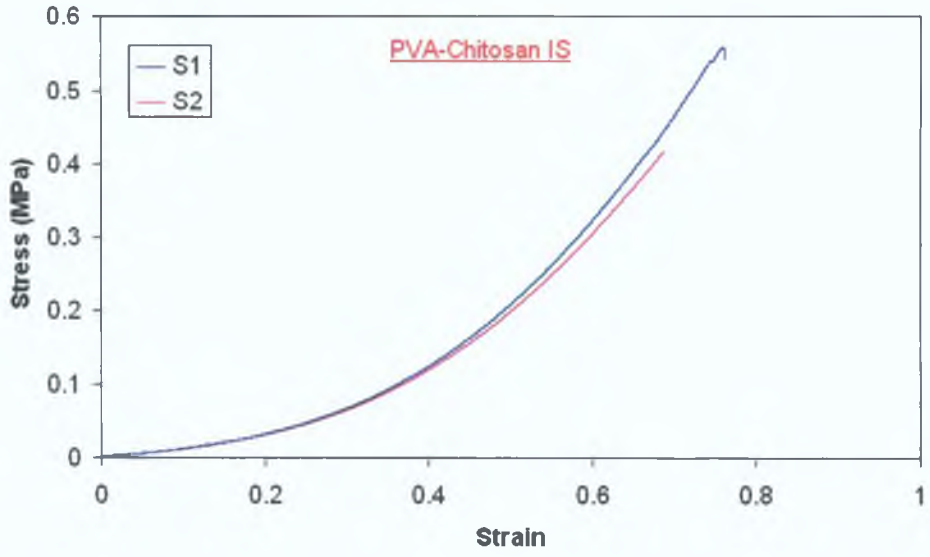

Figure E.4 **Uniaxial stress versus strain data for PVA-chitosan IS hydrogel samples that underwent 4 freeze-thaw cycles (S = Specimen).**

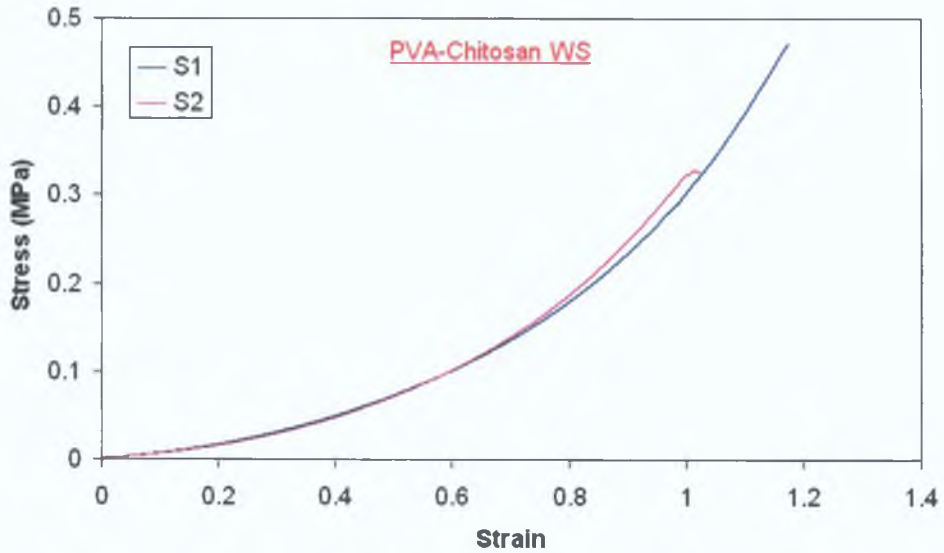

Figure E.5 **Uniaxial stress versus strain data for PVA-chitosan WS hydrogel samples that underwent 1 freeze-thaw cycle (S = Specimen).**

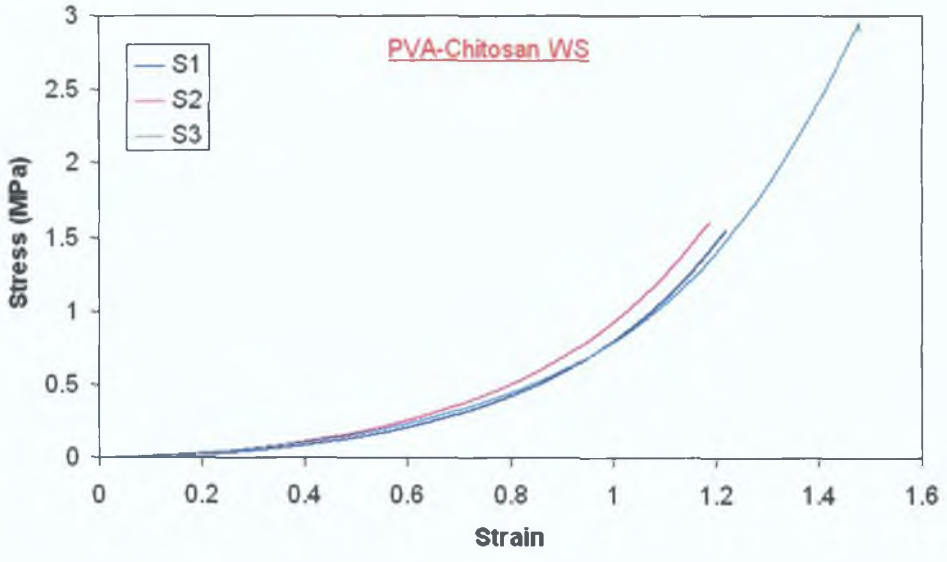

Figure E.6 **Uniaxial stress versus strain data for PVA-chitosan WS hydrogel samples that underwent 2 freeze-thaw cycles (S = Specimen).**

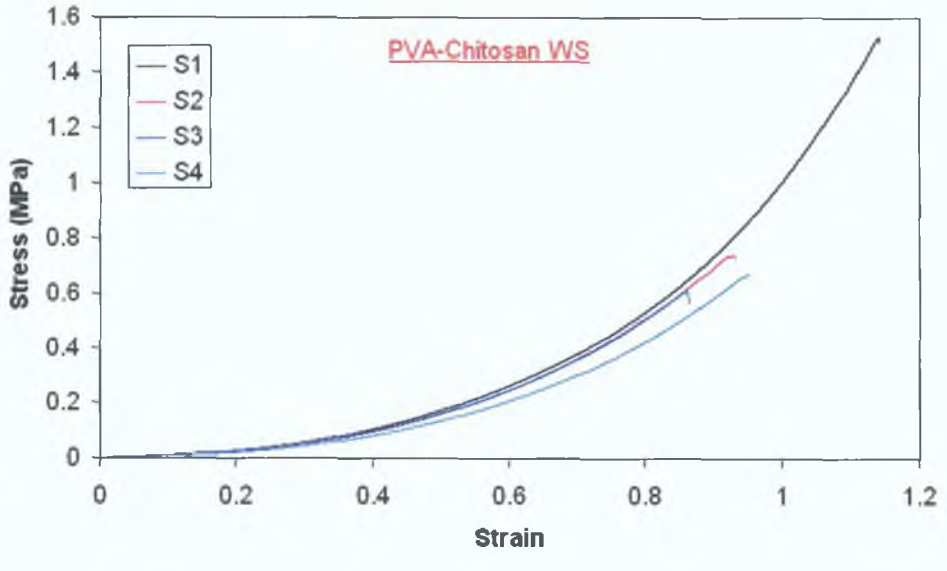

Figure E.7 **Uniaxial stress versus strain data for PVA-chitosan WS hydrogel samples that underwent 3 freeze-thaw cycles (S = Specimen).**

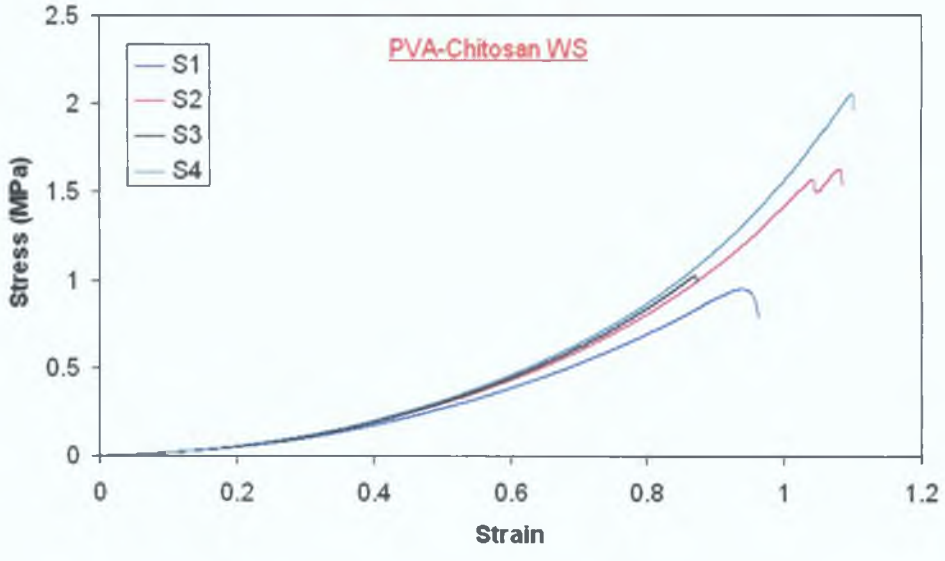

Figure E.8 **Uniaxial stress versus strain data for PVA-chitosan WS hydrogel samples that underwent 4 freeze-thaw cycles (S = Specimen).**

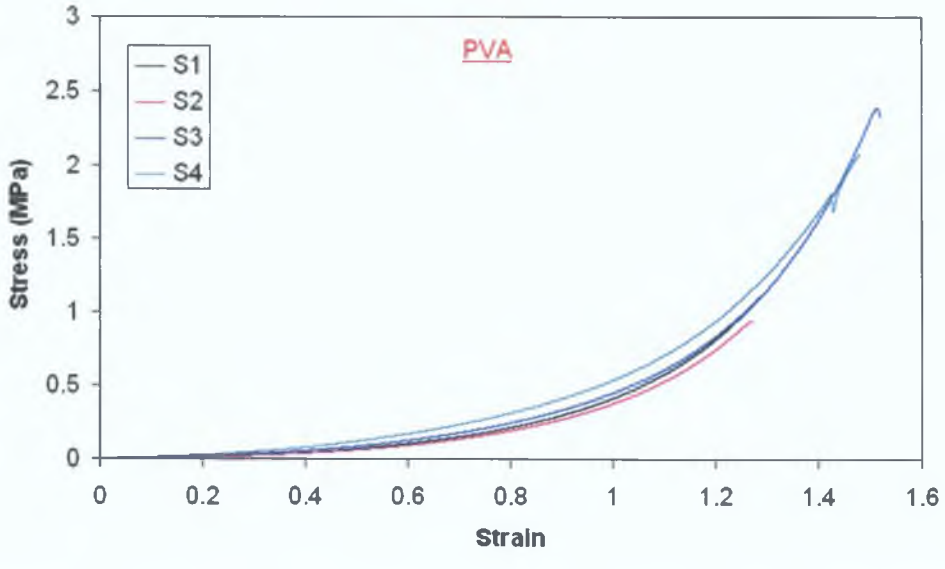

Figure E.9 **Uniaxial stress versus strain data for PVA hydrogel samples that underwent 1 freeze-thaw cycle (S = Specimen).**

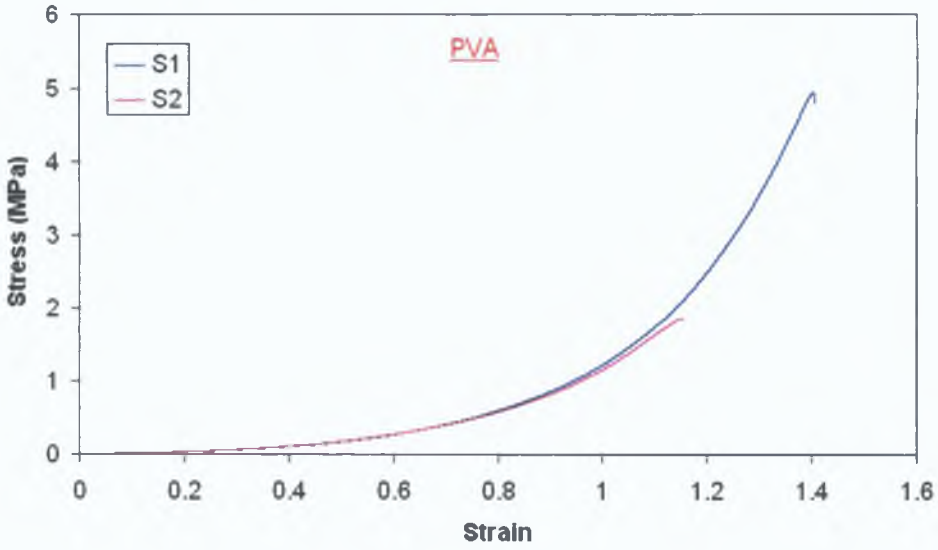

Figure E.10 **Uniaxial stress versus strain data for PVA hydrogel samples that underwent 2 freeze-thaw cyclesf (S = Specimen).**

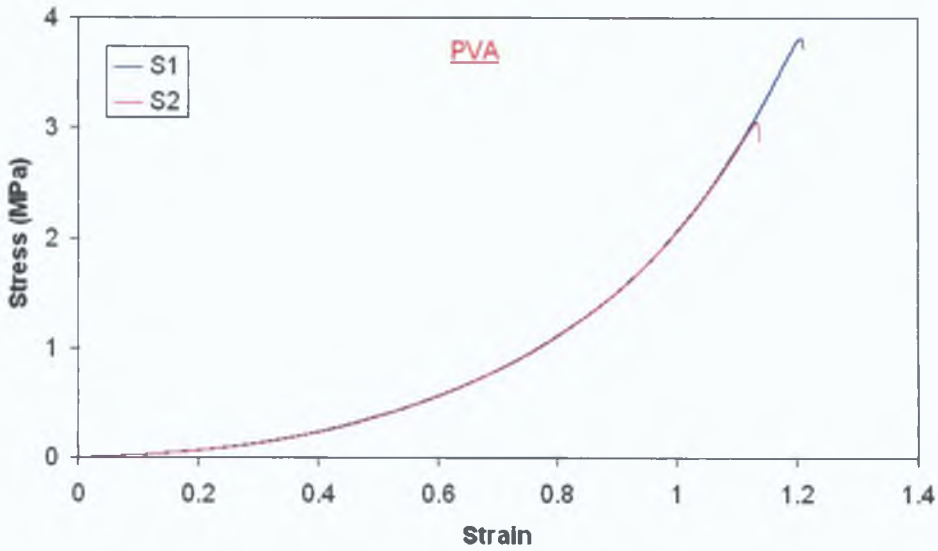

Figure E.11 **Uniaxial stress versus strain data for PVA hydrogel samples that underwent 3 freeze-thaw cycles (S = Specimen).**

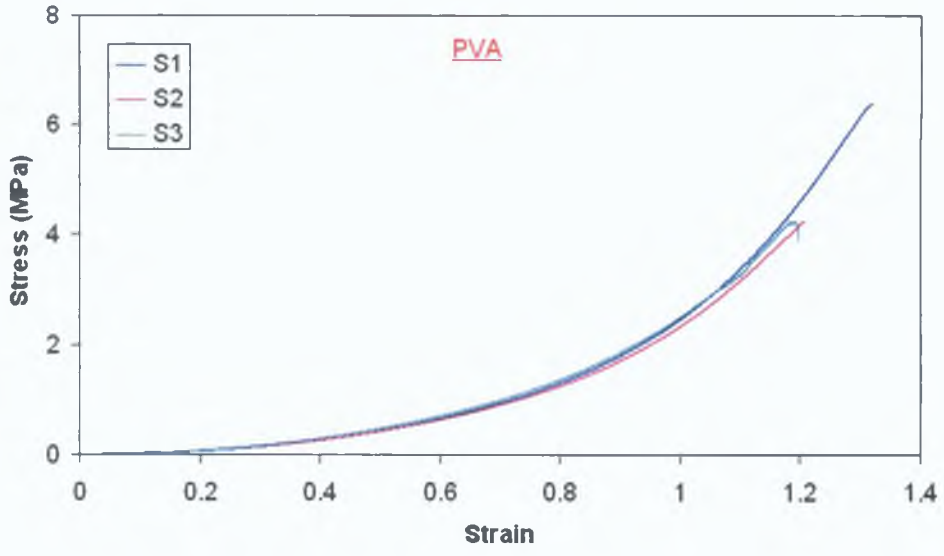

Figure E.12 Uniaxial stress versus strain data for PVA hydrogel samples that underwent 4 freeze-thaw cycles (S = Specimen).

Appendix F

Preconditioning

The uniaxial stress versus strain data illustrates a preconditioning affect on the PVA, PVA-chitosan IS-1 and PVA-chitosan WS-1 hydrogels that underwent 4 freeze-thaw cycles (Figures F.1, F.2 and F.3).

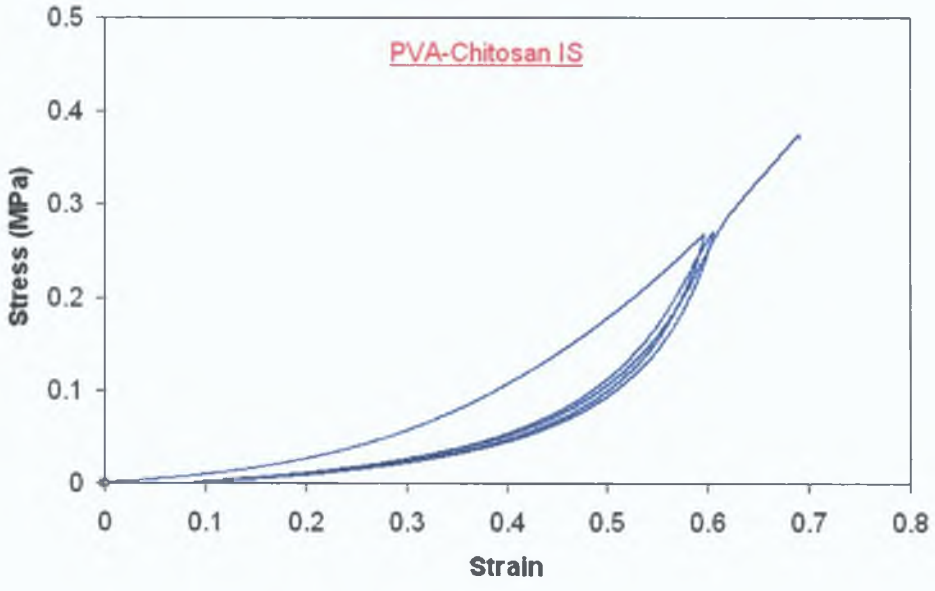

Figure F.1 **Two preconditioning cycles of PVA-chitosan IS to a load of 1N which was then loaded to failure (4 freeze-thaw cycles).**

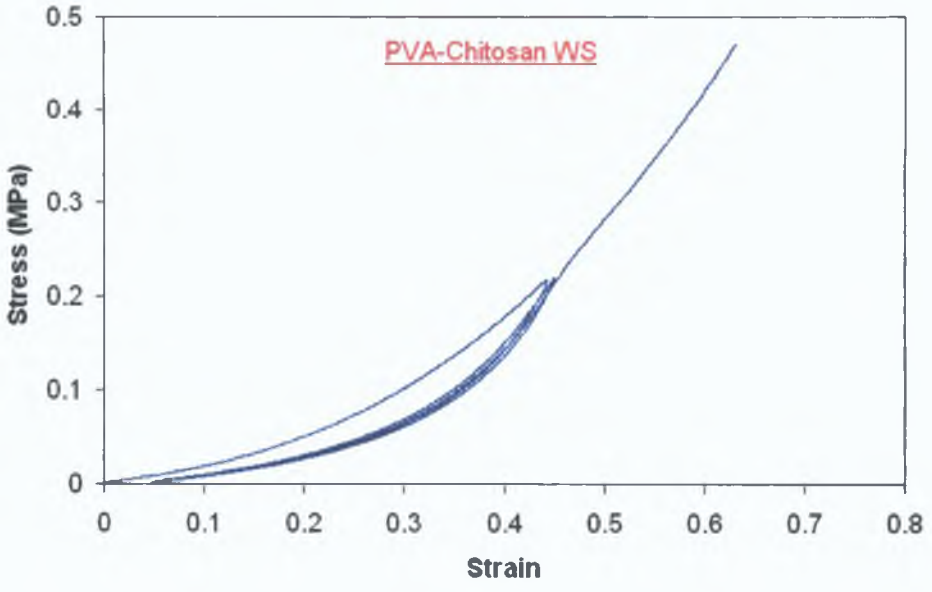

Figure F.2 **Two preconditioning cycles of PVA-chitosan WS to a load of 1N which was then loaded to failure (4 freeze-thaw cycles).**

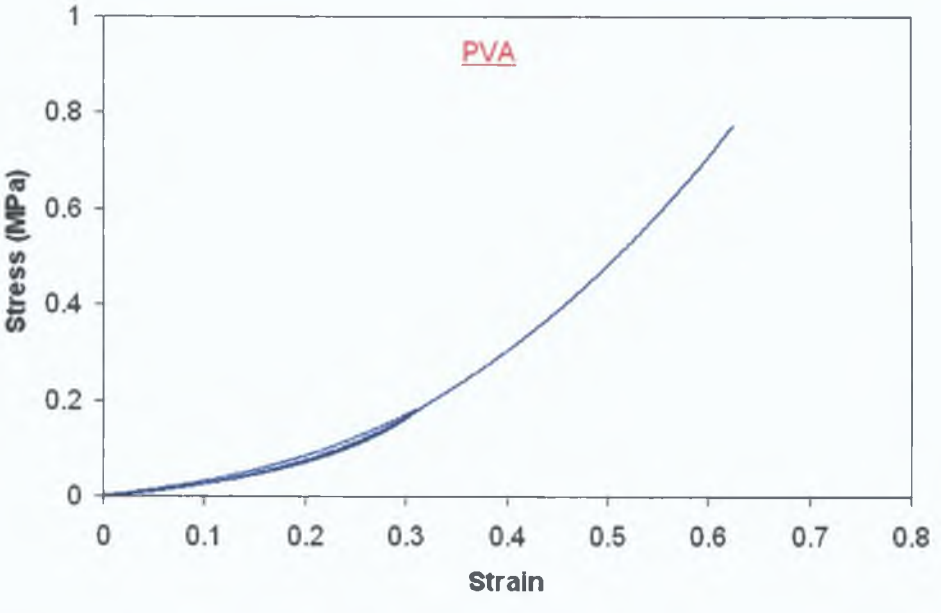

Figure F.3 **Two preconditioning cycles of PVA to a load of 1N which was then loaded to failure (4 freeze-thaw cycles).**